

**Multi-standard Context-aware Cognitive Radio:  
Sensing and Classification Mechanisms**

Von der Fakultät für Elektrotechnik und Informatik  
der Gottfried Wilhelm Leibniz Universität Hannover  
zur Erlangung des akademischen Grades

DOKTOR DER INGENIEURWISSENSCHAFTEN

Dr.-Ing.

genehmigte Dissertation  
von

M.Sc. João Paulo Cruz Lopes Miranda  
geboren am 05. April 1974 in Recife, Brasilien

2013

Referent: Prof. Dr.-Ing. Markus Fidler, Leibniz Universität Hannover  
Korreferentin: Prof. Dr. Linda Doyle, Trinity College Dublin, Ireland  
Vorsitzender: Prof. Dr.-Ing. Jürgen Peissig, Leibniz Universität Hannover  
Tag der Promotion: 20. December 2012



# Zusammenfassung

Die wachsenden Bandbreitenanforderungen an moderne drahtlose Kommunikationsnetze stellen eine große Herausforderung dar, die durch die Einführung neuartiger Anwendungen verschärft wird. Lösungsansätze wurden in der letzten Zeit sowohl in Ingenieurs- und Wirtschaftswissenschaften als auch durch Regulierungsbehörden vorgestellt. Dazu gehört die Verwendung von White Spaces, *d.h.* spektrale Ressourcen, die einem lizenzierten Dienst zugeordnet sind, jedoch zu einem bestimmten Zeitpunkt in einem bestimmten Ort nicht eingesetzt werden sind. In diesem Zusammenhang hat Dynamic Spectrum Access (DSA) besondere Aufmerksamkeit erhalten. Der Grund dafür ist dessen Flexibilität, die in das herkömmliche Spektrum-Management eingeführt werden kann. Aufbauend auf neuer entstehenden Technologien wie Software Defined Radio (SDR) und Cognitive Radio (CR) kann DSA den Einsatz innovativeren rekonfigurierbaren Systemen erleichtern. Unter der Berücksichtigung des Standortes oder auf Basis von Context Awareness, *d.h.* Umgebungswahrnehmung, können DSA-fähige Systeme ihre Betriebsfrequenzen dynamisch wählen.

White Space Devices (WSD) sind DSA-fähige Systeme, die opportunistisch (möglicherweise lizenzfrei) im nicht ausgelasteten Spektrum betrieben werden können. In den vergangenen Jahren haben WSD sowie die darauf basierenden Anwendungen einen Aufschwung genommen. Zuerst hat die International Telecommunications Union (ITU) erklärt das Breitband-Internet als das wichtigste Werkzeug, um die Fortschritte in den Informations- und Kommunikationstechnologien zu steigern. Zweitens haben einige entwickelte Länder White Spaces als effektives Mittel zur Unterstützung des Breitband-Wachstums vorgesehen. Die Einführung von WSD weckte großes Interesse, weil diese das Anbieten einer Reihe von neuen Services ermöglicht. Beispielsweise können Breitband-Internet-Zugang für unterversorgte Gebiete, Backhaul für drahtlose lokale Netzwerke, Datenverkehr Offload aus anderen Netzen, Machine to Machine Communications (M2M) und Smart Grid angeboten werden. Um von den oben genannten Chancen profitieren können, müssen WSD in der Lage sein, White Spaces effektiv auszunutzen und gleichzeitig lizenzierte Dienste ausreichend zu schützen. Geolocation/Database Access (GDA) ist die Methode, die zur Bestimmung von White Spaces im neuen freigewordenen Spektrum der bisherigen TV-übertragung in den USA genutzt wird. Trotz kleiner Unterschiede wird GDA auch von den meisten europäischen Regulierungsbehörden kurz- bis mittelfristig als die am besten geeignete Methode betrachtet. In diesem Zusammenhang kooperieren entwickelte Länder zusammen, um die regulatorische Arbeit zu minimieren sowie ein Mindestmaß an Harmonisierung unter den gewählten Lösungen zu gewährleisten. Trotz dieser Bemühungen stellt sich die Frage, ob die GDA-basierten Lösungen, die mittlerweile in entwickelten Ländern angenommen sind, auch für den weltweiten Einsatz geeignet werden.

In der vorliegenden Dissertation werden alternative Lösungen basierend auf Spectrum Sensing dargestellt. Insbesondere werden Verfahren analysiert, die die Zusammenar-

beit zwischen Sensorknoten ausnutzen, *z.B.* Cooperative Spectrum Sensing (CSS) und Wireless Sensor Networks (WSN). Ein neues Verfahren wird eben auch vorgeschlagen, welches eine Art von Context Awareness verwendet. Dieses stammt von einer Gruppe von WSD, die in der Lage sind Signale zu detektieren und zu klassifizieren. Die Grundidee basiert sich auf einer Kombination von Signalverarbeitungsalgorithmen, die komplementäre Eigenschaften besitzen. Basierend auf seiner Robustheit gegen Mehrwegeausbreitung, Ungewissheit des Rauschens und Frequenzausgleiche wird jeder Stufe der Klassifizierungskaskade der am besten passenden Algorithmus gewählt. Unter solchen unterschiedlichen Betriebsbedingungen sind mit einem kustomisierten Sensing-Plattform zwölf Kandidaten untersucht worden. Das Plattform ist eine virtuelle Testumgebung, die sich von herkömmlichen Matlab-Simulation unterscheidet indem alle Ziel-Signale in detaillierten gemäß den entsprechenden Standards implementiert sind. Die dadurch entstehende Klassifizierungskaskade ist in der Lage mit weltweit eingesetzten TV Standards zu koexistieren. Alternativ kann auch dieser Kaskadenklassifizierer verwendet werden, um Program Making and Special Events (PMSE) in den TV Bändern proaktiv zu schützen. Ferner kann der vorgestellte Klassifizierer die Koexistenz von WSD Systemen verschiedener Art gewährleisten. Die Herleitung eines Verfahrens für Multi-standard Context Awareness in beliebigen wenig ausgelasteten Frequenzbänder ist eine direkte Erweiterung der vorgestellten Arbeit. Ausserdem unterstützt das in dieser Dissertation vorgestellte Konzept die Realisierbarkeit von Sensing basierten Lösungen in den Entwicklungsländern.

**Schlagwörter:** Cognitive Radio, Signaldetektion und -klassifizierung, Spectrum Sensing.

# Abstract

The need to accommodate the increasing bandwidth demands for new applications is a big issue in modern wireless communications. In order to circumvent this problem, substantial effort has been undertaken by engineering, economics, and regulation communities to exploit white spaces, *i.e.* spectral resources that are allocated to some incumbent service but are not used in a particular time in a particular geographic area. Dynamic Spectrum Access (DSA) has received particular attention in the context of white spaces due to its potential to introduce flexibility into the static spectrum management model worldwide adopted. Built on top of emerging technologies such as Software Defined Radio (SDR) and Cognitive Radio (CR), DSA can leverage the deployment of innovative reconfigurable systems that take into account their geographic location, or obtain context awareness by other means, to dynamically select their operating frequencies.

White Space Devices (WSD) are DSA-capable systems that can operate opportunistically, possibly on an unlicensed basis, wherever underutilized spectrum exists. WSD and applications based thereon have recently gained momentum after the International Telecommunications Union (ITU) declared broadband Internet access as the prime tool to boost progress in the Information and Communication Technologies (ICT) domain. The fast-paced introduction of WSD into the market is of great interest as it has potential to open up a new world of opportunities, including broadband Internet access for underserved areas, backhaul for wireless local area networks, offload data traffic from other networks, machine to machine (M2M) communications, and smart grid to name a few. However, ICT societies will only benefit from the aforementioned opportunities if WSD rely on methods able to effectively exploit white spaces while affording sufficient protection to incumbent services. Geolocation/Database Access (GDA) has been the method adopted to allow WSD operation in the spectrum freed up by the TV switchover in the U.S. In spite of some minor differences, most European regulatory agencies also consider GDA as the most feasible method in the short to medium term. However, notwithstanding the efforts to harmonize the solutions adopted among developed countries, one aspect seems to have been overlooked in the rule-making process for WSD: Do GDA-based solutions adopted in developed countries fit developing countries too?

This dissertation deals with alternative solutions based on spectrum sensing, especially those that enforce cooperation among multiple sensing nodes, *e.g.* Cooperative Spectrum Sensing (CSS) and Wireless Sensor Networks (WSN). Instead of relying on geolocation, the proposed approach takes advantage of a kind of context awareness that a set of cooperating WSD obtains by detecting and subsequently classifying the signals conveyed in its cooperation footprint. The underlying idea of multi-standard context awareness is that, by suitably combining different signal processing techniques offering complementary features, one can design cascade classifiers able to deal with the coexistence situations raised by the operation of WSD collocated with incumbent services. The technique that best suits each

stage of the classifier is chosen on the basis of its robustness against issues raised by the practical implementation of spectrum sensing, *e.g.* multipath fading, noise uncertainty, and frequency offsets. Twelve candidate techniques are examined under such different operation conditions using a custom-built virtual testbed, which differs from conventional Matlab simulation in that all target signals are implemented in detailed accordance to corresponding standards. The outcomes of this analysis are used to populate the stages of a cascade signal classifier that is shown able to coexist with the TV broadcast standards most deployed worldwide. Alternatively, the proposed cascade signal classifier can be employed to proactively protect Program Making and Special Events (PMSE) systems, and to provide a contingency for self-coexistence between WSD whenever the standard beacon-based methods fail. The derivation of extensions to obtain multi-standard context awareness in whatever underutilized bands is straightforward along the lines above. In addition to providing a deeper understanding on a number of aspects related to node cooperation, the concept of multi-standard context-aware WSD introduced in this dissertation reinforces the suitability of sensing-based solutions for developing countries.

**Keywords:** Cognitive radio, signal detection and classification, spectrum sensing.

# Acknowledgements

To begin with I would like to thank my advisor Prof. Dr.-Ing. Markus Fidler for having given me the opportunity to carry out my doctoral studies in his group. Working under Markus' supervision was really enjoyable, not only because of his superb technical guidance but his invaluable support. From the technical perspective, I am especially grateful to Markus for his advice on what simulation findings I could investigate also analytically bearing in mind the time constraints of this project. Being the first to demonstrate interest in my financial life in Germany, Markus soon realized that the scholarship I received from CAPES/Brazil was not on an equal footing with the average salary of Ph.D students with our institute. He then offered me a position as Teaching Assistant through which my financial worries could be reduced to a minimum. My deepest appreciation is therefore devoted to Markus.

During the course of this project I was fortunate to work with Prof. Dr. Luiz DaSilva, Virginia Tech, U.S., Prof. Dr. Giuseppe Abreu, Jacobs University, Germany, Jacek Kibiłda, Wrocław Research Centre EIT+, Poland, and my colleague Dr. Sami Akin. My gratitude is expressed to Luiz for helping me putting some of my initial findings in shape for publication and for co-authoring most of them. I am grateful to Giuseppe for his help during the formulation of the research problems addressed in this dissertation and in circumventing some issues raised by the formatting of the final manuscript. I am indebted to Jacek for his invaluable help in writing and debugging the virtual testbed used in my simulations and for co-authoring some of the publications based thereon. My warmest thanks go to Sami for his patience in listening to my research ideas (even the roughest ones) and supporting me with some of the analytical derivations in this dissertation. Working with these exceptional researchers has been a distinct privilege to me.

My gratitude is expressed to Prof. Dr.-Ing. Jürgen Peissig and to Prof. Linda Doyle, from CTVR, Trinity College Dublin, Ireland, for having accepted my invitation for serving as second advisor and external advisor, respectively, on my doctoral committee.

I would like to acknowledge Prof. Dr.-Ing. Hans-Peter Kuchenbecker and Prof. Dr.-Ing. Klaus Jobmann for their interest in hosting a Ph.D. candidate from such a distant country as Brazil. These conversations started back in 2004 but it was not before 2006 that I met Prof. Dr.-Ing. Thomas Kaiser. I am indebted to Prof. Kaiser for having encouraged me to apply for a scholarship and for his patience in each and every one of the several remote iterations we had so as to put together a workplan for a my doctoral studies.

I am also indebted to many colleagues who have helped on the way. In particular, Bamrung Tau Sieskul and Mohamed El-Hadidy for their support in the writing of my doctoral workplan, my first office mates Andrej Tissen, Sebastian Sczyslo, Souhir Daoud and Waldemar Gerok for having helped me settle down after I moved from Göttingen to Hannover, Amīna Ayadi-Mießen, Anggia Anggraini, Christoph Thein, Chung Le, Emil Dimitrov, María



Dolores Pérez Guirao, Ralf Lübben, Sanam Moghaddamnia and Zhao Zhao for the stimulating discussions. A special thanks goes to Amr Rizk, Hanwen Cao, Hugues Tchouankem, Leonid Tomaszpolski and Sami Akin with whom I also enjoyed friendship.

Over the years in Germany I made few but good non-academic friends. Many thanks go to Conrad Finger, Sarah Fischer, Murat and Cigdem Meyer-Adalet, Marco Kirchhof, Kim Lemke, Oliver Kühn, Berti and Edineide Lutz, Rafael Haun, Magda Korycińska, Paulo Alexandre and Sandra Albuquerque for having put some color in the black & white life of a Ph.D. student. Their friendship was of utmost importance to me and my wife, especially to keep us warm when the thermometers went down to  $-26^{\circ}$  Celsius (this is “relatively” cold for people used to an average temperature of  $+27^{\circ}$  Celsius all the year long). I owe special thanks to Rainer and Luciana Koslowski, Raquel Gonzalez Belfort, Bianca Araujo, Fabiola Beller and Eylem Ünlü for being so lovely to us. The number of times these people helped us sort out our issues were definitely too many to count.

Finally, and most importantly, I would like to express my deepest gratitude to my family. I would first like to acknowledge my parents, Antonio and Vania, and my brother Felipe for their constant source of support and boundless love. Despite being 10000 Kilometers apart, they have never let the different latitudes separate us. Whether to push me forward after something went wrong or to celebrate my victories, they have always been present through every single step of my life. While they have inspired me to pursue this project, I would never have managed to circumvent the challenges raised thereby without my wife, Daniela. She also gave me the best souvenir I could ever bring from Germany: our little princess, Letizia. I cannot thank Daniela enough for her love, confidence, almost limitless patience, and encouragement over the passed four years.

This work was supported by a Scholarship from the Brazilian Federal Agency for Support and Evaluation of Graduate Education (CAPES – Brasília/Brasil) under the Grant BEX2770/07-5. It was also partially supported by the European Cooperation in Science and Technology (COST), Action IC0902 “Cognitive Radio and Networking for Cooperative Coexistence of Heterogeneous Wireless Networks”.

João Paulo Cruz Lopes Miranda  
Dublin, April 2013

To my beloved wife Daniela, with deepest love and gratitude



# Contents

|  |              |
|--|--------------|
| <b>Zusammenfassung</b>   | <b>II</b>    |
| <b>Abstract</b>  | <b>V</b>     |
| <b>Acknowledgements</b>  | <b>VII</b>   |
| <b>Table of Contents</b>                                       | <b>X</b>     |
| <b>List of Figures</b>   | <b>XIV</b>   |
| <b>List of Tables</b>  | <b>XVI</b>   |
| <b>Acronyms and Abbreviations</b>                              | <b>XVIII</b> |
| <b>Mathematical Symbols</b>                                    | <b>XXII</b>  |
| <b>1 Introduction</b>  | <b>2</b>     |
| 1.1 Background . . . . .                                       | 3            |
| 1.1.1 Dynamic Spectrum Access . . . . .                        | 3            |
| 1.1.2 Emerging Technologies . . . . .                          | 4            |
| 1.1.3 The Increasing Need for Bandwidth . . . . .              | 5            |
| 1.2 Towards White Space Use . . . . .                          | 6            |
| 1.2.1 Recent Advances in White Space Regulation . . . . .      | 6            |
| 1.2.2 Using White Spaces to Support Broadband Growth . . . . . | 7            |
| 1.3 Determining White Spaces . . . . .                         | 8            |
| 1.3.1 The GDA Method . . . . .                                 | 9            |
| 1.3.2 The Sensing Method . . . . .                             | 13           |
| 1.4 Comparing Coexistence Methods . . . . .                    | 22           |
| 1.4.1 Technical Aspects . . . . .                              | 22           |
| 1.4.2 Non-technical Aspects . . . . .                          | 25           |

|          |   |           |
|----------|---|-----------|
| 1.5      | Chapter Summary and Thesis Objectives . . . . .     | 31        |
| 1.5.1    | Chapter Summary . . . . .                           | 31        |
| 1.5.2    | Thesis Objectives . . . . .                         | 32        |
| 1.6      | Key Contributions . . . . .                         | 33        |
| 1.7      | Chapter Outline . . . . .                           | 34        |
| 1.8      | Publications Record . . . . .                       | 35        |
| <b>2</b> | <b>Related Work</b>                                 | <b>39</b> |
| 2.1      | Tests, Rules & Optimality Criteria . . . . .        | 39        |
| 2.1.1    | Binary Hypotheses . . . . .                         | 40        |
| 2.1.2    | Simple Hypotheses . . . . .                         | 41        |
| 2.1.3    | Composite Hypotheses . . . . .                      | 42        |
| 2.2      | Signal Processing for White Space Devices . . . . . | 42        |
| 2.2.1    | Energy Detection . . . . .                          | 43        |
| 2.2.2    | Eigenvalue-based Detection . . . . .                | 47        |
| 2.2.3    | Spectrum Correlation Detection . . . . .            | 51        |
| 2.2.4    | Cyclostationary Feature Detection . . . . .         | 54        |
| 2.2.5    | Other Feature Detectors . . . . .                   | 61        |
| 2.3      | Chapter Summary . . . . .                           | 67        |
| <b>3</b> | <b>The MESS Platform</b>                            | <b>70</b> |
| 3.1      | Signal Generation Block . . . . .                   | 71        |
| 3.1.1    | The Post-switchover Era . . . . .                   | 72        |
| 3.1.2    | Parameterization of Information Sources . . . . .   | 73        |
| 3.2      | Channel Generation Block . . . . .                  | 80        |
| 3.2.1    | AWGN Channel Model . . . . .                        | 80        |
| 3.2.2    | Multipath Fading Channel Model . . . . .            | 81        |
| 3.3      | Signal Detection Block . . . . .                    | 83        |
| 3.3.1    | Demodulation . . . . .                              | 83        |
| 3.3.2    | Sampling & Pre-detection . . . . .                  | 85        |
| 3.3.3    | Detection . . . . .                                 | 87        |
| 3.4      | Signal Classification Block . . . . .               | 89        |
| 3.4.1    | First Stage: Blind Detector . . . . .               | 92        |
| 3.4.2    | Second Stage: Fast OFDM Classifier . . . . .        | 92        |
| 3.4.3    | Third Stage: Full Signal Classifier . . . . .       | 93        |
| 3.5      | Chapter Summary . . . . .                           | 95        |

|          |  |            |
|----------|--|------------|
| <b>4</b> | <b>Simulation Results</b>                                      | <b>98</b>  |
| 4.1      | Exemplary Statistical Analysis . . . . .                       | 99         |
| 4.2      | AWGN Performance . . . . .                                     | 100        |
| 4.2.1    | OFDM-based Target Signals . . . . .                            | 103        |
| 4.2.2    | Non-OFDM Target Signals . . . . .                              | 109        |
| 4.3      | Multipath Fading . . . . .                                     | 115        |
| 4.3.1    | Impact of Target Signal Type . . . . .                         | 115        |
| 4.3.2    | Impact of Number of Nodes . . . . .                            | 118        |
| 4.4      | Noise Uncertainty . . . . .                                    | 125        |
| 4.4.1    | Impact of Target Signal Type . . . . .                         | 126        |
| 4.4.2    | Impact of Number of Nodes . . . . .                            | 129        |
| 4.5      | Frequency Offsets . . . . .                                    | 141        |
| 4.5.1    | Impact of Target Signal Type . . . . .                         | 142        |
| 4.5.2    | Impact of Sensing Time . . . . .                               | 145        |
| 4.5.3    | Impact of Number of Nodes . . . . .                            | 152        |
| 4.6      | Signal Classification Block (Revisited) . . . . .              | 152        |
| 4.6.1    | Blind Techniques . . . . .                                     | 153        |
| 4.6.2    | Semi-blind Techniques . . . . .                                | 153        |
| 4.6.3    | Signal-specific Techniques for the 2nd Stage . . . . .         | 154        |
| 4.6.4    | Signal-specific Techniques for the 3rd Stage . . . . .         | 155        |
| 4.7      | Chapter Summary . . . . .                                      | 157        |
| <b>5</b> | <b>Conclusions</b>   | <b>159</b> |
| 5.1      | Summary of Contributions . . . . .                             | 160        |
| 5.1.1    | Multi-standard Context-aware WSD . . . . .                     | 160        |
| 5.1.2    | Cooperation based on Signal Specific Techniques . . . . .      | 161        |
| 5.1.3    | A Cascade Classifier for Coexistence in the TV Bands . . . . . | 163        |
| 5.1.4    | The MESS Platform . . . . .                                    | 164        |
| 5.2      | Suggestions for Future Research . . . . .                      | 165        |
| 5.2.1    | Emerging Coexistence Situations . . . . .                      | 165        |
| 5.2.2    | Practical Implementation . . . . .                             | 166        |
| 5.2.3    | Characterization of Classification Performance . . . . .       | 167        |
| 5.2.4    | Applications . . . . .   | 168        |

# List of Figures

|      |   |     |
|------|---|-----|
| 1.1  | Example of coexistence based on the GDA method . . . . .                  | 9   |
| 1.2  | Definition of temporal white spaces . . . . .                             | 15  |
| 1.3  | Definition of spatial white spaces . . . . .                              | 16  |
| 1.4  | Information processes of cooperative spectrum sensing . . . . .           | 19  |
| 2.1  | Block diagram of a typical digital receiver . . . . .                     | 40  |
| 2.2  | Exemplary ROC curves for energy detection ( $M = 1500$ samples) . . . . . | 44  |
| 2.3  | Minimum number of samples obtained via (2.15) . . . . .                   | 45  |
| 2.4  | Minimum number of samples obtained via (2.18) . . . . .                   | 46  |
| 2.5  | Simplified block diagram of a baseband OFDM transmitter . . . . .         | 57  |
| 2.6  | Exemplary cyclic autocorrelation function obtained via (2.72) . . . . .   | 58  |
| 2.7  | Exemplary autocorrelation function obtained via (2.72) . . . . .          | 59  |
| 2.8  | Simplified block diagram of a baseband ATSC transmitter . . . . .         | 64  |
| 3.1  | Functional block diagram of the MESS platform. . . . .                    | 71  |
| 3.2  | Detailed view of the signal generation block. . . . .                     | 73  |
| 3.3  | Pilot insertion patterns adopted in some OFDM standards . . . . .         | 76  |
| 3.4  | Exemplary power spectra of OFDM signals . . . . .                         | 77  |
| 3.5  | Exemplary power spectra of non-OFDM signals . . . . .                     | 78  |
| 3.6  | Exemplary power spectra of wireless microphone signals . . . . .          | 79  |
| 3.7  | Detailed view of the channel generation block . . . . .                   | 80  |
| 3.8  | Detailed view of the signal detection block . . . . .                     | 84  |
| 3.9  | Multi-standard operation environment based on the MESS platform . . . . . | 90  |
| 3.10 | TV broadcast standards most deployed in the Americas . . . . .            | 90  |
| 3.11 | Detailed view of the signal classification block . . . . .                | 91  |
| 4.1  | Exemplary histograms of the test statistic $z_{ED}$ . . . . .             | 101 |
| 4.2  | Exemplary normal plots of the statistic collector “rxfile” . . . . .      | 102 |
| 4.3  | Detection of DVB-T under AWGN . . . . .                                   | 103 |

|      |   |     |
|------|---|-----|
| 4.4  | Detection of ISDB-T under AWGN (CP= 1/4) . . . . .                              | 104 |
| 4.5  | Detection of ISDB-T under AWGN (CP= 1/32) . . . . .                             | 105 |
| 4.6  | Detection of IEEE 802.22 under AWGN . . . . .                                   | 107 |
| 4.7  | Detection of ECMA-392 under AWGN . . . . .                                      | 108 |
| 4.8  | Detection of ATSC under AWGN . . . . .  | 111 |
| 4.9  | Detection of NTSC under AWGN . . . . .  | 112 |
| 4.10 | Detection of PAL under AWGN . . . . .   | 113 |
| 4.11 | Detection of PMSE under AWGN (different WM speaker modes) . . . . .             | 114 |
| 4.12 | Detection of ECMA-392 under multipath (prof. B, $N = 2$ ) . . . . .             | 117 |
| 4.13 | Detection of ECMA-392 under multipath (prof. D, $N = 2$ ) . . . . .             | 118 |
| 4.14 | Impact of multipath on ACD, BTPD, SCD (prof. D, $N = \{2, 10, 20\}$ ) . . . . . | 119 |
| 4.15 | Autocorrelation function of ECMA-392 (prof. B, $N = 1$ ) . . . . .              | 124 |
| 4.16 | Autocorrelation function of ECMA-392 (prof. D, $N = 1$ ) . . . . .              | 125 |
| 4.17 | Impact of noise uncertainty on ED ( $N = 2$ ) . . . . .                         | 129 |
| 4.18 | Impact of noise uncertainty on RLRT ( $N = 2$ ) . . . . .                       | 130 |
| 4.19 | Impact of noise uncertainty on SCD ( $N = 2$ , non-OFDM signals) . . . . .      | 131 |
| 4.20 | Impact of noise uncertainty on SCD ( $N = 2$ , OFDM signals) . . . . .          | 132 |
| 4.21 | Impact of noise uncertainty on ED ( $N = \{2, 10, 20\}$ ) . . . . .             | 133 |
| 4.22 | Impact of noise uncertainty on SCD ( $N = \{2, 10, 20\}$ ) . . . . .            | 134 |
| 4.23 | Spectral masks of ECMA-392 at different SNR ( $\sigma_w^2$ known). . . . .      | 135 |
| 4.24 | Spectral mask and performance of SCD for large $M$ (ECMA-392). . . . .          | 136 |
| 4.25 | Impact of noise uncertainty on RLRT ( $N = \{2, 10, 20\}$ ) . . . . .           | 137 |
| 4.26 | Impact of noise uncertainty on blind EBD ( $N = \{2, 10, 20, 50\}$ ) . . . . .  | 139 |
| 4.27 | Impact of noise uncertainty on blind EBD ( $N = \{2, 10, 20, 50\}$ ) . . . . .  | 140 |
| 4.28 | Impact of SFO on TDSC-NP (DVB-T, 4.48 ms, $N = 2$ ) . . . . .                   | 142 |
| 4.29 | Impact of SFO on TDSC-MRC (DVB-T, 4.48 ms, $N = 2$ ) . . . . .                  | 143 |
| 4.30 | Impact of SFO on TDSC methods (ECMA-392, 0.75 ms, $N = 2$ ) . . . . .           | 144 |
| 4.31 | Impact of SFO on TDSC-NP (DVB-T, 8.96 ms, $N = 2$ ) . . . . .                   | 145 |
| 4.32 | Impact of SFO on TDSC-MRC (DVB-T, 8.96 ms, $N = 2$ ) . . . . .                  | 146 |
| 4.33 | Impact of SFO on TDSC methods (ECMA-392, 1.50 ms, $N = 2$ ) . . . . .           | 147 |
| 4.34 | Impact of SFO on TDSC-NP (ISDB-T, 8.96 ms, $N = \{2, 10, 20\}$ ) . . . . .      | 150 |
| 4.35 | Impact of SFO on TDSC-MRC (ISDB-T, 8.96 ms, $N = \{2, 10, 20\}$ ) . . . . .     | 151 |
| 5.1  | An interaction channel model for iTV over TV white spaces . . . . .             | 169 |
| 5.2  | In-band channel monitoring using quiet periods . . . . .                        | 170 |
| 5.3  | Channel monitoring mechanisms for future C-PMSE systems . . . . .               | 172 |



# List of Tables

|      |  |     |
|------|--|-----|
| 1.1  | Performance limiting factors of GDA and spectrum sensing . . . . .               | 23  |
| 1.2  | Exemplary keep-out regions of GDA and spectrum sensing . . . . .                 | 24  |
| 1.3  | White space detection capabilities of GDA and spectrum sensing . . . . .         | 24  |
| 1.4  | Evolution of the ICT development index by region (2002 – 2010) . . . . .         | 26  |
| 1.5  | Service penetration per 100 inhabitants (2010) . . . . .                         | 26  |
| 1.6  | Evolution of the service affordability by region (2009 – 2010) . . . . .         | 27  |
| 1.7  | Exemplary applications for DSA operational contexts . . . . .                    | 29  |
| 1.8  | Most preferred DSA methods (regulator perspective) . . . . .                     | 30  |
| 1.9  | Most preferred DSA methods (licensed user perspective) . . . . .                 | 30  |
| 1.10 | Most preferred DSA methods (unlicensed user perspective) . . . . .               | 30  |
|      |  |     |
| 3.1  | System parameters of some OFDM-based standards . . . . .                         | 74  |
| 3.2  | System parameters of some non-OFDM standards . . . . .                           | 75  |
| 3.3  | System parameters adopted in PMSE (different WM speaker modes) . . . . .         | 75  |
| 3.4  | Values assigned to $\rho$ in the noise uncertainty analysis . . . . .            | 81  |
| 3.5  | Multipath profiles proposed in the IEEE 802.22 standard . . . . .                | 82  |
| 3.6  | Signal processing techniques currently implemented in MESS . . . . .             | 84  |
| 3.7  | Settings of sensing time and number of samples used in the simulations . . . . . | 86  |
| 3.8  | Summary of requirements for the 1st stage . . . . .                              | 92  |
| 3.9  | Summary of requirements for the 2nd stage . . . . .                              | 93  |
| 3.10 | Allowed subcarrier spacings (in kHz) for 6 MHz channels . . . . .                | 93  |
| 3.11 | Summary of requirements for the 3rd stage . . . . .                              | 94  |
|      |  |     |
| 4.1  | Loss created by multipath fading (OFDM signals) . . . . .                        | 116 |
| 4.2  | Loss created by multipath fading (non-OFDM signals) . . . . .                    | 116 |
| 4.3  | Loss created by noise uncertainty under AWGN (OFDM signals) . . . . .            | 127 |
| 4.4  | Loss created by noise uncertainty under AWGN (Non-OFDM signals) . . . . .        | 127 |
| 4.5  | Loss created by noise uncertainty under multipath (OFDM signals) . . . . .       | 128 |

|     |  |     |
|-----|--|-----|
| 4.6 | Loss created by noise uncertainty under multipath (Non-OFDM signals) . . | 128 |
| 4.7 | Loss created by sampling frequency offsets (TDSC methods) . . . . .      | 141 |
| 4.8 | Summary of the major results of the simulation work . . . . .            | 153 |

# Acronyms and Abbreviations

|        |   |
|--------|---|
| ACD    | Autocorrelation-based Detection                             |
| ACF    | Autocorrelation Function                                    |
| ADC    | Analog-to-Digital Converter                                 |
| AGM    | Arithmetic to Geometric Mean Detector                       |
| A-GPS  | Assisted Global Positioning System                          |
| AM     | Amplitude Modulation  |
| AMD    | Average Method Deviation                                    |
| ARPU   | Average Revenue Per User                                    |
| ASSD   | ATSC Segment SYNC Detector                                  |
| ATSC   | Advanced Television Systems Committee                       |
| AWGN   | Additive White Gaussian Noise                               |
| BPF    | Bandpass Filter   |
| BS     | Base Station  |
| BTPD   | Blind Twin Peak Detector                                    |
| CAF    | Cyclic Autocorrelation Function                             |
| CAGR   | Compound Annual Growth Rate                                 |
| CAPEX  | Capital Expenditure   |
| CBP    | Coexistence Beacon Protocol                                 |
| CEPT   | Conference of Postal and Telecommunications Administrations |
| CFAR   | Constant False Alarm Rate                                   |
| CFD    | Cyclostationary Feature Detection                           |
| CFO    | Carrier Frequency Offset                                    |
| CH     | Cluster Head  |
| CIS    | Commonwealth of Independent States                          |
| CIT    | Cognitive Interactive Terminal                              |
| COST   | European Cooperation in Science and Technology              |
| CP     | Cyclic Prefix   |
| CPC    | Cognitive Pilot Channel                                     |
| CPE    | Customer Premise Equipments                                 |
| C-PMSE | Cognitive Program Making and Special Events                 |
| CR     | Cognitive Radio   |
| CSS    | Cooperative Spectrum Sensing                                |
| DFT    | Discrete-time Fourier Transform                             |
| DSA    | Dynamic Spectrum Access                                     |
| DTMB   | Digital Terrestrial Multimedia Broadcast                    |
| DVB-T  | Digital Video Broadcast-Terrestrial                         |

|        |  |
|--------|--|
| EBD    | Eigenvalue-Based Detection                           |
| ED     | Energy Detection                                     |
| EME    | Energy with Minimum Eigenvalue Detector              |
| E-OTD  | Enhanced Observed Time Difference                    |
| FAR    | False Alarm Rate                                     |
| FBMC   | Filter Bank Multi-Carrier                            |
| FCC    | Federal Communications Commission                    |
| FFT    | Fast Fourier Transform                               |
| FM     | Frequency Modulation                                 |
| FPGA   | Field Programmable Gate Array                        |
| GDA    | Geo-location/Database Access                         |
| GLRT   | Generalized Likelihood Ratio Test                    |
| GNI    | Gross National Income                                |
| GPS    | Global Positioning System                            |
| HSYNC  | Horizontal SYNC                                      |
| ICT    | Information and Communication Technologies           |
| ICI    | Inter-Carrier Interference                           |
| IDI    | ICT Development Index                                |
| IETF   | Internet Engineering Task Force                      |
| IF     | Intermediate Frequency                               |
| IFFT   | Inverse Fast Fourier Transform                       |
| i.i.d. | Independent and Identically Distributed              |
| IS     | Importance Sampling                                  |
| ISDB-T | Integrated Services Digital Broadcasting-Terrestrial |
| ISI    | Inter-Symbol Interference                            |
| ITU    | International Telecommunications Union               |
| iTV    | Interactive Television                               |
| LLRT   | Log Likelihood Ratio Test Statistic                  |
| LO     | Local Oscillator                                     |
| LOS    | Line-Of-Sight  |
| LRT    | Likelihood Ratio Test                                |
| LTE    | Long Term Evolution                                  |
| M2M    | Machine To Machine Communications                    |
| MAD    | Modified Autocorrelation Detector                    |
| MBSS   | Multi-Band Spectrum Sensing                          |
| MC     | Monte Carlo  |
| MD     | Multi-cycle Detector                                 |
| MDR    | Missed Detection Rate                                |
| MED    | Maximum Eigenvalue Detector                          |
| MESS   | Multi-Environment Spectrum Sensing Platform          |
| MF     | Matched Filter                                       |
| MLE    | Maximum Likelihood Estimate                          |

|        |  |
|--------|--|
| MME    | Maximum-Minimum Eigenvalue Detector        |
| MRC    | Maximum Ratio Combining                    |
| MRSS   | Multi-Resolution Spectrum Sensing          |
| NA     | Not Applicable                             |
| NHSD   | NTSC Horizontal SYNC Detector              |
| NLOS   | Non-Line-Of-Sight                          |
| NP     | Neyman-Pearson                             |
| NTSC   | National Television Systems Committee      |
| Ofcom  | Office of Communications                   |
| OFD    | Other Feature Detectors                    |
| OFDM   | Orthogonal Frequency Division Multiplexing |
| OPEX   | Operational Expense                        |
| PAL    | Phase Alternating Line                     |
| PAM    | Pulse Amplitude Modulation                 |
| PAPR   | Peak-to-Average Power Ratio                |
| PAWS   | Protocol to Access White Space Database    |
| p.d.f. | Probability Density Function               |
| p.m.f  | Probability Mass Function                  |
| PDP    | Power Delay Profile                        |
| PMSE   | Program Making and Special Events          |
| PN     | Pseudo Noise                               |
| ppm    | Parts Per Million                          |
| PRBS   | Pseudo Random Binary Sequence              |
| PRU    | Pilot Repetition Unit                      |
| PSD    | Power Spectrum Density                     |
| QPSK   | Quadrature Phase-Shift Keying              |
| RCT    | Return Channel Terrestrial                 |
| REM    | Radio Environment Maps                     |
| RF     | Radio Frequency                            |
| RLRT   | Roy's Largest Root Test                    |
| ROC    | Receiver Operating Characteristic          |
| SCD    | Spectrum Correlation Detector              |
| SCF    | Spectrum Correlation Function              |
| SD     | Single Cycle Detector                      |
| SDR    | Software-Defined Radio                     |
| SFO    | Sampling Frequency Offset                  |
| SNR    | Signal-to-Noise Ratio                      |
| SP     | Scattered Pilot                            |
| SPD    | Scattered Pilot Detector                   |
| SRU    | Scanning Receiver Unit                     |
| ST     | Spherical Test Detector                    |
| STSM   | Short-Term Scientific Mission              |

|       |   |
|-------|---|
| SVD   | Singular Value Decomposition                    |
| TDS   | Time-Domain Synchronous                         |
| TDSC  | Time-Domain Symbol Cross-correlation            |
| TVBD  | TV Band Device                                  |
| UCS   | Urgent Coexistence Situation                    |
| VSF   | Vestigial Side Band                             |
| WiFi  | Wireless Fidelity                               |
| WiMAX | Worldwide Interoperability for Microwave Access |
| WLAN  | Wireless Local Area Network                     |
| WM    | Wireless Microphone                             |
| WRAN  | Wireless Regional Area Network                  |
| WSD   | White Space Device                              |
| WSN   | Wireless Sensor Network                         |
| WSS   | Wideband Spectrum Sensing                       |

# Mathematical Symbols

|                |  |
|----------------|--|
| $A_c$          | Carrier magnitude  |
| $B$            | Channel bandwidth  |
| $C_C$          | Cost of a bidirectional control channel between database and WSD                 |
| $C_{CSS}$      | Incremental cost of cooperative spectrum sensing                                 |
| $C_{DB}$       | Cost of constructing a database  |
| $C_{GDA}$      | Incremental cost of geo-location/database access                                 |
| $C_L$          | Cost of embedding location-aware components in WSD                               |
| $C_l(k)$       | Complex constellation conveyed by the $k$ th subcarrier during the $l$ th symbol |
| $C_S$          | Cost of embedding a sensing receiver in WSD                                      |
| $C_{SN}$       | Cost of constructing a wireless sensor network                                   |
| $C_{WSN}$      | Incremental cost of a wireless sensor network                                    |
| $d_B$          | Margin added to the protected contour of a base station                          |
| $d_C$          | Margin added to the protected contour of a customer premise equipment            |
| $d_P$          | Radius of the protected contour used in geo-location/database access             |
| $d_S$          | Margin added to the protected contour of a sensing-only WSD                      |
| $f_0$          | Channel coherence bandwidth  |
| $f_c$          | Carrier center frequency   |
| $f'_c$         | Mismatched carrier frequency introducing carrier frequency offsets               |
| $f_{dev}$      | Frequency deviation  |
| $f_{dop}$      | Doppler frequency  |
| $f_s$          | Sampling frequency   |
| $f'_s$         | Incorrect sampling frequency introducing sampling frequency offsets              |
| $\mathbb{F}$   | Set of all possible carrier frequencies where PMSE are allowed to operate        |
| $F_Q$          | Number of frames per query   |
| $g$            | Pulse shaping filter   |
| $h$            | Channel impulse response   |
| $h_{ij}$       | Channel coefficient between the $i$ th WSD and the $j$ th licensed transmitter   |
| $\mathbf{h}_j$ | Vector of channel coefficients $h_{ij}, i = 1, 2, \dots, N$                      |
| $\mathbb{H}$   | Wishart matrix   |
| $H_0$          | Null hypothesis (signal is absent)   |
| $H_1$          | Alternate hypothesis (signal is present)   |
| $\mathbf{I}$   | Identity matrix  |
| $K$            | Number of nonoverlapping sequences of a single realization (Bartlett method)     |
| $L$            | Channel order  |
| $L_{ij}$       | Channel order between the $i$ th WSD and the $j$ th licensed transmitter         |
| $m$            | Audio input signal (tone in the context of the speaker modes in Table 3.3)       |

|                                 |  |
|---------------------------------|--|
| $M$                             | Number of samples  |
| $M_{\min}$                      | Minimum number of samples required by a certain point in the ROC         |
| $n_0$                           | Starting sample index  |
| $N$                             | Number of nodes (WSD) engaged in cooperative spectrum sensing            |
| $\mathcal{N}$                   | Normal distribution  |
| $N_c$                           | Number of categories present in a given operation environment            |
| $N_f$                           | Number of possible carrier frequencies                                   |
| $N_1$                           | Number of symbol pairs that have the same scattered pilot pattern        |
| $N_r$                           | Number of independent runs in a Monte Carlo experiment                   |
| $N_s$                           | Number of subcarriers in an OFDM signal                                  |
| $N_{\tau_d}$                    | Number of segment SYNC pairs that are distant $\tau_d$ from each other   |
| NF                              | Noise figure of the sensing receiver used in WSD                         |
| $\mathcal{O}(\cdot)$            | Big O notation   |
| $P$                             | Number of licensed transmitters operating collocated with WSD            |
| $\mathbb{P}$                    | Set of subcarriers onto which scattered pilots are mapped                |
| $P_d$                           | Probability of detection   |
| $\bar{P}_d$                     | Target probability of detection  |
| $P_{fa}$                        | Probability of false alarm   |
| $\bar{P}_{fa}$                  | Target probability of false alarm  |
| $P_{mc}$                        | Probability of missed classification                                     |
| $P_{md}$                        | Probability of missed detection  |
| $\bar{P}_{md}$                  | Target probability of missed detection                                   |
| $P(x)$                          | Prior probability of event $x$   |
| $\Pr(x)$                        | Probability of event $x$ occurring                                       |
| $p(x y)$                        | Conditional probability density function of event $x$ given event $y$    |
| $Q(\cdot)$                      | Marcum Q-Function  |
| $Q_d$                           | Overall probability of detection derived by $N$ cooperating nodes        |
| $Q_{fa}$                        | Overall probability of false alarm derived by $N$ cooperating nodes      |
| $Q_{md}$                        | Overall probability of missed detection derived by $N$ cooperating nodes |
| $r$                             | Received signal  |
| $\mathbf{r}$                    | Vector of received signals $r_i, i = 1, 2, \dots, N$                     |
| $R_x$                           | Autocorrelation function of $x$  |
| $R_x^\alpha$                    | Cyclic autocorrelation function of $x$                                   |
| $R(l, l')$                      | TDSC function of two OFDM symbols that have the same SP pattern          |
| $\mathbf{R}_x$                  | Covariance matrix of $x$   |
| $s$                             | Transmitted signal (target signal in the context of coexistence)         |
| $S_x$                           | Power spectrum density of $x$  |
| $S_x^\alpha$                    | Spectrum correlation function of $x$                                     |
| $\hat{S}_{\text{BAR},x}$        | Bartlett estimate of $S_x$   |
| $\hat{S}_{\text{PER},x}$        | Periodogram estimate of $S_x$  |
| $\hat{S}_{\text{PER},x}^\alpha$ | Cyclic periodogram estimate of $S_x^\alpha$                              |
| SNR                             | Signal-to-noise ratio in linear scale                                    |



|                          |  |
|--------------------------|--|
| $t_0$                    | Channel coherence time   |
| $t_d$                    | Sample timing drift per OFDM symbol  |
| $t_Q$                    | Time required to enquire the database  |
| $t_S$                    | Sensing time per frame   |
| $t_T$                    | Amount of time available for transmission                                    |
| $\bar{t}_M$              | Average medium access time per frame   |
| $T_C$                    | Number of data samples in the cyclic prefix of an OFDM symbol                |
| $T_{CP}$                 | Cyclic prefix duration   |
| $T_{cyc}$                | Cyclic period of a scattered pilot sequence                                  |
| $T_D$                    | Total number of data samples per OFDM symbol                                 |
| $T_{FFT}$                | Useful duration of an OFDM symbol  |
| $T_s$                    | Sampling period  |
| $T'_s$                   | Incorrect sampling period introducing sampling frequency offsets             |
| $T_{SYM}$                | Total duration of an OFDM symbol   |
| $w$                      | Zero-mean additive white Gaussian noise                                      |
| $\mathbf{w}$             | Vector of noise signals $w_i, i = 1, 2, \dots, N$                            |
| $W$                      | Occupied signal bandwidth  |
| $W_{BAR}$                | Discrete-time Fourier transform of a Bartlett window                         |
| $x$                      | Generic variable, symbol, signal   |
| $z$                      | Generic test statistic   |
| $\mathbb{Z}$             | Set of integers  |
| $\alpha$                 | Cycle frequency  |
| $\alpha_l$               | Channel amplitude measured over the $l$ th path of a multipath channel       |
| $\beta_{\max}$           | Eigenvector corresponding to the maximum eigenvalue of $\mathbf{R}_x$        |
| $\chi_{2K}^2$            | Central chi-squared distribution with $2K$ degrees of freedom                |
| $\chi_{\kappa}^2(o)$     | Non-central chi-squared distribution with skewness $\kappa$ and kurtosis $o$ |
| $\delta(\cdot)$          | Dirac delta sequence   |
| $\Delta f$               | Subcarrier spacing   |
| $\Delta l$               | Symbol index difference between two OFDM symbols with same SP pattern        |
| $\Delta \lambda$         | Average of all the eigenvalues of $\mathbf{R}_x$                             |
| $\epsilon_c$             | Normalized carrier frequency offset  |
| $\epsilon_s$             | Normalized sampling frequency offset   |
| $\varphi$                | Autocorrelation function coefficient   |
| $\gamma$                 | Detection threshold  |
| $\eta_{CSS}$             | Transmission efficiency of cooperative spectrum sensing                      |
| $\eta_{GDA}$             | Transmission efficiency of geo-location/database access                      |
| $\eta_{WSN}$             | Transmission efficiency of wireless sensor network                           |
| $\iota$                  | Smoothing factor (used in the context of eigenvalue-based detection)         |
| $\lambda_{\max}$         | Maximum eigenvalue of $\mathbf{R}_x$   |
| $\lambda_{\min}$         | Minimum eigenvalue of $\mathbf{R}_x$   |
| $\boldsymbol{\lambda}_x$ | Vector of eigenvalues of $\mathbf{R}_x$                                      |
| $\nu_{chan}$             | Parameter that determines the channel model in (2.82)                        |

|                         |   |
|-------------------------|---|
| $\theta$                | Random phase  |
| $\theta_l$              | Channel phase measured over the $l$ th path of a multipath channel      |
| $\rho$                  | Parameter that determines the amount of noise uncertainty in (2.19)     |
| $\sigma_x^2$            | Average power of $x$  |
| $\tau$                  | Discrete time lag   |
| $\tau_d$                | Correlation delay in terms of data segments                             |
| $\tau_l$                | Channel delay measured over the $l$ th path of a multipath channel      |
| $\tau_{\max}$           | Maximum excess delay of a multipath channel                             |
| $\tau_s$                | Discrete time lag normalized by a sampling period $T_s$                 |
| $\tau_u$                | Discrete time lag normalized by a useful symbol length $T_{\text{FFT}}$ |
| $\Psi_{\text{SYNC}}$    | Accumulated SYNC function   |
| $\Psi_{\text{TDSC}}$    | Accumulated TDSC function   |
| $*$                     | Convolution operation   |
| $a \succ b$             | Preference relation indicating that $a$ is more preferable than $b$     |
| $\wedge$                | Estimate, maximum likelihood estimate in (2.9)                          |
| $\ell(\cdot)$           | Likelihood ratio  |
| $E(\cdot)$              | Expected value of the argument  |
| $\text{Var}(\cdot)$     | Variance of the argument  |
| $\cdot _{\text{dB}}$    | Value in dB of the linear quantity on the left                          |
| $ \cdot $               | Absolute value of the argument  |
| $ \cdot ^2$             | Energy of the argument  |
| $\ \cdot\ $             | Norm of the argument  |
| $\ \cdot\ ^2$           | Power of the argument   |
| $\lceil \cdot \rceil$   | The smallest integer not less than the argument                         |
| $\lfloor \cdot \rfloor$ | The largest integer not greater than the argument                       |
| $(\cdot)^*$             | Complex conjugate operation   |
| $(\cdot)^T$             | Transposition operation   |
| $(\cdot)^\dagger$       | Hermitian operation   |
| $\text{Re}\{\cdot\}$    | Real part of a complex argument   |
| $\text{Im}\{\cdot\}$    | Imaginary part of a complex argument                                    |
| $\max(\cdot)$           | Maximum of the argument   |
| $\min(\cdot)$           | Minimum of the argument   |
| $\sup(\cdot)$           | Supremum of the argument  |
| $\text{Tr}(\cdot)$      | Trace of the argument   |



# Chapter 1

## Introduction

In the modern society, the radio frequency (RF) spectrum constitutes a vital resource for a number of applications that rely on wireless communications. One issue raised when new wireless applications need to be accommodated is that, though the RF spectrum spans from 3 kHz to 300 GHz, its useful portion lies below 15 GHz for most applications. Eventually, higher frequencies can be used to accommodate larger bandwidth requirements but this results in shorter reach, *i.e.* transmitted signals are received over shorter distances. Therefore, wireless communication systems for frequencies above 15 GHz are more economically viable in dense urban areas or for fixed point-to-point communications. Such technical and economical constraints become even more stringent when it comes to mobile communications. In this case, the use of very low frequencies raises antenna size issues so that the frequencies commercially feasible span only up to about 4 GHz. These reasons render the useful RF spectrum to be regarded as a *limited* resource.

For more than one century, which dates back to the early days of the wireless telegraphy, techniques for improving the efficiency of spectrum usage have been receiving attention from both academy and industry. Thanks to this continued effort, tremendous progress has been achieved on virtually all technological fields that may influence the way a wireless communication system uses the spectrum. This includes, but is not limited to, antenna characteristics, backhaul requirements, duplexing techniques, frequency reuse, interference mitigation, modulation and multiple access schemes, polarization, power control, resource allocation, and routing. However, notwithstanding the progress made thus far, there still exist many reasons for spectrum underutilization.

In this chapter, we describe the causes of spectrum underutilization and review the state of the art in regulatory and technical solutions to mitigate them. We begin in Section 1.1 with some ideas currently under discussion to flexibilize spectrum management. We also overview some emerging technologies aimed at supporting these ideas. In Section 1.2, we summarize the latest moves towards more flexible regulations and explain how they exploit underutilized spectrum to support broadband growth. We continue in Section 1.3 with an in-depth overview about the underlying principles, advantages, and drawbacks of the two methods currently regarded as the most promising to determine underutilized spectrum. This puts in place the technical background for Section 1.4, where we carry out a techno-economical analysis crucial to set out the motivation of this dissertation later on in Section 1.5. Before closing the chapter, we highlight our key contributions in Section 1.6, outline the remainder of the dissertation in Section 1.7, and provide a record of the own publications related to the dissertation in Section 1.8.

## 1.1 Background

This section is divided in three parts that are as follows. First, we look at some promising spectrum management policies and techniques recently advanced as a means to tackle the spectrum underutilization problem. Second, we introduce emerging technologies based on which a number of methods have been proposed to facilitate the flexibilization discussed in the first part. Basically, these methods are able to determine spectrum availability and, in doing so, allow to accommodate future applications using underutilized spectrum. In the third part, we give some figures on the bandwidth needs of such future applications.

### 1.1.1 Dynamic Spectrum Access

Regulatory agencies worldwide typically use allocation and assignment processes to manage the interaction between services in neighboring frequency bands and in different geographical areas. Though this two-step method keeps interference under acceptable levels, its incentives for efficient spectrum utilization are limited because huge regions of spectrum are assigned on a static, long term basis [1]. Apart from this inherent underutilization caused by current spectrum management policies, other sources of underutilization include large peak-to-average power ratio (PAPR) of wireless systems that have dedicated spectrum, limited rejection of practical receivers to adjacent channel interference, and, not surprisingly, the simple fact that population is non-uniformly distributed [2].

Frequency assignment data from regulatory agencies usually shows little or no unassigned spectrum in most bands of interest. However, static frequency charts fail to reflect how well a certain type of service (specific party) is making use of allocated (assigned) frequencies. Monitoring tasks are therefore necessary to determine the actual degree of spectrum usage. Several measurement campaigns carried out at in the recent years at different times and places report similar findings that confirm spectrum underutilization. In [3], utilization levels between 15% and 85% were observed depending on the geographic location and the time of the day. Low spectrum utilization was also perceived by [4], especially in the bands between 3 GHz and 6 GHz. Constant use below 300 MHz and around 900 MHz was reported in [5] but large amounts of “premium” spectral resources showed either any or only sporadic activity in between these frequency bands. More recently, a study on the spectrum occupancy of 11 European countries found that 49% to 56% of the TV channels in the 470–790 MHz bands are unused [6]. Such spectral resources, which though allocated and assigned are not being used at a particular time in a particular geographic area, are referred to as *white spaces*.

To a certain extent, the notion of white space has been modifying the belief that spectrum scarcity is created solely by inefficient regulatory policies. This paradigm change is motivating engineering, economics, and regulation communities to search for novel spectrum management policies and techniques that can allow wireless devices to improve the current spectrum usage by exploiting white spaces. Among some ideas envisioned to tackle this problem, *dynamic spectrum access* (DSA) has been receiving particular attention due to its potential to introduce flexibility into a so far static way of managing spectrum resources. In DSA networks, wireless devices need not be locked into a fixed set of operating frequencies. This flexibility can leverage the deployment of innovative reconfigurable systems that are either *context-aware* or take into account their geographic location to dynamically select operating frequencies.

Various approaches to spectrum reform can be put under the umbrella of DSA. Among these approaches, the one of interest in this dissertation is the *overlay-based hierarchical access model* [7]. This model prioritizes access to spectrum, so that lower priority unlicensed systems are allowed to share spectrum with higher priority licensed systems. As long as unlicensed systems are capable of determining spectrum availability prior to initiate transmissions, they can be sure they will not generate harmful interference to licensed systems. Unlicensed systems can thus convey data *opportunistically* over the frequency bands identified as white spaces. In this fashion, more flexible regulations based on the overlay model can lead to more efficient wireless systems thus improving the current levels of spectrum utilization. As an additional advantage, this model has been regarded in the literature as the most compatible with existing allocation and assign policies [7][8]. Nevertheless, overlay operation brings about several challenges to the practical implementation of DSA, *e.g.* the need for *frequency rendezvous* that comes along with increased flexibility [9]. Unlike traditional wireless systems, which operate using a fixed set of frequencies known a priori, DSA-capable systems need to determine what frequencies to use before commencing operation. Synchronization issues also arise as any two wireless devices need to agree beforehand on what channel to use for establishing a communications link between each other.

### 1.1.2 Emerging Technologies

Considerable research effort has been made over the past decade to meet the complex reconfigurability needs raised by DSA. *Software-defined radio* (SDR) and *cognitive radio* (CR) are emerging technologies regarded as DSA enablers because of the following reasons. With its baseband processing performed in software, SDR possesses the ability to reconfigure operation frequency, modulation type, transmit power, and other physical layer parameters according to the current conditions of the operation environment. This is possible at run-time thanks to recent advances in digital signal processing and generic hardware components used to implement communication functions in SDR, *e.g.* microprocessors, field programmable gate arrays (FPGA) and other software reconfigurable hardware. When built on top of SDR, CR provides wireless devices with the awareness required to understand the context they find themselves in and autonomously configure themselves in response to a predefined set of goals [1]. Simply put, the synergy arising between SDR and CR consists of a software controlled communication vehicle whose control and applications follow CR principles [8][10].

Under the overlay model, CR principles can be guided by any means able to determine spectrum availability and, in doing so, identify white spaces. In this context, approaches that can afford sufficient protection to license holders without posing excessive computational burdens on CR devices are of utmost importance to the commercial feasibility of future DSA networks. A (non-exhaustive) list of methods that can be used to determine spectrum availability include:

- **Geo-location/database access (GDA)** denotes a method for CR devices to obtain from a database a list of permitted channels before initiating operation and without sensing the spectrum for licensed signals [11]. Exemplary information available at the database includes the services granted protection, their locations, protection requirements, and operation channels.

- In **spectrum sensing**, the problem to be solved at the CR device translates into the estimation of a specific parameter of the licensed signal (to be detected) using a test statistic. Decision on the channel availability is made via statistical hypothesis testing, *e.g.* by constructing a test statistic and comparing it to a detection threshold based on some test criterion [12].
- **Disabling beacons** are digitally modulated signals especially designed to convey information to sensing-capable CR devices [13]. Within an area covered by disabling beacons, CR devices can be instructed about what channels to avoid so as not to interfere with other licensed systems operating nearby.
- **Cyclostationary signatures** are similar to beacons in the sense that they can be intentionally embedded in digital signals for the sake of facilitating signal detection and classification. Additional uses of cyclostationary features include frequency acquisition, network identification, and frequency rendezvous [14].
- The concept of **cognitive pilot channel (CPC)** refers to a dedicated RF link used to convey information to CR devices. Including available frequency bands, services, load situation, and network policies, CPC information allows CR devices to connect to whatever service available on whatever frequency [15].

### 1.1.3 The Increasing Need for Bandwidth

The modern society is becoming increasingly mobile and more dependent of information and communication technologies (ICT). An issue common in such ICT societies is the increasing bandwidth needs of innovative features and applications. Typically, this growing bandwidth demand is introduced along with new generations of smartphones, tablets, and laptops, which are high-end mobile devices having potential to multiply the traffic created by basic mobile phones in up to five hundred times [16]. Current estimates point out that the mobile data traffic by 2015 will exhibit a 26-fold increase over 2010, corresponding to a compound annual growth rate (CAGR) of 92%. Adding up the contributions of fixed Internet and managed Internet protocol, expected to be about 32% and 24%, respectively, results in an overall traffic growth of 32% in the same period [17].

Clearly, the success of future wireless services depends on the ability of ICT societies to accommodate the growing demands for capacity and quality. Aiming at finding solutions, regulatory and technical work is currently being undertaken through a number of authorities. The International Telecommunications Union (ITU) is responsible for both global and regional levels. At the regional level, further harmonization efforts are usually necessary to adequate and implement the ITU recommendations, *e.g.* the regulation activities carried out by the European Conference of Postal and Telecommunications Administrations (CEPT). Locally, the RF spectrum framework is set and managed by national regulatory agencies such as the Federal Communications Commission (FCC) in the U.S., and the Office of Communications (Ofcom) in the U.K.

In the next section, we summarize the latest moves towards more flexible regulations. The first part of the section briefly overviews the arguments used by the FCC, Ofcom, and CEPT to define a preferred method for determining white spaces. The second part describes how some exemplary plans set out in both global, regional, and national levels intend to exploit white spaces to support broadband growth.

## 1.2 Towards White Space Use

### 1.2.1 Recent Advances in White Space Regulation

The practicality and efficiency of methods aimed at determining white spaces have been largely discussed by regulatory agencies, both in country- and region-wide levels. Pioneering work has been carried out in the U.S., where the FCC will allow unlicensed operation of CR-based *TV band devices* (TVBD) in the spectrum freed up by the digital switchover. The TV bands were selected due to their superior propagation and penetration characteristics (as compared to higher frequencies) and static behavior (changes in location and frequency of TV transmitters occur unfrequently). In [18], the FCC determines that TVBD can use GDA as the sole means to identify white spaces. Subsequently, multiple database administrators were selected for an initial period of 5 years [19] and the first public trials were concluded without any report of critical nature [20]. The reasoning used by the FCC to drop the sensing requirement, mandated to be combined with GDA in an earlier Report & Order [21], is that license holders will be granted adequate protection by means of GDA and other provisions of the rules. As such, mandatory sensing requirements would impose additional burdens to TVBD. According to the FCC, this could slow down the introduction of TVBD to the market, thus making the uptake of unlicensed applications based on CR more difficult. In parallel, based on experience acquired through extensive prototype testing [22], the FCC recognizes spectrum sensing as a promising method and defines requirements for sensing-only TVBD. Device certification will occur under a rigorous “proof-of-performance” standard in this case, meaning that sensing-only TVBD have to pass laboratory and field tests prior to certification.

The Ofcom refers to GDA as the most important method in the short to medium term and allows both GDA and spectrum sensing methods to be used independently [23]. Despite of the similarities between the approaches ruled by the FCC and Ofcom, differences exist under some aspects. The most distinguishing aspect is that the Ofcom intends to specify algorithms for determining white spaces [24][25], whereas the FCC leaves the database structure, administrative functions, and services up to the market [18]. While the focus of the Ofcom seems to be on facilitating harmonization, a vital task within the European regulatory framework, the FCC seems to be aiming at an optimized database design. With respect to spectrum sensing, the Ofcom believes that there may be advantages in aligning requirements for sensing-only TVBD on an international basis, *i.e.* through CEPT. So, rule making activities for such devices are waiting for developments in Europe.

In [26], the CEPT points out GDA as the most feasible method and argues that spectrum sensing is not required as long as GDA can provide sufficient protection to license holders. The CEPT agrees that the combined use of GDA and sensing may be positive but its benefits need to be further investigated. European countries that decide to adopt GDA will have the flexibility to select the parameters and algorithms for the database according to their own national circumstances. A certain degree of harmonization will be ensured by providing exemplary algorithms and general guidelines for the exchange of information between TVBD and the database.

Technical standards have recognized importance as their employment provides advantages, such as *economies of scale*, interoperability, and efficient usage of spectrum and energy. Aware of these advantages and driven by the latest regulatory decisions discussed above, the Internet Engineering Task Force (IETF) has started working on a protocol to access



white space databases (PAWS) [27]. In essence, PAWS consists of an effort to standardize a data model for databases and a query method for TVBD to retrieve information from databases. Both tasks are important for the development of end devices. At the time of this writing, the IETF is determining use cases and requirements on top of which PAWS will be defined. The use cases addressed in the first drafts include broadband Internet access in rural and underserved areas, backhaul for wireless local area networks (WLAN), and offload data traffic from other networks.

Though conceptually different, GDA, disabling beacons, and CPC are similar in the sense that they require additional infrastructure from stakeholders and coordination efforts from regulators. As disabling beacons and CPC compete with GDA as enabler of prior knowledge, they have received less support in the context of DSA. The Ofcom addresses disabling beacons in its studies but concludes that the method does not merit further investigation [23]. The rationale behind this conclusion builds on top of the three main drawbacks of the beacon approach. First, TVBD within an area covered by the disabling beacon can be “shielded” from receiving beacon signals such that interference protection cannot be ensured. Second, efficiency concerns arise as TVBD access to white spaces may be unnecessarily prohibited if the area covered by beacons is larger than needed. Finally, spectrum otherwise available for TVBD is required for the beacon transmission. Neither disabling beacons nor CPC is considered by the FCC [18]. This makes of the ECC the only regulatory agency that considers further investigating the use of disabling beacons. This, however, seems to be conditioned to the standardization of the CPC along the lines proposed in [28].

### 1.2.2 Using White Spaces to Support Broadband Growth

Due to its proven potential to create job opportunities, increase productivity, and boost economies, broadband Internet access has been considered by the ITU as the prime tool to tackle today’s challenges. In what is intended to be the beginning of a series of reports, the ITU’s Broadband Commission for Digital Development presents an approach to benefit healthcare, education, energy efficiency, environmental protection, public safety, civic participation, and economic growth [29]. In a second report, the ITU provides some facts and figures to help bringing recommendations into effect [30]. Also, related policy challenges are addressed through a roadmap of regulatory issues that includes the establishment of consistent licensing frameworks for broadband deployment and optimization of RF spectrum use.

So as not to lose the opportunities above, support for broadband growth should be coordinated on a countrywide basis. In line with the goals set by the ITU, countries worldwide are planning to release larger amounts of RF spectrum and reallocate them for new purposes. In the U.S., the FCC will make available 500 MHz of spectrum for wireless broadband until 2015, 300 MHz of which exclusively for mobile use [31]. Concerning white spaces, the recommendation 5.13 of the American National Broadband Plan is of particular interest as it promotes the development and deployment of opportunistic uses across *more* radio spectrum. The first action proposed to meet this goal is to provide more technical room for innovation by supporting the development of CR technologies, *e.g.* by allowing them to use spectrum currently held by the FCC. In a second action, the FCC will investigate ways to apply GDA to frequencies *other* than the TV bands. As license holders will be protected by means of GDA, TVBD that are also capable of spectrum sensing can carry

out parallel measurements to assess the actual spectrum usage in these bands. Reporting these findings back to the database can help improve opportunistic uses.

Europe’s vision for the period 2010 – 2020 was set out in the first quarter of 2010. With smart growth, sustainable growth, and inclusive growth as mutually reinforcing priorities, Europe 2020 [32] defines seven initiatives to catalyze progress and support targets put forward by the European Commission. One of these initiatives establishes a digital agenda [33] aimed at accelerating the roll-out of broadband Internet in Europe. Thereby, broadband access should be made available for all citizens by 2013. By 2020, the aim is to deliver speeds of at least 30 Mbps for all citizens and reach 50% of the households subscribing to speeds above 100 Mbps. Each member state should develop and make operational its own national broadband plan by 2012, including the spectrum allocations needed to meet the target of 100% coverage of 30 Mbps by 2020. As economies of scale can be leveraged by using the same equipment and by offering the same services, the European Commission will harmonize spectrum bands where necessary.

Targeting at having Europe’s best broadband network by 2015, the British government also intends to release spectrum below 5 GHz over the next 10 years. Accordingly, 500 MHz should be released for new mobile communication uses. To meet this ambitious target, a first draft of plan was set out over-viewing public sector holdings, market demand, as well as the key next steps [34]. The draft classifies candidate bands as prioritized for release, subject to immediate investigation, or subject to posterior investigation. Spectrum below 1 GHz was left to posterior investigation despite the wide range of possible applications for these bands, *e.g.* business radio, terrestrial TV broadcasting, wireless broadband access, cognitive white space use, machine to machine communications (M2M), and utilities like smart metering and *smart grid*. The reason is that the U.K. government is expecting such applications to be accommodated using TV white spaces [35].

### 1.3 Determining White Spaces

As seen in the previous section, substantial regulation effort is being undertaken to facilitate white space exploitation. In well developed ICT societies, such as the U.S. and the U.K., white spaces are being already regarded as an effective means to accommodate the increasing bandwidth needs bring about by future wireless applications. This, *per se*, puts in place the motivation for the *bigger picture* goal of this dissertation, which involves the study of methods to determine white spaces. Therefore, in the first two parts of this section, we provide some background on the fundamental operation principles of GDA and spectrum sensing. Our emphasis is solely on GDA and spectrum sensing because, as seen in Section 1.2, the former is the method with the best chances of reaching the market first and the latter comes as the second most preferred by regulators. In the third and last part of this section, we present a high-level comparison between GDA and spectrum sensing. Rather than in the related work, the comparison established here is “unbiased” in the sense that we look at the detection capability and performance limiting factors of each method regardless of regulatory trends and political/commercial reasons.

Recalling that the investigation of potential white space use in frequency bands other than in the TV bands has been already directed in the U.S. [31], we denote CR-based unlicensed devices hereafter as *white space devices* (WSD). Instead of mere TVBD, whose operation is confined strictly to the TV bands, WSD can operate wherever underutilized

spectrum exists. Therefore, we think the use of WSD is more appropriate than TVBD to reflect the intrinsic flexibility of DSA devices and networks.

### 1.3.1 The GDA Method

GDA can be viewed as a kind of management system that assists WSD in selecting operational frequencies, thus eliminating the need for sensing the spectrum for licensed signals. Frequency selection is carried out on the basis of information on available frequencies associated with locations in the database and location information received from WSD [26]. Approaches based on GDA use RF propagation models to estimate the electromagnetic field strength received at the geographical location of WSD. Through this process, it is possible to determine a *protected contour* within which WSD are not allowed to transmit co-channel with the licensed system that should be granted protection. *Keep-out regions* determine the limits above which undesired field strengths at the protected contour exceed acceptable levels. In practice, keep-out regions are obtained by adding safety margins to the protected contour. So are specified the areas beyond which WSD can use white spaces without causing harmful interference to those licensed receivers operating at the edge of the protected contour [36].

A pictorial view of the GDA method is given in Figure 1.1, where the main tower in the middle plays the role of a licensed transmitter registered in the database. The peripheral systems placed outside the protected contour of radius  $d_P$  are GDA-capable WSD systems, each composed of a *base station* (BS) and multiple *customer premise equipments* (CPE). The margins  $d_B$  and  $d_C$  are added to protected contour  $d_P$  so that the resulting keep-out regions can accommodate specific transmission characteristics of BS and CPE, respectively, *e.g.* antenna height, front-to-back ratio, and transmit power. It is clear from

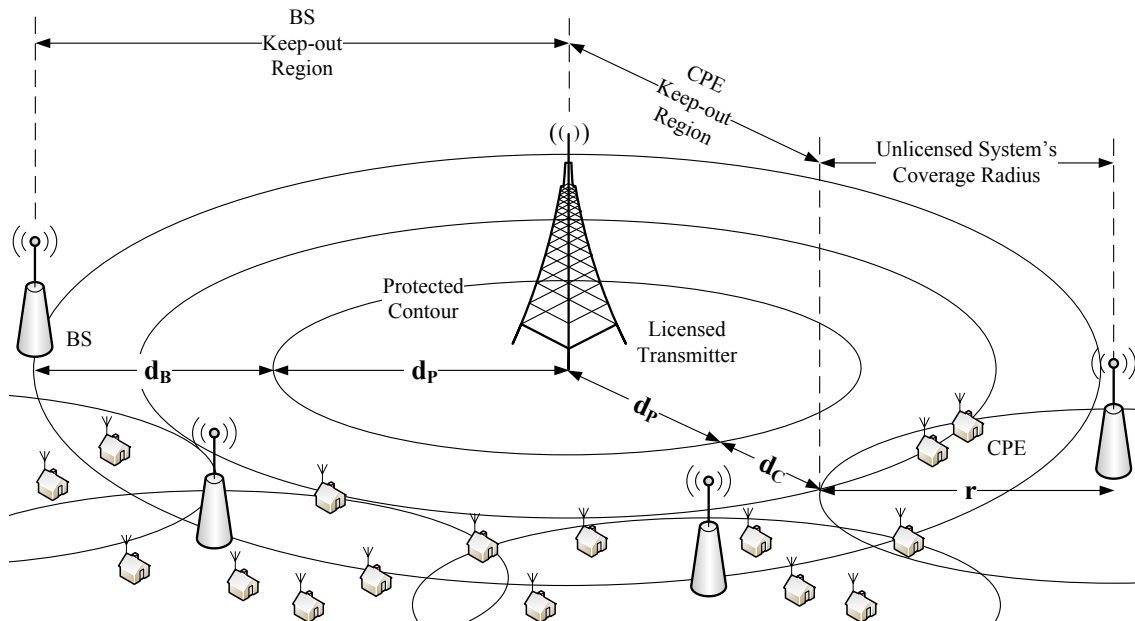


**Fig. 1.1:** The protected contour  $d_P$  adopted in GDA delimits the area within which WSD are prohibited to transmit co-channel with the licensed transmitter. Margins  $d_B$  and  $d_C$  are further required to keep undesired field strengths at the edge of the protected contour below acceptable levels.

the figure that protection to a given licensed system can only be granted as long as the operation details of that system are registered in the database. If this information contains errors, or cannot be known far in advance to be registered in the database, protection against harmful interference from WSD *cannot* be guaranteed using GDA.

Advance registration in the database is particularly difficult for itinerant *program making and special events* (PMSE) systems that are not at fixed locations and operate in intermittent, occasional, or one-time basis. To protect such use cases, the FCC and CEPT adopt different strategies: the former will reserve *safe harbor* channels where WSD are not allowed to operate [18], whereas the latter will allow both stationary and temporary sites to have their locations stored in the database [37]. However, if the number of transmitters operating simultaneously is too large to be accommodated in the safe harbor channels, PMSE will likely have to compete with WSD for unused frequencies. This will be the case of major sport contests or live theatrical productions that fail to register in the database. According to [38], this condition could be avoided by reserving more safe harbor channels in each location. The FCC decided not to reserve more spectrum to PMSE usage but continues to pursue the issues above in a pending proceeding, targeted at more efficient PMSE operation and improved immunity to interference.

Even in the case that the service to be protected has its operation details correctly and timely stored in the database, there exist other reservations about the use of GDA. Depending on the accuracy of RF propagation modeling, determination of white spaces by means of GDA may be imperfect. A *false alarm* occurs when a white space is overlooked, *i.e.* a channel that is actually idle is deemed to be occupied by mistake. A *missed detection* occurs if a channel actually occupied is misperceived as idle. False alarms and missed detections must be avoided to increase spectrum utilization and minimize harmful interference to (and from) licensed services, respectively. Since both errors are intrinsic to the process of determining white spaces by any practical method, false alarm rate (FAR) and missed detection rate (MDR) are the metrics typically used to characterize the accuracy with which WSD are able to identify white spaces.

The accuracies of four well known propagation models used in GDA are quantified in [39]. The FAR of the free space model, the simplest model analyzed, is higher than 90%. More complex, the Longley-Rice model considers a large set of parameters in the estimation of field strengths including climactic effects, soil conductivity, permittivity, Earth's curvature, and surface refractivity. Still, with FAR higher than 30%, the Longley-Rice model results in an unacceptably large white spaces loss. A major finding provided in [39] is that elevation data can greatly improve accuracy, *e.g.* the Longley-Rice model *with terrain* loses only about 8% of the available channels and gives zero MDR. This matches well the concerns about the complexity of GDA raised in [18] and [24], where the required efficiency is expected to call for highly sophisticated and computationally expensive signal propagation models.

In order to get instructed about white space availability, a WSD needs first to determine its own location and report it to the database. The database then estimates the frequencies available at that location and reports back to that WSD on which frequencies and with which power levels it can transmit at the indicated location<sup>1</sup>. This process gives rise to two issues discussed in the sequel: location determination and dissemination of location information.

---

<sup>1</sup> In the U.K., the Ofcom mandates the database to provide additional information, *e.g.* a notification about whether complementary sensing should be performed too [25].

### 1.3.1.1 Location Determination

The process of determining location of WSD has important implications in any GDA system because it involves establishing system parameters such as resolution, accuracy, and reliability. A possible approach to cope with resolution issues is to pick the BS location instead of the individual locations of its served CPE. In this case, the GDA method will allow WSD to use only those channels available in the BS's coverage area. This rather conservative approach avoids determining location on a too frequent basis (*e.g.* every time a new WSD has joined the unlicensed network or has moved in between two database updates) but results in a median white space loss above 80%. This means that GDA is largely dependent of the accuracy of the position determination carried out by WSD. In fact, it is shown in [39] that location errors ranging from 1.6 Km to 4 Km can yield white space losses from 20% to 80%. So, to be efficient, the GDA method imposes the need of CPE able to determine individual locations with error not larger than 800 m. However, as observed by the Ofcom [25] and the ECC [26], the required accuracy depends on the granularity used for coverage modeling, *i.e.* the size of the *pixel* used to represent a given geographical location. Each pixel is associated with a list of available frequencies and the pixel size depends on the planning decisions made when populating the database. Too large pixels prevent WSD from using an area larger than actually necessary to protect the licensed system, whereas too small pixels imply both larger number of computations at the database and larger amount of data to be transferred to and stored at WSD. Hence, depending on the pixel size and WSD location accuracy, the location uncertainty region may cover several pixels. Such complexity issues can be tackled using the concept of *location uncertainty*, whereby lower granularity grid points are assigned the minimum allowed transmit power within the location uncertainty region [11]. The transmit powers, to be minimized within this region, come from a higher granularity grid computed by the database. Since only lower granularity grids are sent to WSD, the approach reduces communication bandwidth and storage size at the expense of transmit power levels that decrease as the amount of location uncertainty increases.

The dependency of GDA on the performances of each individual WSD can be illustrated with an example. Assume that the database relies on a sophisticated propagation model to estimate the field strengths received in a certain geographical area. Assume further that this area is represented using a pixel size so small that the allowed transmit powers can be mapped onto a highly granular grid. In this setting, the excessive burden imposed on both database and individual WSD leads to efficient white space use only if each WSD can determine its position with accuracy compatible with the pixel size. Solutions to this problem are mostly based on over-the-air techniques, some of which have been assessed in the context of WSD in [40]. Accordingly, enhanced observed time difference (E-OTD) and methods based on the cell ID of a mobile phone caller need 4 s to 6 s to determine a location. Beside capable of providing very low latencies, solutions that rely on the cell ID are *network-centric* and, as such, impose no impact on the WSD design. As for the disadvantages, the use of the cell ID can yield location errors as large as the cell area, *e.g.* 150 m in a pico-cell or more than 30 Km in a large cell. E-OTD is fast too but, with errors in the range 40 – 400 m, it is in most cases not accurate enough to meet the  $\pm 50$  m requirement mandated by the FCC [18]. A position solution that is accurate to 5 – 20 m is the global positioning system (GPS). However, the use of GPS for WSD applications is made difficult due to its acquisition time of at least 30 s (up to 15 min), high power consumption, and low availability. Other issues arise as GPS cannot detect the

weak signals that result from small-sized antennas used in portable WSD and/or indoor use cases where availability of satellite signals is difficult to guarantee. These limitations can be overcome by using stronger signals from *other* networks to assist the GPS receiver [41]. In such assisted GPS (A-GPS), signals from mobile phone networks are used to allow accurate localization even in dense, urban, and indoor scenarios where plain GPS signals are attenuated by 20 dB. In another approach, known as TV-GPS [42], TV signals are used as an alternative to cellular signals. The higher transmit power, better penetration, frequency diversity, and larger bandwidth of TV signals allows TV-GPS to provide power margins up to 50 dB over plain GPS. Nevertheless, both A-GPS and TV-GPS introduce extra costs to WSD design and are useful only if the required signals are available in the area where the WSD of interest finds itself in.

### 1.3.1.2 Location Dissemination

It is evident from the discussion above that the performance of GDA is limited by the ability of each individual WSD in determining its position. Even in the case that WSD are accurate enough (relative to the pixel size), another performance limiting factor of GDA relates to how actual is the information exchanged between the databased and WSD. White space information made available via GDA to WSD suffers from two types of delays. The first delay type is introduced by the estimation of available frequencies, which may not reflect the current spectrum availability. Such delays are intrinsic to any GDA approach because the signal propagation models used in the estimation process do *not* measure the actual field strengths. The second delay type results from the time interval required by each WSD to get instructed about eventual changes in the sets of available frequencies and power levels allowed at its location. This may occur in a number of situations, *e.g.* a WSD has been activated from power-off condition, the database has been updated, or a WSD has moved from its last position reported to the database.

The frequency of database checks and re-checks raises concerns on database burden too, particularly in case of portable WSD. The challenge here is to find an update frequency that can balance between the different needs of licenced services and WSD. The FCC mandates WSD to poll the database (for updates) at least on a daily basis and everytime operation position changes by more than 100 m [18]. A second requirement implies adding a mobility margin to the keep-out region. This latter approach contributes to increased white space losses because it prohibits a WSD from using channels available at its current position but blocked off within the extended keep-out region required to handle mobility. This condition can be illustrated with an example, where a portable WSD is moving at, say, 100 km/h. If this WSD accurately determines its location and re-checks the database each and every minute, the required additional margin of 1.6 Km will result in a medium white space loss of 20% [39]. To prevent such loss, the Ofcom follows a different approach and requires the database to append an *area of validity* and a *time-validity stamp* to the information provided to WSD [25]. Following this additional information, a WSD must cease transmissions either if the time validity expires or if that WSD moves outside the area of validity.

White space losses introduced by the aforementioned mobility margins can be mitigated by programming WSD to poll the database at higher frequencies. Since this implies additional burden both to database and WSD, an alternative approach is to let the database push updates to WSD. Whether in poll- or push-based architectures, WSD need to provide

information to the database before having received any information from the database. Hence, a WSD that relies solely on GDA has no other means to determine spectrum availability prior to report its location to the database. Such “uninformed” transmissions have potential to generate harmful interference to licensed systems, so WSD should be prohibited to transmit in this case. In turn, without WSD location (or at least a location uncertainty region), GDA cannot feed the propagation model and the task of estimating available frequencies becomes impossible. Considering that a common channel, *e.g.* some sort of CPC, may not be available across the entire coverage area of the BS, beacon signals can be advanced to avoid the *bootstrapping* problem above [39]. However, in addition to the drawbacks of the beacon method discussed earlier in this section, this approach makes use of the BS position and thus may lead to inefficient usage of white spaces.

### 1.3.2 The Sensing Method

*Spectrum sensing* denotes the process whereby WSD detect and/or classify RF signals transmitted in a given channel or frequency band. The bottom line in the sensing process is that the sensing receivers used in WSD, hereafter referred to simply as WSD, pick up intended and unintended signals [1]. As unintended signals can drown out and mask intended signals, approaches based on sensing must ensure that WSD can properly distinguish the signals transmitted by licensed systems from those due to the noise ground and interference generated by other systems operating nearby. As we will see later in Chapter 2, such decision-making is accomplished via statistical hypothesis testing that basically consists of using a test criterion to compare a test statistic to a detection threshold. The test statistic depends on the signal processing technique used to sample the channel, whereas the detection threshold determines a WSD sensitivity, *i.e.* the weakest signal that WSD is able to detect. The test criteria applied to spectrum sensing are typically binary, composite, or sequential [12]. Since each test criterion relies on different assumptions, it is possible to optimize different aspects of the decision-making process, *e.g.* maximize detection rate for a given constant FAR (CFAR), minimize prior knowledge of unknown signal parameters, minimize number of samples required for detection, etc.

In contrast to GDA, spectrum sensing allows a WSD to determine white spaces by measuring the *actual* field strength within its sensitivity region. Though capable of operating without any reliance on propagation models, sensing-based WSD largely depend on the signal processing technique used to collect the channel samples. The choice of the signal processing technique constitutes a crucial step in the design of sensing approaches because it not only determines the test statistic but dictates the amount of prior information required for detection, *e.g.* knowledge about the structure of the signals to be detected, number of samples needed to produce a certain desired accuracy, computational complexity, etc. Depending on the signal processing technique used, spectrum sensing also can provide for signal classification ability, robustness against different RF impairments, among other advanced features useful for WSD applications.

Signal processing techniques for spectrum sensing can be grouped as follows. *Blind techniques* do not need to know anything about the signals to be detected. This minimum amount of prior information required for detection allows for flexibility in the sense that the same detector can be used to scan the spectrum for virtually any signal type. Blind techniques carry out detection irrespective to the signal type, so they are particularly suitable for operation scenarios where WSD operate collocated with multiple licensed

systems based on different standards. This, of course, as long as the desired performance levels can be met. *Semi-blind* techniques differ from their blind counterparts in the sense that they need to know the noise power in order to work. However, it is generally hard to distinguish between two different signals using techniques that are blind or semi-blind. In this case, it is advisable to use *signal specific techniques* that rely on the underlying features inherent to the structure of a certain signal type. Techniques that exploit specific features may fail entirely for a signal type other than the intended one. Even for the intended signal type, the performance obtained by using signal specific techniques may vary significantly depending on the parameterization of the signal *feature* used for detection. This is particularly true for licensed systems that dynamically select one among multiple transmission modes, each assigning different values to the feature (in order to fit different operation conditions) exploited in the detection process.

For a fixed operation bandwidth, it is straightforward that the *agility* of a signal processing technique also can be assessed in terms of the number of samples required for detection. Techniques that require less samples are thus faster than those that need more samples to give the same accuracy. Such techniques, which offer low sensing time requirements, are referred to as *fast techniques*. Blind and semi-blind techniques are usually classified as fast because they typically work based on a reduced number of samples, *e.g.* collected over a sensing time that corresponds to a single received symbol. Specific features may be spread through several symbols, so signal specific techniques are frequently referred to as *fine techniques*. In view of the fact that different signal processing techniques usually require different amounts of information to work, alternative criteria to compare different sensing techniques might be based on (i) the minimum amount of information that should be available a priori or (ii) arbitrarily setting the sensing time so as to guarantee that the number of samples collected is large enough.

In the sequel, we overview the state of art in spectrum sensing with respect to a number of aspects including its categories, the assumptions usually made and their corresponding implications, the performance limiting factors, and the issues arising in practical implementation. Similarly to what we have done for GDA, our goal here is to provide subsidies to the comparison that we will carry out later on in Section 1.4.

### 1.3.2.1 Single-band Spectrum Sensing

Sensing the spectrum for licensed signals is not always a hard task but it may become challenging depending on some technical limitations and regulatory assumptions that can be made during the rule making of WSD operation. In what follows, we will see that these limitations include the number of dimensions used to represent white spaces, the type of licensed device to be detected (receiver or transmitter), the bandwidth of the operation environment (narrowband or wideband), and the degree of standardization of licensed signals, to name some.

To begin with, we observe that the amount of underutilized spectrum that can be identified via sensing is largely affected by the signal dimensions used to represent white spaces. Assuming a bidimensional signal space, we define a *temporal white space* as a channel that is perceived as idle after a WSD has observed the channel for sufficient time, *i.e.* the signal processing technique has collected enough channel samples. Following this definition, temporal white spaces can be exploited regardless of WSD location. As shown in Figure 1.2, this extremely simplifies the sensing task because WSD can operate inside the coverage



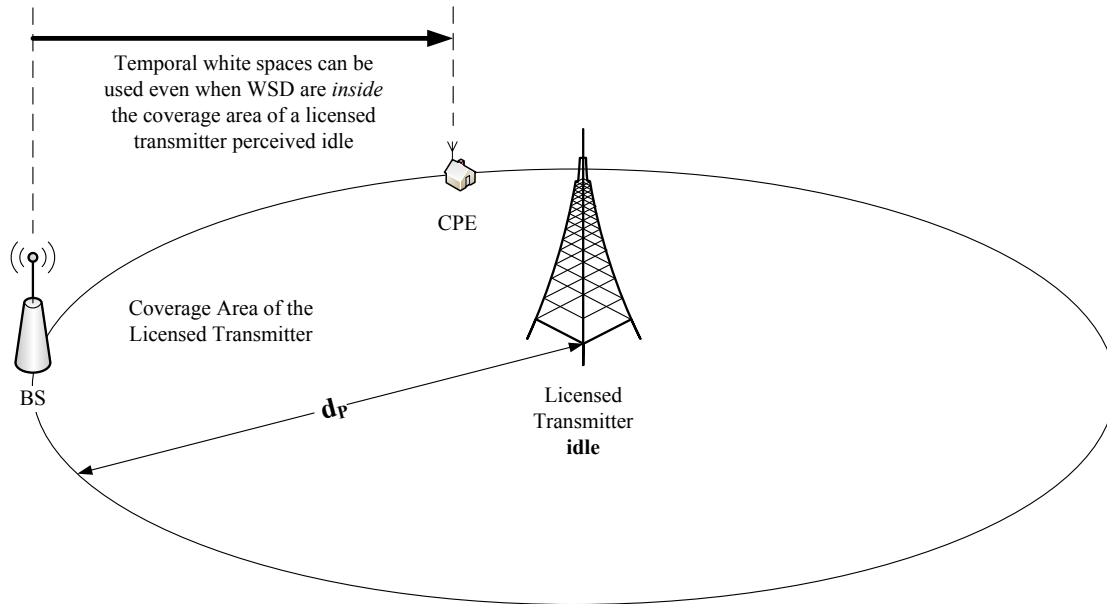


**Fig. 1.2:** As temporal white spaces are defined over a bidimensional signal space (time and frequency), the sensing task can be simplified by reducing the sensitivity requirement imposed on WSD to that of ordinary licensed receivers.

area<sup>2</sup> of the licensed system. The licensed signals captured by WSD are strong enough in this case, so temporal white spaces can be determined with sensitivity similar to that of ordinary licensed receivers and without placing any unnecessary computational burden on WSD [43]. Nevertheless, the notion of temporal white space fails to reflect the case of a channel occupied in a certain area but idle outside that area.

Defined over a three-dimensional signal space, *spatial white spaces* can be exploited to increase spectrum utilization, particularly when WSD operate outside the coverage area of the licensed system. Because of the inherent uncertainty about the location of licensed receivers, caused by their “passive” nature, it is commonly assumed that licensed receivers are much harder to detect than licensed transmitters [7]. Under this assumption, there is room for a condition to occur whereby WSD accurately detect the activity of a given licensed transmitter but generate interference to licensed receivers which operate on the coverage edge of that detected licensed transmitter. This worst-case condition, referred to as the *hidden terminal problem*, is examined in Figure 1.3. Required to avoid interference at licensed receivers, the protection margin  $d_S$  increases with the transmit power of WSD and decreases with the power margin factor of the licensed system. The power margin factor gives minimum conditions for a licensed receiver to successfully receive licensed signals under different RF impairments including path loss, shadowing, and multipath fading [43]. Though able to alleviate the hidden terminal problem, the protection margin  $d_S$  implies the need of a detection threshold low enough to maintain a larger sensitivity region with radius  $d_p + d_S$ . As with any method aimed at determining white spaces, prohibiting access to underutilized spectral regions that are larger than actually needed leads to increased white space losses.

<sup>2</sup> We think it is more suitable *not* to use the terms protected contour and coverage area interchangeably because (i) the corresponding radius of these areas need not necessarily be equal and (ii) the former is defined in the context of GDA, whereas the latter is typically used in spectrum sensing.

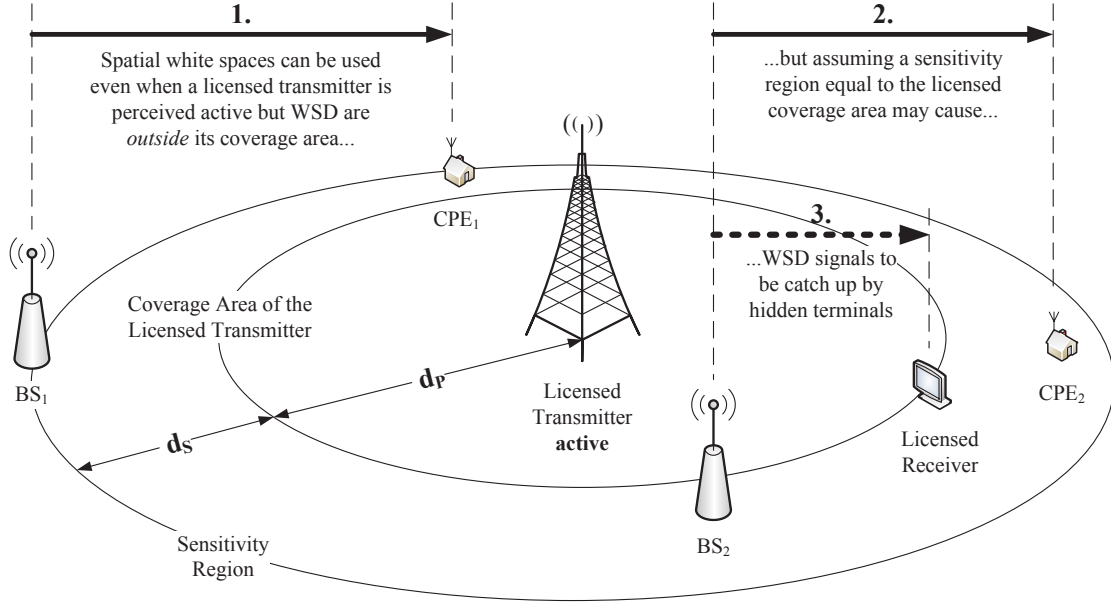


**Fig. 1.3:** Defined over a three-dimensional signal space (time, frequency, and space), spatial white spaces reveal more underutilized spectrum but bring about new challenges. For instance, by adding the margin  $d_s$  we can tackle the hidden terminal problem at the expense of increased sensitivity requirements.

*Macroscopic white space* is the term used to denote underutilized spectrum that implies the absence of active licensed transmitters in a large sensitivity region. Exploitation of macroscopic white spaces is characterized by a binary power mask that allows WSD to transmit with maximum power in the absence of licensed transmissions or not to transmit at all otherwise. In [44], a power/rate control and channel assignment optimization problem is formulated to exploit *microscopic white spaces* even when licensed and WSD systems are close to each other. The proposed algorithms rely on multi-level power masks that are set according to spatial variations in white space availability. Thereby, sensitivity regions can be made as small as the coverage area of the licensed transmitter. This eliminates potential white space losses caused by the introduction of the protection margins required to alleviate the hidden terminal problem.

As an alternative to eliminate protection margins, WSD can “look” at the reverse RF leakage emitted by heterodyne-type receivers. Present in both analog and digital receivers, RF leakages are due to local oscillator (LO) power that inevitably couples back through the input port and radiates out of the receiver antenna [45]. The received LO leakage is an unmodulated frequency tone, so it can be detected by using narrowband techniques. Apart from these benefits, one practical issue raised by receiver detection is the error introduced by the variability of the LO leakage power level, *e.g.*  $-30$  dBm to  $-90$  dBm for analog receivers [45] and  $-72$  dBm to  $-90$  dBm for digital receivers [46]. In either case, these high variable power levels make it difficult for practical WSD to detect LO leakages. Also, the approaches in [45] and [46] have limited applicability (short-range communications only) and need prior knowledge of the receiver’s intermediate frequency (IF). Specifically, the approach in [46] is based on a sophisticated signal processing technique that is onerous to WSD implementation.

Sensing algorithms are tailored to detect the presence of licensed signals over a pre-determined signal space. Though the utilization of other signal dimensions, such as the

code dimension, may not be straightforward, multi-dimensional awareness has potential to allow more efficient spectrum utilization [47]. This, however, may come at the expense of larger sensitivity regions that require more sophisticated signal processing and additional computational complexity.

### 1.3.2.2 Multi-band, Multi-resolution, and Wideband Spectrum Sensing

One may believe at this point that all the “pains” of the sensing process are caused by the number of dimensions over which white spaces are defined, and by the need to transform the problem of detecting licensed receivers in that of detecting licensed transmitters [7]. In fact, this is not the case as the hidden terminal problem can be caused by other factors that include severe multipath fading and shadowing [47]. To protect potential hidden terminals, regulators mandate stringent protection margins that typically translate into sensitivities below the noise floor [18][23][26]. Along with such physical limitations and regulatory requirements, the opportunistic nature of DSA networks may require sensing-based WSD to scan several GHz of spectrum to find white spaces.

The simplest way to tackle the latter problem is to break wide operation bandwidths into multiple non-overlapping subbands. Known as *multi-band spectrum sensing* (MBSS), this method allows WSD to sense the resulting subbands using more simple narrowband signal processing techniques. Subbands are sensed one at a time, so some degradation in agility is expected when determining white spaces via MBSS. To minimize the detection delay, which is a performance-critical factor in DSA, it is preferable to sense multiple bands in parallel [48]. At the RF front-end, MBSS can rely on either tunable narrowband bandpass filters (BPF) or digital windowing techniques, *e.g.* based on the fast Fourier transform (FFT). Analog solutions lack on flexibility because they require bulky filter banks [52], whereas digital solutions imply extremely high rates that are difficult to implement in practice. The Nyquist sampling theorem can be satisfied by high-resolution high-speed analog-to-digital converters (ADC), but the cost and power consumption burdens on a hardware design having such requirements are likely prohibitive for most WSD applications [53]. As another drawback, the finite length of the FFT window may cause digital domain filtering to suffer from energy leakages that lead to degraded FAR [54]. Whether implemented in analog or digital domain, MBSS usually assumes independent and identically distributed (i.i.d.) noise samples that require ideal filter design [49]. This is difficult to achieve in practice, so the required robustness against narrowband noise is usually provided at the expense of additional filters. See, *e.g.* [50] and [51] for applications of interference alleviating filters and prewhitening filters in the context of WSD.

Recent advances in information theory demonstrate that signal sparsity allows the exact recovery of signals sampled at sub-Nyquist rates [55][56]. Such *compressive sensing* sets a fixed sampling rate according to the maximum sparsity order of the underutilized spectrum. As this information is subject to temporal and spatial variations, better reduction of acquisition costs can be achieved with techniques that estimate the actual sparsity order and are thus able to adaptively minimize the sampling rates used [57]. Algorithms based on matrix completion and joint sparsity recovery seem also capable of providing effective solutions [58]. However, concerning the practical implementation of compressive sensing, efforts are still underway to catch up experimentation with theory. An example of what is being done in this sense can be found in [59], which presents a new compressive sensor that does not require a high-speed clock anywhere in the sensing path.

*Multi-resolution spectrum sensing* (MRSS) is similar to compressive sensing in the sense that it can be implemented using low-power hardware. MRSS is a digitally-assisted analog technique that needs no analog filter in the RF signal path [60]. In MRSS, the received signals are correlated with a window signal generated in the digital domain and subsequently sampled using a low-bandwidth ADC. This allows to flexibility in bandwidth adjustment (not available in purely analog approaches) and relaxed requirements on power consumption (not available in purely digital approaches). As for the shortcomings of MRSS, all of which are common to MBSS, joint decisions over multiple frequency bands are not considered and the frequency allocation plan of the licensed system is required for detection. The first disadvantage is specially critical when the available white spaces are spread over several non-contiguous bands. Joint decisions on the spectrum availability made across these bands could maximize the aggregate opportunistic throughput [52][61]. The second disadvantage relates to the need of using other means to obtain additional information about the operation center frequencies and bandwidths (in some cases not available in practice) prior to the application of MBSS or MRSS.

In fact, MBSS and MRSS are special cases of a more abrangent concept denoted *wideband spectrum sensing* (WSS). In contrast to single-band, multi-band, and multi-resolution methods, whose performance can be characterized in terms of FAR and MDR only, WSS approaches depend on other types of errors. These errors may include the notions of sub-carrier occupancy error rate, band occupancy error, and wideband spectral error discussed in [62]. Notwithstanding its *channel bonding* ability, *i.e.* to transmit over non-contiguous white spaces, WSS still needs substantial research to become practical. For a survey on WSS and its open research issues, see, *e.g.* [49] and the references therein.

### 1.3.2.3 Cooperative Spectrum Sensing

So far in this section, we have discussed spectrum sensing from the perspective of an individual WSD. Thereby, white spaces are determined locally in a standalone fashion. Type and color of the noise process, shadowing, fading, location of the licensed system, and limited detection capability constitute some sources of *uncertainty* that make it difficult for a single WSD to detect weak licensed signals attenuated by bad channel conditions. A well investigated remedy to this fundamental problem is *diversity*. If copies of a signal are conveyed (or received) over multiple physical channels, the risk that all channels simultaneously experience shadowing or fading can be dramatically reduced [63]. The higher the number of channels the more probable will be the accurate detection of at least one of the copies. Reception at different locations makes independently faded copies of the signal available at WSD, thus generating a kind of *spatial diversity*. Whether obtained on the transmitter or receiver side, diversity usually requires devices equipped with more than one antenna. Multi-antenna techniques are power-hungry, costly, and complex, so that they are more advantageous for some applications than for others. In particular, the distance among antennas required to guarantee channel independence may make the use of multiple antennas impractical for mobile devices, *e.g.* in case of portable WSD that are limited by size and/or hardware complexity.

Techniques that “mimic” antenna arrays can be employed to obtain diversity under the above restrictions. One such technique is *cooperative spectrum sensing* (CSS), whereby multiple spatially distributed WSD share their individual antennas to form a virtual multi-antenna array. The increase in reliability obtained by instructing multiple WSD, referred

to as *nodes* in the context of CSS, to scan the *same* channel can significantly mitigate the hidden terminal problem [64]. When directed to scan *different* channels, multiple nodes can alternatively “team up” to reduce detection delays or to scan wideband operation environments without the need of WSS [52]. In either case, CSS has been regarded in the literature as a promising approach to maintain a high global performance with relaxed requirements on individual nodes. Most of the issues arising in local spectrum sensing can be thus resolved through cooperation. However, to obtain a more accurate picture of the current spectrum occupancy, CSS needs to exchange and posteriorly combine the sensing information acquired locally by each WSD engaged in cooperation. While the processes of information acquisition, information exchange, and information fusion are essential to any CSS scheme, each of them is composed of elements for which different *design options* can be selected. A pictorial description of CSS is provided in Figure 1.4, where each information process is represented as a “folder” containing several “boxes”. Each box accounts to an element for which design options, shown in the figure as floating text, can be selected to address different system needs. The boxes inside the information acquisition folder have already been described earlier in this section. Hence, in what follows our emphasis is put on the processes of information exchange and information fusion.

In the information exchange process, the *cooperation scheme* dictates how node interaction takes place [12][43]. As this has implications in agility, power consumption, and robustness, the scheme used exerts preponderant influence in the performance achievable in CSS. *Centralized architectures* are managed by some kind of master node, which is usually the only entity able to make decisions. When implementing centralized CSS in centralized networks, it is natural to let the BS act as master node. In this case, besides typical control tasks, the BS sends enabling signals to instruct its served CPE about which channel to sense, when to sense, and for how long to sense. *Distributed architectures* are characterized by the lack of a central entity. All nodes communicate among themselves and decisions are made on a local basis. As long as some consensus can be ensured by using algorithms that avoid selfish node behavior, it seems natural to implement distributed CSS in distributed networks. Alternatively, at the expense of increased node complexity, centralized CSS lends itself also to distributed networks. In this case, any ordinary node playing the role of the master node can coordinate the tasks of sensing and information fusion.

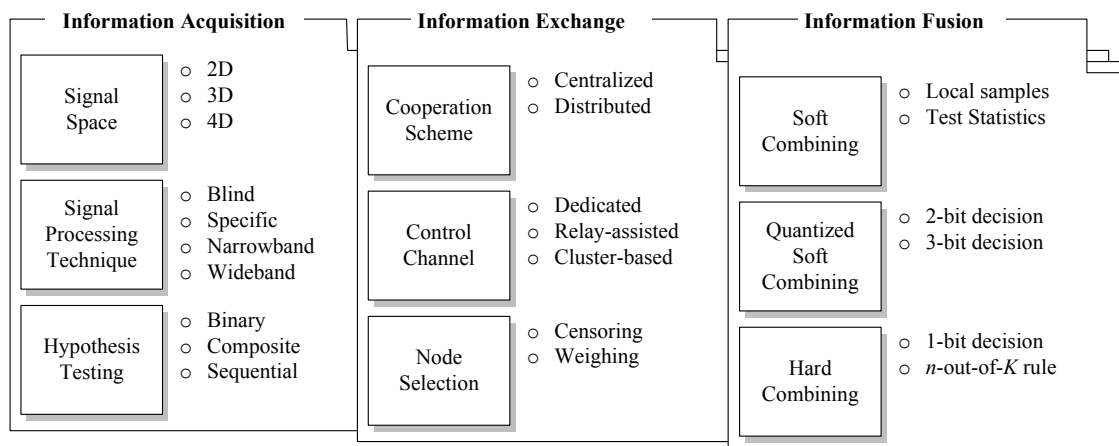


**Fig. 1.4:** A pictorial description of CSS. “Folders” depict information processes common to any CSS scheme. “Boxes” correspond to elements for which design options, shown as floating text, can be selected to address different system needs.

Both centralized and distributed architectures require a bidirectional *control channel*. The master node broadcasts control signals in the downlink whereas ordinary nodes send local information back to the master in the uplink. On the one hand, we have seen in Section 1.2 that approaches requiring licensed (or at least harmonized) spectrum for signalling and control tasks are typically less supported by regulators. On the other hand, establishing a point-to-point link between each ordinary node and the master node becomes challenging on an unlicensed basis [12]. In this context, *dedicated solutions* are not applicable because control channels have to be dynamically allocated according to the white space availability. Also, like any wireless channel, control channels over white spaces will also be susceptible to RF impairments. Hence, the gains achieved via CSS will be limited in practice by errors that occur when local information is exchanged over imperfect control channels [65].

Originally proposed to increase transmission rates, maximize spatial reusability, and enlarge coverage range in various types of networks (see [66] and references therein), *relay nodes* are used in CSS to increase the reliability of the information exchange process. The bottom line in relaying is to let those nodes assigned a bad control channel forward their local information to their neighbors. Among the neighbors, the node with the best path towards the master node serves as relay node. Increased accuracy can be obtained by pairing the nodes such that the “stronger” node in each pair acts as relay for the “weaker” one. In case of *amplify-and-forward* relaying, CSS is known to reduce detection delays but this agility gain largely depends on the power level received at the relay nodes, and on the power they use to retransmit the received signals [67]. As another advantage, spatial white spaces can be exploited also in the direction dimension by forming a distributed zero-forcing beamformer of relay nodes. If combined with rateless coding, such *cooperative beamforming* can efficiently exploit discontinuous white spaces while keeping complexity at acceptably low levels [68]. Reliable exchange of information can also be achieved in CSS by grouping cooperating nodes in *clusters*. A node selected to act as cluster head (CH) can play the role of relay node or accumulate functions of both relay node and master node. In relay mode, cluster-based CSS can reduce errors introduced by the report of local information over faded control channels [69]. As in relay-assisted CSS, the premise for this to work is that CH have control channel gains larger than the ordinary nodes in the cluster. A CH operating in master mode is responsible for combining local information collected in its cluster and for forwarding these findings to other CH, so network-wide decisions on white space availability can be made. In general, regardless of how the control channel is implemented, practical channels used to this end typically have limited bandwidth. This constitutes a problem in the implementation of CSS, particularly when the number of nodes is large.

While being an optional element in the information exchange process, *node selection* can address the above issues by *censoring* unreliable nodes. A simple censoring approach for narrowband CSS schemes that rely on binary hypothesis testing and hard combining consists of using *two* detection thresholds. Reliable nodes, allowed to report their local information to the master node, are those nodes whose test statistics lie below the smallest threshold and above the largest threshold. If the test statistic lies in the region between the two thresholds, the node is classified as unreliable and prohibited to report its findings to the master node. This approach decreases the average number of bits sent to the master node, over both perfect and imperfect reporting channels, with little performance loss in comparison to the case where any censoring scheme is employed [70]. One aspect to keep in mind is that the optimization of individual thresholds (not necessarily equal) is a hard task [71] that becomes harder when multiple thresholds need to be set for each single

node. Provided that the nodes are well synchronized, censoring can also be performed by allowing a node to gain (or lose) confidence whenever its decision matches (or not) the global consensus and prohibiting low-confidence nodes to report [72]. Another alternative, suitable for performance critical applications where concerns about the bandwidth of the control channel may be milder, is to distinguish reliable nodes from unreliable nodes by assigning different *weights* to the summary statistics. If the weight coefficients are selected so as to represent the impact of each individual contribution to the global decision, the aggregate opportunistic throughput of the unlicensed network can be maximized. Optimum weight assignments can be obtained along the lines used in [52], where a linear combination of summary statistics is proposed for narrowband CSS and then extended to more sophisticated MBSS and WSS cases.

It is evident from the discussion above that CSS can achieve different levels of performance depending on the format (data or decision), precision (infinite or finite), and size (raw sensing data, multi-bit decisions, or one-bit decisions) of the local information available at the master node. In *soft combining*, each node reports with infinite precision by sending either its entire set of collected samples or a summary of test statistics. Though larger amounts of sensing information allow to achieve a certain detection performance using less nodes [73], this imposes large sensing overheads to the information exchange process. Therefore, practical implementation of CSS requires a balance between amount of information exchanged and number of nodes. The motivation for *quantized soft combining*, where raw sensing data is represented with less precision, is that simple messages are better suitable for energy-constrained systems. Despite of the additional noise introduced by quantization, two or three bits can be employed in most cases without noticeable performance loss. Though this makes it easier to convey local information over practical bandwidth-limited report channels, the performance of quantized soft combining still requires tight synchronization among nodes. If frequency offsets cannot be avoided, sensing overheads can be cut down by using one-bit decisions. As this minimum bandwidth requirement is achieved at the expense of virtually any performance degradation [64], *hard combining* becomes an interesting solution under bandwidth and synchronization constraints. In contrast to the complex algorithms required in soft combining, hard combining is simple to implement using sub-optimum fusion rules. One well known example of such rules is the  $k$ -out-of- $N$  rule, which has AND logic ( $k = 1$ ), majority logic ( $k \geq N/2$ ), and OR logic ( $k = N$ ) as special cases.

Other performance limiting factors of CSS relate to the *operation environment* where all information processes in Figure 1.4 take place. For CSS to obtain diversity, the nodes must be *spread* throughout a *cooperation footprint* [64]. Otherwise, correlated shadowing will hinder the contributions of nodes placed physically close to one another from improving the global performance achievable through cooperation [74]. The master node could drop those contributions found to be correlated before fusion but this is not efficient in the sense that energy would have already been wasted to report “useless” information. Node mobility constitutes another big issue because it makes the required node density more difficult to maintain. For instance, allowing the nodes to move in a cluster-based setting may cause the node density to vary over time inside each cluster. In this case, each CH has to be concerned about minimizing the probability of assigning sensing tasks to nodes that are not currently associated with its cluster [75]. In fact, ensuring detection within a certain cooperation footprint depends not only on the number of nodes but also on their sensitivity and position. These are well-known issues in *wireless sensor networks* (WSN), where the nodes have small batteries of finite energy and follow some wake-up

cycle to extend the network lifetime. If wake-up cycles are scheduled so as to minimize the areas covered by multiple active nodes, the number of nodes required by a deterministic node placement is one order of magnitude lower than by scattering them randomly [76]. While this gain is a decreasing function of the fraction of time during which the nodes are powered on, the distribution of active and sleeping times does not affect detection delays significantly. In fixed WSN, the node density required to assist a set of “passive” WSD, *i.e.* neither sensing capable nor allowed to engage in CSS, is known to be reasonable [77]. Also, at the expense of additional control signalling and tighter synchronization requirements, some room for improvement can be envisioned by allowing sensing-capable WSD within the coverage range of the WSN to contribute their local findings.

## 1.4 Comparing Coexistence Methods

In this two-part section, we establish a high-level comparison between GDA and spectrum sensing. The first part of the section capitalizes on the previous section to compare GDA and spectrum sensing from a purely technical perspective, whereas the second one introduces non-technical concerns that are important to allow white space use in developing countries too. Ensuring universal access to white spaces constitutes a task of utmost importance to optimize usage of RF spectrum, particularly in the developing world where WSD and applications based thereon can hopefully leverage the ITU’s broadband strategies aimed at speeding up ICT progress.

### 1.4.1 Technical Aspects

GDA and spectrum sensing rely on different principles to determine white spaces. Each principle has its advantages but also drawbacks that give rise to different implementation issues. Hence, even when we look at one of these methods in isolation, the performance achievable by a certain implementation can largely vary depending on a number of performance limiting factors. For the discussion that follows, we provide in Table 1.1 a “quick-reference” guide that summarizes the major issues and performance limiting factors discussed in Section 1.3.

As seen in Table 1.1, the resulting performance achieved by using either method depends on a series of parameters and settings that are implementation dependent. This makes it difficult to draw conclusions without making assumptions on the underlying specifications related to how each method is implemented. One possible way to establish a high-level comparison, perhaps the only one available in the literature at the time of this writing, is to represent the sensitivity requirements adopted in spectrum sensing in terms of the keep-out regions used in GDA [11]. In this fashion, both methods can be analyzed on the basis of field strengths as illustrated in Table 1.2 [78]. On the one hand, considering that GDA and spectrum sensing require keep-out regions 12% and 74% larger than the protected contour, respectively, it seems natural to argue that this discrepancy reflects the extent to which the former is more efficient than the latter [11]. On the other hand, the received power level may fall down far below the mandatory sensitivity level before the pictures observed at a TV receiver start to degrade [23]. Thus, TV receivers operating well beyond the protected contour can be protected by spectrum sensing but *not* by GDA. The FCC seems to misinterpret this fact in [22], where it classifies *any* detection outside



**Table 1.1:** Performance limiting factors of GDA and spectrum sensing.

| Method                        |                         | Issue                      | Limited/dictated by       | Ref.                        |
|-------------------------------|-------------------------|----------------------------|---------------------------|-----------------------------|
| GDA                           | Information acquisition | • Signal propagation model | [6][39]                   |                             |
|                               |                         |                            | • Location dimension      | [39]                        |
|                               |                         | Location determination     | • Resolution (pixel size) | [6][25][26]                 |
|                               | • Location accuracy     |                            | [40][41][42]              |                             |
|                               | • Location reliability  |                            | [11]                      |                             |
|                               | Location dissemination  | • Update frequency         | [18]                      |                             |
|                               |                         | • Mobility margins         | [25][39]                  |                             |
|                               |                         | • Bootstrapping            | [39]                      |                             |
|                               | Spectrum Sensing        | Narrowband                 | Information acquisition   | • Signal space dimension    |
| • Signal processing technique |                         |                            |                           | [12][43]                    |
| • Hypothesis testing          |                         |                            |                           | [12]                        |
| Wideband                      |                         | Subband division           | • BPF design              | [48][49]                    |
|                               |                         |                            | • Windowing technique     | [54]                        |
|                               |                         | Power consumption          | • ADC resolution          | [53]                        |
|                               |                         | Sampling rates             |                           | • Sparsity order estimation |
| Cooperative                   |                         | Operation environment      | • Cooperation footprint   | [12][64]                    |
|                               |                         |                            | • Node spread (diversity) | [64][76]                    |
|                               |                         |                            | • Node density (mobility) | [75][77]                    |
|                               |                         | Information exchange       | • Cooperation scheme      | [43][67][69]                |
|                               |                         |                            | • Control channel         | [65]                        |
|                               |                         |                            | • Node selection          | [70][72]                    |
|                               |                         | Information fusion         | • Decision format         | [12][73]                    |
|                               |                         |                            | • Decision precision      |                             |
| • Decision size               | [12][64]                |                            |                           |                             |
| • Fusion rule                 |                         |                            |                           |                             |

the protected contour as a false alarm. As observed in [78], *some* of these detections may have been true detections as long as the prototype testing was conducted outside the protected contour but inside the keep-out region.

Though capable of providing a rough picture of how efficiently GDA and spectrum sensing can protect licensed services, the above approach entirely fails to capture the performance dependencies shown in Table 1.1. The methodology used to set the field strengths, taken as basis in the comparison, raises fairness concerns too. The field strengths of GDA are predicted using the statistical ITU model [79], whereas those reflecting the sensitivity of spectrum sensing are computed in terms of mandatory protection requirements. Recently, a comparison between the Longley-Rice model with terrain and the ITU model has revealed that the former leads to larger local variability than the latter but the amount of white spaces detected is in average *similar* for both models [6]. This means that both [11] and [78] consider a GDA approach relying on one of the *most* efficient propagation models available. In contrast, they evaluate spectrum sensing based on the mandatory sensitivity rather than on its *actual* capabilities.

Other evidences that there has always been some inclination in favouring GDA can be found in the literature, *e.g.* the issues raised by the processes of determining location and of disseminating such information are usually ignored. In contrast, spectrum sensing is analyzed from a perspective that highlights all those issues that a standalone WSD might experience. As seen in Section 1.3, such local issues can be solved (or at least largely

**Table 1.2:** Exemplary keep-out regions of GDA and spectrum sensing [78].

| Type                    | Minimum field strength (dBu) | Distance (Km) |
|-------------------------|------------------------------|---------------|
| Protected contour       | 41                           | 125           |
| GDA keep-out region     | 36                           | 131           |
| Sensing keep-out region | 19                           | 218           |

alleviated) by enforcing node cooperation. An attempt to address this gap for the case of distributed CSS is provided in [80]. The message left is that even high-level conclusions are hard to draw without picking a specific implementation of each method.

At the time we started working on coexistence methods for WSD applications, a question that arose was whether we should go with GDA or spectrum sensing in this dissertation. The trivial answer to this fundamental question could be “pick the method that can *best* determine white spaces”. However, as seen above, the notion of best is implementation dependent in this case, so none of the contributions available in the literature could provide us with a clear path to follow. To overcome this limitation, we recall that the amount of available white spaces is likely as dependent of the cardinality of the signal space as on the method used to determine white spaces. So, if high-level comparisons are unavoidable, it seems more appropriate to compare GDA and spectrum sensing on the basis of the *same* number of signal space dimensions. In Table 1.3, we classify a GDA approach as “typical” or “advanced” according to its ability to process additional location information, *e.g.* terrain information. Spectrum sensing approaches are classified according to their capabilities of achieving reliable detection over a given signal space. “Local” sensing can exploit temporal white spaces only, while “cooperative” approaches additionally exploit spatial and microscopic white spaces. Approaches that rely on cooperative beamforming to exploit directional white spaces are denoted as “advanced” sensing. Using Table 1.3 it is possible to perform high-level comparisons where GDA and spectrum sensing are more likely to stand on equal footing. Low-level assessment is of course more laborious but it has the advantage of taking into account the *actual* capabilities of each method. In either case, the most important aspect here is that there is not *any* fair baseline based on which GDA and local sensing can be compared.

In general, *any* method aimed at *efficiently* determining white spaces will have its advantages but will also bring about practical implementation challenges. This is due to the fact that coexistence in DSA networks encompasses non trivial tasks that need to be implemented to simultaneously commit to antagonistic goals. Of utmost importance among these goals are the maximization of the overall system performance (accuracy, agility, reli-

**Table 1.3:** White space detection capabilities of GDA and spectrum sensing.

| Signal Space | GDA     |          | Spectrum Sensing |             |          |
|--------------|---------|----------|------------------|-------------|----------|
|              | Typical | Advanced | Local            | Cooperative | Advanced |
| 2D           | •       | •        | •                | •           | •        |
| 3D           | •       | •        |                  | •           | •        |
| 4D           |         | •        |                  |             | •        |

ability, and robustness) and the minimization of system costs (computational complexity, bandwidth requirements, and power consumption). CSS solves some local detection problems but the processes of information exchange and information fusion introduced thereby impose additional requirements. Nevertheless, most issues arising in CSS can be tackled at the *network level* thus reducing cost, power, and computational burdens imposed to individual WSD. In contrast, the treatment of two out of three systemic issues associated to the implementation of GDA is limited by the way individual WSD are designed.

## 1.4.2 Non-technical Aspects

It turns out from Section 1.2 that the regulatory efforts to promote DSA are being led virtually by developed countries only. To minimize unnecessary work, the FCC and CEPT have been collaborating, an effort that has its value as it allows to some harmonization between the solutions adopted in the U.S. and Europe. In this process, one aspect that seems to have been overlooked is whether such solutions fit developing markets too. Precarious infrastructure, low household income, and low education are typical issues of developing markets that impose additional requirements on the adoption of new technologies. At a first glance, the goals of spectrum management should be broadly the same in both developed and developing countries – regardless of the existence of differentiating factors between these environments [81].

### 1.4.2.1 The Digital Divide

Before elaborating on the statement made in [81], let us look at some recent trends that are shaping ICT market developments. We begin examining the latest values of the *ICT development index* (IDI). IDI accounts to a composite indicator used by the ITU to track ICT progress with respect to readiness (level of networked infrastructure and access), intensity (level of use), and impact (resulting from efficient use) [82][83]. The current indicators embedded in the IDI are fixed telephony, mobile telephony, international Internet bandwidth, households with computers, and households with Internet (for readiness); Internet users, fixed broadband, and mobile broadband (for intensity); adult literacy and gross secondary and tertiary enrolment (for impact).

Notwithstanding the overall improvement in the IDI observed in the recent years, Table 1.4 reveals disparities in both intra- and inter-regional levels. In the intra-regional level, we represent such disparities as *gaps* resulting from the deduction of the lowest IDI from the highest one. The increasing gaps, exhibited from 2002 to 2010 in Africa, Asia & Pacific, and Commonwealth of Independent States (CIS), suggest that high ranked countries are improving more than low ranked countries in these regions. This is a global tendency until the Arab States, Europe, and the Americas showed gap decreases of 0.05, 0.12, and 0.41, respectively, from 2008 to 2010. In the inter-regional level, Europe is the benchmark because it is the world’s leading region in ICT infrastructure and services uptake. Considering the best ranked country in each region, we see that Asia & Pacific, the Arab States, and CIS improved 0.32, 0.60, and 0.43 more than Europe, while Africa and the Americas improved 0.81 and 0.33 less than Europe. With gaps as large as 0.35 in the Americas and 1.30 in Africa, all regions improved less than Europe in terms of the worst ranked country in each region. *Digital divide* is the term used to denote these gaps [84].

**Table 1.4:** Evolution of the IDI by Region (adapted from [82] and [83]).

| IDI  |     | A    | B    | C    | D    | E    | F    |
|------|-----|------|------|------|------|------|------|
| 2002 | max | 2.57 | 5.84 | 3.36 | 2.71 | 5.99 | 5.18 |
|      | min | 0.52 | 0.99 | 1.07 | 1.77 | 2.00 | 1.05 |
|      | gap | 2.05 | 4.85 | 2.29 | 0.94 | 3.99 | 4.13 |
| 2007 | max | 3.44 | 7.23 | 5.20 | 4.13 | 7.27 | 6.33 |
|      | min | 0.73 | 1.06 | 1.41 | 2.11 | 2.74 | 1.29 |
|      | gap | 2.71 | 6.18 | 3.80 | 2.02 | 4.54 | 5.04 |
| 2008 | max | 3.64 | 7.68 | 6.11 | 4.54 | 7.85 | 6.54 |
|      | min | 0.79 | 1.08 | 1.46 | 2.25 | 3.12 | 1.35 |
|      | gap | 2.85 | 6.60 | 4.66 | 2.29 | 4.73 | 5.19 |
| 2010 | max | 4.00 | 8.40 | 6.19 | 5.38 | 8.23 | 7.09 |
|      | min | 0.83 | 1.38 | 1.58 | 2.50 | 3.61 | 2.31 |
|      | gap | 3.16 | 7.02 | 4.61 | 2.88 | 4.61 | 4.78 |

A: Africa, B: Asia & Pacific, C: Arab States,  
D: CIS, E: Europe, F: The Americas.

Whether between developed and developing countries or within a single region or country, digital divides are typically characterized in terms of aspects such as penetration rates, mobile cellular subscriptions, Internet users, and personal computers. Table 1.5 illustrates the digital divide observed in 2010 in terms of service penetration per 100 Inhabitants. Taken in isolation, any of these indicators fails to reflect the big picture of the digital divide. This explains why the IDI has been advanced as a more powerful tool. Revisiting Table 1.4 from this perspective suggests that the digital divide between developed and developing countries is *increasing* on a global basis and, in some cases, on a regional basis too. The ITU adds that the cost of ICT services constitutes a main barrier to their uptake because it influences or even determines their use. Between 2008 and 2009, an average price fall of 42% was verified for fixed broadband services, the largest one if compared to mobile cellular (25%) and fixed telephony (20%) [82]. However, as shown in Table 1.6 as a percentage of the average monthly gross national income (GNI) per capita, mobile cellular prices increased on a global basis from 2009 to 2010. This condition is particularly alarming in Africa, where penetration rates are still quite low in some countries. Also, substantial variations in the average broadband prices still exist across regions. These disparities in relative costs per region indicate that much more of the household income has to be spent in developing countries (unaffordable 112%) than in developed countries (1.5%) [83].

In view of these facts, we *partially* agree with the statement in [81] that developed and developing countries have the same spectrum management goals. On the one hand, the underlying principles used to establish, leverage, and maintain flexible and efficient spectrum management systems may eventually be the same in both environments. On the

**Table 1.5:** Service penetration per 100 inhabitants in 2010 (adapted from [83]).

| Service         | Developing Countries | Developed Countries |
|-----------------|----------------------|---------------------|
| Mobile Cellular | 70.1                 | 114.2               |
| Internet        | 21.1                 | 68.8                |
| Fixed Broadband | 4.2                  | 23.6                |

**Table 1.6:** Evolution of the service affordability by region (adapted from [82] and [83]).

| Service         |      | A     | B    | C    | D    | E   | F    | G   | H     |
|-----------------|------|-------|------|------|------|-----|------|-----|-------|
| Fixed Telephony | 2009 | 17.4  | 3.6  | 4.0  | 1.3  | 1.3 | 2.9  | 1.2 | 7.7   |
|                 | 2010 | 17.0  | 3.8  | 4.4  | 1.1  | 1.1 | 3.1  | 1.1 | 7.8   |
| Mobile Cellular | 2009 | 17.7  | 3.0  | 4.7  | 2.7  | 1.1 | 3.0  | 1.2 | 7.5   |
|                 | 2010 | 24.6  | 4.6  | 7.4  | 4.1  | 1.6 | 5.1  | 2.0 | 11.4  |
| Fixed Broadband | 2009 | 482.8 | 46.0 | 71.0 | 10.4 | 1.8 | 10.1 | 2.0 | 173.9 |
|                 | 2010 | 291.3 | 27.3 | 52.6 | 7.3  | 1.4 | 22.4 | 1.5 | 112.2 |

A: Africa, B: Asia & Pacific, C: Arab States, D: CIS, E: Europe,  
F: The Americas, G: Developed Countries, H: Developing Countries.

other hand, from Tables 1.4-1.6, it is evident that the rule making for white spaces should not neglect the business implications of technically feasible methods, *e.g.* with respect to specific social and economical factors. In this regard, it is necessary to provide stakeholders with estimatives of what consumers are willing/able to pay for before introducing white space services into the market. Some questions arising in this techno-economical context might include:

1. What is the preferred method among GDA, CSS, and WSN?
2. What aspects make one method preferred over the other?
3. Are these preferences equal for developed and developing countries?

Answers for the above questions can be formulated along the lines in [85] and [86]. Based on simple expressions for transmission efficiency and *incremental cost*, *i.e.* the additional capital expenditure (CAPEX) over a simple SDR arrangement, these contributions suggest that the selection of a given coexistence method depends on aspects that are closely related to the perspective taken in the analysis. In what follows, we use this framework to examine the business models discussed in [80] and [87] as potential candidates to introduce WSD into the market and then draw our replies to questions 1 to 3 above.

#### 1.4.2.2 Techno-economical Analysis

From Table 1.1, we can infer that the minimum implementation costs of GDA involve constructing a database ( $C_{DB}$ ), embedding location-aware components in WSD ( $C_L$ ), and establishing a bidirectional control channel to provide connectivity between the database and WSD ( $C_C$ ). The incremental cost of GDA is then given by

$$C_{GDA} = C_{DB} + N \times (C_S + C_L + C_C), \quad (1.1)$$

where the number of nodes ( $N$ ) and the cost of the sensor equipping each individual node ( $C_S$ ) reflect the assumption in [85] that WSD do not register in the database but are able to perform spectrum sensing. Under this assumption, the transmission efficiency of GDA can be expressed as the ratio of the amount of time available for transmission ( $t_T$ ) to the total amount of time corresponding to tasks other than data transmission

$$\eta_{GDA} = \frac{t_T}{t_T + t_S + \bar{t}_M + t_Q/F_Q}, \quad (1.2)$$

where  $t_S$  is the sensing time per frame,  $\bar{t}_M$  is the average medium access time per frame,  $t_Q$  is the time to enquire the database, and  $F_Q$  is the number of frames per query.

As seen in the Section 1.3, WSN can alleviate requirements on node spread/density thus addressing diversity and mobility issues that arise in CSS. In an alternative implementation, information about the channel availability can be received from some CPC and forwarded to those WSD within the coverage area of the WSN [85]. The incremental cost of this approach can be written as

$$C_{\text{WSN}} = C_{\text{SN}} + N \times (C_L + C_C), \quad (1.3)$$

where  $C_{\text{SN}}$  is the cost of constructing the WSN and  $N$ , with some slight abuse of notation, represents the number of nodes in the WSN (though they do not possess sensing capabilities here). The transmission efficiency of this approach has the same form of (1.2) and is therefore omitted. It is worth noting, however, that (1.3) eliminates sensing costs but introduces other costs associated with location-aware hardware (as each node needs to know its location). Also, it does not model the costs of coordination and regulatory efforts required to harmonize spectrum for CPC. Hence, it is clear that the actual incremental cost of such CPC-WSN combined approach is higher than that derived in [85].

The infrastructure costs  $C_{\text{DB}}$  and  $C_{\text{SN}}$  in (1.1) and (1.3) pose high CAPEX to stakeholders, so that GDA and WSN may make *less* economic sense in countries where minimum telecommunications infrastructure lacks. Even if stakeholders and governments agree to share CAPEX and prioritize such deployments, high operational expenses (OPEX) to maintain both database and WSN will still exist. According to the business models proposed in [80], CAPEX and OPEX of GDA can be funded by charging database administrators with license fees and consumers with subscription or per-query fees. In [87], stakeholders that already hold licensed spectrum form a kind of *joint venture* to cooperatively exploit white spaces in the spectrum resulting from the sum of their licensed frequency bands. It is then shown through cash flow analysis that WSN-aided operation of WSD can be profitable in urban and suburban areas but, as in conventional infrastructure telecommunication projects, stakeholders have to think long-term. In a well developed telecommunication market, where the average revenue per user (ARPU) comes from subscription fees, the minimum pay-back period is about five years.

While the business models in [80] and [87] may work fine in well developed countries, Table 1.6 suggests that any additional burden on consumers, even if minimum, will discourage white space use in the developing world. In contrast to GDA and WSN, CSS does require *neither* infrastructure *nor* location awareness, so its CAPEX is limited to the development and implementation of sensing-based WSD that are of lower cost. Also, depending on the regulatory framework and business model adopted, consumers may operate WSD free of license and subscription fees in a fashion that could be similar to typical WLAN devices broadly deployed today. The corresponding OPEX in this case is almost exclusively limited to WSD power consumption, which should be low. The incremental cost and transmission efficiency of CSS are then [85]:

$$C_{\text{CSS}} = N \times (C_S + C_C) \quad (1.4)$$

$$\eta_{\text{CSS}} = \frac{t_T}{t_T + t_S + \bar{t}_M}. \quad (1.5)$$

Another aspect that is relevant to the present discussion is connectivity. Loss of connectivity between WSD-database, WSD-WSD, or WSD-WSN constitute concerns that are

common to all methods under analysis here. In the developed world, connectivity between WSD and the database will be over the Internet. According to Table 1.5, this is hard to provide in the developing world where around 80% of the people are still excluded from using the Internet. Even in the event that WSD could access the database over mobile cellular networks, the opportunities unleashed by white space would be limited to about 70% of the people living in developing countries. In either case, we know from Table 1.6 that the corresponding cost  $C_C$  is certain to be much higher in developing countries than in developed countries. As for CSS and WSN, connectivity issues are milder because these methods do not necessarily require access to the Internet. The control channel can be implemented by other means, *e.g.* *in-band* coexistence beacons can be used to convey control signalling over white spaces at the expense of some throughput loss. Hence, since  $C_C$  can be reduced to a minimum, the use of CSS and WSN seems particularly appealing in areas where the Internet is not available or for service connectivity applications such as video streaming that do not require Internet access [88]. Finally, it can be seen from (1.2) and (1.5) that GDA performs *at most* as efficient as CSS (for  $F_Q$  arbitrarily large) so its use in the developing world seems thus far hard to justify.

This impression finds support in [85], where preference relations are shown to depend also on the operation environment where candidate methods are to be deployed in. Such operational contexts are given along with some exemplary applications in Table 1.7, where the symbol “–” stands for the lack of either feasible combinations or known applications. As seen in Table 1.8, GDA is the most preferred method by regulators for environments where the occurrence of white spaces remains static in both time and space, *e.g.* in the TV bands. For environments where this is not the case, and white space availability may follow stochastic processes in time, space, or both, the solutions based on CSS or WSD dominate as the most preferred by regulators. The aforementioned study is further extended in [86] to show that different stakeholders are prone to assign different weights to different aspects. This makes it possible for different preference relations to arise when we rank the same set of methods yet from different perspectives. Licensed users are granted the right to use spectrum on a primary basis, so the preferences given in Table 1.9 are exactly the same as those of regulators as long as white spaces do not exhibit stochastic behavior. Otherwise, the symbol “x” stands for the fact that licensed users do not care about the method used so that no preference arises. However, when we look at the preferences of unlicensed users, shown in Table 1.10, we see that WSN dominates as the most preferred coexistence method.

Our analysis of non-technical issues suggests that developing countries need to *minimize* CAPEX and OPEX related to infrastructure. In contrast, developed countries will likely

**Table 1.7:** Characteristics & Applications of DSA Operational Contexts (adapted from [85]).

|          |            | Spatial           |                |               |
|----------|------------|-------------------|----------------|---------------|
|          |            | Static            | Periodic       | Stochastic    |
| Temporal | Static     | TV broadcast      | WSN            | CDMA mobile   |
|          | Periodic   | Daytime broadcast | Rotating radar | –             |
|          | Stochastic | WLAN              | –              | Public Safety |

**Table 1.8:** Most preferred DSA methods from the regulator perspective (adapted from [85]).

|          |            | Spatial |          |            |
|----------|------------|---------|----------|------------|
|          |            | Static  | Periodic | Stochastic |
| Temporal | Static     | GDA     | WSN      | CSS/WSN    |
|          | Periodic   | GDA     | WSN      | CSS/WSN    |
|          | Stochastic | CSS/WSN | CSS/WSN  | CSS/WSN    |

**Table 1.9:** Most preferred DSA methods from the licensed user perspective (adapted from [86]).

|          |            | Spatial |          |            |
|----------|------------|---------|----------|------------|
|          |            | Static  | Periodic | Stochastic |
| Temporal | Static     | GDA     | WSN      | x          |
|          | Periodic   | GDA     | WSN      | x          |
|          | Stochastic | x       | x        | x          |

*capitalize* on existent infrastructure to create new business opportunities. That being said, our answers to the questions posed earlier in this section are as follows:

1. What is the preferred method among GDA, CSS, and WSN?

**A:** In general, GDA and CSS are the preferred methods for static and stochastic environments, respectively, but a specific preference relation cannot be established without knowledge of the stakeholder assuming the implementation costs.

2. What aspects make one method preferred over the other?

**A:** Stakeholders account to a major aspect here because they largely influence the analysis outcomes. Other aspects include but are not limited to: cost-effectiveness,

**Table 1.10:** Most preferred DSA methods from the unlicensed user perspective (adapted from [86]).

|          |            | Spatial |          |            |
|----------|------------|---------|----------|------------|
|          |            | Static  | Periodic | Stochastic |
| Temporal | Static     | x       | WSN      | WSN        |
|          | Periodic   | Trading | WSN      | WSN        |
|          | Stochastic | WSN     | WSN      | WSN        |



transmission efficiency, accuracy, and ability to deal with broader (regulatory and institutional) contexts.

3. Are these preferences the same for developed and developing countries?

**A:** Provided that the stakeholders are aware of what consumers can pay for, we rank  $GDA \succ CSS \succ WSN$  and  $GDA \succ WSN \succ CSS$  as the preference relations more likely to arise in developed countries. In such markets, large infrastructure projects are typically less budget constrained due to the higher ARPU and shorter pay-back period. Developing countries are characterized by the need of minimizing both CAPEX and OPEX, so the stakeholders need to make the most out of their choice, *e.g.* by choosing the method that is the most preferred for the majority of potential operation environments. Depending on the budget limitations, we expect either  $CSS \succ WSN \succ GDA$  or  $WSN \succ CSS \succ GDA$  to arise.

## 1.5 Chapter Summary and Thesis Objectives

### 1.5.1 Chapter Summary

Make use of white spaces is a natural path towards increased spectrum efficiency. Whether in the TV bands or in whatever bands where the spectrum is underutilized, DSA can help meet the increasing bandwidth needs that new wireless devices and services bring about. This is particularly important to boost the growth of broadband Internet, regarded by the ITU as the prime tool to tackle a number of global issues and leverage ICT progress. Innovative policies and plans are currently being set out to accelerate both DSA development and the roll-out of broadband Internet.

In our opinion, the benefits envisioned by the ITU are doable provided that DSA policies and broadband plans to be implemented do not contribute to an increase in the (currently increasing) digital divide. White spaces access needs to be granted on a universal basis. In this context, we define a *universal solution* as a set of policies, plans, and methods intended at leveraging white space use – also in the developing world. As defined here, the notion of universal solution calls for methods capable of determining white spaces in most operation environments, while posing low CAPEX, low OPEX, and keeping computational burdens as low as they can possibly be.

GDA cannot compose a universal solution because its use suits spatially static environments only and is limited to developed markets where the Internet has large penetration. Another intrinsic drawback of GDA is that most issues arising in its practical implementation are not solvable at the database side, thus imposing higher costs, power consumption, and computational burdens to WSD.

Approaches that enforce cooperation among nodes, such as CSS and WSN, are better suitable to take part in a universal solution because of their broader scope of application and the fact that most of their practical implementation issues can be tackled at the network level. Indeed, provided that individual nodes are made of low complexity and low cost, both CSS and WSN can compose a universal solution. In either method, the overall computational complexity depends on the design options used to implement the processes of acquisition, exchange, and fusion of information shown in Figure 1.4. Nevertheless, when

fabrication costs come into consideration, we have to consider not only the complexity of such network-centric schemes but also their ability to achieve economies of scale.

## 1.5.2 Thesis Objectives

The observations made in the previous section have motivated us to rewrite our bigger picture goal as the study of spectrum sensing methods that determine white spaces by enforcing cooperation among nodes. We have seen in Section 1.3 that most work available in the CSS literature focusses on the processes of exchange and fusion of information, whereas the information acquisition process has received less attention to date. The literature also has analyzed local spectrum sensing in terms of blind and semi-blind techniques *only*, so there are practically *no* counterparts of these analyses for the case where individual nodes rely on signal specific techniques. Low complexity and low, or possibly any, requirements of prior knowledge of the structure of the signals to detect are interesting for more general applications. However, lack of signal classification ability is one limitation of blind and semi-blind techniques that may difficult operation in different markets, thus hindering future WSD from achieving economies of scale. Analyses that extend the related work on CSS with signal specific techniques are therefore desirable, both for a better understanding of the information acquisition process as well as a design guide for future WSD.

This sets out the specific goal of the present dissertation, which is to develop an approach to leverage economies of scale in the information acquisition process, *i.e.* in terms of signal processing tasks carried out at the local level. The proposed approach takes advantage of the *context awareness* that a set of cooperating WSD obtains when it is capable of detecting, and subsequently classifying, the RF signals conveyed in its cooperation footprint. The underlying idea is that, by suitably combining different signal processing techniques offering complementary features, we can define a *unique* design that is able to deal with a number of coexistence situations raised by the introduction of WSD into practical markets where multiple standards are deployed. The design of multi-standard context-aware WSD is worth research because it allows universal white space exploitation and, in doing so, has potential to contribute to the decrease of digital divides in both regional and global levels.

For the specific case of the TV bands, we propose a three-stage cascade signal classifier that allows WSD to coexist with the TV broadcast standards most deployed worldwide. Beside the requirements on context awareness and universality mentioned above, the other design directives of the proposed cascade classifier are committed to complexity, reliability, agility, robustness, and ability to cope with most challenges raised by practical multi-standard environments. Alternatively, the proposed cascade classifier can be employed to protect PMSE systems on a proactive fashion or to provide a contingency for self-coexistence among future TVBD standards in case other methods fail, *e.g.* IEEE 802.22 CBP, IEEE 802.22.1 disabling beacons, or ECMA-392 alien beacons. While we illustrate our approach for multi-standard context-aware WSD in the context of the TV bands, the construction of cascade classifiers aimed at facilitating coexistence in whatever underutilized bands should be straightforward along the lines discussed in this dissertation.

## 1.6 Key Contributions

This section lists our key contributions. The first contribution, perhaps the most important made in this dissertation, is the introduction of the concept of multi-standard context-aware WSD. By exploiting the distinguishing features of this novel concept, we provide a deeper understanding on CSS using signal specific techniques. On top of these two contributions, we design a cascade classifier that allows to coexistence in the TV bands while mitigating digital divides and leveraging economies of scale. We also substantialize our performance assessments through extensive simulation work. This is realized using MESS, a spectrum sensing platform that we developed using Matlab.

In the sequel, we briefly describe each of these contributions.

- **Multi-standard context-aware WSD:** At the time of this writing, the majority of publications available in the literature evaluated detection performance having only digital TV broadcast in mind. In a few very rare exceptions, the literature addressed the detection of TV broadcast signals in both digital and analog formats. Even in those cases, the study was always restricted to a single market, *e.g.* North America or Europe. Our concept of multi-standard context-aware WSD can be distinguished from the related work, as well as from the literature on spectrum sensing in general, in the sense that it considers multiple markets where a larger number of different incumbent systems may operate in. Built on top of this broader scope of application, our analysis of CSS reveals nuances of signal specific techniques that are less understood from the perspective of the traditional single-target single-market approach. As nuances we mean those signal type dependencies that, though negligible in case of blind or semi-blind techniques, yield significant performance variations in case of signal specific techniques. Also, in most cases of interest, the literature has not managed yet to perform standard classification. Multi-standard context-aware WSD exploit explicit signal features that, in contrast to implicit signal features, can be extracted without going into the “internal details” of the signal. This reduces the signal processing needs placed on the classification process.
- **Cooperation based on signal specific techniques:** One interesting open question in the context of CSS is how the use of different signal processing techniques affects the performance improvement derived via cooperation. This dissertation largely contributes to a better understanding on this aspect as it shows that: (i) the achievable cooperation gain depends on the signal processing technique used at the local level, (ii) the extent to which CSS can be beneficial depends on several aspects other than the number of cooperating nodes, (iii) these performance limiting aspects include both type and amount of uncertainty present in the operation environment, (iv) there may be some advantages in using node selection algorithms when only imperfect knowledge of the noise power is available, (v) noise uncertainty affects most techniques equally, regardless of target signal type, but detrimental synergies may occur when the feature used for detection oscillates, and (vi) CSS can compensate for performance degradations introduced by sampling frequency offsets.
- **A cascade classifier for coexistence in the TV bands:** Recalling the current levels of spectrum underutilization and the typically static behavior of TV band incumbents, a WSD will likely spend much of its operation time on channel monitoring tasks. Therefore, it is desirable to implement the first stage of our cascade

classifier using blind or semi-blind techniques. They are fast, so detection delays can be kept low. With respect to signal classification, we exploit in the second stage the fact that most standards deployed today adopt multi-carrier transmission schemes. In this case, a natural way to obtain classification ability is to use a classifier that exploits the periodicities introduced by the cyclic prefix. This is relatively efficient, of low complexity, and agile too. Those less numerous cases that cannot be resolved on the basis of the cyclic prefix are treated at the third stage. There, our focus is on achieving advanced classification abilities even if, in doing so, some detection delay is introduced. The highlight of the proposed cascade classifier is that its stages are carefully designed to possess complementary features. In addition to the desired multi-standard classification ability, this allows to a level of robustness hard to be obtained using individual signal processing techniques.

- **The MESS platform:** Originally envisioned as a standardized evaluation scenario to comparing approaches proposed by different research groups on a fair basis, the MESS platform ended up becoming much more than we had ever thought it could be. It was based on what we call *virtual testbed*, a concept that differs from conventional Matlab simulation in the sense that all target signals are implemented in detailed accordance to corresponding standards. This allows to visualize (and gain insight on) issues that cannot be captured by other means. Beside of accomplishing its major goal of allowing our thorough assessment of several signal processing techniques (not available in the literature at the time of this writing), MESS has its value as integrating research platform, enabler of own algorithm development, baseline for future research, and, particularly, as a promising commercial product to support the assessment, development, and implementation of signal processing techniques for WSD. To the best of our knowledge, such a product is currently available neither in the academy nor in the industry.

## 1.7 Chapter Outline

This dissertation is organized as follows. In Chapter 2, we review the related work that has served as the basis for the contributions provided in this dissertation. We start with the essential steps that any digital receiver follows when performing signal detection. Having the basics in place, we introduce the underlying elements composing the spectrum sensing problem and discuss the assumptions usually made to formulate it as a decision problem. We survey selected publications, which contribute to the signal processing techniques currently regarded as the most promising for WSD. We close the chapter with a list of gaps identified in the related work.

Chapter 3 is mostly devoted to MESS, the simulation tool that we developed to evaluate the signal processing techniques surveyed in the related work. Written in Matlab, MESS consists of four major functional blocks: signal generation, channel generation, signal detection, and signal classification. Along with careful descriptions of each of these functional blocks, we explain what sources of uncertainty of the operation environment are taken into account and how these uncertainties are modeled in MESS. Our approaches to generalize the results in the related work and obtain context-awareness via signal classification are also discussed in this chapter.

In chapter 4, we present a thorough performance assessment of virtually all signal processing techniques surveyed in the related work. The chapter begins presenting our simulation results obtained under ideal operation conditions. Taking this ideal performance as baseline for comparisons, we then extend our assessment to the case where different sources of uncertainty are considered. This includes multipath fading, noise uncertainty, frequency offsets, and joint impacts observed in the presence of two (or more) of these sources. From this simulation work, we identify the pros & cons of each candidate method, draw our conclusions and, based on them, determine the signal processing techniques required by the concept of multi-standard context-aware WSD introduced in this dissertation.

Chapter 5 summarizes the contributions made in this dissertation. Here, we make our final remarks and highlight the insights gained during the long process of studying, implementing, assessing, and selecting signal processing techniques for multi-standard context-aware WSD. We also list some key issues in which we believe promising future research can be carried out. This includes extensions for two different scenarios, studied in our previous work, where the results presented in this dissertation may find application.

## 1.8 Publications Record

From May 2010 to June 2012 we contributed with the European Cooperation in Science and Technology (COST) within the scope of the IC0902 Action. Entitled “Cognitive Radio and Networking for Cooperative Coexistence of Heterogeneous Wireless Networks”, IC0902 aims at integrating the CR concept across all layers of a communication system. The IC0902’s deliverables will be used to define an European platform for CR and CR networks by December 2013. Specifically, we worked with the IC0902’s working group 2 on the definition of cognitive mechanisms that take advantage of cooperation of devices in spatial proximity. This work resulted in the following first-author papers:

1. J. P. Miranda, M. D. Pérez Guirao, A. Lambertucci, and L. A. DaSilva, “Worst Case Analysis of Single-stage Sensing in WRANs”, 1st Workshop of the COST Action IC0902, Bologna, Italy, Nov. 2010.
2. J. P. Miranda, J. Kibiłda, and L. A. DaSilva, “Spectrum Sensing by Program Making and Special Events in the Post-switchover Era: Achievements of a Short Term Scientific Mission”, 2nd Workshop of the COST Action IC0902, Barcelona & Castelldefels, Spain, Oct. 2011.

Particularly, part of the results in 2. was obtained during a one-week short-term scientific mission (STSM) carried out in April 2011 at CTVR, the telecommunications research centre headquartered in Trinity College Dublin, Ireland.

The work in 1. and 2. consists of smaller sets of results, which were subsequently extended and published in the following first-author papers:

3. J. P. Miranda, H. Tchouankem, J. Kibiłda, and L. A. DaSilva, “Return Path for iTV using Whitespaces: A Novel Application for 802.22 WRAN”, In Proc. of IEEE Wireless Advanced, pp. 95-100, London, U.K., June 2011.

4. J. P. Miranda, J. Kibilda, and L. A. DaSilva, “Semi-blind Channel Monitoring Mechanisms for Post-switchover Wireless Microphones”, In Proc. of IEEE Globecom, pp. 1-6, Houston, U.S., Dec. 2011.

The papers 1. to 4. contain preliminary ideas and results that relate directly to the two applications described in the Chapter 5 of this dissertation. In 3., we introduce the idea of providing the return path for interactive TV (iTV) over white spaces. The advantages of this approach over other access technologies currently used in iTV are multi-fold: interactive data can be transmitted in overlay with higher priority broadcast data, the fact that home users are not likely to interact all the time can be exploited to set the return path on an on-demand basis, and broadcasters are not required to cooperate (and share revenues) with telecommunications or Internet service providers. A second idea, introduced in 4., aims at improving immunity to interference in future CR-based PMSE systems. Unlike in the usual overlay-based hierarchical access model, where TVBD should detect and avoid licensed services and PMSE, the proposed approach is concerned about spectrum sensing carried out *by* PMSE rather than *for* PMSE. Within this framework, we provide in-band and out-of-band channel monitoring mechanisms to ensure quality of service of future PMSE. We then show via simulation that the proposed mechanisms are capable of exploiting complementary features of multiple signal processing techniques while incurring no performance loss in comparison to their use in isolation.

In parallel to the above, we worked from February 2010 to June 2012 as a teaching assistant supporting the course “Cognitive Wireless Networks”. Our main task was to design, test, operationalize, and supervise laboratory experiments for undergraduate students. This work was documented in the following handouts:

5. J. P. Miranda, C. König, and M. D. Pérez Guirao, “Implementation of a Simple Air-interface for Overlay-based Cognitive Radio”, Skriptum zum Laboratorium für Netze und Protokolle (NUP), chapter 4, pp. 59-86, Apr. 2010.
6. J. P. Miranda and H. Tchouankem, “Simple Air-interface for Energy-based Cooperative Spectrum Sensing”, Skriptum zum Laboratorium für Netze und Protokolle (NUP), chapter 5, pp. 55-75, Apr. 2011.
7. J. P. Miranda and H. Tchouankem, “Simple Air-Interface for Energy-based Cooperative Spectrum Sensing”, Skriptum zum Laboratorium für Netze und Protokolle (NUP), chapter 5, pp. 53-73, June 2012.

The testbed consists of a single licensed user following a cyclic hopping pattern and operating collocated with a network of CR devices. In order to avoid collisions, the CR network monitors a shared RF environment defined by five non-overlapping channels in the 5.745 – 5.845 GHz range. Our major contribution here was the continuous improvement of the single-node setting initially used in 5. The modifications introduced in 6. and further improved in 7. made the CR network capable of operating also in multi-node mode, and were of utmost importance for the measurement campaigns that generated the real-world CSS results in 3.

Finally, some joint work with the colleague H. Cao (discussed in his own Ph.D dissertation) was performed on cyclostationary signatures:

8. H. Cao, Q. Cai, J. P. Miranda, and T. Kaiser, "Cyclostationary Multitone Beacon Signal for Opportunistic Spectrum Access", In Proc. of the 4th ICST Crowncom, pp. 1-6, Hannover, Germany, June 2009.
9. H. Cao, Q. Cai, J. P. Miranda, and T. Kaiser, "Cyclostationary Beacon for Assisting Spectrum Sensing in Opportunistic Spectrum Access", *Majlesi Journal of Electrical Engineering*, vol. 5, No. 1, pp. 65-72, Mar. 2011.
10. H. Cao, J. P. Miranda, and J. Peissig, "Enhanced Spectrum Awareness with Extended Information Carried on Embedded Cyclostationary Signatures for Cognitive Radio", In Proc. of IEEE Globecom, pp. 1506-1512, Anaheim, U.S., Dec. 2012.





# Chapter 2

## Related Work

This chapter reviews the related work that has served as the basis for the contributions presented later on in this dissertation. We start in Section 2.1 with a brief review of the essential steps that digital receivers follow when performing signal detection. We then introduce the underlying elements composing the detection problem and, as these are introduced, discuss the assumptions available to formulate the sensing problem as a decision problem. After these basics are put in place, we arrive at the core of this chapter, Section 2.2, where we review some selected publications in a summary of the signal processing techniques currently regarded as the most promising for WSD. Section 2.3 closes the chapter with a list of gaps identified in the related work, whose subsequent investigation has provided the backbone of the present dissertation.

### 2.1 Tests, Rules & Optimality Criteria

Consider the continuous-time received signal

$$r(t) = s(t) * h(t) + w(t), \quad (2.1)$$

where  $s(t)$  denotes the *target signals*, *i.e.* the signals that WSD need to detect for coexistence reasons,  $h(t)$  is the channel impulse response,  $w(t)$  is a zero-mean additive white Gaussian noise (AWGN) process introduced by the channel, and “\*” stands for the convolution operation. As shown in Figure 2.1, the task of any digital receiver encompasses three basic processes: demodulation, sampling, and detection. Usually placed at the receiver front-end, the demodulator is composed of a frequency down-conversion block and a receiving filter. After the demodulator,  $r(t)$  is recovered to a baseband pulse  $z(t)$  that is made available to the sampler. The baseband pulse is then sampled at sampling frequency  $f_s = 1/T_s$  so that a test statistic  $z(nT_s)$  can be constructed at the end of each sampling period  $T_s$ . At the detector, decision-making is performed to determine the meaning of  $z(nT_s)$ . If the receiving filter used in the demodulator is linear, its output is also a Gaussian process and  $z(nT_s)$  is a continuous-valued random variable [91].

Unlike typical digital receivers, WSD need not necessarily demodulate the received signals. This means that the sensing task reduces to signal detection, eventually followed by signal classification depending on the application needs. Viewed this way, the detection process can be formulated as a statistical decision problem that consists of a set of hypotheses, a

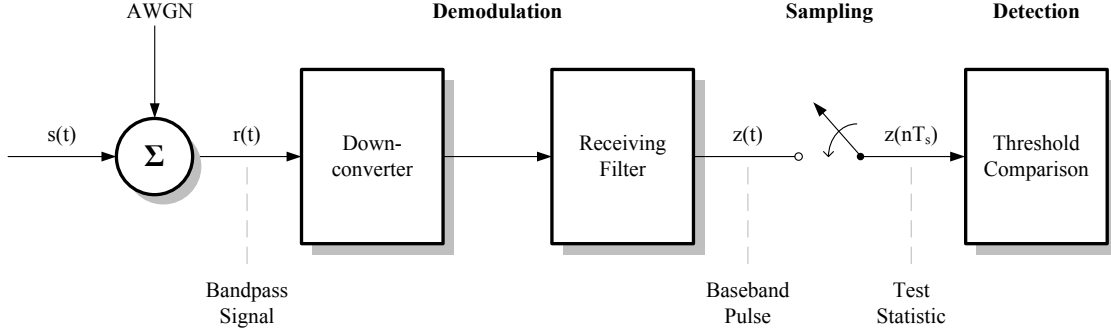


**Fig. 2.1:** Simplified block diagram of a typical digital receiver (adapted from [91]).

test statistic, a decision rule, and a criterion of optimality. Different performance levels can be achieved depending on how the signal detection process is modeled. In what follows, we discuss the fundamental assumptions that may be used to formulate the detection process as a decision problem. Specifically, according to the type of hypotheses used to represent the true states of nature, we overview the rules and optimality criteria usually applied to support the decision-making in spectrum sensing.

### 2.1.1 Binary Hypotheses

In the context of spectrum sensing, the true states of nature correspond to two possible channel statuses. *Idle channels*, where  $s(n)$  is absent, are interpreted as white spaces and thus perceived by WSD as available to use. *Occupied channels*, where  $s(n)$  is deemed to be present, should be avoided by WSD. Let a channel be declared idle under the null hypothesis and occupied otherwise. The detection problem can be represented in discrete-time domain by using the following binary hypotheses set

$$\begin{cases} H_0 : r(n) = w(n) \\ H_1 : r(n) = \sum_{m=0}^{L-1} h(m)s(n-m) + w(n), \end{cases} \quad (2.2)$$

where  $n = 1, 2, \dots, M$  are the samples collected and  $L$  is the channel order. In such *binary hypothesis testing*, detection is performed by choosing the hypothesis that results from the comparison

$$z(n) \underset{H_1}{\overset{H_0}{\leq}} \gamma, \quad (2.3)$$

where  $\gamma$  denotes the *detection threshold* and the condition  $z(n) = \gamma$  means that decision is arbitrary. Hereafter, for ease of notation, we write the test statistic  $z(nT_s)$  simply as  $z(n)$  and assume that the functional dependence on the sampling period  $T_s$  is implicit.

It is evident from (2.3) that how well the detection process can distinguish between  $H_0$  and  $H_1$  is crucial to minimize both white space losses and interference to licensed systems. By misperceiving  $H_0$  for  $H_1$ , WSD will “see” the channel as occupied when it is actually idle and will not transmit on this channel. Such false alarms lead white spaces to be overlooked and must be avoided to increase spectrum utilization. Likewise, if WSD misperceive  $H_1$  for  $H_0$ , they may initiate transmissions on this channel and in doing so will greatly interfere

with “hidden” licensed systems. Therefore, the accuracy of the detection process is usually expressed in terms of the probability of false alarm and the probability of detection

$$P_{\text{fa}} = \Pr[z(n) > \gamma | H_0] = \int_{Z_1} p(z|H_0) dz \quad (2.4)$$

$$P_{\text{d}} = \Pr[z(n) > \gamma | H_1] = \int_{Z_0} p(z|H_1) dz, \quad (2.5)$$

where  $p(z|H_i)$  is the conditional probability density function (p.d.f.) of  $z$ ,  $Z_i$  is the decision region under hypothesis  $H_i$ ,  $i \in \{0, 1\}$ , and  $P_{\text{md}} = 1 - P_{\text{d}}$  denotes the probability of missed detection.

### 2.1.2 Simple Hypotheses

The utmost goal of WSD is to identify the presence of licensed signals, while making sure that both  $P_{\text{fa}}$  and  $P_{\text{md}}$  are kept as low as they possibly can be. If false alarms and missed detections are equally costly, the optimum criterion that minimizes the average number of incorrect decisions is the *likelihood ratio test* (LRT) [91]:

$$\frac{p(z|H_0)}{p(z|H_1)} \underset{H_1}{\overset{H_0}{\gtrless}} \frac{P(H_1)}{P(H_0)}. \quad (2.6)$$

Supposing that the licensed system and WSD do not communicate, the prior probabilities  $P(H_i)$ ,  $i \in \{0, 1\}$ , in (2.6) are unknown to WSD. In this case, the *Neyman-Pearson* (NP) criterion is optimum in the sense that it can be applied to minimize  $P_{\text{md}}$  constrained to a fixed  $P_{\text{fa}}$ . If  $\bar{P}_{\text{fa}}$  denotes the target  $P_{\text{fa}}$  required by some application (or mandated in some standard), the NP criterion can be implemented as a LRT with  $\gamma$  given by the Lagrange multiplier that satisfies [92]

$$P_{\text{fa}} = \int_{Z_1} p(z|H_0) dz = \int_{\gamma}^{\infty} p(\ell|H_0) d\ell = \bar{P}_{\text{fa}}, \quad (2.7)$$

where  $\ell(z)$  is the likelihood ratio on the left side of (2.6). When determined on the basis of a certain fixed  $P_{\text{fa}}$ , the detection threshold  $\gamma$  is said to ensure CFAR detection. Here we should mention that the NP criterion is flexible in the sense that it can be used to construct LRT where any of the hypotheses is rejected in favour of the other hypothesis. The reason why  $\gamma$  is usually determined as a function of  $\bar{P}_{\text{fa}}$ , instead of the target probability of missed detection  $\bar{P}_{\text{md}}$ , will become evident a little later on in Section 2.2.

LRT and its NP-based variation are referred to as *simple hypothesis testing* because they assume that each of the hypotheses corresponds to a single distribution for  $z$  [93]. However, the null hypothesis of (2.2) describes a situation where only noise is received, though WSD actually pick up interference from unintended signals too. If  $w(n)$  is treated as *noise floor*,  $p(z|H_0)$  depends solely on the sum of the power of all noise sources and unwanted signals within the WSD sensitivity region [1]

$$\sigma_w^2|_{\text{dB}} = -174 + \text{NF} + 10 \log B, \quad (2.8)$$

where  $B$  is the channel bandwidth and NF accounts to the noise figure (in dB) of WSD, *i.e.* the ratio of the actual output noise to that which would remain if the WSD itself did not introduce noise. Based on the notion of noise floor, it seems reasonable to assume simple hypothesis testing under  $H_0$ . However, the received noise level observed in practice may change over time thus making it difficult for WSD to obtain an accurate estimation of  $\sigma_w^2$  in some cases [49]. Thus, despite of having eliminated the parameters of unintended signals,  $p(z|H_0)$  is still dependent of knowledge of  $\sigma_w^2$  that may be unavailable. Several parameters are unknown under  $H_1$ , not only because the fundamental information about  $s(n)$  may not be available to WSD but also due to the lack of synchronization between WSD and licensed transmitter, and degrading effects introduced by the channel.

In the sequel, we describe a way to model the condition where many possible distributions can occur under a single hypothesis.

### 2.1.3 Composite Hypotheses

The existence of at least one unknown parameter characterizes *composite hypothesis testing*. Thereby, each hypothesis can be viewed as a family of distributions on  $z$  indexed by the values of the unknown parameters [93]. In contrast to simple hypothesis testing, each of these values describes a situation where  $s(n)$  is actually absent (under  $H_0$ ) or present (under  $H_1$ ). To handle composite hypothesis-testing problems, it is possible to construct a test taking as input the estimatives of all possible unknown parameters instead of their actual values. One such test is the *generalized likelihood ratio test* (GLRT) [94]

$$\frac{p(z|\hat{s}_{H_1}, \hat{w}_{H_1})}{p(z|\hat{w}_{H_0})} \underset{H_1}{\overset{H_0}{\gtrless}} \gamma, \quad (2.9)$$

where the unknown parameters of target signal and noise are replaced with their maximum likelihood estimates (MLE), here identified by the superscript “ $\wedge$ ”. Though not optimum, GLRT is robust, easy to implement [12], and its use has been recently advanced for acquisition purposes in the context of global navigation satellite [94]. GLRT also finds application in some cases where analysis based on the NP criterion is mathematically intractable [52].

## 2.2 Signal Processing for White Space Devices

The previous section has described the underlying elements composing the spectrum sensing problem, as well as the options available to model it. Independent of the decision rule and the optimality criterion used, the test statistic largely affects the outcome of the sensing process. This impact is multi-fold in the sense that the performance that results from using different test statistics is essentially different, not necessarily in terms of accuracy only, but also with respect to several other performance and operational metrics. Such metrics include agility, amount of prior knowledge required for detection, computational complexity, classification ability, and robustness, to name some. The extent to which such variations in performance occur closely relates to the meaning of the test statistic, which, in turn, depends on the signal processing technique used in the sampling process.

In the remainder of this section, we summarize the most promising signal processing techniques for WSD. In the first part, which comprehends the subsections 2.2.1 and 2.2.2, we address blind and semi-blind techniques that impose minimum requirements on the amount of prior information required for detection. Spanning from subsections 2.2.3 to 2.2.5, the second part is devoted to signal specific techniques that improve accuracy, robustness, and/or provide signal classification ability at the expense of longer sensing time, increased knowledge about the structure of  $s(n)$ , or both.

Throughout the rest of this dissertation, we refer to each of these subsections as a *class* of signal processing techniques. Except for Section 2.2.5, each class relies on the same underlying principle to perform detection but different levels of performance can be achieved by different test statistics within a class. We refer to the test statistics used to implement the sensing methods simply as *methods*.

## 2.2.1 Energy Detection

We have seen in the previous section that the detection of target signals in the presence of noise implies choosing between two situations in (2.2). An intuitive way to accomplish this task is to use the average energy of the received signal  $r(n)$  as test statistic:

$$z_{\text{ED}}(n) = \frac{1}{M} \sum_{n=0}^{M-1} |r(n)|^2. \quad (2.10)$$

The test that results from substituting (2.10) into (2.3) is known as *energy detection* (ED). ED is a semi-blind signal processing technique that is simple, of low complexity, and does not require any knowledge about the structure of  $s(n)$ . As for the disadvantages, distinction between the target signals and WSD signals cannot be established based on  $|r(n)|^2$ . The use of ED is therefore limited to applications where sensing tasks need not be performed while other WSD simultaneously transmit. At the expense of tight synchronization requirements, one can enforce quiet periods during which all WSD cease transmissions and (eventually engage in CSS to) scan the operation environment for white spaces.

### 2.2.1.1 Performance Analysis

Despite of the limitations above, ED is by far the most regarded method in the context of local spectrum sensing and one of the couple of methods considered when it comes to CSS. One reason for this popularity is that the performance analysis of ED can be made quite simple provided that some assumptions are put in place. As (2.10) corresponds to a sum of  $M$  i.i.d. Gaussian random variables, the distribution of  $z_{\text{ED}}$  is central and non-central chi-squared with  $M$  degrees of freedom under  $H_0$  and  $H_1$ , respectively [43]. For  $M$  large enough, the central limit theorem can be applied to model  $z_{\text{ED}}$  as asymptotically normally distributed

$$z_{\text{ED}}(n) \sim \begin{cases} H_0 : \mathcal{N}(M\sigma_w^2, 2M\sigma_w^4) \\ H_1 : \mathcal{N}(M\sigma_w^2 + M\sigma_s^2, 2M\sigma_w^4 + 4M\sigma_w^2\sigma_s^2), \end{cases} \quad (2.11)$$

where  $\sigma_s^2 = \|s\|^2/M$  is the average power of  $s(n)$ . The sensing time required to achieve an acceptable detection accuracy typically requires  $M \geq 20$ , so the Gaussian approximations in (2.11) are of practical interest. Based on this assumption, the performance of ED can be analyzed in closed-form using [52]

$$P_{\text{fa}}^{\text{ED}} = \Pr[z_{\text{ED}}(n) > \gamma | H_0] \approx Q\left(\frac{\gamma - M\sigma_w^2}{\sigma_w^2 \sqrt{2M}}\right) \quad (2.12)$$

$$P_{\text{d}}^{\text{ED}} = \Pr[z_{\text{ED}}(n) > \gamma | H_1] \approx Q\left(\frac{\gamma - M\sigma_w^2 - M\sigma_s^2}{\sigma_w \sqrt{2M\sigma_w^2 + 4M\sigma_s^2}}\right), \quad (2.13)$$

where the Marcumm Q-Function

$$Q(x) = \frac{1}{\sqrt{2\pi}} \int_x^{+\infty} e^{-x^2/2} dx \quad (2.14)$$

gives the tail probability of a zero-mean unit-variance Gaussian random variable. Closed-form expressions for the performance of ED under Rayleigh, Nakagami, and Rician fading channels can be found in [95]. In general, the detection performance of a method is characterized in terms of its *receiver operating characteristic* (ROC) where  $P_{\text{d}}$  is plotted against  $P_{\text{fa}}$ . Figure 2.2 illustrates the ROC of ED, which is concave and lies above the line  $P_{\text{d}} = P_{\text{fa}}$  as in any continuous LRT [93]. The *complementary ROC* plots  $P_{\text{md}}$  against  $P_{\text{fa}}$ .

Ideally, the larger the number of samples over which  $r(n)$  is averaged the more accurately ED can distinguish between  $H_0$  and  $H_1$ . The minimum number of samples required to achieve any operation point ( $P_{\text{fa}}, P_{\text{d}}$ ) in the ROC can be computed using [52]

$$M_{\text{min}}^{\text{ED}} = \left\lceil 2 \left[ Q^{-1}(P_{\text{fa}}) - Q^{-1}(P_{\text{d}}) \sqrt{1 + 2\text{SNR}} \right]^2 \text{SNR}^{-2} \right\rceil, \quad (2.15)$$

where  $\lceil y \rceil = \min\{x \in \mathbb{Z} | x \geq y\}$  is the ceiling function and the *signal-to-noise ratio* (SNR) in linear scale is given by:

$$\text{SNR} = \frac{\sigma_s^2}{\sigma_w^2} = \frac{\|s\|^2}{M\sigma_w^2}. \quad (2.16)$$

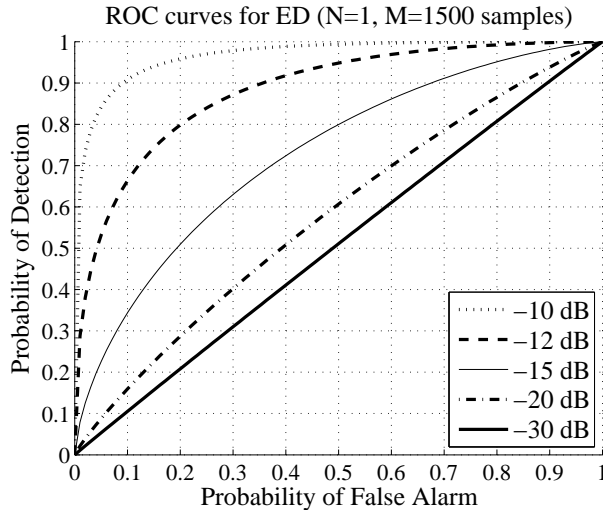


**Fig. 2.2:** Family of ROC curves illustrating the performance of ED obtained via (2.12) and (2.13) for different SNR values with  $M = 1500$  samples.

According to Figure 2.3, the number of samples that ED requires to meet any operation point  $(P_{fa}, P_d)$  in the ROC asymptotically scales as  $\mathcal{O}(1/\text{SNR}^2)$  in the low SNR regime. Hence, the challenge of scanning the frequency band of interest is not just about accurately determining white spaces but doing it in a timely manner. In this process, the average power of the target signal will change depending on the characteristics of  $s(n)$  and the distance between licensed transmitter and WSD. Since this information is likely unknown at sensing-only WSD,  $\sigma_s^2$  is difficult to estimate and the sensing receiver can never know its operating SNR exactly. Recalling the performance expressions of ED, (2.12) needs to know only  $\sigma_w^2$  whereas (2.13) imposes the need of additional information about  $\sigma_s^2$ . Due to this reason, the detection threshold is usually set based on the p.d.f. of  $z_{\text{ED}}$  under  $H_0$ . In this case, the NP criterion can be applied to rewrite (2.7) as [1]:

$$\gamma_{\text{ED}} = \sigma_w^2 \left[ 1 + \frac{Q^{-1}(\bar{P}_{fa})}{\sqrt{M}} \right]. \quad (2.17)$$

### 2.2.1.2 Noise Uncertainty and SNR Walls

As a semi-blind technique, ED is optimum in terms of the NP criterion when only  $\sigma_w^2$  is known a priori [52]. In the ideal case that  $\sigma_w^2$  is perfectly known, (2.15) ensures that reliable detection is possible at arbitrarily low SNR by suitably increasing  $M$ . Moreover, threshold determination is straightforward using (2.17). However, the received noise level changes over time in practice. It may be possible to obtain a rough estimate of  $\sigma_w^2$  based on noise-only samples [96] but, whenever the availability of noise-only samples becomes difficult to guarantee, ED becomes highly susceptible to noise uncertainty [49]. This susceptibility to noise uncertainty can be portrayed by rewriting (2.15) as

$$M_{\min}^{\text{ED}} \approx \frac{2 [Q^{-1}(P_{fa}) - Q^{-1}(P_d)]^2}{\left[ \text{SNR} - \left( \rho - \frac{1}{\rho} \right) \right]^2}, \quad (2.18)$$

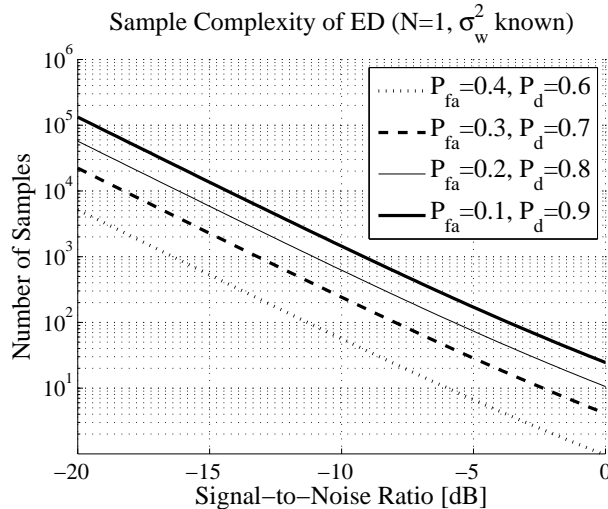


**Fig. 2.3:** Minimum number of samples obtained via (2.15) for different operation points  $(P_{fa}, P_d)$  and SNR values.

where the parameter  $\rho$  determines the knowledge of  $\sigma_w^2$  available for detection and the estimated noise power  $\hat{\sigma}_w^2 \in [(1/\rho)\sigma_w^2, \rho\sigma_w^2]$ . If  $\rho = 1$ , perfect knowledge of  $\sigma_w^2$  is assumed and (2.18) converges to (2.15). Otherwise,  $\rho > 1$  indicates that WSD cannot be sure about the actual  $\sigma_w^2$  and this uncertainty increases with  $\rho$ . According to this model, ED can detect the presence of  $s(n)$  as long as  $\gamma_{\text{ED}} > \rho\hat{\sigma}_w^2$ . In practice, however, the achievable performance will be constrained even under a moderate degree of noise uncertainty because the number of samples  $M \rightarrow \infty$  as  $\text{SNR} \downarrow (\rho - \frac{1}{\rho})$ . This inability of ED in detecting signals with power smaller than that of  $\gamma_{\text{ED}} - \sigma_w^2$  creates a *SNR wall*

$$\text{SNR}_{\text{wall}} = \frac{\rho^2 - 1}{\rho} \quad (2.19)$$

in the neighborhood of which the number of samples required for detection approaches infinity. Figure 2.4 shows how the imperfect knowledge of  $\sigma_w^2$  introduces SNR walls that can fairly degrade the performance of ED. From this figure it is clear to see why the notion of SNR wall has been advanced as representation for the *limit* to the SNR under which reliable detection is impossible no matter how many samples are collected.

The detection of weak signals “buried” in noise of uncertain power is a big issue. This fundamental limitation was first identified in [97] but later on shown to be not an exclusive drawback of ED. Indeed, it is well known today that SNR walls exist for *every* moment detector and for *any* practical detector with finite dynamic range [98]. More generally, the detection limits of a certain method depend on its prior knowledge of  $s(n)$ , *i.e.* the SNR walls of different methods are created by the different kinds of uncertainties present in the operation environment [99]. Uncertainty in the marginal noise distribution is pointed as the *sole* reason for the SNR walls in ED, whereas other sources of uncertainty *jointly* contribute in the case of signal specific techniques, *e.g.* color of the noise and time-selectivity of the fading process.

In general, the impact of such modeling uncertainties is an open research problem in the context of CSS but some ED-based insights can be found in the literature. For instance, if soft combining is used, CSS cannot improve the nominal SNR wall defined in (2.19) but can effectively mitigate the impact of noise uncertainty provided that the SNR walls

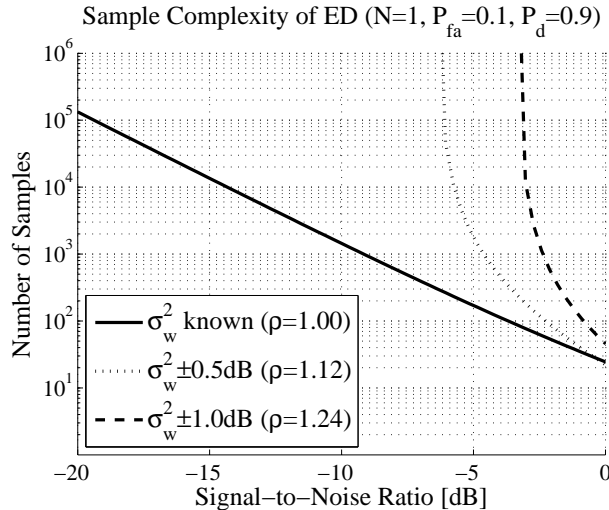


**Fig. 2.4:** Impact of noise uncertainty on the minimum number of samples obtained via (2.18) for different SNR values using  $(P_{\text{fa}}, P_{\text{d}}) = (0.1, 0.9)$ .



are defined in average or on probability [100]. The intuition behind this finding is that the variance of the test statistic decreases as the number of WSD engaged in cooperation increases. Hence, any closed subinterval of  $[(1/\rho)\sigma_w^2, \rho\sigma_w^2]$ , within which  $\hat{\sigma}_w^2$  varies with certain probability, can be made narrower. Similar results are obtained for hard combining in [101], where OR logic is shown to be the fusion rule least susceptible to noise uncertainty while AND logic is the most. Also, according to [102], the use of AND logic in the presence of noise uncertainty is not advisable because it may cause the global detection performance obtained via CSS to be *worse* than that achieved by a single WSD.

## 2.2.2 Eigenvalue-based Detection

The signal processing techniques that have been proposed to overcome the performance degradation associated with the SNR wall phenomenon are mostly based on signal specific methods. Among these methods, *eigenvalue-based detection* (EBD) has been receiving particular attention because it is a signal processing technique that is able to work blindly or semi-blindly. In contrast to ED, EBD relies on spatial diversity (obtained either through multi-antenna techniques or CSS) to exploit the underlying properties of the covariance matrix of  $r(n)$ . As seen in Section 1.3, multi-antenna techniques are power-hungry, costly, complex, and thus less simple to implement in portable WSD. In what follows, we assume that portable WSD are of limited size and complexity and, as such, use CSS as the natural diversity enabler for EBD.

### 2.2.2.1 General Approach

Consider an operation environment where  $i = 1, 2, \dots, N$  WSD operate collocated with  $j = 1, 2, \dots, P$  licensed transmitters, each device being single-antenna device. If the number of WSD within the cooperation footprint is  $N > P$ , from the perspective of the  $i$ th WSD the binary hypotheses set in (2.2) becomes

$$\begin{cases} H_0 : r_i(n) = w_i(n) \\ H_1 : r_i(n) = \sum_{j=1}^P \sum_{m=0}^{L_{ij}} h_{ij}(m) s_j(n-m) + w_i(n), \end{cases} \quad (2.20)$$

where  $L_{ij}$  and  $h_{ij}(m)$  are respectively the channel order and the channel coefficient between the  $j$ th licensed transmitter and the  $i$ th WSD. As inherent in CSS,  $h_{ij}(m)$  can be independent or correlated for different  $i$  depending on how the WSD engaged in cooperation are spatially distributed.

By making  $L_j = \max_i(L_{ij})$ , it is possible to define the vectors

$$\mathbf{r}(n) = [r_1(n), r_2(n), \dots, r_N(n)]^T \quad (2.21)$$

$$\mathbf{h}_j(n) = [h_{1j}(n), h_{2j}(n), \dots, h_{Nj}(n)]^T \quad (2.22)$$

$$\mathbf{w}(n) = [w_1(n), w_2(n), \dots, w_N(n)]^T, \quad (2.23)$$

where the superscript “ $T$ ” stands for transpose. This vectorial representation is convenient as it allows to rewrite (2.20) as:

$$\begin{cases} H_0 : \mathbf{r}(n) = \mathbf{w}(n) \\ H_1 : \mathbf{r}(n) = \sum_{j=1}^P \sum_{m=0}^{L_j} \mathbf{h}_j(m) s_j(n-m) + \mathbf{w}(n). \end{cases} \quad (2.24)$$

After some straightforward computation (shown in detail in [103]), the statistical covariance matrix of  $\mathbf{r}(n)$  can be obtained under the two hypotheses

$$\mathbf{R}_r = E [\hat{\mathbf{r}}(n)\hat{\mathbf{r}}^\dagger(n)] = \begin{cases} H_0 : \sigma_w^2 \mathbf{I}_{N_\iota} \\ H_1 : \mathbb{H} \mathbf{R}_s \mathbb{H}^\dagger + \sigma_w^2 \mathbf{I}_{N_\iota}, \end{cases} \quad (2.25)$$

where  $E(\cdot)$  denotes taking the expectation, the superscript “ $\dagger$ ” stands for transpose-conjugate (Hermitian),  $\iota$  is a smoothing factor,  $\mathbf{I}_{N_\iota}$  is the identity matrix of order  $N_\iota$ , and the Wishart matrix  $\mathbb{H} = [\mathbb{H}_1, \mathbb{H}_2, \dots, \mathbb{H}_P]$  has coefficients of the form:

$$\mathbb{H}_j = \begin{bmatrix} \mathbf{h}_j(0) & \dots & \dots & \mathbf{h}_j(\iota_j) & \dots & 0 \\ & \ddots & & & \ddots & \\ 0 & \dots & \mathbf{h}_j(0) & \dots & \dots & \mathbf{h}_j(\iota_j) \end{bmatrix}. \quad (2.26)$$

Now let  $\lambda_{\max} = \lambda_1 \geq \lambda_2 \geq \dots \geq \lambda_{N_\iota} = \lambda_{\min} > 0$  denote the eigenvalues of  $\mathbf{R}_r$  ordered in strictly decreasing order. Following [104], the distributions of  $\lambda$  under  $H_0$  and  $H_1$  are respectively given by  $p(\lambda_i|H_0) = \sigma_w^2, \forall i$ , and

$$p(\lambda_i|H_1) = \begin{cases} \sigma_i^2 + \sigma_w^2 & 1 \leq i \leq P \\ \sigma_w^2 & P \leq i \leq N_\iota, \end{cases} \quad (2.27)$$

where  $\sigma_1^2, \sigma_2^2, \dots, \sigma_P^2$  are the target signal powers received at the  $i$ th WSD.

### 2.2.2.2 Test Statistics

It is evident from (2.27) that the eigenvalues of  $\mathbf{R}_r$  can be used as test statistic. In practice, since the sensing task is usually limited to a number of samples that is finite and possibly small, only a sample of the statistical covariance matrix in (2.25) will be available to WSD. If  $M$  samples are collected, this sample covariance matrix can be computed as [103]:

$$\mathbf{R}_r(n) = \frac{1}{M} \sum_{n=\iota-1}^{\iota-2+M} \hat{\mathbf{r}}(n)\hat{\mathbf{r}}^\dagger(n). \quad (2.28)$$

It is possible to construct several detection methods that use the eigenvalues of  $\mathbf{R}_r(n)$  as test statistic. Under simple hypothesis testing, a NP-based LRT can be written as the ratio of the p.d.f. of all eigenvalues under  $H_1$  to the p.d.f. of all eigenvalues under  $H_0$ :

$$z_{\text{LRT}}(n) = \frac{p(\lambda_1, \lambda_2, \dots, \lambda_{N_\iota}|H_1)}{p(\lambda_1, \lambda_2, \dots, \lambda_{N_\iota}|H_0)}. \quad (2.29)$$

In the asymptotical regime, it is shown in [105] that the above LRT reduces to the *Roy's largest root test* (RLRT)

$$z_{\text{RLRT}}(n) = \frac{\lambda_{\max}}{\sigma_w^2}, \quad (2.30)$$

which decides  $H_1$  if  $\lambda_{\max} > \sigma_w^2$  and  $H_0$  if  $\lambda_{\max} = \sigma_w^2$ . From the denominator of (2.30) it is clear that RLRT relies on prior knowledge of the noise power to distinguish between the two hypotheses and thus it is a semi-blind technique just like ED.

For  $M \gg \iota$ , a comparison between ED and RLRT can be established along the lines in [103] and [105]. First, rewrite (2.10) for the case of  $N$  cooperative WSD:

$$z_{\text{ED}}^{\text{CSS}}(n) = \frac{1}{MN} \sum_{i=1}^N \sum_{n=0}^{M-1} |r(n)|^2. \quad (2.31)$$

Next, define  $\Delta\lambda$  as the average of all the eigenvalues of  $\mathbf{R}_r(n)$

$$\Delta\lambda(n) = \frac{1}{N\iota} \text{Tr}[\mathbf{R}_r(n)] \quad (2.32)$$

$$= \frac{1}{MN\iota} \sum_{n=L-1}^{L-2+M} \hat{\mathbf{r}}(n)\hat{\mathbf{r}}^\dagger(n) \quad (2.33)$$

$$\approx z_{\text{ED}}^{\text{CSS}}(n), \quad (2.34)$$

where  $\text{Tr}(\cdot)$  denotes the trace of a matrix. ED and RLRT respectively test  $\Delta\lambda$  and  $\lambda_{\max}$  against  $\sigma_w^2$ , so the former has reduced statistical power as compared to the latter [105].

Robustness against noise uncertainty can be obtained by combining the energy samples collected via simple ED. An obvious criterion is to choose the combining matrix such that the resultant signal has the largest SNR. Let  $\boldsymbol{\beta}_{\max}$  denote the eigenvector corresponding to the maximum eigenvalue of the statistical covariance matrix of  $\mathbf{r}(n)$ . By exploiting the properties of the trace of a matrix, it can be show that  $\boldsymbol{\beta}_{\max}$  corresponds to the optimal combining matrix [108]. This fact is used in a kind of “blindly combined” ED denoted as *maximum eigenvalue detector* (MED):

$$z_{\text{MED}}(n) = \frac{1}{M} \sum_{n=0}^{M-1} \left| \hat{\boldsymbol{\beta}}_{\max}^T \mathbf{r}(n) \right|^2 \quad (2.35)$$

$$= \frac{1}{M} \sum_{n=0}^{M-1} \hat{\boldsymbol{\beta}}_{\max}^T \mathbf{r}(n) \mathbf{r}^T(n) \hat{\boldsymbol{\beta}}_{\max} \quad (2.36)$$

$$= \hat{\boldsymbol{\beta}}_{\max}^T \mathbf{R}_r(n) \hat{\boldsymbol{\beta}}_{\max} \quad (2.37)$$

$$= \lambda_{\max}. \quad (2.38)$$

MED decides  $H_1$  if  $z_{\text{MED}}(n) > \frac{\gamma}{N\iota} \text{Tr}[\mathbf{R}_r(n)]$  and  $H_0$  otherwise. The threshold  $\gamma$  depends only on  $P_{\text{fa}}$  and on the number of samples  $M$ , so MED is immune to noise uncertainty. The method that results from assuming  $\boldsymbol{\beta}_{\max}$  known a priori, denoted in [108] as “optimally combined” ED, is essentially the same as the RLRT detector in (2.30).

Other well-known EBD methods that are blind, and thus robust against noise uncertainty, are *maximum-minimum eigenvalue* (MME) and *energy with minimum eigenvalue* (EME). The mathematical intuition behind the MME method is that  $\lambda_1 = \lambda_2 = \dots = \lambda_{N\iota} = \sigma_w^2$  under  $H_0$  and thus  $\lambda_1/\lambda_{N\iota} = 1$ . Since it is highly probable that  $\lambda_1/\lambda_{N\iota} > 1$  under  $H_1$ , we can construct a test statistic using the ratio

$$z_{\text{MME}}(n) = \frac{\lambda_{\max}}{\lambda_{\min}} \quad (2.39)$$

to decide  $H_1$  if  $z_{\text{MME}}(n) > 1$  [103] and  $H_0$  if  $z_{\text{MME}}(n) = 1$ . The same intuition lends itself to construct the test statistic of EME. By replacing  $\lambda_{\text{max}}$  in (2.39) by  $\Delta\lambda$  we get

$$z_{\text{EME}}(n) = \frac{\Delta\lambda(n)}{\lambda_{\text{min}}} \approx \frac{z_{\text{ED}}^{\text{CSS}}(n)}{\lambda_{\text{min}}}, \quad (2.40)$$

which decides  $H_1$  if  $z_{\text{EME}} > N$  and  $H_0$  if  $z_{\text{EME}} = 1$ .

Prior knowledge of parameters other than  $\sigma_w^2$  may be not available to WSD in practice. As seen in Section 2.1, the usual procedure in this case is to formulate the detection problem using composite hypothesis testing and then apply some sub-optimal test. For the specific case of unknown channel gains  $\mathbf{h}_j(n)$ , we can rewrite the GLRT in (2.9) as

$$\frac{\sup_{\mathbf{h}, \sigma_w^2} p(\mathbf{r}|\mathbf{h}, \sigma_w^2)}{\sup_{\sigma_w^2} p(\mathbf{r}|\sigma_w^2)} \underset{H_1}{\overset{H_0}{\gtrless}} \gamma, \quad (2.41)$$

where  $\sup(\cdot)$  denotes taking the supremum. For  $P = 1$ , *i.e.* provided that WSD operate collocated with a single licensed system only, (2.41) assumes the form [105]:

$$z_{\text{GLRT}}(n) = \frac{\lambda_{\text{max}}}{\frac{1}{N} \text{Tr}[\mathbf{R}_r(n)]}. \quad (2.42)$$

Another method based on the GLRT principle is the *arithmetic to geometric mean* (AGM) detector. As the name suggests the test statistic of AGM [109]

$$z_{\text{AGM}}(\boldsymbol{\lambda}_r) = \frac{\frac{1}{N} \sum_{i=1}^N \lambda_{i,r}}{(\prod_{i=1}^N \lambda_{i,r})^{1/N}} \quad (2.43)$$

is based on the ratio of the arithmetic mean to the geometric mean of the  $N$  eigenvalues of  $\mathbf{R}_r(n)$ , which we assume are collected into the vector  $\boldsymbol{\lambda}_r = [\lambda_{1,r}, \lambda_{2,r}, \dots, \lambda_{N,r}]$ .

### 2.2.2.3 Performance Analysis

Thus far a number of EBD-based methods have been presented but their performances still remain to be investigated. This involves the tasks of finding the p.d.f. of each test statistic under  $H_0$  and  $H_1$  and defining a suitable procedure to set the detection threshold  $\gamma$ . Both tasks have received great attention recently, with treatments available in the EBD literature ranging from semi-asymptotical [103] and asymptotical [106] to exact methods [104] among others [107]. The derivation of eigenvalue distributions and the definition of thresholds for each of the EBD-based methods described in the aforementioned references transcend the scope of the present dissertation. In any EBD method, however, we observe that the bottom line is to take advantage of the fact that the target signals either occupy a subspace of dimension strictly smaller than  $N$  or have non-white spectrum [109]. EBD is therefore particularly suitable when the samples are highly correlated and ideal ED is not optimum anymore. This is exactly the case of narrowband PMSE signals, which occupy less than 1/30 of a TV channel [108]. Neither ED nor EBD requires accurate synchronization but the former *always* suffers from SNR walls whereas the latter is robust against noise uncertainty depending on the method used [103].

As another advantage, the performance of EBD has been shown to be robust in faded and time-dispersed channels for the following signal types:

- Advanced Television Systems Committee (ATSC) captures [103].
- Randomly generated signals and PMSE signals [103][108][109].
- Other generic or non-specified signals [104][105][107].

### 2.2.3 Spectrum Correlation Detection

Signal processing techniques that are blind or semi-blind are advantageous because they require little or no prior knowledge of  $r(n)$ . As such, they can be used to detect virtually any kind of target signal. In practice, however, some prior knowledge about the structure of  $s(n)$  will be frequently available to WSD. If this is the case, there may be advantages in constructing test statistics to examine the correlation of this a priori information with an estimate locally computed based on  $r(n)$ .

#### 2.2.3.1 General Approach

Wireless channels are generally perturbed by multipath fading, so it is reasonable to model the received signals as being second-order stationary random processes [50]. Under this assumption, the second-order moment of such a process can be described in the time domain by its *autocorrelation function* (ACF)

$$R_r(\tau) = E[r(t)r^*(t - \tau)], \quad (2.44)$$

where  $\tau$  is the time lag and the superscript “\*” stands for complex-conjugate. Examining (2.44) under the two hypotheses in (2.2) yields

$$\begin{cases} H_0 : R_r(\tau) = \sigma_w^2 \delta(\tau) \\ H_1 : R_r(\tau) = R_s(\tau) + \sigma_w^2 \delta(\tau), \end{cases} \quad (2.45)$$

where  $\delta(\cdot)$  is the Dirac delta sequence. If the autocorrelation sequence  $\{R_s(\tau)\}$  is absolutely summable and has finite energy, the Wiener-Khinchin theorem guarantees that the discrete-time Fourier transform (DFT), also called *power spectrum density* (PSD)

$$S_s(f) = \sum_{\tau=-\infty}^{\infty} R_s(\tau)e^{-j2\pi f\tau}, \quad (2.46)$$

exists and uniformly converges for all  $f \in [0, 1]$ . This allows us to rewrite (2.45) in terms of its frequency domain description:

$$\begin{cases} H_0 : S_r(f) = \sigma_w^2 \\ H_1 : S_r(f) = S_s(f) + \sigma_w^2. \end{cases} \quad (2.47)$$

Since the target signals typically exhibit unique spectral patterns, distinction between  $H_0$  and  $H_1$  can be made by examining the spectral correlation between  $S_s(f)$  and  $S_r(f)$ . The test statistic of this *spectrum correlation detector* (SCD) is [93]:

$$z_{\text{SCD}}(f) = 2\pi \int_0^1 S_r(f)S_s(f)df. \quad (2.48)$$

Even in the case that  $S_s(f)$  is available a priori,  $S_r(f)$  is always corrupted by noise and therefore needs to be estimated. Since ACF and PSD form a Fourier pair  $R_r(\tau) \Leftrightarrow S_r(f)$ , the spectrum estimation task is usually viewed as equivalent to that of estimating  $R_r(\tau)$  and then Fourier transforming the estimated ACF. Though the ACF can be determined in the limit by using the time-average

$$R_r(\tau) = \lim_{M \rightarrow \infty} \frac{1}{2M+1} \sum_{n=-M}^M r(n)r^*(n-\tau), \quad (2.49)$$

the practical amount of data available to WSD will be limited to a finite set of samples  $n = 0, 1, \dots, M-1$  and hence it is more realistic to use the finite sum [110]

$$\hat{R}_r(\tau) = \frac{1}{M} \sum_{n=0}^{M-1} r(n)r^*(n-\tau) \quad (2.50)$$

$$= \frac{1}{M} \sum_{n=0}^{M-1-\tau} r(n)r^*(n-\tau), \quad (2.51)$$

where  $\tau = 0, 1, \dots, M-1$ . The last step leading to (2.51) is just to ensure that the  $r(n)$  values falling outside the interval  $[0, M-1]$  are excluded from the sum.

### 2.2.3.2 Test Statistics

The class of spectrum estimation techniques that rely on the DFT of an estimated ACF to obtain the desired PSD is referred to as *non-parametric methods*. Once an estimate of the ACF is available, one computationally simple alternative is the *periodogram*

$$\hat{S}_{\text{PER},r}(f) = \sum_{\tau=-M+1}^{M-1} \hat{R}_r(\tau) e^{-j2\pi f\tau}, \quad (2.52)$$

which is an *asymptotically unbiased* estimator, *i.e.* the PSD estimates are on the average equal to the true power spectra as the number of samples goes to infinity [110]:

$$\lim_{M \rightarrow \infty} E[\hat{S}_{\text{PER},r}(f)] = S_r(f). \quad (2.53)$$

A periodogram-based SCD can be constructed by rewriting the test statistic in (2.48) as

$$z_{\text{PER}}(\tau) = \frac{1}{M} \sum_{\tau=0}^{M-1} \hat{S}_{\text{PER},r}(\tau) S_s(\tau), \quad (2.54)$$

which asymptotically converges to LRT at low SNR and, thus, is optimal according to the NP criterion [50]. A major disadvantage of the periodogram is that it is not a *consistent estimator*, *i.e.* its variance does not go to zero as the number of samples goes to infinity. Instead, the variance of the periodogram is proportional to the squared magnitude of the actual PSD [110]:

$$\lim_{M \rightarrow \infty} \text{Var}[\hat{S}_{\text{PER},r}(f)] \approx S_r^2(f). \quad (2.55)$$

Other non-parametric methods, such as the Bartlett method (periodogram averaging), the Welch method (averaging of modified periodograms), and the Blackman-Tukey method (periodogram smoothing), are designed to reduce the statistical variability of the periodogram thus providing consistent estimates of  $S_r(f)$ . To see how spectrum estimation can be realized consistently via periodogram averaging, assume that  $K$  uncorrelated realizations of  $r(n)$ , denoted as  $r_i(n), i = 1, 2, \dots, K$ , are observed over  $0 \leq n < M'$ . The periodogram of the  $i$ th realization and the average of all  $K$  periodograms are [110]

$$\hat{S}_{\text{PER},i}(f) = \frac{2\pi}{M'} \left| \sum_{n=0}^{M'-1} r_i(n) e^{-j2\pi fn} \right|^2 \quad (2.56)$$

and

$$\hat{S}_{\text{AVG}}(f) = \frac{1}{K} \sum_{i=1}^K \hat{S}_{\text{PER},i}(f), \quad (2.57)$$

respectively. If  $W_{\text{BAR}}(f)$  denotes the DFT of a Bartlett window extending from  $-M'$  to  $M'$ , it can be seen from the expectation and variance of (2.57)

$$E \left[ \hat{S}_{\text{AVG}}(f) \right] = E \left[ \hat{S}_{\text{PER},i}(f) \right] = S_r(f) * W_{\text{BAR}}(f) \quad (2.58)$$

$$\text{Var} \left[ \hat{S}_{\text{AVG}}(f) \right] = \frac{1}{K} \text{Var} \left[ \hat{S}_{\text{PER},i}(f) \right] \approx \frac{S_r^2(f)}{K} \quad (2.59)$$

that  $\hat{S}_{\text{AVG}}(f)$  is a consistent estimator because it is asymptotically bias-free and its variance approaches zero as  $K$  approaches infinity. In the Bartlett method, the assumption of uncorrelated realizations can be relaxed by partitioning a *single* realization of  $r(n)$  into  $K$  non-overlapping sequences of length  $M'$ . The corresponding estimate is obtained by making  $r_i(n) = r(n + iM')$  in (2.56)

$$\hat{S}_{\text{BAR},r}(f) = \frac{2\pi}{M} \sum_{i=0}^{K-1} \left| \sum_{n=0}^{M'-1} r(n + iM') e^{-j2\pi fn} \right|^2, \quad (2.60)$$

where  $M = KM'$  is the length of the single realization  $r(n)$ . Hence, for the Bartlett-based SCD, the test statistic in (2.48) can be rewritten as:

$$z_{\text{BAR}}(\tau) = \frac{1}{M'} \sum_{\tau=0}^{M'-1} \hat{S}_{\text{BAR},r}(\tau) S_s(\tau). \quad (2.61)$$

### 2.2.3.3 Performance Analysis

By exploiting the linearity of the DFT, it can be shown that the quadratic term in (2.60) follows a central chi-square distribution with two degrees of freedom and, as consequence of this fact, (2.61) has a central chi-squared distribution with  $2K$  degrees of freedom. This can be well approximated by a non-central chi-squared distribution  $\chi_{\kappa}^2(o)$  as long as the parameters  $\kappa$  and  $o$  are set such that the skewnesses of  $\chi_{\kappa}^2(o)$  and  $z_{\text{PER}}$  are equal and the kurtoses of  $\chi_{\kappa}^2(o)$  and  $z_{\text{PER}}(n)$  are reduced to a minimum [50]. This approximation allows

the probability of false alarm of the Bartlett-based SCD to be evaluated numerically in closed-form using

$$P_{\text{fa}}^{\text{SCD-BAR}} = \Pr [z_{\text{BAR}}(n) > \gamma | H_0] \quad (2.62)$$

$$= 1 - P \left( \frac{\gamma - c_1}{\sqrt{c_2}} \sigma_{\chi^2} + \mu_{\chi^2}; \kappa, o \right), \quad (2.63)$$

where the first two cumulants

$$c_1 = \frac{1}{M'} \sum_{\tau=0}^{M'-1} E \left[ \hat{S}_{\text{BAR},r}(\tau) \right] S_s(\tau) = \sigma_w^2 S_s \quad (2.64)$$

$$c_2 = \frac{1}{(M')^2} \sum_{\tau=0}^{M'-1} \text{Var} \left[ \hat{S}_{\text{BAR},r}(\tau) \right] S_s^2(\tau) = \frac{\sigma_w^4}{KM'^2} \sum_{\tau=0}^{M'-1} S_s^2(\tau) \quad (2.65)$$

are obtained from the moment generating function of (2.61) and  $\mu_{\chi^2}$  and  $\sigma_{\chi^2}$  account to mean and variance, respectively, of the proposed  $\chi_{\kappa}^2(o)$  distribution.

Also according to [50], the SCD in (2.61) can reliably detect TV signals at very low SNR. This is illustrated for the U.S. market, where analogue broadcast is easier to detect than digital broadcast. This is so because the signals compliant with the National Television Systems Committee (NTSC) standard have three sharp spectral features (corresponding to the luminance, chrominance, and audio carriers), while those based on ATSC have only one (the pilot tone located at the channel lower edge).

## 2.2.4 Cyclostationary Feature Detection

Modern communications rely on processes that, like source coding and modulation, are known to couple stationary message signals with pulse trains, sinusoidal carriers, and other periodic signals. Additional periodicities can be introduced by other processes along the transmit chain, such as sampling and multiplexing. This relaxes the classical assumption of stationarity and let the second and the higher order statistics of the target signals vary periodically over time. Cyclostationary signal analysis reveals underlying cyclostationarities that cannot be visualized in the PSD. This advantage can be exploited in a multitude of contexts that include interference rejection, blind channel equalization/identification, blind antenna array beam/null steering, signal identification and detection, and synchronization [111]. In this section, we provide a minimum background on cyclostationary signal processing theory required to discuss the theoretical implementations of *cyclostationary feature detectors* (CFD). Considering the low complexity requirements that are introduced by portable WSD, we then describe a couple of more practical CFD that will be used throughout the remainder of this dissertation.

### 2.2.4.1 General Approach

A discrete process  $x(t)$  is said to exhibit second order cyclostationarity if its mean and time-varying correlation are periodic with some period  $T$  [112]

$$\mu_x(t+T) = \mu_x(t) \quad (2.66)$$

$$R_x(t+T, \tau) = R_x(t, \tau) \quad (2.67)$$



with mean and autocorrelation defined as:

$$\mu_x(t) = E[x(t)] \quad (2.68)$$

$$R_x(t, \tau) = E[x(t)x^*(t - \tau)]. \quad (2.69)$$

The right hand of (2.67) can be expanded in Fourier series [112]

$$R_x(t, \tau) = \sum_{\alpha} R_x^{\alpha}(\tau) e^{j2\pi\alpha t} \quad (2.70)$$

with Fourier coefficients given by:

$$R_x^{\alpha}(\tau) = E[R_x(t, \tau) e^{-j2\pi\alpha t}] \quad (2.71)$$

$$= E[x(t)x^*(t - \tau) e^{-j2\pi\alpha t}]. \quad (2.72)$$

The Fourier coefficients above represent the cyclostationarity of  $x(t)$  in the time domain and are referred to as the *cyclic autocorrelation function* (CAF) of  $x(t)$ . For each time lag  $\tau$ , the CAF measures the strength of the sinusoid in  $t$  at a given cycle frequency  $\alpha$ . The CAF is not identically zero for all nonzero  $\alpha$  iff (2.69) contains an additive periodic component, *i.e.* if  $x(t)$  is cyclostationary.

Provided that  $T$  exceeds the width of the CAF, the Parseval's relation for Fourier transforms can be invoked to approximate (2.72) in terms of its *spectrum correlation function* (SCF) [112]:

$$S_x^{\alpha}(f) = \int_{-\infty}^{\infty} R_x^{\alpha}(\tau) e^{-j2\pi f\tau} d\tau. \quad (2.73)$$

#### 2.2.4.2 Test Statistics

Now that we have put in place the expressions that describe the Fourier pair  $R_x^{\alpha}(\tau) \Leftrightarrow S_x^{\alpha}(f)$  we can turn our attention into their application in the context of CFD. The bottom line of CFD is that nonlinearities are used to regenerate a spectral line of the received noisy signal at a cycle frequency  $\alpha$ . The test statistic of such *generic* CFD can be represented by a quadratic time-invariant system of the form

$$z_{\text{CFD}}(n) = \int_{-\infty}^{\infty} \int_{-\infty}^{\infty} k_{\alpha}(\tau_{s_1}, \tau_{s_2}) x(n - \tau_{s_1}) x(n - \tau_{s_2}) d\tau_{s_1} d\tau_{s_2}, \quad (2.74)$$

where  $\tau_{s_1}$  and  $\tau_{s_2}$  are time lags normalized by a sampling period  $T_s$ . If the kernel  $k_{\alpha}(\tau_{s_1}, \tau_{s_2})$  is selected so as to maximize the SNR of the regenerated spectral line, it can be shown that the optimum detector is the *single-cycle detector* (SD) [113]

$$z_{\text{SD}}(n, f) = \int_{-\infty}^{\infty} S_s^{\alpha}(f) * \hat{S}_{\text{PER},r}^{\alpha}(n, f) df e^{j2\pi\alpha n}, \quad (2.75)$$

where the ideal  $S_s^{\alpha}(f)$  is obtained from a stored noise-free replica of the target signal  $s(t)$  and then correlated with the *cyclic periodogram* of the received signal  $r(n)$

$$\hat{S}_{\text{PER},r}^{\alpha}(n, f) = \frac{1}{T} R_T(n, f + \alpha/2) R_T^*(n, f - \alpha/2), \quad (2.76)$$

where  $R_T(n, f)$  represents the sampled complex envelope of a narrowband spectral component with center frequency  $f$  and bandwidth on the order of  $1/T$ . Consistency can be achieved by smoothing/averaging cyclic periodograms [114], just like discussed in the previous section for the case of conventional periodograms.

It is evident from (2.75) and (2.76) that SD measures the cyclic periodograms of  $r(n)$  only at a single cycle frequency contained in  $s(t)$ . To regenerate all possible spectral lines, their complex envelopes need to be summed over all cycle frequencies. This likelihood-ratio detector is known as *multi-cycle detector* (MD):

$$z_{\text{MD}}(n, f) = \sum_{\alpha} z_{\text{SD}} e^{-j2\pi\alpha n} \quad (2.77)$$

$$= \sum_{\alpha} \int_{-\infty}^{\infty} S_s^{\alpha}(f) * \hat{S}_{\text{PER},r}^{\alpha}(n, f) df. \quad (2.78)$$

SD and MD offer robustness against noise uncertainty and ability to detect very weak signals in the presence of noise as major advantages. As for the disadvantages, both detectors are less practical from the implementation point of view because they are of high complexity and require substantial prior knowledge of target signals. In MD, the quantities  $S_s^{\alpha}(f)$  are phase-dependent so that the method is optimal only if the phases of  $s(t)$  are known. SD is a suboptimum solution that employs only one harmonic of the fundamental cycle frequency but still requires additional information about  $s(t)$ . The SCF computation common to both SD and MD involves bidimensional transforms that, unlike the real-valued unidimensional transforms typical in PSD-based analysis, are in general complex-valued.

To alleviate the complexity and energy burdens due to FFT computations, signal detection can be performed in the time domain by constructing test statistics based on the CAF of  $r(t)$ . This approach is particularly interesting for “blind” detection of orthogonal frequency division multiplexing (OFDM) signals because the lack of information about the number of subcarriers may cause a mismatch of FFT parameters, thus reducing the performance of FFT-based methods [115]. In case of OFDM, the target signals can be represented in continuous-time domain as

$$\tilde{s}(t) = \sum_{k=0}^{N_s-1} \sum_{l=-\infty}^{\infty} C_l(k) g(t - lT_{\text{SYM}}) e^{j2\pi\Delta f k(t - lT_{\text{SYM}})}, \quad (2.79)$$

where  $k$  is the subcarrier index,  $l$  is the symbol index,  $C_l(k)$  is the complex constellation transmitted by the  $k$ th subcarrier during the  $l$ th symbol,  $g(t)$  is a pulse shaping filter,  $T_{\text{SYM}}$  is the symbol duration, and  $lT_{\text{SYM}} \leq t \leq (l+1)T_{\text{SYM}}$ . The discrete-time representation of (2.79) is obtained by using a sampling period  $T_s$ , *i.e.*  $s(n) = \tilde{s}(nT_s)$ , so the subcarrier spacing is  $\Delta f = 1/(N_s T_s)$ . Observing the form of the  $l$ th symbol

$$\tilde{s}_l(t) = \sum_{k=0}^{N_s-1} C_l(k) e^{j\frac{2\pi}{N_s T_s} k(t - lT_{\text{SYM}} T_s)} \quad (2.80)$$

it is convenient to generate the samples corresponding to each symbol by taking the inverse FFT (IFFT) of  $C_l(k)$ ,  $k \in [0, N_s - 1]$ . This yields each symbol having duration equal to the IFFT length, *i.e.*  $T_{\text{SYM}} = T_{\text{FFT}}$ , so the subcarrier spacing becomes  $\Delta f = 1/T_{\text{FFT}}$ .

To absorb the inter-symbol interference (ISI) caused by time-dispersed channels, a cyclic prefix (CP) is added before transmission. If the CP duration is  $T_{CP}$ , this cyclic extension is accomplished by copying the last  $T_{CP}/T_{FFT}$  samples of a symbol and appending them to the front of the same symbol. In this fashion, a guard period is created in the time domain and the symbol duration becomes  $T_{SYM} = T_{CP} + T_{FFT}$ . Nevertheless, CP-based multi-carrier systems remain sensitive to synchronization errors. Such errors may compromise the independence among subcarriers and thus degrade performance, particularly when  $N_s$  is large. In most existing OFDM-based standards, this drawback is mitigated by allocating pilot symbols with the same amplitude in the frequency domain. The pilot positions are predefined and follow a pilot insertion pattern created by some pseudo random binary sequence (PRBS) so as to reduce PAPR. As we will see in Chapter 3, the OFDM-based target signals considered in this dissertation have both CP and frequency-domain pilots, so the signal generation process follows the block diagram depicted in Figure 2.5.

Figure 2.6 illustrates how the detection process can take advantage of the cyclostationarities induced by the CP to distinguish between  $H_0$  and  $H_1$ . The discrete autocorrelation surfaces are highlighted by normalizing  $\alpha$  and  $\tau$  to  $T_{SYM}$  and  $T_{FFT}$ , respectively. For both  $s(n)$  and  $r(n)$ , these surfaces occur at  $\alpha = n/T_{SYM}$ ,  $n = \pm 1, \pm 2, \dots$ , with peaks of similar magnitude at  $\tau/T_{FFT} = \pm 1$ . Unlike, the CAF of a stationary process such as AWGN exhibits magnitudes that are essentially zero for any  $\alpha$  except for a peak at  $\alpha = \tau = 0$ . This explains the noticeable magnitude gain verified at  $\alpha = \tau = 0$  in the CAF of the received signal. It is evident that CFD needs to know the cycle frequencies where the cyclostationarities occur in order to determine the presence of  $r(n)$  based on its CAF. Substantial complexity and time savings can be obtained by performing cyclostationary analysis in the time domain (as compared to SD-based analysis in the frequency domain), but the full computation of the CAF may still be prohibitive for some applications. To overcome this practical shortcoming, we can use a “simplified” CAF that measures all cycle frequencies yet only at some (a priori known) lags of interest, measures  $\alpha = 0$  at all lags, or a combination of both. For  $\alpha = 0$ ,  $R_x^\alpha(\tau)$  and  $S_x^\alpha(f)$  reduce to the conventional ACF and PSD, respectively.

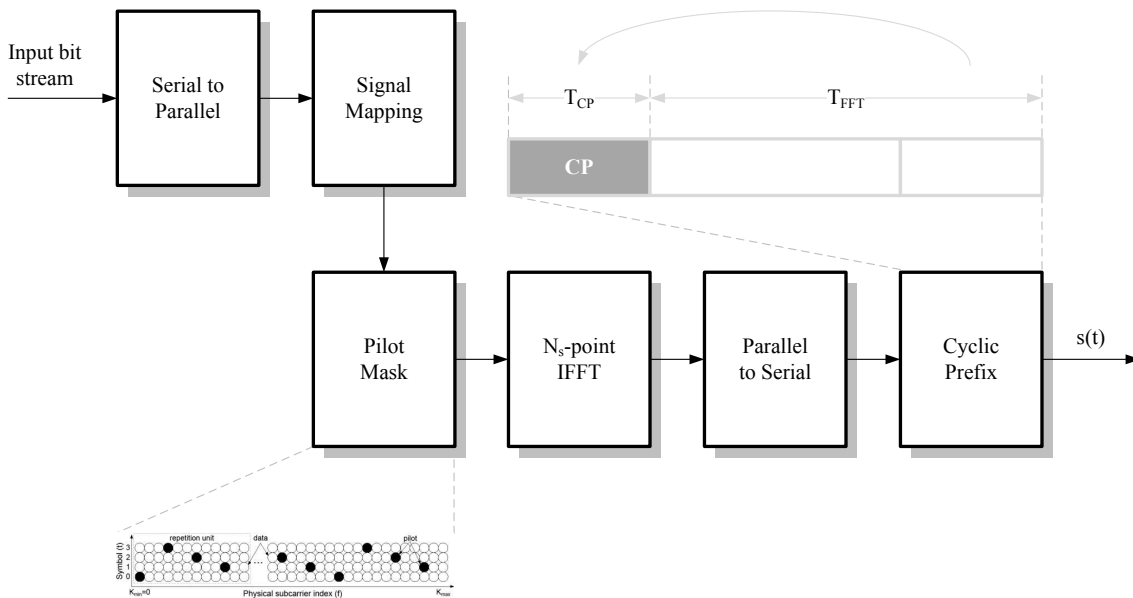
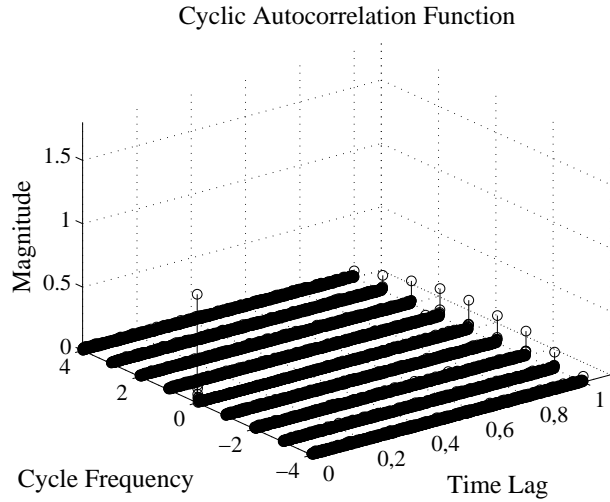
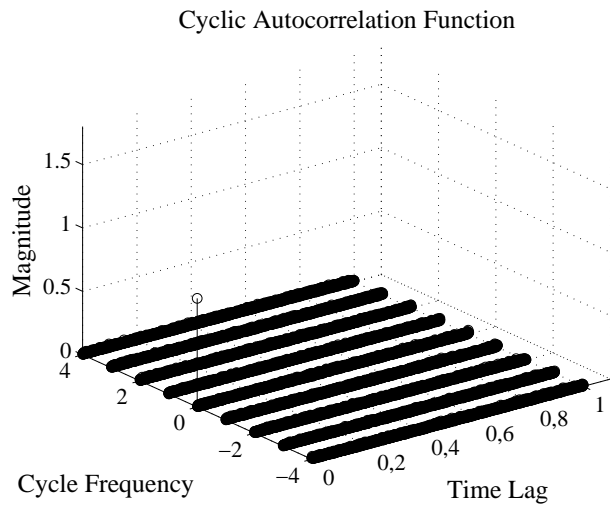


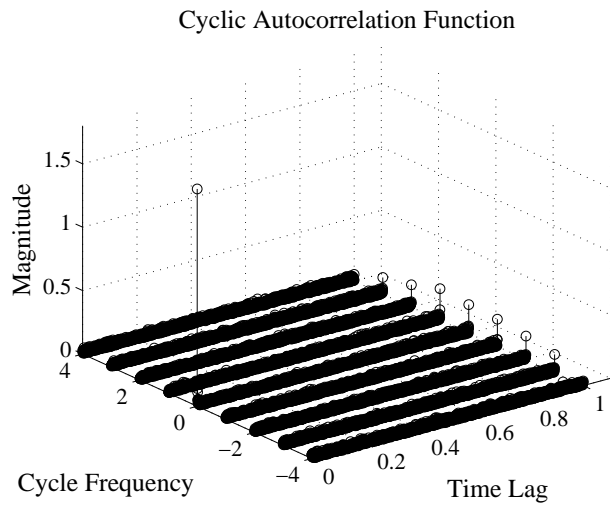
Fig. 2.5: Simplified block diagram of a baseband OFDM transmitter.



(a) Transmitted signal



(b) Noise signal



(c) Received signal ( $\text{SNR}|_{\text{dB}} = -3 \text{ dB}$ )

**Fig. 2.6:** Exemplary CAF plots obtained by making  $x(t)$  equal to three OFDM symbols in (2.72). The negative (symmetric) time lags were omitted for simplicity ( $N_s = 2048$ ,  $\text{CP} = 1/4$ ).

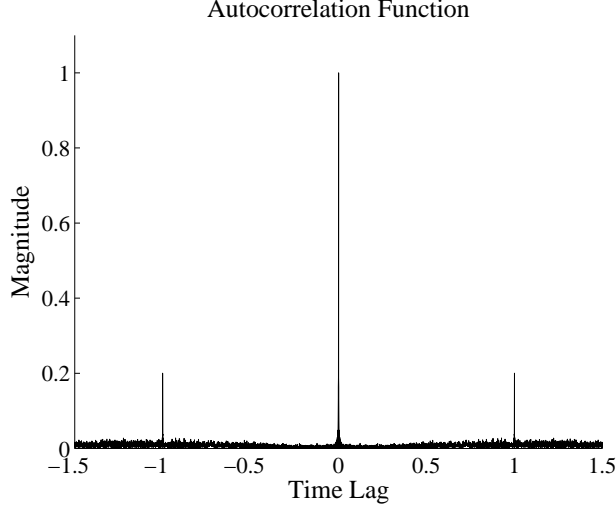


**Fig. 2.7:** Exemplary ACF plot obtained by making  $\alpha = 0$  and  $x(t)$  equal to three OFDM symbols in (2.72). Time lags are normalized by the useful symbol length  $T_{\text{FFT}}$  ( $N_s = 2048$ ,  $\text{CP} = 1/4$ ).

Figure 2.7 suggests that we can construct a test statistic to exploit the fact that the time interval between the major peak (at  $\tau = 0$ ) and any secondary peak (at  $\tau = \pm 1$ ) in the ACF of an OFDM signal should be equal to the useful symbol length  $T_{\text{FFT}}$ . In fact, it can be shown that the ACF coefficients at lags  $\tau = \pm T_{\text{FFT}}$  correspond to the log likelihood ratio test statistic (LLRT) in the low SNR regime [116]. If  $T_D = T_{\text{FFT}}/T_s$  and  $T_C = T_{\text{CP}}/T_s$  respectively denote the total number of data samples per symbol and the number of samples in the CP of a symbol, the hypotheses in (2.2) can be rewritten in terms of the ACF coefficient  $\varphi(\tau) = E[x(t)x^*(t - \tau)] / E[x(t)x^*(t)]$

$$\begin{cases} H_0 : \varphi(\pm T_D) = 0 \\ H_1 : \varphi(\pm T_D) = \varphi_{\text{chan}} \end{cases} \quad (2.81)$$

with the value under  $H_1$  given by [116]

$$\varphi_{\text{chan}} = \frac{T_C}{(T_D + T_C)} \frac{\nu_{\text{chan}} \sigma_s^2}{(\nu_{\text{chan}} \sigma_s^2 + \sigma_w^2)}, \quad (2.82)$$

where the parameter  $\nu_{\text{chan}}$  dictates the channel model, *i.e.*  $\nu_{\text{chan}} = 1$  for AWGN and  $\nu_{\text{chan}} = \sum_{m=0}^{L-1} E[|h(m)|^2]$  for a multipath channel of order  $L$ .

Based on the NP criterion with CFAR, two test statistics and their corresponding distributions under  $H_0$  and  $H_1$  are derived in [116] for *autocorrelation-based detectors* (ACD) that require different amounts of prior knowledge of target signals. The first proposed ACD entirely lacks information about the CP length, whereas the second one requires both CP length and synchronization for detection. On the one hand, perfect synchronization between WSD and licensed transmitters may be quite unrealistic in practice. On the other hand, some information about  $T_C$  or  $T_D$  will typically be available or can be obtained by testing different values from a likely small set of allowed options.

While the assumptions that the CP length is known and synchronization is perfect can provide an upper bound on the performance of that would result otherwise, *i.e.* in case this information partially or entirely lacks [116], it is more realistic to keep the amount

of prior information of target signals at a minimum. An alternative ACD, which needs to know only the number of data samples per symbol  $T_D = T_{\text{SYM}}/T_s$  has the following test statistic [118]

$$z_{\text{ACD}}(n) = \frac{\frac{1}{M-T_D} \sum_{n=0}^{M-T_D-1} \text{Re} \{r(n)\}}{\frac{1}{M} \sum_{n=0}^{M-1} |r(n)|^2}, \quad (2.83)$$

which evaluates the ACF of  $r(n)$  at just one side peak induced by the CP and normalizes the outcome by the energy of  $r(n)$ . For a real-valued ACF coefficient,  $\varphi(\tau) = \varphi(-\tau)$  and any of the side peaks can be used in (2.83) without loss of generality.

By inspecting Figure 2.7 again, we see that the ACF of an OFDM signal exhibits symmetric secondary peaks. This allows one to construct an alternative test statistic that exploits this symmetry property. The test statistic of this *blind twin peak detector* (BTPD) is [119]

$$z_{\text{BTPD}}(n) = \sum_{\tau_s} \frac{1}{M} \sum_{n=0}^{M-1} r(n)r^*(n - \tau_s), \quad (2.84)$$

where  $\tau_s$  are time lags normalized by a sampling period  $T_s$ . After having computed the ACF of  $r(n)$ , BTPD carries out a peak search to determine the secondary peaks on both sides of the ACF, *i.e.* at  $\tau_s = \pm T_{\text{FFT}}$ . The channel is declared occupied in case symmetry holds. As a by-product of this process, the position of the positive peak relative to  $\tau_s = 0$  can be used to determine the subcarrier spacing  $\Delta f$ .

### 2.2.4.3 Performance Analysis

The performance analysis of CFD is in general mathematically intractable and the Monte Carlo (MC) method has to be used for setting threshold and evaluating  $P_{\text{fa}}$  and  $P_{\text{d}}$  [52]. The performances of some ACD (not considered in this dissertation) are investigated via simulation in [116] when generic OFDM signals are detected under AWGN, multipath, and shadowing scenarios. If different nodes “see” independent channels it is shown that cooperation can mitigate the undesirable effects introduced by shadowing. The detection of signals based on the Digital Video Broadcast-Terrestrial (DVB-T) standard [117] over Rayleigh and Rice fading channels is considered in [118], where it is shown that the frequency selectivity of the channel does not influence much the performance of ACD. Among the five state-of-the-art OFDM detectors investigated therein, the ACD in (2.83) shows performance similar to that of other detectors but has the advantage of needing only  $T_D$  to work. The detection of DVB-T signals in noise of uncertain power is investigated in [119] and [120] when BTPD operates under AWGN and multipath fading, respectively. Among the four CP-based methods discussed therein, BTPD is the one that offers the best compromise between detection performance and complexity in real-time implementation and is robust against noise uncertainty. The double of  $\tau_s$  values required in (2.84) makes BTPD twice as complex as ED (and ACD) but this apparent disadvantage can be used to obtain a posteriori knowledge of  $\Delta f$ . Once  $\Delta f$  has been determined, we can employ BTPD to distinguish between two OFDM signals that have different subcarrier spacings. Obtaining signal classification ability at the expense of some increase in complexity seems reasonable and may become quite desirable if WSD need to resolve for different OFDM-based target signals within a multi-standard operation environment. As a disadvantage, ACD and BTPD are dependent of the number of subcarriers and the CP length of the

target signal. This dependence is studied in [115] for multi-mode generic OFDM signals and confirmed in [121] for CP-based methods in general.

CFD is applicable to detect non-OFDM signals too. The cyclostationary features embedded in Phase Alternating Line (PAL) signals [122] and frequency-modulated (FM) signals, conveyed by PMSE, are exploited in [123] to detect the presence of such analogue systems under AWGN. In case of PAL, it is assumed that prior knowledge of the picture and audio carriers is available so that a couple of SD can be used to detect the four spectral peaks induced at  $\pm 3.5$  MHz and  $\pm 15.5$  MHz, respectively. However, we will see later in this section that the narrowband FM-based signals used in PMSE can be centered anywhere within the TV channel. This means that, in practice, no prior information is available in this case. This issue is addressed using MRSS under AWGN in [124] and then extended to multipath fading channels in [125]. Basically, the idea is to construct test statistics to maximize the SCF over all cyclic frequencies. Beside of being highly complex (MD is required), both approaches are slightly susceptible to noise uncertainty.

## 2.2.5 Other Feature Detectors

A number of *other feature detectors* (OFD), not necessarily cyclostationary, can be used as signal specific techniques. To keep the sensing time requirements low, it is preferable to select a feature that is transmitted the most frequently as possible. Since the availability and strength of a feature largely depend on the target signal, the structure of this section slightly differs from the rest of this chapter in the sense that: (i) for simplicity, we group methods having different working principles in the OFD class; and (ii) we discuss the related work in terms of OFDM-based signals and non-OFDM signals.

### 2.2.5.1 OFDM-based Signals

In emerging TVBD standards, such as IEEE 802.22 [126] and ECMA-392 [127], the use of *preambles* is advanced to perform a number of tasks including synchronization, channel estimation, frequency offset estimation, and received power estimation. Detection based on preambles has the advantage of allowing different levels of sensitivity, *e.g.* depending on whether the entire preamble is detected or just part of its training sequences [128]. In general, preambles are not used in digital TV standards so that synchronization and channel estimation have to be realized by other means. Similar to DVB-T, the Integrated Services Digital Broadcasting-Terrestrial (ISDB-T) standard [129] is OFDM-based and mandates the use of *scattered pilots* (SP) modulated at boosted power level to accomplish these tasks. In contrast, the Digital Terrestrial Multimedia Broadcast (DTMB) standard relies on time-domain synchronous OFDM (TDS-OFDM) where the CP is replaced by a known pseudo noise (PN) sequence that, beside of playing the role of a guard interval, allows to channel estimation and synchronization in the time domain. Together with ATSC, discussed later on in this section, DVB-T and ISDB-T account for the absolute majority of TV broadcasts in digital format around the globe, while DTMB is deployed only in China, Hong Kong, and Macau. Therefore, and since SP are also available in IEEE 802.22 and ECMA-392 signals, we limit the discussion that follows to CP-OFDM signals. For TDS-OFDM, some sensing algorithms that utilize the PN sequences embedded in the DTMB frame headers can be found in [130].

Consider the OFDM signal represented in continuous-time domain

$$\tilde{s}_p(t) = \sum_{k=0}^{N_s-1} \sum_{l=-\infty}^{\infty} C_l(k) e^{j2\pi\Delta f k(t-T_{\text{CP}}-lT_{\text{SYM}}T_s)}, \quad (2.85)$$

where  $lT_{\text{SYM}} \leq t \leq (l+1)T_{\text{SYM}}$  and the indexes  $(k, l)$  are in the set  $\mathbb{P}$  of subcarriers onto which the SP are mapped. As long as the OFDM parameters of the target signals are available, the coefficients  $C_l(k)$  will be fixed and known for  $k, l \in \mathbb{P}$ . In this case,  $\tilde{s}_p(t)$  becomes deterministic and can be exploited for detection. If  $f_s$  is a standard-compliant elementary sampling frequency, *i.e.* determined such that target signals fulfill standardized bandwidth requirements, the test statistic of this *scattered pilot detector* (SPD) is [118]

$$z_{\text{SPD}}(n) = \max_{\tau_s \in \{0, 1, \dots, T_{\text{cyc}}-1\}} \left| \sum_{n=0}^{M-1-\tau_s} s_p(n) r^*(n + \tau_s) \right|, \quad (2.86)$$

where the sequence  $s_p(n) = \tilde{s}_p(nT_s)$  is cyclic with period  $T_{\text{cyc}}$ . Though capable of outperforming ED and other four state-of-the-art OFDM detectors under AWGN (at the expense of an increased amount of information of the target signals), the SPD in (2.86) can poorly detect DVB-T signals when operating under multipath fading [118].

The drawback above can be overcome by exploiting the property that the mean of the *time-domain symbol cross-correlation* (TDSC) of two OFDM symbols is nonzero as long as those symbols have the same frequency-domain SP. The *accumulated TDSC function* can be defined as

$$\Psi_{\text{TDSC}}(\Delta l) = \frac{1}{N_1 N_s} \sum_{l'-l=\Delta l}^{N_1} \sum_{n=0}^{N_s-1} x_l(n) x_{l'}^*(n), \quad (2.87)$$

where the indexes  $l$  and  $l'$  denote the symbols that have the same SP pattern,  $\Delta l = l' - l$  is the symbol index difference, and  $N_1$  is the number of correlated symbol pairs having the same SP pattern. In the context of CR, (2.87) was originally introduced in [121] along with two different TDSC approaches. The first one, based on the NP criterion, works only for  $\Delta l$  fixed. The test statistic is:

$$z_{\text{TDSC-NP}}(\Delta l) = |\Psi_{\text{TDSC}}(\Delta l)|. \quad (2.88)$$

The second approach relies on *maximum ratio combining* (MRC) to improve performance by combining the various  $\Psi_{\text{TDSC}}(\Delta l)$  that arise when different  $\Delta l$  are used. This allows one to construct a new test statistic

$$z_{\text{TDSC-MRC}}(\Delta l, \Delta l + \xi) = \left| \sum_{\Delta l} N_1 N_{1+\xi} \Psi_{\text{TDSC}}(\Delta l) \Psi_{\text{TDSC}}^*(\Delta l + \xi) \right|, \quad (2.89)$$

where the products  $N_1 N_{1+\xi}$  are the combining coefficients and  $\Psi_{\text{TDSC}}(\Delta l) \Psi_{\text{TDSC}}^*(\Delta l + \xi)$  expresses the conjugate product of two accumulated TDSC functions.

TDSC methods perform similarly under both AWGN and multipath fading channels (Rice and Rayleigh) and are not impacted by DVB-T signals with different CP lengths, though TDSC-MRC outperforms TDSC-NP at the expense of increased complexity [121]. MRC is known to be the optimal combining scheme but since it requires knowledge of all the



fading parameters its optimality comes at the expense of increased complexity and amount of channel information [131]. TDSC methods are further investigated in [132], where real-world DVB-T captures and filter bank multi-carrier (FBMC) signals are detected when knowledge of the noise power and synchronization are both imperfect. Under such practical operation conditions, it is shown via simulations that the performance of TDSC methods is independent of noise uncertainty and carrier frequency offsets (CFO) but TDSC-NP is more robust than TDSC-MRC against sampling frequency offsets (SFO).

CFO and SFO need to be modeled for a better understanding of how the detection process is impaired in the presence of synchronization errors. Assuming synchronized sampling, the individual impact of CFO can be considered by passing (2.80) through the channel and receiving its noisy version at a mismatched carrier frequency  $f'_c$  [133]

$$\tilde{r}_l(t) = \frac{1}{N_s} \sum_{k=0}^{N_s-1} H(k)C_l(k)e^{j\frac{2\pi}{N_s T_s}k(t-lT_{\text{SYM}}T_s)}e^{j\frac{2\pi}{N_s T_s}\epsilon_c t} + w_l(t), \quad (2.90)$$

where it is seen that the normalized CFO  $\epsilon_c = (f'_c - f_c)/\Delta f$  equally affects all subcarriers. If the licensed transmitter and WSD are not synchronized but  $f_c$  is known a priori by the former ( $\epsilon_c = 0$ ), then the individual impact of SFO results from sampling (2.80) using an incorrect sampling period  $T'_s$ . This introduces a sample timing drift per OFDM symbol  $t_d = (T'_s - T_s)T_{\text{SYM}}$  that yields

$$r_l(n) = \frac{1}{N_s} \sum_{k=0}^{N_s-1} H(k)C_l(k)e^{j\frac{2\pi}{N_s}k\left[n\left(\frac{T'_s}{T_s}\right) - lT_{\text{SYM}}\left(\frac{\epsilon_s}{1+\epsilon_s}\right)\right]} + w_l(n), \quad (2.91)$$

where  $\epsilon_s = (f'_s - f_s)/f_s$  is the normalized SFO. The detrimental effects introduced by CFO and SFO are better perceived by looking at the frequency-domain samples of (2.90) and (2.91). In this fashion, it is shown in [134] that CFO causes the same amplitude reduction and phase shift of  $C_l(k), \forall k$ , whereas these impacts are not equal for all subcarriers in case of SFO. In addition, both types of frequency offsets create inter-carrier interference (ICI) due to the loss of orthogonality between subcarriers.

### 2.2.5.2 Non-OFDM Signals

We have seen that the detection of OFDM signals can be greatly facilitated by exploiting the cyclostationarity introduced by appending the CP or correlating the SP mask in the time domain. Depending on the standard under consideration, non-OFDM signals may also possess several distinguishing features that can be exploited for detection. The first step when searching for such features is to examine the structure of the target signals. For instance, ATSC signals are structured in frames, fields, and data segments, each data segment consisting of 832 symbols [135]. The first four symbols, denoted as *data segment SYNC*, provide synchronization within a data segment. The remaining 828 symbols of a data segment carry data, which is modulated using eight-level pulse amplitude modulation (PAM). At the field level, synchronization is provided by PN sequences referred to as *data field SYNC*. As shown in Figure 2.8, after the frames are formatted and multiplexed with SYNC signals, a in-phase pilot is added to every symbol to facilitate carrier recover at the ATSC receiver.

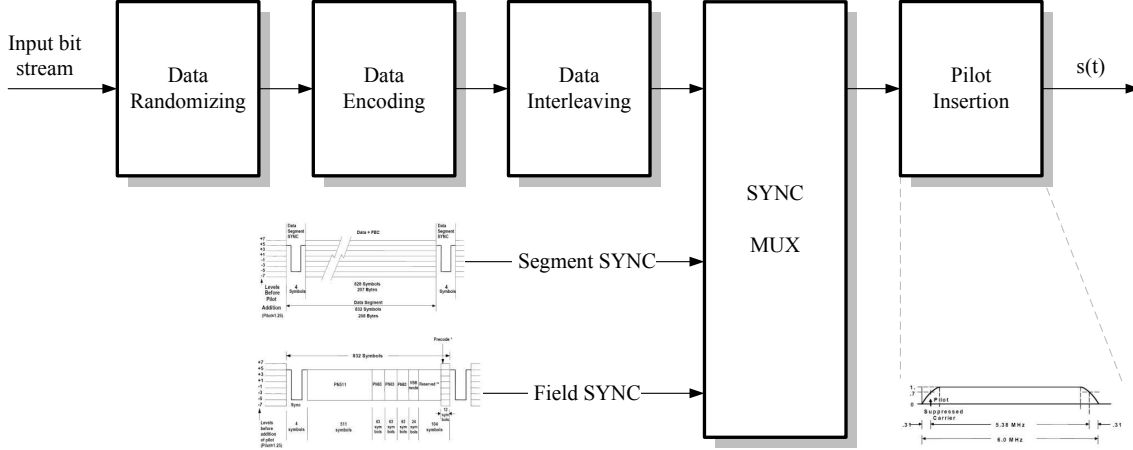


**Fig. 2.8:** Simplified block diagram of a baseband ATSC transmitter (adapted from [135]).

Since the pilot sits at a known location relative to the signal (about 310 kHz away from the lower channel edge) it is perhaps the most widely feature used in spectrum sensing for ATSC signals. Algorithms based on the energy and location of the pilot are proposed in [136] and evaluated using a set of signals especially created in laboratory so as to reflect real-world conditions. In some of these signals, the pilot tone is attenuated due to multipath fading thus causing performance losses up to 6.5 dB in both algorithms. All in all, the pilot-energy algorithm performs slightly ( $\approx 1$  dB) better than the pilot-location algorithm. Nevertheless, an advantage of the algorithms exploiting the pilot location is that the noise power needs not be exactly known, whereas algorithms that measure the pilot energy are susceptible to noise uncertainty.

Whether targeting at the energy or the position of the pilot tone, reliable detection becomes hard if strong signals are transmitted in the lower adjacent channel, *i.e.* the pilot can be easily shadowed by the power leakage. This issue can be overcome by using interference alleviating filters before detection, exploiting other signal features, or a combination of both. Though this cannot be seen in Figure 2.8, the SYNC signals used in ATSC have distinguishing features. Unlike the ordinary 8-PAM data symbols, they are periodic binary modulated signals that are not passed through any randomizer, encoder, nor interleaver. The PN sequences used in data field SYNC signals are inserted into the data stream at most every 24.20 ms, while the data segment SYNC symbols occur regularly at intervals of  $77.30 \mu\text{s}$ . It is evidently better to exploit the data segment SYNC symbols because their higher repeating rate will allow to reduced sensing time requirements. Also, as compared to the pilot, the data segment SYNC provides a stronger feature for detection because its power is spread almost over the whole TV channel. The idea of exploiting the correlation of two data segment SYNC elements to detect ATSC signals is presented in [51]. The derivation of a test statistic to this purpose follows the lines used to construct the test statistics of TDSC methods. To begin with, define the *accumulated SYNC function*

$$\Psi_{\text{SYNC}}(n_0, \tau_d) = \frac{1}{4N_{\tau_d}} \sum_{n=0}^{N_{\tau_d}-1} \sum_{l=0}^3 r(n_0 + l + 832n) r^*[n_0 + l + 832(n + \tau_d)], \quad (2.92)$$

where  $n_0$  is the starting sample index,  $l$  the symbol index in a data segment SYNC,  $\tau_d$  is a non-zero positive integer representing the correlation delay in terms of data segments, and  $N_{\tau_d}$  is the number of pairs of data segment SYNC that are distant  $\tau_d$  data segments from each other.

For a certain sensing time, the noise embedded in (2.92) is low correlated for different  $\tau_d$  values. This means that performance can be improved by linearly combining the various  $\Psi_{\text{SYNC}}(n_0, \tau_d)$  that result from different  $\tau_d$ . The test statistic of this *ATSC segment SYNC detector* (ASSD) is

$$z_{\text{ASSD}}(n_0, \tau_d) = \max_{0 \leq n_0 \leq 831} \left| \sum_{\tau_d} N_{\tau_d} N_{\tau_d+1} \Psi_{\text{SYNC}}(n_0, \tau_d) \Psi_{\text{SYNC}}^*(n_0, \tau_d+\xi) \right|, \quad (2.93)$$

where  $N_{\tau_d} N_{\tau_d+1}$  are the combining coefficients and  $\xi = 1$  allows to efficient utilization of all conjugate products of two accumulated SYNC functions  $\Psi_{\text{SYNC}}(n_0, \tau_d) \Psi_{\text{SYNC}}^*(n_0, \tau_d+\xi)$  obtained in a fixed sensing time.

Signals compliant with the NTSC standard have a rate of 29.97 frames/s and consist of 525 lines per frame, each line having duration of 63.55  $\mu\text{s}$  [122]. All but the first nine lines within a field contain a horizontal SYNC (HSYNC) signal, most followed by a color burst that serves as a reference signal to the receiver. Since this is analogous to the data segment SYNC of ATSC, (2.92) and (2.93) can be modified to yield a *NTSC horizontal SYNC detector* (NHSD). The performances of ASSD and NHSD have been investigated in [51] when field captured data files are detected under AWGN. The densities of the HSYNC signal and the data segment SYNC are about 7.40% and 0.48%, respectively, so NHSD outperforms ASSD in all cases studied. Intuitive extensions to scenarios other than AWGN can be made by noting that  $\tau_d$  is sufficiently large in ATSC and NTSC. Both detectors should experience the same timing offsets, frequency offsets, and multipath effects.

In contrast to standard-compliant target signals, PMSE signals are technically more challenging to detect. PMSE systems adopt devices such as wireless microphones (WM) that convey nonstandardized signals and thus may fail to make efficient use of spectrum. As seen in Section 1.3, this is one of the reasons that motivated the FCC in not reserving more spectrum to WM use in the U.S. [18]. In parallel, significant effort towards improving the spectrum efficiency of PMSE has been put on digital technologies that rely on proprietary modulation schemes. Thanks to this effort, it is possible today to pack about 30 digital WM units into a 6 MHz channel. Other critical issues, such as quality of service, have also been addressed and some chipsets currently available can deliver very high audio quality with delay as low as 1.89 ms [137]. Nevertheless, to the best of our knowledge, the task of detecting signals conveyed by hybrid and digital WM has not been addressed to date<sup>1</sup>. Particularly, in the context of WSD, most emphasis has been put on the problem of detecting FM-based WM operated by PMSE in the TV bands.

Consider the FM signal represented in continuous-time domain [51]

$$\tilde{s}_{\text{FM}}(t) = A_c \cos \left[ 2\pi f_c t + 2\pi f_{\text{dev}} \int_0^t m(u) du + \theta \right], \quad (2.94)$$

where  $A_c$ ,  $f_c$ , and  $f_{\text{dev}}$  are the magnitude, center frequency, and frequency deviation of the carrier used to modulate the audio signal  $m(t)$  and the random phase  $\theta$  is uniformly

<sup>1</sup> This may be due to the fact that digital WM operation is typically targeted at higher frequency bands, *e.g.* 2.4 GHz and 6.1–6.6 GHz bands. Another possible reason is that, despite of its potential to improve efficiency, digitisation is still controversial because of the concerns it raises about battery lifetime and suitability for some PMSE use cases. Hence, though some manufacturers have already started offering hybrid analogue/digital and purely digital systems, the currently deployed WM are mostly based on FM.

distributed in  $(0, 2\pi)$ . Typically, the values assumed by  $m(t)$  and  $f_{\text{dev}}$  make (2.94) resemble a pure sinusoid at low SNR. In the frequency domain, this corresponds to a “spike” that can be *theoretically* exploited for detection because of the SNR *boost* created by the ratio of the occupied signal bandwidth and the much larger bandwidth of a TV channel.

When the WM input is silent, the phase  $\theta$  changes very slowly with the time so that the PSD of a practical WM signal may contain more than a single narrowband spike. Distinction between the intended WM signals and other unintended signals becomes hard in this case due to a number of issues [138]. Firstly, the presence of multiple narrowband spikes also characterizes other signals including spurious emissions, quantization noise, leakages from adjacent channels, and other RF impairments. This is the reason why the laboratory tests in [22] had to be carried out in an anechoic chamber. Secondly, lack of standardization results in operational parameters that vary according to manufacturer and device model, *e.g.*  $f_c$ ,  $f_{\text{dev}}$ , and side-tone placements. Since  $f_c$  is not fixed, multiple WM units are free to operate *anywhere* within a TV channel. This issue reinforces the importance of blind techniques, among which EBD and wavelet-based MRSS have been receiving special attention. While EBD usually assumes perfect knowledge of  $f_c$  [103][108][109], this assumption can be relaxed in MRSS because the sensing resolution can be matched to the occupied signal bandwidth ( $W$ ) [124]. Wherever the application permits, more sophisticated spectrum estimation techniques may be used to estimate  $f_c$  before performing detection. This is the case of the *pseudospectra* obtained via autoregressive modeling. The magnitude of the peaks exhibited in the pseudospectrum no longer represent the actual power levels but it can be used to extract the center frequencies of the sinusoids buried in noise [139]. See [140] for an application of pseudospectra in the context of WM signals.

In the U.S., the FCC mandates that PMSE operation should be 25 kHz offset from the upper and lower limits of a 6 MHz channel. Formed from a combination of adjacent 25 kHz segments,  $W$  should not exceed a maximum of 200 kHz. This limits the total number of possible carrier frequencies to  $N_f = 1 + (6 \text{ MHz} - 100 \text{ kHz}) / (25 \text{ kHz}) = 237$  carriers. If all possible carrier frequencies are collected into the set  $\mathbb{F} = f_{c_0}, f_{c_1}, \dots, f_{c_{N_f-1}}$ , one can take advantage of this prior knowledge using the test statistic [51]

$$z'_{\text{MF}}(f_c) = \max_{f_c \in \mathbb{F}} z_{\text{MF}}(f_c) \quad (2.95)$$

with the test statistic for each individual  $f_c$  being a *matched filter* (MF) of the form

$$z_{\text{MF}}(f_c) = \sum_{\tau_s} R_r(\tau_s) \cos(2\pi f_c \tau_s), \quad (2.96)$$

where  $\tau_s$  are time lags normalized by a sampling period  $T_s$  and the autocorrelation  $R_r(\tau_s)$  is computed for and averaged over different  $\tau_s$  values. Since  $\tilde{s}_{\text{FM}}(t)$  and  $n(t)$  are both zero-mean and independent processes,  $R_r(\tau_s)$  can be obtained from the sum of ACFs

$$R_r(\tau_s) = R_s(\tau_s) + R_n(\tau_s), \quad (2.97)$$

where the  $R_s(\tau_s)$  that results from plugging (2.94) into (2.44) can be simplified to

$$R_s(\tau_s) \approx \frac{A_c^2}{2} 2\pi f_c \tau_s \quad (2.98)$$

provided that  $f_c$  is much larger than both  $f_{\text{dev}}$  and  $\tau_s$  [51].

In general, MF is known to be the optimum detector that maximizes the received SNR when prior knowledge of the target signal is available. Another distinguishing feature of MF is that the required number of samples scales only as  $\mathcal{O}(1/\text{SNR})$  in the low SNR regime, thus allowing to achieve a given operation point  $(P_{\text{fa}}, P_{\text{d}})$  in the ROC using shorter sensing time than ED. As for the disadvantages, the use of MF imposes tight synchronization, high implementation complexity, and high power consumption [47]. With respect to the specific implementation in (2.96), the optimality of MF holds only when  $f_c$  is known. Otherwise, the exhaustive search performed in (2.95) results in increased complexity and degraded performance. It is also worth noting that, even in case of known  $f_c$ , (2.96) acts as a tone detector and as such it is sensitive to those unintended spikes typically present in practical operation environments.

## 2.3 Chapter Summary

In this chapter, we have reviewed the related work that served as the basis for the contributions made in this dissertation. Specifically, based on a number of selected publications, we have summarized the most promising signal processing techniques for TVBD and more general WSD applications. From this survey, it turns out that the related work currently lacks contributions on the following aspects:

- **Baseline for comparison:** Number of samples, channel bandwidth, sensing time, type and characteristics of target signals, channel model (along with multipath profiles where appropriate), and number of runs over which the results obtained through MC simulation are averaged constitute aspects that play a crucial role in the resulting performance of any method. In the absence of one or more of these settings, as typical in the literature, it is hard to establish *fair* comparisons even when the methods being compared belong to the same class, the assumptions made when modeling the detection process are the same, and/or the operation environment taken into account is similar.
- **Broader scope of application:** At the time of this writing, the majority of publications available in the spectrum sensing literature used to evaluate the performance of proposed methods having only a *single* market in mind, *e.g.* the detection of ATSC signals in the U.S. or of DVB-T signals in Europe. As we have advocated in Chapter 1, the commercial success of WSD based on a given method depends on the ability of that method in achieving economies of scale. This calls for WSD designed to operate in *multiple* markets where different types of licensed systems, not necessarily collocated deployed, may be operating. On the one hand, it may seem tempting for those supporting the use of GDA to fulfill this goal by equipping WSD with additional hardware to determine location. On the other hand, we also have seen in Chapter 1 that GDA introduces extra costs to WSD design, suits only spatially static environments, and cannot alleviate the digital dividend. Cooperation-based approaches like CSS and WSN are thus more advantageous because they are network-centric (alleviate burdens to WSD design) and offer a broader scope of application. However, we have seen in this chapter that much has been done in terms of signal detection but the literature on signal classification has not managed yet to distinguish target signals based on multiple standards. See, *e.g.* [141] and the references therein for a survey on signal classification approaches.

- **Deeper understanding of information acquisition:** While most work on CSS relates to the processes of exchange and fusion of information, the information acquisition process has received less attention to date. At the local level, spectrum sensing has been typically modeled using techniques that are blind (EBD) or semi-blind (ED). Therefore, it is hard to name a single contribution that deals with the case where the nodes engaged in cooperation rely on signal specific techniques to perform local sensing. In this context, an interesting research question that remains open is whether different local sensing methods allow to different cooperation gains. Likewise, the benefits of cooperation have been illustrated mostly in the presence of multipath fading and shadowing though it is intuitive that CSS also may have potential to alleviate the losses introduced by other sources of uncertainty, *e.g.* actual noise level, carrier and sampling frequencies used at the licensed transmitter, etc.
- **Realistic operation environments:** Robust signal detection using ED is known to be limited by SNR walls when the uncertainty about the actual noise level is taken into account. The detection of target signals buried in noise of uncertain power has received some attention recently, but the literature has not managed thus far to address the effect of other underlying uncertainties present in the operation environment. This includes, for instance, the impact exerted on the detection process by the lack of exact knowledge of channel fading coefficients, carrier and sampling frequencies used at the licensed transmitter, and even the type of target signal currently being detected. Apart from ED and some CP-based methods, *e.g.* ACD and BTPD, less is known about how such sources of uncertainty affect the performance of signal specific techniques.

We deal with all the aspects above in the remainder of this dissertation. Instead of studying each of them on an individual basis, we develop a comprehensive simulation-based framework that also allows us to analyze the synergies created when two or more of the above aspects are considered simultaneously. Using this approach, we expect to contribute to a deeper understanding of the related work and, eventually, shed light on some promising research avenue that has been less investigated to date. The outcomes of this study, including a thorough analysis on the issue of method selection for future testbed/demonstrator implementation and the determination of theory gaps that are worth analytical investigation, will hopefully support the development of WSD and their posterior introduction to the market.



# Chapter 3

## The MESS Platform

We have seen in Chapter 1 that the choice of the method used to determine white spaces plays a crucial role in the feasibility of future WSD. Under the assumption that candidate methods should additionally commit to the decrease of the digital divide, we have argued that sensing-based approaches that enforce cooperation among nodes are more preferred for developing markets. Next, we have observed that even such network-centric approaches will only make economic sense if the cost and complexity of individual nodes is as low as it can possibly be. Thus, economies of scale can be achieved provided that WSD can determine the region where they currently operate. In the specific case of the TV bands, the operation region can be determined on the basis of the signals broadcasted over the air within the sensitivity region of WSD. The bottom line is that two different digital (or analog) standards are in general not deployed collocated, so a WSD can take advantage of the current TV broadcast deployments to identify the region where it finds itself in. In view of these facts, we have suggested that the context awareness required to distinguish among different regions can be obtained via signal classification.

In our search for candidate methods that can fit the purpose of signal classification, we have reviewed in Chapter 2 the signal processing techniques currently regarded as the most promising for WSD. Since we intend to classify different signal types, it is important to assess each method not only in terms of its detection performance but also the *strength* of the feature that method uses for detection. This kind of assessment calls for a standardized (or widely accepted) evaluation scenario that allows to establish comparisons without the need of implementing each and every method. Unfortunately, no such an evaluation scenario exists and the related work frequently lacks basic information about the settings used in the simulation work. This makes it difficult to compare two approaches proposed by different research groups. Such lack of baseline for comparison provided us with the initial motivation to construct a sensing platform using Matlab. Additional motivation was provided by the mathematical intractability of some methods (whose performance can only be evaluated via MC simulation), and, of course, by our interest in contributing to a better understanding of the gaps highlighted in Section 2.3.

Having these goals in mind, the major design requirement of our sensing platform was the simulation of multiple detection methods when target signals based on multiple standards are detected in a realistic operation environment where multiple sources of uncertainty may be present. Our implementation effort resulted in the *multi-environment spectrum sensing* (MESS) platform, described in this chapter in terms of Figure 3.1. We start in Section 3.1 with an approach to generalize the results in the related work. Basically, we



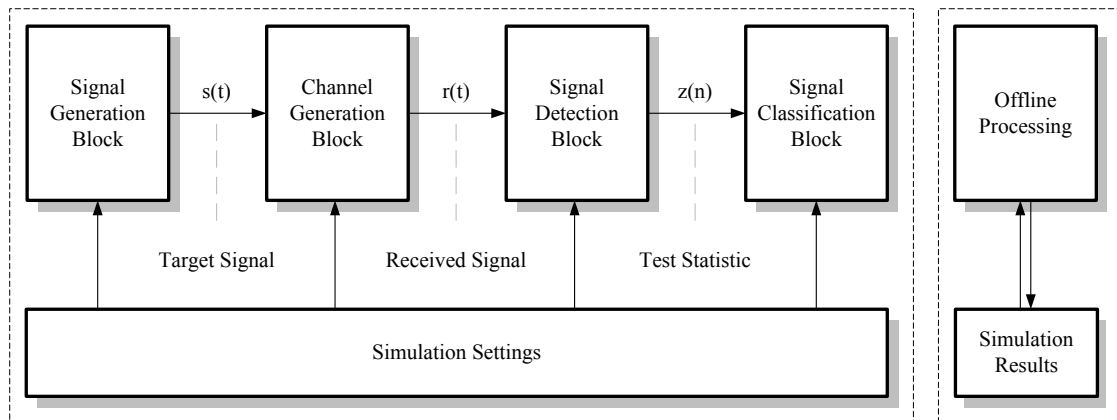


**Fig. 3.1:** Functional block diagram of the MESS platform.

rely on a comprehensive signal generation process that creates target signals in compliance with the TV broadcast standards most deployed worldwide, non-standardized FM-based PMSE, and emerging TVBD standards. We continue in Sections 3.2 and 3.3, where we respectively describe our implementations for the processes of channel generation and signal detection. Both sections include detailed explanations about what underlying uncertainties of these processes are taken into account and how they are modeled in MESS. In Section 3.4, we explain how WSD can obtain context awareness via signal classification in the TV bands, present the structure of a generic three-stage signal classification block, and summarize the candidate methods that may be implemented at each stage. We close the chapter in Section 3.5 with some remarks that, along with our simulation work in Chapter 4, will guide us into the definition of the method to be used in each stage.

### 3.1 Signal Generation Block

To be efficient and reliable, the exploitation of white spaces imposes stringent requirements on WSD. We have seen in Chapter 1 that such requirements are more or less static for GDA but become tougher or more relaxed for spectrum sensing depending on the operation environment<sup>1</sup>. Also, it turns out from the related work discussed in Chapter 2 that the majority of contributions available in the spectrum sensing literature has considered simplified operation environments where the goal of WSD is to detect at most two different types of target signals. The target signals considered are either in compliance with a given standard, usually a well deployed digital TV broadcast standard, or based on transmission schemes like OFDM. Eventually, this “common” approach is due to the three following facts. First, blind techniques perform independently of the received signal, so the performances obtained for different target signals should be essentially the same. Second, signal specific techniques may work well for a given type of signal but make less (or any) sense for other signal types. Finally, it is evident that assuming a single type of target signal largely simplifies analysis. In particular, provided that certain conditions are satisfied, the real performance of a method may be approximated by closed-form expressions for the sake of facilitating the numerical analysis. Clearly, this common approach

<sup>1</sup> Different protection levels can be granted to high- and low-power TV stations by proportionally specifying larger and smaller protected contours in the database, whereas spectrum sensing cannot distinguish between these two types of services.

has been accomplishing the task of providing insights on in what direction signal processing for WSD is going and should further evolve. However, the *post-switchover era* brings about more challenging operation conditions that WSD will likely have to cope with. In what follows, we characterize such operation conditions for the case of the TV bands.

### 3.1.1 The Post-switchover Era

The digital switchover in the TV bands translates into the immediate need for WSD to coexist with digital TV standards and the non-standardized WM operated by PMSE. The ability to coexist with analog TV standards is crucial too because it finds application in those markets where *simulcast services* are still offered, *i.e.* TV broadcast is made available both in analog and digital formats. In most countries, analog TV stations have not been fully switched off yet due to a number of technical, commercial, and policy issues arising in the switchover process [142]. Experience has shown that the transition from analog to digital TV may occur relatively fast (*e.g.* fully completed within two years in Norway, Sweden, and Switzerland) but may also involve longer periods (*e.g.* five years in the U.K., six years in Germany, and approximately seven years in the U.S). In addition to these coexistence requirements, future WSD need to minimize mutual interference when sharing channels in a common operating area. Mechanisms that allow for this kind of coexistence, referred to as *self-coexistence*, have been specified in some emerging TVBD standards that we discuss in the sequel.

IEEE 802.22 is probably the most prominent standard among all TVBD standards that have proliferated recently. Regarded as the first standard for operation in TV white spaces, IEEE 802.22 has been announced in the end of 2011 as the recipient of the IEEE standards association emerging technology award. Within IEEE 802.22, a self-coexistence operation mode is used to address the condition where multiple BS having overlapping coverage areas share the same channel [126]. To avoid mutual interference, the channels are shared on a per frame basis whereby a subset of the frames in a superframe is exclusively allocated to each coexisting BS. The degree of self-coexistence obtained through this channel allocation process can be further improved by regularly transmitting *coexistence beacon protocol* (CBP) bursts that convey the identity of the currently transmitting devices.

The IEEE 802.22 standard was modified to allow operation of portable WSD only at a later standardization step. In contrast, the ECMA-392 standard was designed from its very beginning to allow both fixed and portable WSD [127]. This is perhaps the reason why ECMA-392 includes distributed and centralized mechanisms for different self-coexistence situations. The distributed mechanism allows WSD to detect *alien beacons* (*e.g.* 802.22 CBP or 802.22.1 disabling beacons [13]), adjust the beacon period and superframe structure adopted in ECMA-392 with those of alien WSD, and dynamically control the number of beaconing WSD to avoid unnecessary large overheads. In the centralized mechanism, several schemes can be applied depending on whether the self-coexistence situation occurs between two master-slave networks, two peer-to-peer networks, or a peer-to-peer network and a master-slave network.

Though both IEEE 802.22 and ECMA-392 mandate mechanisms for self-coexistence, only the latter addresses coexistence between its standard-compliant WSD and other WSD. Recalling the recent advancements in white space policy seen in Section 1.2, additional requirements may be necessary in some markets to address the coexistence between different TVBD standards. In such markets, spectrum sensing can be directed to detect and

classify signals transmitted by future TVBD standards, *i.e.* other than ECMA-392, thus protecting IEEE 802.22 operation from harmful interference. Since the intended WSD can be shielded from receiving the beacon signals, we envision the use of spectrum sensing as a contingency tool in case of failure of the self-coexistence mechanisms mandated in ECMA-392. Due to these reasons, we represent the post-switchover era in this dissertation by a multi-standard operation environment where WSD share a geographical area with digital TV, analog TV, PMSE, and emerging TVBD systems. In this realistic operation scenario, the ability of sensing the spectrum for different types of target signals is a factor critical to the successful deployment of WSD. This is modeled in MESS through the signal generation process shown in Figure 3.2. Despite of looking like a “sampler”, the switch on the farthest left side of this figure actually indicates that only one type of information source is considered per simulation campaign at a time. Assuming that self-coexistence between IEEE 802.22 and ECMA-392 is ensured through the mechanisms provided by the latter, this reflects well a market where only a single TV broadcast standard is deployed. Markets where simulcast services are still offered need to be analyzed in two distinct simulation campaigns, one for each format.

### 3.1.2 Parameterization of Information Sources

The information sources currently implemented in MESS include the TV broadcast standards most deployed worldwide both in digital (ATSC, DVB-T, and ISDB-T) and in analog (NTSC and PAL) formats, non-standardized (FM-based) PMSE, and emerging TVBD standards (IEEE 802.22 and ECMA-392). By parameterizing all information sources for operation on 6 MHz channels, the only channel bandwidth available in ATSC and NTSC, we ensure that WSD scan roughly the same bandwidth regardless of the target signal. In case of OFDM, the signal generation process follows the steps in Figure 2.5 with the input bit stream being random quadrature phase-shift keying (QPSK) symbols with unitary power. The mandatory system parameters and pilot insertion patterns are given in Table 3.1 and Figure 3.3, respectively. In all standards, the occupied signal bandwidth  $W$  is almost equal to the entire channel bandwidth  $B$ . Apart from the pilot insertion pattern, signals compliant with DVB-T and IEEE 802.22 have the same parameterization,

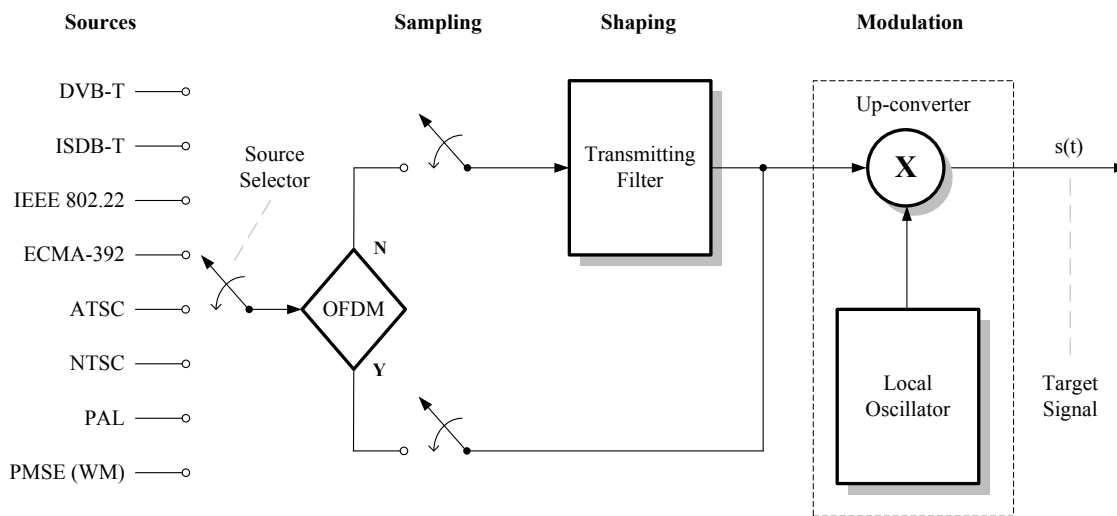


Fig. 3.2: Detailed view of the signal generation block.

**Table 3.1:** System parameters of OFDM-based standards ( $B = 6$  MHz).

| Parameter              | DVB-T         | ISDB-T        | IEEE 802.22   | ECMA-392       |
|------------------------|---------------|---------------|---------------|----------------|
| $N_s$                  | 2048          | 2048          | 2048          | 128            |
| CP ratio               | 1/32 to 1/4   | 1/32 to 1/4   | 1/32 to 1/4   | 1/32 to 1/8    |
| $T_{CP}(\mu\text{s})$  | 9.33 to 74.67 | 7.87 to 63.00 | 9.33 to 74.67 | 0.58 to 2.33   |
| $T_{FFT}(\mu\text{s})$ | 298.67        | 252.00        | 298.67        | 18.67          |
| $T_{SYM}$ (ms)         | 0.31 to 0.37  | 0.26 to 0.31  | 0.31 to 0.37  | 0.019 to 0.021 |
| $\Delta f$ (kHz)       | 3.35          | 3.97          | 3.35          | 53.57          |
| $f_s$ (MHz)            | 6.86          | 8.13          | 6.86          | 6.86           |
| $W$ (MHz)              | 5.71          | 5.57          | 5.62          | 5.52           |

so we expect all but TDSC methods to deliver similar performance when detecting such signals. ISDB-T mandates the same CP ratios adopted in DVB-T and IEEE 802.22 but slightly differs from these standards in terms of the useful symbol duration  $T_{FFT}$ . This renders the sampling period  $T_s$  to be shorter in ISDB-T than in DVB-T and IEEE 802.22. In contrast, WSD based on ECMA-392 convey information using shorter symbols, *i.e.* around only 20  $\mu\text{s}$  long as compared to more than 300  $\mu\text{s}$  in case of DVB-T, ISDB-T, and IEEE 802.22. Later in this chapter, we exploit this fact to investigate the effect of the FFT length on detection performance without incurring the longer simulation times that would result from the use of the larger modes (4k and 8k) allowed in DVB-T and ISDB-T. Hence, without any loss of generality, all simulation results obtained for multi-mode OFDM-based standards are based on the 2k mode unless explicitly stated otherwise. The typically flat spectra of the OFDM-based target signals used in this dissertation are shown in Figure 3.4. The ISDB-T spectrum is essentially the same as that of DVB-T and therefore omitted.

MESS can also generate non-OFDM signals. The current version of the platform is capable of generating ATSC, NTSC, and PAL signals in accordance with the values given in Table 3.2. In contrast to OFDM, where baseband signals are transmitted ( $f_c = 0$ ), non-OFDM standards are represented here using bandpass signals. The reason for this is twofold. First, currently non-OFDM TV receivers typically select the desired channel from a number of available channels and down-convert it to standardized IF values. This has implications in terms of computational complexity and higher sampling rates but mimics well the way that non-OFDM TV receivers currently operate. Second, bandpass signals have been used in [51] with the sampling rates of ATSC and NTSC signals set to  $4 \times f_c$  and  $3 \times f_c$ , respectively. No “clue” about where these values come from is provided therein, so we got started with  $f_s = 2.1 \times f_c$  to set the sampling rates used in MESS. This is roughly the sampling rate we ended up using for ATSC. Before being sampled, the ATSC signal is 8-PAM modulated (except for the data segment SYNC which is transmitted in binary form) and passed through a vestigial side band (VSB) modulator to eliminate the spectral redundancy typical in PAM. Unlike in OFDM, where the IFFT process accommodates the signal in the transmitted bandwidth, the ATSC spectrum needs to be shaped by a square root raised cosine filter [135]. This shaping results in 620 kHz transition regions (310 kHz on each side), so the target ATSC signal occupies a bandwidth of 5.38 MHz. However, in NTSC and PAL, the number of samples collected by using  $f_s = 2.1 \times f_c$  was apparently too low to properly generate the color burst [122]. We solved this issue by progressively increasing  $f_s$  until we ended up with  $f_s = 200$  MHz, which is roughly the

**Table 3.2:** System parameters of some non-OFDM standards ( $B = 6$  MHz).

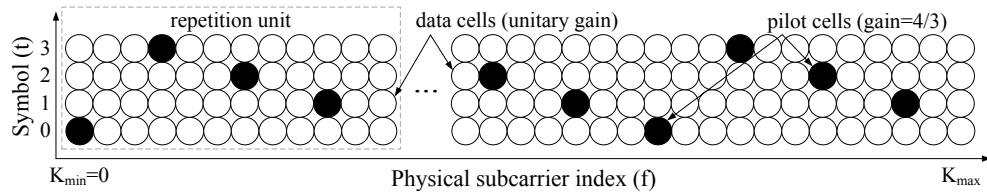
| Parameter          | ATSC   | Parameter                | NTSC   | PAL    |
|--------------------|--------|--------------------------|--------|--------|
| Segments/frame     | 313    | Lines/frame              | 525    | 625    |
| Symbols/segment    | 832    | Frame rate (fps)         | 29.87  | 25.00  |
| Segment ( $\mu$ s) | 77.30  | Line ( $\mu$ s)          | 63.55  | 64.00  |
| $f_c$ (MHz)        | 44.00  | Video $f_c$ (MHz)        | 45.75  | 45.75  |
| $f_s$ (MHz)        | 100.00 | $f_s$ (MHz)              | 200.00 | 200.00 |
| $W$ (MHz)          | 5.38   | $W_{\text{video}}$ (MHz) | 4.20   | 4.20   |

same sampling rate used in [51]. Another peculiarity inherent to analog TV broadcast is that the reception of *composite signals* requires two different IF values, one for the video signal, the other for the audio signal. Since WSD are aimed at detecting the presence of the target signal rather than actually “understanding” the information it conveys, we decided to use video-only signals for the sake of simplicity. The standard-compliant video signals are passed through a lowpass filter, amplitude modulated (AM), and further VSB modulated so that the occupied signal bandwidth is 4.20 MHz for NTSC and PAL. The power spectra of the non-OFDM TV broadcast signals used in this dissertation are shown in Figure 3.5.

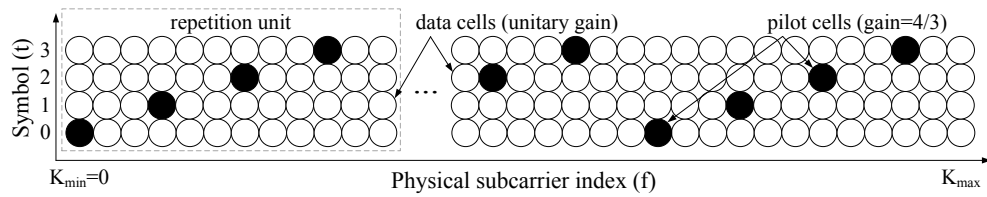
The last type of target signal available in MESS reflects the operation of PMSE, where FM signals are conveyed by WM. In this case, since standardized system values entirely lack, we implemented the signal generation process along the lines of the signal simulation method proposed in [143]. The deterministic model and the test scenarios proposed therein allow to a controlled and reproducible form of WM detection evaluation, which served as the basis for assessing different methods within the scope of the IEEE 802.22 standard. As shown in Table 3.3, different speaker modes can be created by suitably selecting the tone signal, used to represent the audio input  $m(t)$ , and the frequency deviation  $f_{\text{dev}}$ . The resulting target signal is a sum of carrier and tone signal in the silent mode, whereas in the soft and louder modes it is the carrier with moderate and near the maximum amount of deviation, respectively. Following the work in [51], we set the carrier frequency  $f_c$  to 100 times of the maximum frequency deviation (32.6 KHz in loud speaker mode), so that  $f_c \gg f_{\text{dev}}$  and (2.98) holds. The sampling frequency used is  $f_s = 2.1 \times f_c$  and the occupied signal bandwidth (measured at  $-80$  dB/Hz) is always below 200 kHz regardless of the speaker mode used. The power spectra of the WM signals used in this dissertation are shown in Figure 3.6 for all the three speaker modes.

**Table 3.3:** System parameters of different WM speaker modes (adapted from [143]).

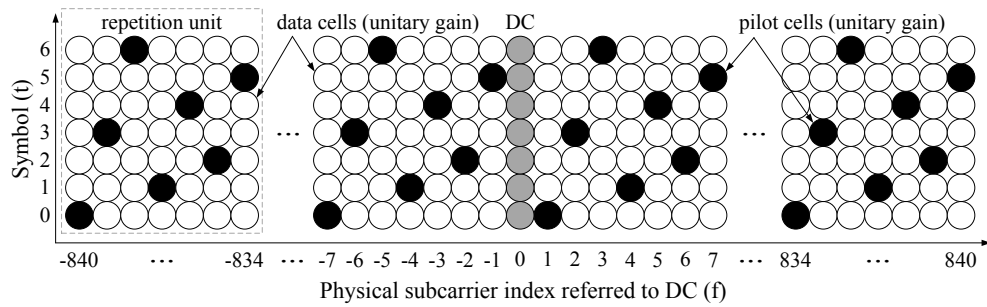
| Parameter              | Silent    | Soft       | Loud       |
|------------------------|-----------|------------|------------|
| $m(t)$ (kHz)           | 32.0      | 3.9        | 13.4       |
| $f_{\text{dev}}$ (kHz) | $\pm 5.0$ | $\pm 15.0$ | $\pm 32.6$ |
| $f_c$ (MHz)            | 3.26      | 3.26       | 3.26       |
| $f_s$ (MHz)            | 6.85      | 6.85       | 6.85       |
| $W$ (kHz)              | 87.00     | 87.00      | 135.00     |



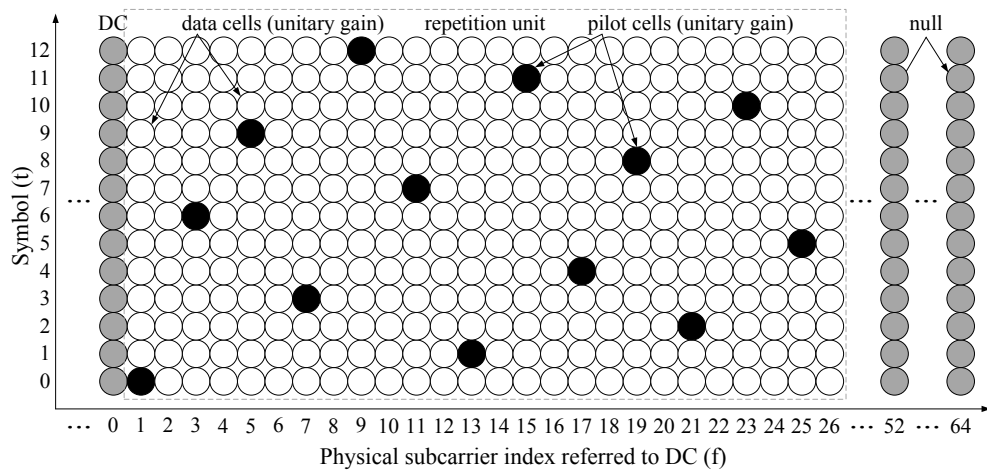
(a) DVB-T 2k (PRBS:  $x^{11} + x^2 + 1$ ).



(b) ISDB-T 2k (PRBS:  $x^{11} + x^9 + 1$ ).

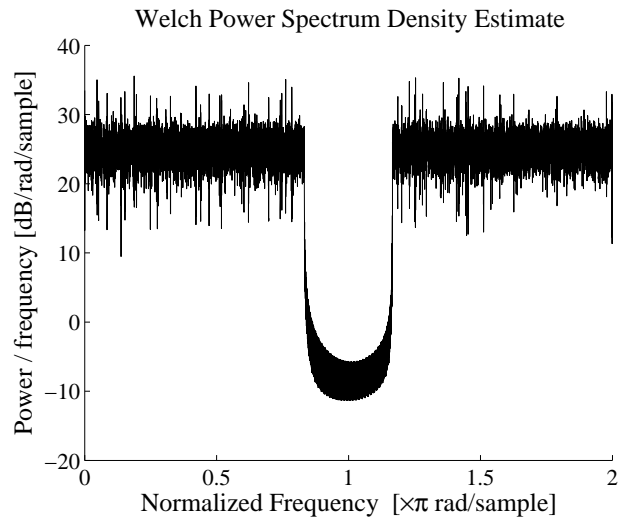


(c) IEEE 802.22 (PRBS:  $x^{15} + x^{14} + 1$ ).

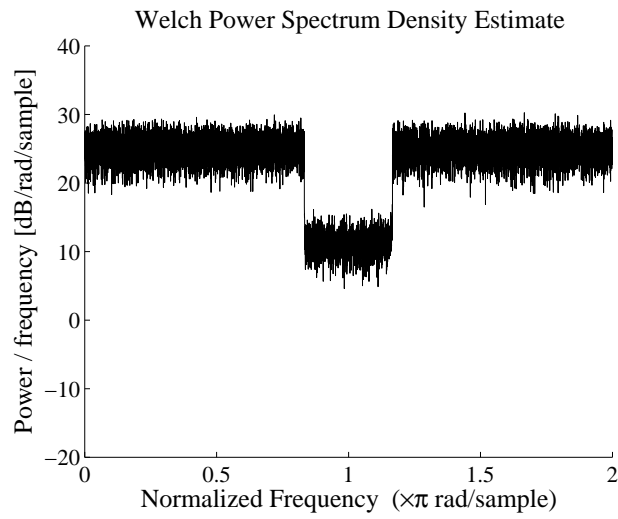


(d) ECMA-392 (PRBS:  $x^9 + x^4 + 1$ , symmetric negative carriers omitted).

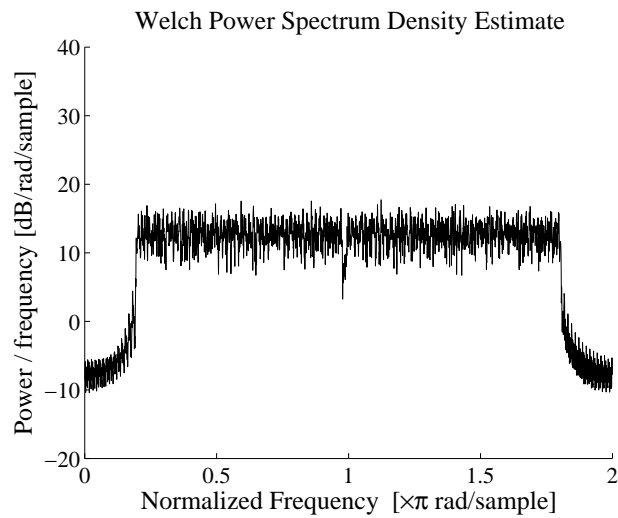
**Fig. 3.3:** Pilot insertion patterns adopted in the OFDM-based standards implemented in MESS ( $B = 6$  MHz).



(a) DVB-T (Mode 2k CP=1/4).

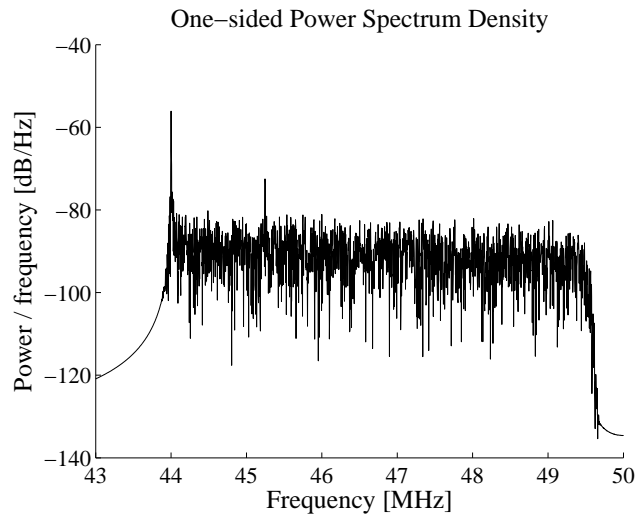


(b) IEEE 802.22 (CP=1/4).

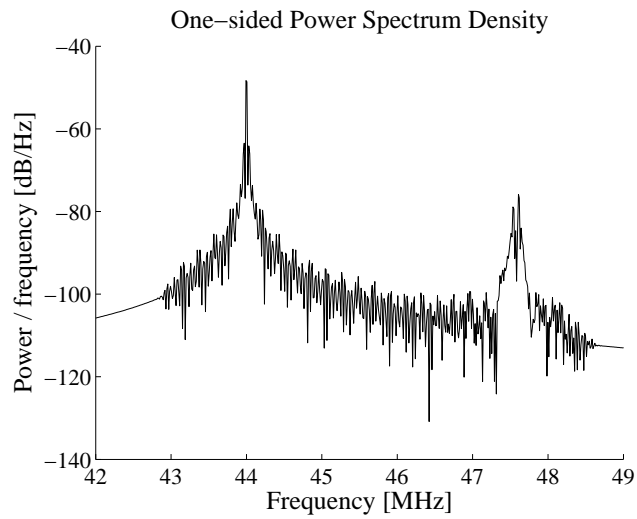


(c) ECMA-392 (CP=1/8).

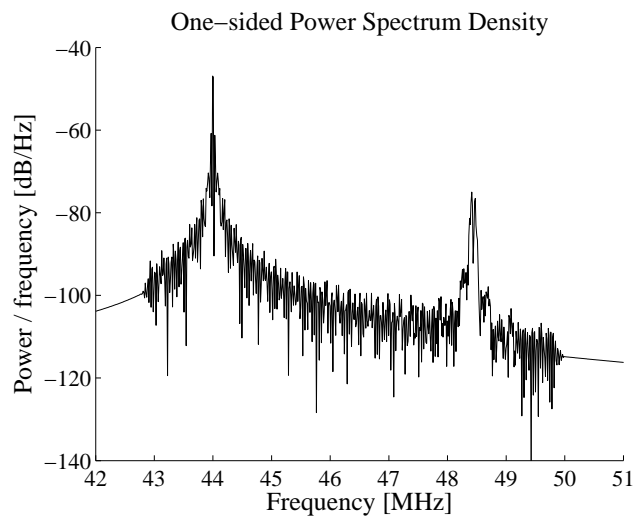
**Fig. 3.4:** Power spectra of OFDM signals created according to Table 3.1 and Figure 3.3.



(a) ATSC.



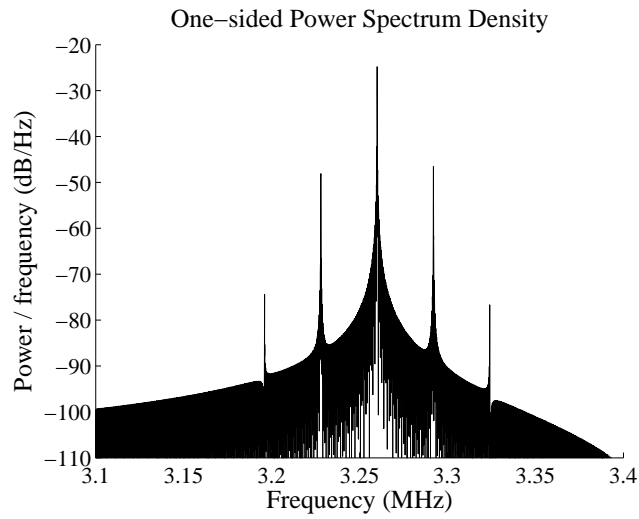
(b) NTSC (video-only signal).



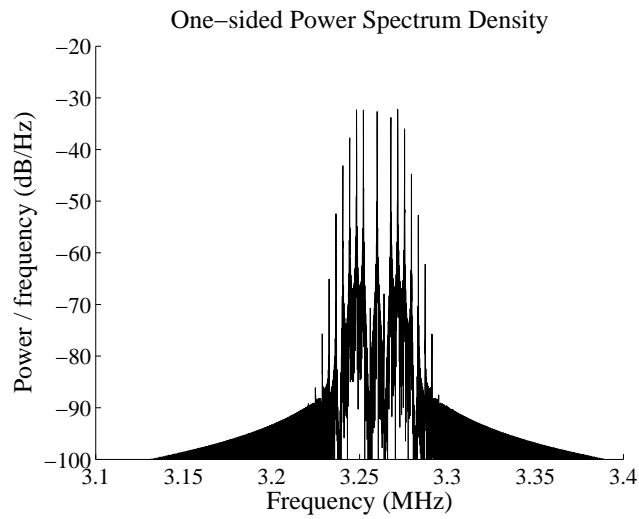
(c) PAL (video-only signal).

**Fig. 3.5:** Power spectra of non-OFDM signals created according to Table 3.2.

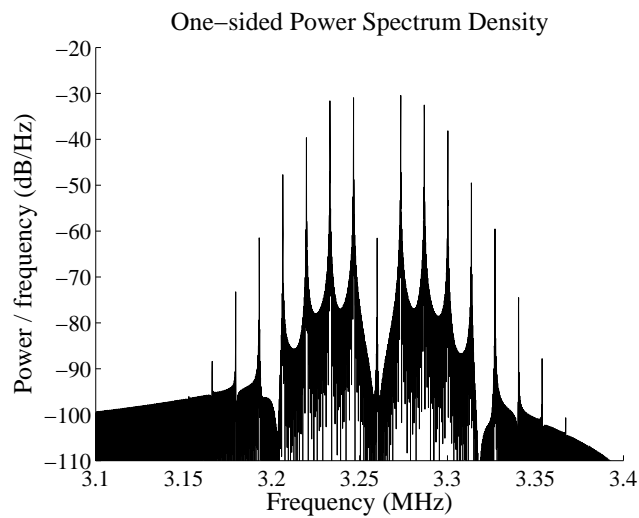




(a) Silent mode.



(b) Soft mode.



(c) Loud mode.

**Fig. 3.6:** Power spectra of WM signals created according to Table 3.3.

## 3.2 Channel Generation Block

### 3.2.1 AWGN Channel Model

In MESS, the channel generation is modeled as shown in Figure 3.7. The switch on the left side of the figure is a channel selector that allows us to choose between a pure AWGN channel or multipath fading conditions. Though not explicitly depicted in the figure, the AWGN process is created as independent in phase (I) and in quadrature (Q) components having their amplitudes attenuated so as to reflect the SNR received at the WSD front-end.

However, as seen in Chapter 2, perfect knowledge of the noise power is hard to obtain in practice due to variations in the received noise level. Our first step to model such limitation is to compute the actual SNR based on  $\sigma_w^2$  perfectly known. Then, we create two replicas of this ideal SNR and artificially introduce uncertainty about the actual value of  $\sigma_w^2$  in them. This allows the replicas to be viewed as SNR estimates computed based on an estimated noise power  $\hat{\sigma}_w^2$ . The amount of uncertainty introduced in each replica is selected so that the estimation error  $\Delta\sigma_w^2 = \hat{\sigma}_w^2 - \sigma_w^2$  lies within the practical uncertainty bounds proposed in [49]. Specifically, the detection of target signals in noise of uncertain power is simulated in this dissertation using the values shown in Table 3.4. As in [98][99], each  $\rho$  value imposes a different uncertainty range that corresponds to different deviations in the estimated noise power  $\hat{\sigma}_w^2$ . Negative and positive deviations are implemented as lower and upper bounds on the actual SNR.

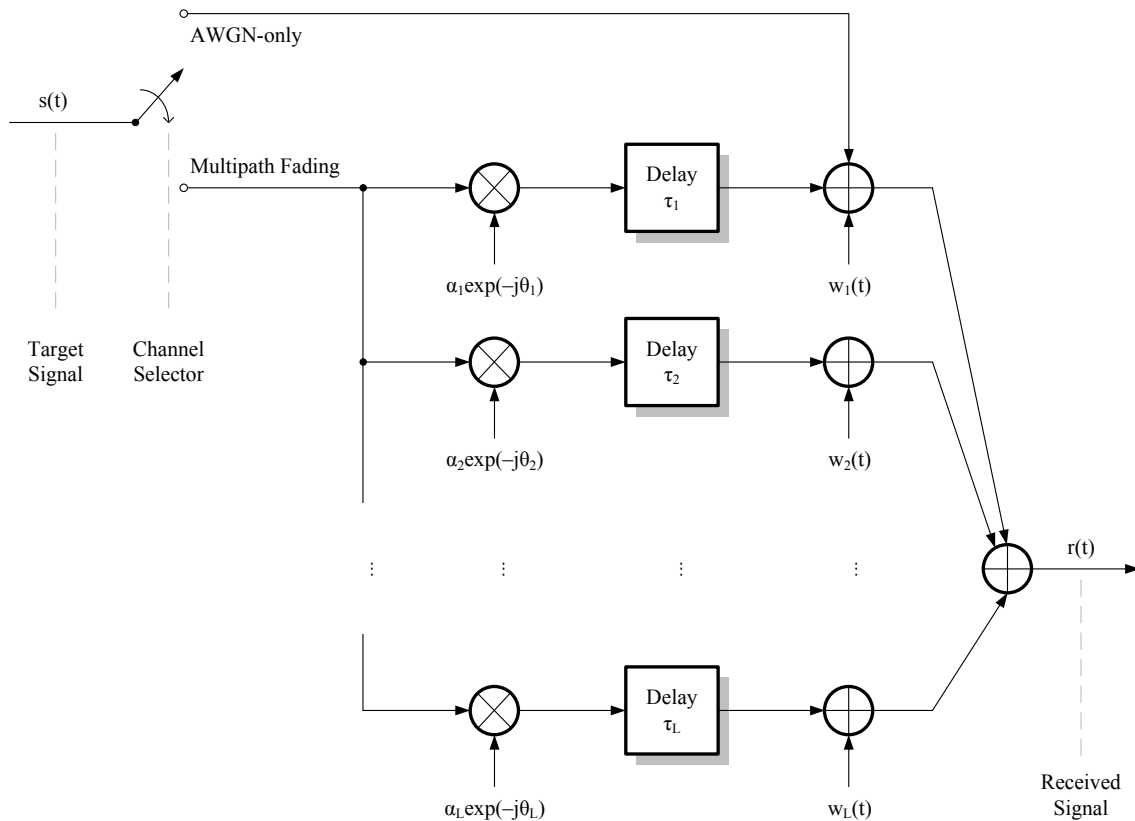


**Fig. 3.7:** Detailed view of the channel generation block.

**Table 3.4:** Values assigned to  $\rho$  in the noise uncertainty analysis.

| $\rho$ | Estimate Range  | $\Delta\hat{\sigma}_w^2$ (dB) |
|--------|---|-------------------------------|
| 1.00   | $\hat{\sigma}_w^2 = \sigma_w^2$ (ideal case)            | none                          |
| 1.12   | $\hat{\sigma}_w^2 \in [0.89\sigma_w^2, 1.12\sigma_w^2]$ | $\sigma_w^2 \pm 0.50$         |
| 1.24   | $\hat{\sigma}_w^2 \in [0.80\sigma_w^2, 1.24\sigma_w^2]$ | $\sigma_w^2 \pm 1.00$         |

### 3.2.2 Multipath Fading Channel Model

Under AWGN conditions, the I and Q components are simply added to the real and imaginary parts of the target signal  $s(t)$ , so that there are no other multiplicative mechanisms at work. When under multipath fading,  $l = 1, 2, \dots, L$  replicas of  $s(t)$  are received over independent paths, each path modeled as a flat fading channel. After passing through the fading channels, each replica is further perturbed by complex AWGN that is statistically independent from path to path. Such multipath fading channel can be fully determined by  $\{\alpha_l\}_{l=1}^L$ ,  $\{\theta_l\}_{l=1}^L$ , and  $\{\tau_l\}_{l=1}^L$ , which denote the sets of channel amplitudes, phases, and delays, respectively [131]. In addition, mobility issues raised by the relative motion between the licensed transmitter and portable WSD are incorporated into the model by allowing the amplitude of each path to vary according to the Doppler frequencies in the set  $\{f_{\text{dop},l}\}_{l=1}^L$ . None of these fading parameters is known a priori by WSD.

The above multipath fading process can be set in MESS as time-invariant or time-variant. In time-invariant channels, the  $l$ th path is fully characterized by a combination of amplitude and delay denoted *power delay profile* (PDP). In this case, since the Doppler shifts are not taken into account, the amplitudes in  $\{\alpha_l\}_{l=1}^L$  vary only with the random phases in  $\{\theta_l\}_{l=1}^L$  and the PDP describes the amount of energy in  $s(t)$  that is likely to arrive with a certain delay from the transmission of a Dirac impulse. The replica of  $s(t)$  travelling along the direct path, *i.e.* transmitted in line-of-sight (LOS), gives rise to the earliest arriving contribution to which delay zero is assigned. This earliest contribution is usually used as reference to set the relative amplitudes of the non-line-of-sight (NLOS) contributions, where  $s(t)$  is attenuated by obstructing objects [144]. Unless explicitly stated otherwise, all simulations carried out in this dissertation are based on time-varying channels where the amplitudes in  $\{\alpha_l\}_{l=1}^L$  are affected by both the random phases in  $\{\theta_l\}_{l=1}^L$  and Doppler frequencies in  $\{f_{\text{dop},l}\}_{l=1}^L$ .

Despite of the fact that the fading processes arising in LOS and NLOS propagation conditions can be respectively characterized by Ricean and Rayleigh distributions, several efforts have been done to establish channel models to characterize multipath behavior. In MESS, the channel generation is flexible in the sense that the channel specifications can be configured to fit a given application and support algorithm design, validation, and performance prediction in the context of that application. Recalling that we are interested in evaluating algorithms for WSD, it seems natural to use a channel model conceived for this kind of application. One such model is the simplified multipath channel model proposed in [144] to evaluate wireless regional area network (WRAN) technologies within the scope of the IEEE 802.22 standard. In what follows, we examine the profiles in Table 3.5 with respect to the type of degradation that they can create. Our goal is to minimize unnecessary simulation efforts by using a smaller set of profiles, namely those exhibiting the most representative and interesting fading features for WSD applications.

**Table 3.5:** Multipath profiles proposed within the scope of the IEEE 802.22 standard with profile D set to its worst case (adapted from [144]).

| <b>Profile A</b>               | <b>Path 1</b> | <b>Path 2</b> | <b>Path 3</b> | <b>Path 4</b> | <b>Path 5</b> | <b>Path 6</b> |
|--------------------------------|---------------|---------------|---------------|---------------|---------------|---------------|
| Excess delay ( $\mu\text{s}$ ) | 0             | 3             | 8             | 11            | 13            | 21            |
| Amplitude (dB)                 | 0             | -7            | -15           | -22           | -24           | -19           |
| Doppler freq. (Hz)             | 0             | 0.10          | 2.50          | 0.13          | 0.17          | 0.37          |
| <b>Profile B</b>               | <b>Path 1</b> | <b>Path 2</b> | <b>Path 3</b> | <b>Path 4</b> | <b>Path 5</b> | <b>Path 6</b> |
| Excess delay ( $\mu\text{s}$ ) | -3            | 0             | 2             | 4             | 7             | 11            |
| Amplitude (dB)                 | -6            | 0             | -7            | -22           | -16           | -20           |
| Doppler freq. (Hz)             | 0.10          | 0             | 0.13          | 2.50          | 0.17          | 0.37          |
| <b>Profile C</b>               | <b>Path 1</b> | <b>Path 2</b> | <b>Path 3</b> | <b>Path 4</b> | <b>Path 5</b> | <b>Path 6</b> |
| Excess delay ( $\mu\text{s}$ ) | -2            | 0             | 5             | 16            | 24            | 33            |
| Amplitude (dB)                 | -9            | 0             | -19           | -14           | -24           | -16           |
| Doppler freq. (Hz)             | 0.13          | 0             | 0.17          | 2.50          | 0.23          | 0.10          |
| <b>Profile D</b>               | <b>Path 1</b> | <b>Path 2</b> | <b>Path 3</b> | <b>Path 4</b> | <b>Path 5</b> | <b>Path 6</b> |
| Excess delay ( $\mu\text{s}$ ) | -2            | 0             | 5             | 16            | 22            | 60            |
| Amplitude (dB)                 | -10           | 0             | -22           | -18           | -21           | +10           |
| Doppler freq. (Hz)             | 0.23          | 0             | 0.10          | 2.50          | 0.17          | 0.13          |

To begin with, we observe that typical outdoor environments are characterized by excess delays around  $10 \mu\text{s}$ . Such *post-echoes* are the most significant in practice, in both power and number. The profile B is interesting because most of its delays lie within this range. In contrast, the profiles A, C, and D describe areas surrounded by large and distant structures where larger delays may occur. Despite the similarities between the profiles C and D, the 6th path of the latter accepts ranges of amplitudes  $\alpha_D \in [-30, +10]$  and delays  $\tau_D \in [0, 60]$  that allow us to model obstacle mobility. To make the most of this distinguishing feature, we set the 6th path of the profile D so as to model *pre-echoes* where  $s(t)$  is received at higher power than that of the direct path. Another distinguishing feature of the profiles B and D is that they exhibit the least and the largest *maximum excess delay*  $\tau_{\max}$  in Table 3.5. Defined as the time interval between the first and the last received components [91],  $\tau_{\max}$  provides a time-domain indication about the type of degradation introduced by the multipath fading channel. The channel is said frequency-selective if the received multipath components of a symbol extend beyond the symbol duration  $T_{\text{SYM}}$  and flat otherwise.

The analysis of time-spreading in the time-delay domain classifies the fading phenomenon well as long as the target signals are in digital format. For analog target signals, where no symbols are conveyed, we need to establish a similar relationship in the frequency domain by comparing the occupied signal bandwidth  $W$  to the channel *coherence bandwidth*  $f_0$ . The spectral components received within the frequency range described by  $f_0 \approx 1/\tau_{\max}$  are affected in a similar manner (flat fading), whereas the channel impact on those components received outside this range is frequency dependent (frequency-selective fading) [131]. It follows from this approximation that the coherence bandwidths of the profiles in Table 3.5 are  $f_{0,A} = 47.62 \text{ kHz}$ ,  $f_{0,B} = 71.43 \text{ kHz}$ ,  $f_{0,C} = 28.57 \text{ kHz}$ , and  $f_{0,D} = 16.13 \text{ kHz}$ . Recalling Tables 3.1 and 3.2, it is clear that we always have  $f_0 \ll W$ . Hence, for any profile in Table 3.5, the wideband target signals used in MESS will undergo frequency-selective fading. As for narrowband WM signals, conveyed according to Table 3.3, the channel will introduce some frequency selectivity but the impact should be definitely milder (compared to wideband signals) because  $f_0$  is at most one order of magnitude smaller than  $W$ .

We have assessed the profiles in Table 3.5 in terms of their time-spreading properties thus far. However, despite of the insights brought by  $\tau_{\max}$  and  $f_0$  about the type of degradation introduced by our fading channel model, we still lack an understanding about its time-varying nature, *i.e.* how  $\{\alpha_l\}_{l=1}^L$  and  $\{\theta_l\}_{l=1}^L$  vary according to changes caused by motion. A measure of the time duration over which the channel is expected to respond in an invariant fashion is given by its *coherence time*  $t_0$ . Viewed in the time domain, the time variance of the channel can be described as fast fading when  $t_0 < T_{\text{SYM}}$  and as slow fading otherwise. The reciprocal relation  $t_0 \approx 1/f_{\text{dop}}$  allows us to examine the degradations due to time variance in the Doppler-shift domain, where fast fading is characterized by  $W < f_{\text{dop}}$  and slow fading otherwise [91]. It is then evident that, for the target signals considered in MESS, all profiles in Table 3.5 have less destructive slow fading characteristics because of their (same) low maximum  $f_{\text{dop}} = 2.50$  Hz.

Based on the above discussion, the simulations under multipath fading conditions carried out in this dissertation rely only on the profiles B and D.

### 3.3 Signal Detection Block

#### 3.3.1 Demodulation

Once the target signal has been generated and passed through the channel, the next step according to Figure 3.1 is to detect it. In MESS, the signal detection process is implemented as shown in Figure 3.8. There, the first task performed at the receiver front-end after receiving the RF signal from the antenna is demodulation. In *coherent detection*, the down-converter used to this end is assumed able to reconstruct the received carrier with *perfect* knowledge of its phase and frequency. While desirable for improved performance and versatility, coherent operation WSD requires tight synchronization and as such places complexity burdens on their design. The trade-off between performance and complexity can be addressed by designing more simple WSD able to operate *without* demodulating the received signal before detecting it. Such *noncoherent detectors* make no attempt to estimate the actual value of the phase of the received signal, so the demodulation process is typically performed using a local carrier with phase arbitrarily set to zero. Alternatively, depending on the specific method used for detection, complexity requirements can be further reduced by *directly* sampling the received complex bandpass signal.

Noncoherent detection is clearly of lower complexity. Therefore, it seems reasonable to assume that noncoherent implementations are better suitable for WSD whose utmost goal is to detect target signals without undergoing an unnecessary demodulation process. Having this in mind, we implemented the signal detection process of MESS with emphasis on non-coherent methods as shown in Table 3.6. Except for the MF defined in (2.96), which performs coherent detection, all other methods in MESS do not actually demodulate the received signal. For the sake of simplicity, we use the term *class* throughout the rest of this dissertation to refer to a set of methods that rely on the same underlying principle to work. The classes that are singleton sets will be simply referred to as the corresponding method. In general, SCD is a non-singleton class composed of methods that estimate the PSD of the received signal  $r(n)$ . However, preliminary results obtained using MESS suggested that the use of periodogram averaging methods, such as Bartlett and Welch, provide the same detection performance as the periodogram but this comes at the expense

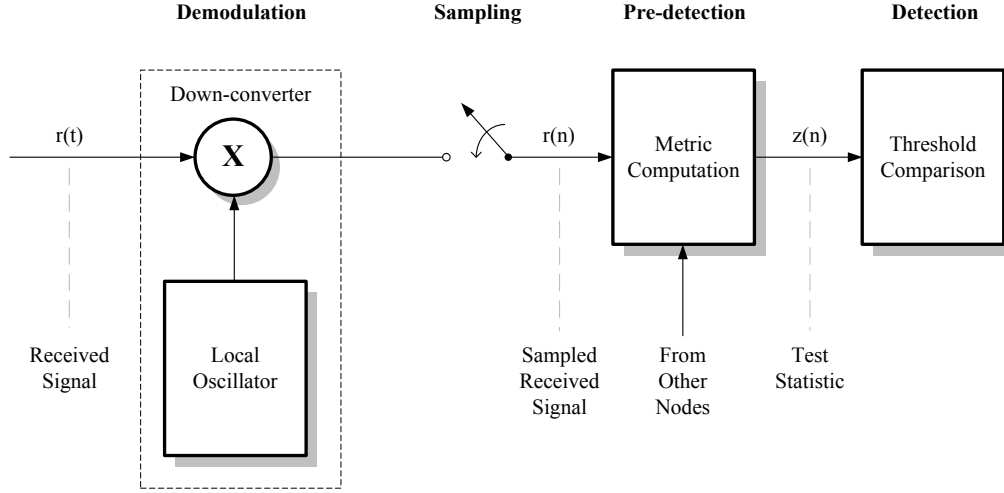


**Fig. 3.8:** Detailed view of the signal detection block.

of substantially longer simulation times. Therefore, unless explicitly stated otherwise, we consider the periodogram in all simulations involving the SCD method.

Coherent detection is usually carried out by creating a demodulation reference at the receiver, *e.g.* by generating local replicas whose phases and frequencies are identical to those used by the up-converter [91]. Unfortunately, such replicas are derived from the received signal and ideal synchronization is hard to meet. In practice, there often exists some offset between the clocks used at receiver and transmitter. A well-known effect of clock offsets is the mismatch between the local oscillators used in the down- and up-converters of receiver and transmitter. Our focus on noncoherent methods renders demodulation less necessary in MESS, but we end up keeping the down-converting block in Figure 3.8 to emphasize that oscillator mismatches are taken into account. We have seen in Chapter 2 that if the CFO introduced by using a mismatched carrier frequency  $f'_c$  is larger than the number of subcarriers  $N_s$ , the orthogonality between the subcarriers may get compromised and thus impair the demodulation of OFDM signals. Since ICI rapidly increases with the amount of CFO, the impact of the mismatch  $f'_c - f_c$  on the detection process is of practical interest (particularly when  $N_s$  is large). In single carrier systems, clock offsets are usually small

**Table 3.6:** Signal processing techniques currently implemented in MESS.

| Target   | Class  | Underlying Principle       | Metric                            | Method   | Test   |
|----------|--------|----------------------------|-----------------------------------|----------|--------|
| Any      | ED     | Received signal energy     | $ r(n) ^2$                        | ED       | (2.10) |
|          | EBD    | Sample covariance matrix   | $\mathbf{R}_r(n)$                 | AGM      | (2.43) |
|          |        |                            |                                   | GLRT     | (2.42) |
|          |        |                            |                                   | MME      | (2.39) |
| RLRT     | (2.30) |                            |                                   |          |        |
|          | SCD    | PSD estimate (periodogram) | $\hat{S}_{\text{PER},r}(\tau)$    | SCD      | (2.54) |
| Any OFDM | CFD    | Autocorrelation function   | $R_r(\tau)$                       | ACD      | (2.83) |
|          |        |                            |                                   | BTPD     | (2.84) |
|          | OFD    | Accumulated TDSC function  | $\Psi_{\text{TDSC}}(\Delta l)$    | TDSC-NP  | (2.88) |
|          |        | Accumulated SYNC function  | $\Psi_{\text{SYNC}}(n_0, \tau_d)$ | TDSC-MRC | (2.89) |
| ATSC     |        | Accumulated SYNC function  | $\Psi_{\text{SYNC}}(n_0, \tau_d)$ | ASSD     | (2.93) |
| PMSE     |        | Autocorrelation function   | $R_r(\tau)$                       | MF       | (2.96) |

compared to the symbol rate so that the performance degradation due to CFO is dominated by a “fading-like” reduction of the useful signal power. This causes single carrier systems to be in general less sensitive to CFO than OFDM systems.

In MESS, we model the impacts of CFO on performance by intentionally injecting different frequency offsets in the target signal. Hence, as with simulcast services, a distinct simulation campaign is needed for each CFO value. In case of OFDM-based signals, we analyze the impact of the loss of orthogonality between subcarriers by selecting the normalized CFO values so that  $\epsilon_c > \Delta f$ . The resulting amplitude reduction and phase rotation is then artificially created as in (2.90), yet at the transmitter side. As for non-OFDM signals, the only difference is that the amount of CFO is given in terms of  $f'_c - f_c$ , *i.e.* the difference (in Hz) between the mismatched and the actual carrier frequencies.

### 3.3.2 Sampling & Pre-detection

In addition to determining the individual performance of each method, we are interested in assessing the strength of the features used for detection. Unlike in most of the related work discussed in Chapter 2, we direct MESS to perform metric derivations over sensing times that are *not* arbitrarily set to produce the best possible results. Here the sensing time is set in terms of *fundamental units*, which we use to represent the minimum requirement of the feature used for detection. In the computation of all the test statistics in Table 3.6, we set the sensing time so that it corresponds to the minimum number of fundamental units plus one fundamental unit. The additional fundamental unit, not strictly necessary, is intended to improve the fairness by allowing all methods to overcome issues that may eventually arise later on in the pre-detection process, *e.g.* due to lack of synchronization. Whenever we analyze a given target signal, we direct blind and semi-blind techniques to use the *same* sensing time as the techniques specific for that signal type.

Specifically, the fundamental units, sensing time, and number of samples used in the simulations performed in this dissertation are given in Table 3.7. The minimum requirement for the CFD class translates into the need of sampling at least two OFDM symbols, so we compute the test statistics of ACD and BTPD over three OFDM symbols. According to Table 3.1, the corresponding sensing times range from  $57.75 \mu\text{s}$  (ECMA-392, CP= 1/32) to 1.12 ms (DVB-T Mode 2K, CP= 1/4). Likewise, TDSC methods rely on the correlation between the transmitted and received SP patterns to perform signal detection. In this case, it is desirable to collect a number of samples high enough to allow the correlation of at least two pilot repetition units (PRU). As seen in Figure 3.3, the PRU is standard dependent and can span over a different number of OFDM symbols. Using the PRU as fundamental unit, we compute the test statistics of TDSC methods over sensing times ranging from 0.75 ms (ECMA-392, CP= 1/32) to 4.48 ms (DVB-T Mode 2K, CP= 1/4). Extending the rationale to the ASSD method and taking the duration of a data segment SYNC as fundamental unit yields the sensing time of 0.23 ms used to detect ATSC.

The intuition behind the rationale above stems from the fact that autocorrelation-based methods need to be fed with a minimum of two fundamental units to detect the target signal. However, since HSYNC signals are not present in the first 9 lines within a NTSC field, the minimum sensing time required by the NHSD method should not be less than the time duration corresponding to 11 lines [51]. Similarly, taking into consideration the same principle to detect PAL signals, a minimum of 8 lines is required because no HSYNC signals are conveyed in the first 6 lines of each field [122]. If we define the line duration

**Table 3.7:** Simulation settings used for signal specific techniques. For a certain type of target signal, the same settings are used for blind and semi-blind techniques.

| Target   | Class | Method              | Unit    | Number of Units | Sensing Time  | Number of Samples |
|----------|-------|---------------------|---------|-----------------|---------------|-------------------|
| Any OFDM | CFD   | ACD                 | Symbol  | 3               | 57.75 $\mu$ s | 12480             |
|          |       | BTPD                |         |                 | 1.12 ms       | 61440             |
|          |       | TDSC-MRC            | PRU     | 3               | 0.75 ms       | 5616              |
|          |       | TDSC-NP             |         |                 | 4.48 ms       | 30720             |
| ATSC     | OFD   | ASSD                | Segment | 3               | 0.23 ms       | 23211             |
| NTSC     |       | Not yet implemented | Line    | 12              | 0.76 ms       | 152532            |
| PAL      |       |                     |         | 9               | 0.57 ms       | 115200            |
| PMSE     |       | MF                  | Time    | 1               | 1.00 ms       | 6846              |

as fundamental unit for analog TV broadcast, the sensing times used to detect NTSC and PAL signals are 0.76 ms and 0.57 ms, respectively<sup>2</sup>. As for PMSE, where WM signal features (if any) are not strong enough to serve as fundamental unit, we arbitrarily set the sensing time to 1.00 ms.

Another issue raised by the presence of clock offsets is that the receiver cannot adapt its sampling frequency to match that of the transmitter. The only option available for the receiver in this case is to operate at fixed sampling frequency. This condition, known as *non-synchronized sampling*, introduces SFO that can potentially create both ICI and ISI. As long as the ISI created thereby can be absorbed by the CP, its impact is negligible and ICI becomes the dominant impact on the performance of OFDM systems. In MESS, the impact of SFO is modeled in the same fashion of CFO as described earlier in this section. In case of OFDM-based signals, the sample timing drift  $t_d$  that results from a normalized SFO  $\epsilon_s$  is artificially introduced as in (2.91), yet at the transmitter side. As for non-OFDM signals, the amount of SFO is given in terms of  $f'_s - f_s$ , *i.e.* the difference (in Hz) between the mismatched and the actual sampling frequencies. Though both normalized frequency offsets  $\epsilon_c$  and  $\epsilon_s$  are dimensionless quantities, the latter assumes very small values and thus is more suitably represented in parts per million (ppm).

The next step in the signal detection process depicted in Figure 3.8 is pre-detection. This step encompasses all signal processing tasks carried out on  $r(n)$  so as to produce a generic test statistic  $z(n)$ . As shown in Table 3.6, this includes the derivation of method-dependent quantities or functions based on which the specific test statistics are constructed. Among these quantities, the computation of the sampled covariance matrix in (2.28) deserves particular attention due to the following aspects. First, the limitation of the signal generation block in dealing with one information source at a time can be interpreted as if the  $N$  nodes engaged in CSS operate collocated with a single licensed transmitter ( $P = 1$ ). Second, it has been assumed in Chapter 2 that the nodes are single-antenna devices and that  $N > P$  [103]. This means that, since  $\mathbf{R}_r(n)$  relies on spatial diversity to work, we have to ensure that at least two nodes are deployed and operational within the cooperation footprint. For the sake of fairness, and despite of the fact that all classes other than EBD need only a single node to work, all simulations in this dissertation are carried out for  $N = 2$  unless

<sup>2</sup> As seen in Table 3.6, no signal specific technique aimed at detecting NTSC and PAL signals is currently implemented in MESS. However, in our future work, we intend to investigate the NHSD method and adapt it to detect PAL signals. Therefore, in this dissertation, detection of NTSC and PAL using blind techniques is set so as to allow future comparisons with signal specific techniques.



explicitly stated otherwise. This makes the pre-detection process dependent of the contributions of all nodes. In MESS, this is modeled by allowing each node to experience an individual channel that is generated as in Figure 3.7. Also, as explained in Chapter 1, the emphasis of this dissertation is on the information acquisition process. This allows us to rely on the following abstractions for the processes of exchange and fusion of information. First, we do not care about how the information exchange process takes place. Each node uses a dedicated control channel to report its local findings to the master node (either a BS or any ordinary node currently serving as master node). The control channels used are not bandwidth constrained and are always available, so neither censoring nor weighing is needed. Second, for the sake of simplicity, the information fusion process considers hard combining (based on AND and OR logic) and the issues related to node density and node spread are not taken into account.

### 3.3.3 Detection

The last step depicted in Figure 3.8 is detection. As seen in Chapter 2, this step accounts to the decision-making process that results from the comparison of a generic test statistic  $z(n)$  against a pre-defined detection threshold  $\gamma$ . In this process, the definition of procedures to set  $\gamma$  is important because it largely affects the resulting detection performance. Basically, the procedure to obtain a closed-form expression for  $\gamma$  consists of the derivation of the p.d.f. of  $z(n)$  under the hypotheses  $H_0$  and  $H_1$  followed by the application of some decision criterion such as LRT or NP. In the case of ED and the Bartlett-based SCD, this procedure has been illustrated in the steps that yield to (2.17) and (2.63), respectively. Both expressions can be used to evaluate  $\gamma$  numerically as a function of  $P_{fa}$ , *i.e.* by using  $p(z|H_0)$ . As for the remaining methods in Table 3.6, however, it is more difficult to employ closed-form formulae due to the following reasons. In EBD, this difficulty arises not because of the lack but the multitude of available approaches (see, *e.g.* [103], [104], [106], [107] and the references therein). Closed-form expressions are also available for some methods and in the OFD class, yet each of them depends on a different heuristic adjusting factor added artificially to account for the assumptions made in [51] (for ASSD) and in [121] (for TDSC). As for the CFD class, performance analysis is in general mathematically intractable and no closed-form expressions are known for the specific cases of ACD and BTPD implemented in (2.83) and (2.84). Threshold setting through MC simulation is still commonly adopted to tackle such cases where analysis is mathematically intractable. In our particular situation, where a number of different methods need to be assessed via simulation, the MC method becomes attractive as the *standard* procedure to set  $\gamma$ . Fairness and consistency concerns that could be raised otherwise, *e.g.* by using the method-dependent procedures mentioned above, can be thus avoided.

In view of the facts above, we use MC simulation to set the threshold  $\gamma$  and to evaluate the method performances in MESS. Our MC experiment, as usual, assigns a one to a success and a zero to a failure. A success indicates that the value computed for  $z(n)|H_1$  exceeds  $\gamma$ , *i.e.* a correct detection. A failure indicates the otherwise case, *i.e.* a missed detection. For each SNR value, we repeat the MC experiment for  $N_r$  independent runs and store the values of the test statistics  $z(n)|H_0$  and  $z(n)|H_1$  into the statistic collectors “wfile” and “rxfile”. Next, we sort out the statistic collector “wfile” in ascending order so that its values can be used to set  $\gamma$  for a certain  $P_{fa}$  (fixed and equal for all nodes). Since we are interested in evaluating performance under different CFAR requirements, we parallel

assign two values to  $\gamma$  so as to ensure  $P_{\text{fa}} = 0.1$  and  $P_{\text{fa}} = 0.01$  at each node<sup>3</sup>. Finally, by dividing the number of successes by the number of runs, we obtain an estimate of  $P_{\text{d}}$  for each pair (SNR,  $P_{\text{fa}}$ ). If the noise power  $\sigma_w^2$  is perfectly known, we have

$$P_{\text{d}}(\text{SNR}) = \frac{\sum \{\text{rxfile} > \text{sort}[\text{wfile}(P_{\text{fa}})]\}}{N_{\text{r}}}, \text{ for } \sigma_w^2 \text{ known}, \quad (3.1)$$

which corresponds to the ratio of the number of times that the test statistics in “rxfile” exceed  $\gamma$  to the number of runs. In the practical case that some estimation error  $\Delta\sigma_w^2$  is present, we compute the test statistic  $z(n)|H_0$  from the lower limit of the noise PSD and the test statistic  $z(n)|H_1$  from the upper limit on the actual SNR. The corresponding statistic collectors that result from this pessimistic assumption<sup>4</sup> are denoted as “wfileL” and “rxfileU”. The same threshold obtained by sorting out “wfileL” in ascending order is used to determine the presence of the target signal at the upper limit of the noise PSD (lower limit on the actual SNR). In contrast to the case of known  $\sigma_w^2$ , here we choose a different  $\gamma$  value for each combination of  $P_{\text{fa}}$  and  $\rho$  values. Hence, for each triplet (SNR,  $P_{\text{fa}}$ ,  $\rho$ ), we parallel compute  $P_{\text{d}}$  for all  $\rho \neq 1$  in Table 3.4 using

$$P_{\text{d}}(\text{SNR}) = \frac{\sum \{\text{rxfileU} > \text{sort}[\text{wfileL}(P_{\text{fa}}, \rho)]\}}{N_{\text{r}}}, \text{ for } \sigma_w^2 \text{ estimated}. \quad (3.2)$$

In MESS, (3.1) and (3.2) are used to evaluate the detection performance obtained without using fusion rules, *i.e.* in case of EBD methods and non-EBD methods relying on a single node. For the case of  $i = 1, 2, \dots, N$  nodes that are based on non-EBD methods, the global probability of detection  $Q_{\text{d}}$  and the global probability of false alarm  $Q_{\text{fa}}$  resulting from the combination of the individual node contributions will depend on the fusion rule used. If  $\sigma_w^2$  is perfectly known, we calculate  $Q_{\text{d}}$  using

$$Q_{\text{d}}^{\text{OR}}(\text{SNR}) = \sum_{i=1}^N P_{\text{d}}^i = \frac{\max \{\text{rxfile}_i > \text{sort}[\text{wfile}_i(P_{\text{fa}})]\}}{N_{\text{r}}} \quad (3.3)$$

$$Q_{\text{d}}^{\text{AND}}(\text{SNR}) = \prod_{i=1}^N P_{\text{d}}^i = \frac{\min \{\text{rxfile}_i > \text{sort}[\text{wfile}_i(P_{\text{fa}})]\}}{N_{\text{r}}} \quad (3.4)$$

and  $Q_{\text{fa}}$  using

$$Q_{\text{fa}}^{\text{OR}}(\text{SNR}) = \sum_{i=1}^N P_{\text{fa}}^i = \frac{\max \{\text{wfile}_i > \text{sort}[\text{wfile}_i(P_{\text{fa}})]\}}{N_{\text{r}}} \quad (3.5)$$

$$Q_{\text{fa}}^{\text{AND}}(\text{SNR}) = \prod_{i=1}^N P_{\text{fa}}^i = \frac{\min \{\text{wfile}_i > \text{sort}[\text{wfile}_i(P_{\text{fa}})]\}}{N_{\text{r}}} \quad (3.6)$$

from where it can be seen that each node is assigned its own threshold. The expressions for  $Q_{\text{d}}$  under unknown  $\sigma_w^2$  are obtained by substituting the statistic collectors “rxfile<sub>*i*</sub>” and “wfile<sub>*i*</sub>” by “rxfileU<sub>*i*</sub>” and “wfileL<sub>*i*</sub>”, respectively, in (3.3) and (3.4). Likewise, the expressions for  $Q_{\text{fa}}$  are obtained by substituting “wfile<sub>*i*</sub>” by “wfileL<sub>*i*</sub>” in (3.5) and (3.6).

<sup>3</sup>  $P_{\text{fa}} = 0.1$  is mandated in the standard IEEE 802.22, whereas  $P_{\text{fa}} = 0.01$  has been adopted in the literature to represent more stringent CFAR requirements.

<sup>4</sup> This assumption is pessimistic in the sense that it yields a detection process designed to cater for worst case noise uncertainty scenarios.

One final remark with respect to the CSS implementation in MESS is that, though the channel is generated independently for each node, all nodes experience the same fading parameters and the same SNR. This does not reflect the classical CSS application, where the nodes with higher SNR (*e.g.* in LOS with the licensed transmitter) help the nodes with lower SNR (*e.g.* in NLOS or suffering from a deep fade). But still, our implementation models well the case where a group of nodes experiencing low (possibly the same) SNR team up to improve the performance that each of them would obtain otherwise in a standalone manner. In this case, since  $P_d^i$  will almost surely be less than one,  $\forall i \in [1, N]$ , we can see from (3.3) and (3.4) that non-EBD methods will always exhibit  $Q_d^{\text{OR}} > P_d^i$  and  $Q_d^{\text{AND}} < P_d^i$ . However, according to (3.5) and (3.6), the cooperation gain achievable via OR logic comes at the expense of  $Q_{\text{fa}}^{\text{OR}} > P_{\text{fa}}^i$  whereas AND logic results in  $Q_{\text{fa}}^{\text{AND}} < P_{\text{fa}}^i$ . As the SNR decreases, the probabilities of detection  $P_d$  and  $Q_d$  will in general converge to the probabilities of false alarm  $P_{\text{fa}}$  and  $Q_{\text{fa}}$ . The exact values depend, of course, on the detection method used.

### 3.4 Signal Classification Block

Detection and classification are closely related signal processing tasks. Either one involves decision-making on the basis of received noisy replicas of the target signal. If only a single type of target signal is transmitted in the operation environment, as in Figure 3.1, the goal is to exploit the a posteriori knowledge obtained from the observation of  $r(n)$  to infer the presence or absence of  $s(t)$ . In contrast, signal classification finds application in operation environments where multiple types of target signals can be transmitted simultaneously. In those cases, the classification task can be regarded as *complementar* to detection since it additionally allows to distinguish between at least two types of target signals corrupted by noise. Despite of these similarities, an aspect that differentiates detection from classification is that the former can be carried out blindly or semi-blindly whereas the latter is not possible without reliance on signal specific techniques. Therefore, signal classification for practical multi-standard environments will typically require the combined use of multiple *classifiers*, *i.e.* signal specific techniques that possess complementary signal classification abilities. A generic implementation of such multi-standard operation environment is depicted in Figure 3.9 in terms of the underlying blocks of the MESS platform. After the presence of “some” signal is determined, the output of the method that has detected that signal can be further used to trigger the signal classification block.

For the specific case of the TV bands, we have seen in Chapter 2 that some prior knowledge about the structure of standardized target signals is frequently available and this information can be used for detection as well as for classification. Also, as explained in Section 3.1, TV standards are deployed in most markets in a fashion that follows certain patterns, *e.g.* different TV broadcast standards having the same format are usually not adopted in a single market, the use of both analog and digital formats in the post-switchover era is still common in some markets, etc. Since the TV broadcast standards currently deployed (or under assessment for deployment) in a country constitute publicly available information, we can greatly facilitate the signal classification task by exploiting that information. In doing so, the context awareness obtained when a WSD detects and subsequently classifies certain combinations of target signals constitutes helpful information for determining the market where that WSD currently operates in.

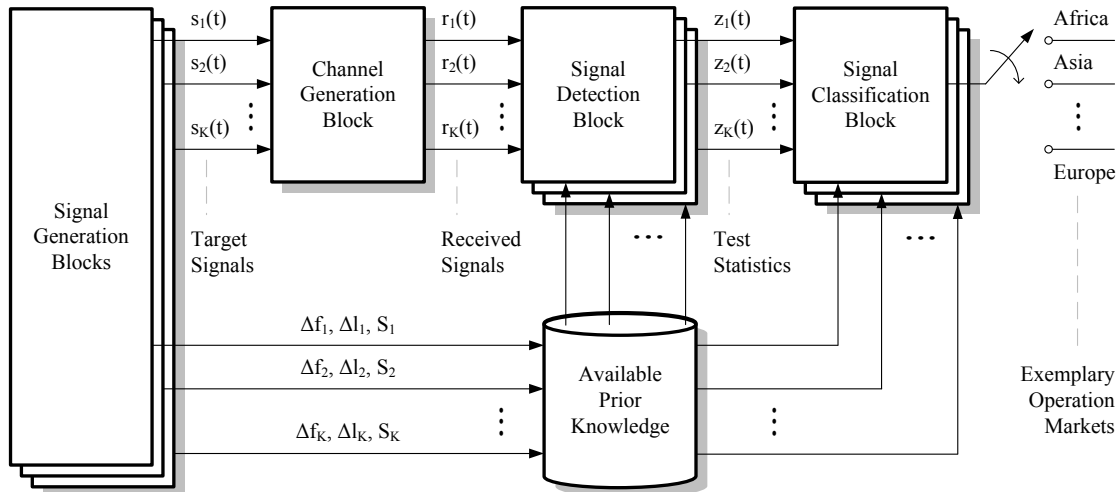


**Fig. 3.9:** Generic multi-standard operation environment based on the MESS platform.

Figure 3.10 illustrates how signal classification can be used in the determination of some exemplary markets. If WSD classify the detected signals as NTSC-compliant, the operation market will be most likely the Americas. Likewise, the presence of ATSC or ISDB-T signals provides an indication that WSD operate either in North America or in South America, respectively. Improved context awareness can be achieved by combining the information obtained from both analog and digital formats. For instance, if WSD are able to perceive that ISDB-T signals are simulcast in PAL, we can delimit the operation market to three countries: Argentina, Brazil, and Uruguay. In some cases, the operation market can be determined with resolution equal to a single country, *e.g.* Colombia (DVB-T simulcast in NTSC) and Greenland (DVB-T simulcast in PAL). Hence, based on the output of the signal classification block, a WSD can autonomously react to current operation conditions on a market-wide basis. Examples of reaction include but are not limited to the reduction of adjacent channel interference by fine tuning the receiving filter according to the allowed

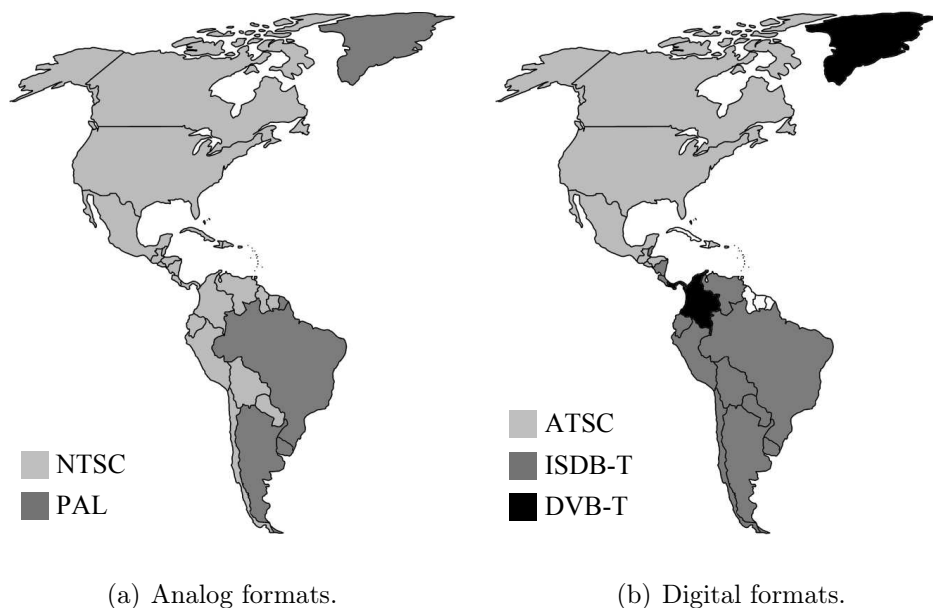


**Fig. 3.10:** TV broadcast standards most deployed in the Americas.

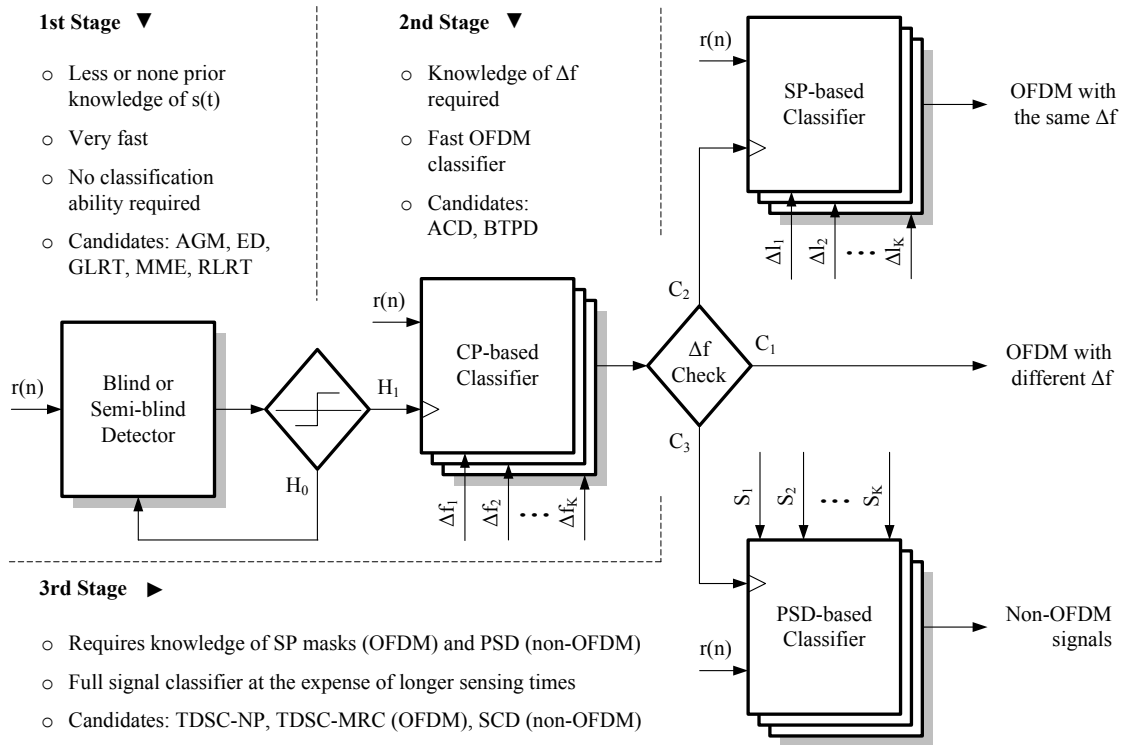


**Fig. 3.11:** Detailed view of the signal classification block.

channel bandwidth (6, 7, or 8 MHz), use of prior information about how PMSE operates in that market to set the resolution used in wavelet-based MRSS or to feed the MF-based exhaustive search in (2.95), return information about the *actual* spectrum occupancy to the database (if sensing is used in conjunction with GDA), etc.

Market distinction based on signal classification becomes less straightforward in Africa, Asia & Pacific, Europe, and the CIS because most countries in these regions adopt (or are considering adopting) DVB-T as the digital counterpart of the analog PAL. In this case, WSD can further improve context awareness by additionally scanning the spectrum for signals based on IEEE 802.22 and/or ECMA-392. However, such future TVBD standards are not deployed yet, so a more immediate alternative might be exploit the small (yet allowed) variations in the parameterization<sup>5</sup> of target signals based on the PAL standard [122], *e.g.* transmission band (VHF or UHF), channel bandwidth (7 or 8 MHz), bandwidth of the video signal (5.0, 5.5, or 6.0 MHz), and particularly the position of the sound subcarrier (5.5, 6.0, or 6.5 MHz). This might be an option until 2020, when most countries should have analog TV stations switched off. This is reasonable time for TVBD standards to become popular or for other standards currently under development to enter the market.

The signal classification block is implemented in MESS as the three-stage cascade signal classifier shown in Figure 3.11. The requirements imposed to each stage, shown as floating text in the figure, are described in the sequel.

<sup>5</sup> To cope with extreme ambiguous scenarios, we envision power-plugged WSD able also to classify electric voltage and frequency. This would make it possible for fixed WSD, as well as for portable WSD while being charged, to determine the operation market with better resolution, *e.g.* Western Europe (230 V, 50 Hz) or Eastern Europe and CIS (220 V, 50 Hz).

### 3.4.1 First Stage: Blind Detector

As seen earlier in this section, signal detection may be carried out prior to classification in order to minimize unnecessary signal processing efforts. Accordingly, the first stage of the cascade classifier in Figure 3.11 is a simple detector, so no classification ability is required at that point. The goals are to monitor the operation environment and trigger the second stage whenever  $H_1$  is perceived true. For this to work efficiently, it is important for the first stage to be capable of providing accurate channel occupancy information in a timely manner even in the low SNR regime. This keeps the detection delay low and avoids unnecessary classification measures due to false alarms. If we further impose that less or none prior knowledge of target signals should be required for detection, then the best design option is to implement the first stage using blind techniques such as AGM, GLRT, or MME. Alternatively, we can use semi-blind techniques like ED or RLRT at the expense of degraded robustness against noise uncertainty.

The computational complexity of these methods is given in Table 3.8 in terms of number of real multiplications (RM) and number of real additions (RA). Each complex multiplication requires four RM and two RA, and each complex addition requires two RA. The other columns of the table indicate whether the method possesses classification ability (CA) and the prior knowledge that it requires to work (PK). All methods in this table but ED perform EBD, which comprises of two basic tasks. The first, posing  $\text{RM} = MN^2\iota$  and  $\text{RA} = N^2\iota(M - 1)$ , is the estimation of the sample covariance matrix in (2.28) [103]. As for the second task, related to the eigenvalue decomposition, the exact number of real operations depends on the algorithm used, *e.g.* it is on the order of  $\mathcal{O}(N^3\iota^3)$  multiplications and additions in case of singular value decomposition (SVD) [145]. If the same number of nodes is used both in ED and EBD, the complexity of the latter is about  $N\iota$  times that of the former but still linear with the number of samples. For  $M \gg N\iota$ , *i.e.* the number of samples is much larger than the smoothing factor, the dominant term is  $MN^2\iota$ .

### 3.4.2 Second Stage: Fast OFDM Classifier

Most target signals implemented in MESS are OFDM-based. It is therefore natural to start classifying them by performing a simple check to determine the presence of periodicities induced by the CP. This can be performed by a CP-based classifier, made fast and of low complexity by using either ACD or BTPD. Let  $N_c$  be the number of *categories*, *i.e.* the number of types of target signals present in the operation environment. As shown in Table 3.9, and again assuming  $N$  cooperating nodes, ACD is as complex as ED but needs to know *all* symbol lengths used in the operation environment to compute  $\{T_{D_c}\}_{c=1}^{N_c}$ . BTPD can

**Table 3.8:** Summary of requirements for the 1st stage.

| Method | RM                                    | RA                | CA   | PK           |
|--------|---------------------------------------|-------------------|------|--------------|
| AGM    | $MN^2\iota + \mathcal{O}(N^3\iota^3)$ | $N^2\iota(M - 1)$ | None | None         |
| GLRT   | $MN^2\iota + \mathcal{O}(N^3\iota^3)$ | $N^2\iota(M - 1)$ | None | None         |
| MME    | $MN^2\iota + \mathcal{O}(N^3\iota^3)$ | $N^2\iota(M - 1)$ | None | None         |
| ED     | $4MN$                                 | $2N(2M - 1)$      | None | $\sigma_w^2$ |
| RLRT   | $MN^2\iota + \mathcal{O}(N^3\iota^3)$ | $N^2\iota(M - 1)$ | None | None         |

**Table 3.9:** Summary of requirements for the 2nd stage.

| Method | RM    | RA           | CA  | PK                                    |
|--------|-------|--------------|-----|---------------------------------------|
| ACD    | $4MN$ | $2N(2M - 1)$ | Yes | $\{T_{D_c}, \Delta f_c\}_{c=1}^{N_c}$ |
| BTPD   | $8MN$ | $2N(4M - 1)$ | Yes | $\{\Delta f_c\}_{c=1}^{N_c}$          |

**Table 3.10:** Allowed subcarrier spacings (in kHz) for 6 MHz channels.

| Target      | 128   | 2k   | 4k   | 8k   |
|-------------|-------|------|------|------|
| DVB-T       | –     | 3.35 | 1.67 | 0.84 |
| ISDB-T      | –     | 3.97 | 1.98 | 0.99 |
| IEEE 802.22 | –     | 3.35 | –    | –    |
| ECMA-392    | 53.57 | –    | –    | –    |

detect OFDM signals blindly but is twice as complex as ACD. However, in the context of signal classification, we observe that both ACD and BTPD require additional knowledge of *all* subcarrier spacings  $\{\Delta f_c\}_{c=1}^{N_c}$ . This information is summarized in Table 3.10 for the case of the multi-standard operation environment considered in this dissertation. It can be seen that different  $\Delta f$  are adopted in multi-mode standards, such as DVB-T and ISDB-T. Hence, for multi-mode standards,  $N_c$  is the sum of the number of modes adopted by all standards deployed in the market of interest. Moreover, the larger  $\Delta f$  adopted in ECMA-392 makes it easier to distinguish that category from all others. Distinction among those categories representing multiple modes of DVB-T and ISDB-T is possible too, but we expect the performance of the CP-based classifier to decrease in this case because there will be less room to accommodate the error inherent to the estimation of  $\Delta f$  from the noisy  $r(n)$ . Generally speaking, as long as all categories have different  $\Delta f$  and the SNR is high enough, the condition  $C_1$  in Figure 3.11 occurs almost surely so that the second stage is able to accurately classify OFDM-based standards.

Different conditions arise when ambiguous categories exist. If  $\Delta f$  is the only information used to define a category, there are at least two cases of ambiguity that cannot be resolved at the second stage. The first case, highlighted using light grey color in Table 3.10, is observed regardless of the SNR experienced by WSD when  $\Delta f = 3.35$  kHz. If it is crucial to distinguish between DVB-T Mode 2k and IEEE 802.22 (depends on market, application, etc), we need to instruct the second stage to trigger a third SP-based stage. This condition is identified as  $C_2$  in Figure 3.11. Another example of ambiguity is represented by condition  $C_3$ , under which the estimate of  $\Delta f$  obtained by the second stage does not match to any value in Table 3.10. This condition occurs when the SNR is very low or simply because no CP-induced periodicities can be found in the signals we are attempting to classify, *e.g.* they belong to non-OFDM categories. In either case, we cope with condition  $C_3$  by triggering a third PSD-based stage.

### 3.4.3 Third Stage: Full Signal Classifier

We refer to the third and last stage of the signal classification block as full signal classifier because it has been designed to accurately classify *any* category out of those generated in

MESS. This means that, at the expense of longer classification time and increased requirements of prior knowledge and complexity, here we can tackle *all* ambiguous conditions left unresolved by the second stage. Signal classification on the basis of  $\Delta f$  is not always possible but, provided that additional information about the SP insertion pattern is available, Figure 3.3 ensures us that DVB-T Mode 2k and IEEE 802.22 can be distinguished. If this is the case, we can resolve condition  $C_2$  using a SP-based classifier that relies either on TDSC-NP or on TDSC-MRC. As seen in Table 3.11, both methods need to know *all* symbol index differences between two OFDM symbols with the same SP pattern. Unlike in the second stage, where  $\Delta f$  varies with the operation mode,  $\Delta l$  is fixed within a given standard and thus (since  $N_c = N_{\text{St}}$ ) we have  $\{\Delta l_c\}_{c=1}^{N_{\text{St}}}$ . From this table, we also see that TDSC-MRC is more complex than TDSC-NP. The reason is that the former takes into account multiples of  $\Delta l_0$ , *i.e.* the shortest difference between two OFDM symbols with the same SP pattern, in the correlation whereas the latter considers a single  $\Delta l$ .

We have seen in Chapter 2 that non-OFDM standards, whether analog or digital, typically do not convey SP. Instead, in ATSC, NTSC, or PAL, synchronization tasks carried out at the receiver are supported by periodically inserting SYNC symbols into the data stream at the transmitter. For this kind of target signals, it is evident that the SP-based classifier above cannot resolve for condition  $C_3$  because there are no SP to correlate. This condition calls for a classifier that relies on non-OFDM signal specific techniques, such as ASSD or SCD. By comparing (2.89) to (2.93), we see that ASSD and TDSC-MRC share the same underlying principle. One drawback of ASSD, also present in its NTSC counterpart and eventual extension to PAL, is that SYNC symbol densities are much lower than those of SP. Therefore, we expect the performance of ASSD to degrade faster as compared to TDSC-MRC, particularly in the low SNR regime. SCD seems a more promising candidate to classify non-OFDM target signals because it is fast, exploits features other than SYNC symbols, and is originally designed to work at very low SNR. The prior knowledge that SCD requires for classification accounts for the set of noise-free replicas of the PSD of the transmitted signal  $\{S_c(f)\}_{c=1}^{N_c}$ . Non-OFDM standards do not make use of multiple operation modes, so this set is composed by the power spectra shown in Figure 3.5.

Though the sharp spectral features present in the spectra of FM-based WM signals shown in Figure 3.6 make SCD interesting also for detection (and eventual classification) of PMSE, it is worth noting that this is *out of the scope* of the proposed signal classification block. The reason is that PMSE and TV broadcast are fundamentally different due to the nonstandardized nature of the former. Even under the assumption that the target signal is FM modulated (can be AM, FM, or digitally modulated in practice), the peaks in its PSD do not occur at fixed positions as opposed to in ATSC, NTSC, and PAL. Also, as seen in Chapter 2, operational parameters such as  $f_c$ ,  $f_{\text{dev}}$ , and  $W$  vary depending on a number of factors that include manufacturer, device model, and operation market. In the

**Table 3.11:** Summary of requirements for the 3rd stage.

| Method   | RM                       |  |                  | RA                               |  | CA  | PK                           |
|----------|--------------------------|--|------------------|----------------------------------|--|-----|------------------------------|
| TDSC-NP  | $4N N_1 T_D$             |  |                  | $2N (N_1 - 1) [T_D + (T_D - 1)]$ |  | Yes | $\{\Delta l_c\}_{c=1}^{N_c}$ |
| TDSC-MRC | $4N$                     | $\frac{N_1}{\Delta l_0} + \left(\frac{N_1}{\Delta l_0}\right)^2$ | $\Delta l_0 T_D$ | $2N$                             | $\frac{N_1}{\Delta l_0} + \left(\frac{N_1}{\Delta l_0}\right)^2 [T_D + (T_D - 1)]$ | Yes |                              |
| SCD      | $2MN (2M + \frac{1}{2})$ |  |                  | $2MN (2M + \frac{5}{2}) - 2$     |  | Yes | $\{S_c(f)\}_{c=1}^{N_c}$     |



unlikely event that all possible combinations of these parameters are available a priori, the amount of information required for detection would still be too large to be handled by practical WSD. While the detection of PMSE requires sophisticated spectrum estimation techniques [139][140], signal classification in this more practical context is to date an open research problem<sup>6</sup>.

## 3.5 Chapter Summary

This chapter has described MESS, a Matlab-based sensing platform that we developed to assess the performance achieved when different types of target signals are detected in the presence of different types of uncertainty. The major goal of MESS is to provide us with a baseline for comparisons, thus far not available in the literature, so it is possible to compare different methods on a fair basis. Such performance analysis, to be carried out in Chapter 4, will help us clarify some aspects observed during the implementation of MESS and define the method to be used in each classifier of the three-stage signal classification block in Figure 3.11. These aspects include:

- **1st Stage:** ED seems the most promising candidate for the first stage in view of its low complexity. However, it is likely the worst method when it comes to robustness against noise uncertainty. RLRT is also susceptible to noise uncertainty but possesses higher statistical power than ED. Hence, we expect RLRT to be more robust than ED when  $\sigma_w^2$  is not exactly known. As complex as any other EBD method, RLRT will be attractive only if the limitation in performance introduced by SNR walls is not that significant as compared to what we can achieve using blind EBD methods. If this is not the case, our choice will be restricted AGM, GLRT, or MME. Performance should be similar, though GLRT has potential to outperform MME as the number of cooperating nodes increases, *i.e.* as  $\frac{1}{N} \text{Tr}[\mathbf{R}_r(n)]$  becomes lower than  $\lambda_{\min}$ .
- **2nd Stage:** If the prior knowledge in Table 3.9 is available, ACD offers the same classification ability as BTPD but is half less complex. If this is the case, then both methods are capable of accurately classifying categories composed of OFDM signals that have different subcarrier spacings. This makes of ACD the most promising candidate for the second stage, though our previous work [90] raises one concern about that method. We showed through simulations that the single-node performance of ACD is poor when ECMA-392 signals are detected under multipath fading. While this suggests that it is better to ensure multipath robustness at the expense of increased complexity, *i.e.* by using BTPD, it remains to be investigated why and under what circumstances this condition occurs as well as whether it can be mitigated by enforcing cooperation among multiple nodes.
- **3rd Stage:** Our goal with respect to the third stage is two-fold. First, we need to choose one TDSC method to implement the SP-based classifier. Ideally, TDSC-MRC outperforms TDSC-NP at the expense of increased complexity. In the practical case of imperfect synchronization, TDSC-NP becomes attractive because its performance is similar to that of TDSC-MRC. This behavior was observed in single-node simulations in the presence of SFO [132], but still lacks an analytical treatment, *e.g.*

---

<sup>6</sup> Among the applications discussed in Chapter 5, we describe an alternative approach that may be used to ensure PMSE coexistence in the post-switchover era.

as done in [121] for CFO. Second, Figure 3.5 suggests that differentiation among ATSC, NTSC, and PAL signals is possible on the basis of the sharp spectral features present in their spectra. While this makes SCD the most promising method to implement the PSD-based classifier, we still need to check whether SCD can also be used to detect the typically flat spectrum of OFDM-based signals. In the event that SCD can exploit the different signal edges of the spectra in Figure 3.4(a) and Figure 3.4(b) to reliably distinguish between DVB-T Mode 2k and IEEE 802.22, we could drop the SP-based classifier and use a single (PSD-based) classifier to resolve for both condition  $C_2$  and condition  $C_3$ .



# Chapter 4

## Simulation Results

In this chapter, we use MESS to carry out a thorough assessment of the detection performance that each method in Table 3.6 achieves when detecting different target signals under different operation conditions. The results presented in what follows are derived from an extensive series of simulations conducted from October 2011 to May 2012 at the high-performance parallel computing cluster system of the Regional Computing Center of Lower Saxony [146]. The task of dealing with the huge amount of data generated during over 50000 simulation hours was challenging from a number of perspectives, particularly with respect to the presentation of the outcomes. Our concern was about figuring out a way to present the results of interest while keeping redundancy reduced to a minimum. Therefore, throughout the remainder of this dissertation, we use the notion of *best-case curves* to characterize the performance that a class obtains when we (i) use the fusion rule yielding the highest  $Q_d$  (OR logic) to (ii) combine the local results of the most accurate method belonging to that class (iii) under the mildest CFAR requirement ( $P_{fa} = 0.1$ ). Conversely, *worst-case curves* describe the performance that results from (i) the combined use of the fusion rule yielding the lowest  $Q_d$  (AND logic) and (ii) the least accurate method within a class (iii) under the most stringent CFAR requirement ( $P_{fa} = 0.01$ ). Whenever we realize that further support is necessary for our exposition of ideas, we provide *detailed analysis* plots. Such additional plots are intended to help us explaining the (eventually large) gaps between best- and worst-case curves, *e.g.* by comparing the methods within a class in terms of all combinations of fusion rule and CFAR requirement, rescaling axes so as to improve visualization, combinations of both, etc. Unless explicitly stated otherwise, the gains and losses mentioned in our discussions are measured at the operation region of interest, *i.e.* in terms of the SNR where  $P_d \geq 0.99$  is first met.

The remainder of this chapter consists of seven parts that are organized as follows. In the first part, we carry out an exemplary statistical analysis on the sample data accumulated on the statistic collectors “wfile” and “rxfile”. The second part presents the results obtained under AWGN when no uncertainty is present in the operation environment. Such “ideal” performance will serve as the baseline for comparisons with the case where different sources of uncertainty are considered. In parts three to five, we extend the AWGN analysis to the case when uncertainty about channel fading parameters, noise power, the carrier frequency and the sampling rate used at the licensed transmitter is present in the operation environment. For each source of uncertainty, we consider the impact exerted by the type of target signal and number of nodes on the performance degradation introduced by that source. This allows us to rank each method in terms of its robustness against multipath

fading, noise uncertainty, and clock offsets. Specifically, we are interested in checking if there exist methods that exhibit substantial performance degradation (as compared to the AWGN case) when detecting some but not all types of target signals. A second aspect that we are interested in is to look at whether the fundamental detection limits of those methods can be further shifted by using an increased number of cooperating nodes. Other operation conditions known to influence the AWGN performance, such as fusion rule, CFAR requirement, symbol length, and CP ratio are also taken into account in the analysis. In the sixth part, we summarize the lessons learned, draw our conclusions, and use them to determine a specific structure for the generic signal classification block in Figure 3.11. Part seven closes the chapter.

## 4.1 Exemplary Statistical Analysis

The underlying principle of MC simulation relies on the strong law of large numbers, which states that the arithmetic mean of a sequence of i.i.d. random variables converges almost surely to an expected value that is the same for all variables in that sequence [147]. This central result in probability theory allows us to approximate the expected value of a random event by arithmetically averaging a number of independent experiments, each and every experiment having the same distribution as the event of interest. As in any stochastic method, there will always exist some error related to the ability of the MC estimate in approximating the exact expected value. When characterized by the standard deviation of the difference between the MC estimate and the exact expected value, this error is on the order of  $1/\sqrt{N_r}$  [148]. Hence, at the expense of significant effort (in terms of computer run time), we can minimize the error associated to the MC estimate simply by making  $N_r$  arbitrarily large. Similar accuracy improvements can be achieved by decreasing the variance of the MC estimate. When it comes to variance reduction, a number of numerical techniques can be applied to exploit known information about the problem and use this information to improve the accuracy of the MC experiment. For instance, more efficient experiments can be obtained by modifying the statistical properties of the random processes input to the simulator. Some techniques, *e.g. importance sampling* (IS), modify the underlying sampling p.d.f.'s to bias the sampling. This *artificially* increases the likelihood that a run produces a nonzero score. To compensate for this biasing, the weight assigned to each run is selected so that unbiased scores can still be produced. However, despite of its potential to reduce the simulation run time, an IS experiment is context-dependent in the sense that the simulation densities and weights introduced thereby have to be designed for each individual problem at hand [148]. One strong implication of this fact is that the power of the IS technique largely depends on the choice of such parameters and this choice often poses a nontrivial problem.

In our specific case, the test statistics implemented in MESS may follow different distributions. This means that at least each class in Table 3.6 requires its own IS scheme<sup>1</sup>. Even if we neglect the development and integration efforts required to implement IS on MESS, this implementation would suit only those methods whose test statistics follow (or can be approximated by) distributions that are well understood. This is not the case here, so

---

<sup>1</sup> This issue is in general common to variance-reduction techniques, where the price of acquiring and dealing with the required information has to be paid *before* actually achieving some (if any) reduction in variance [148].

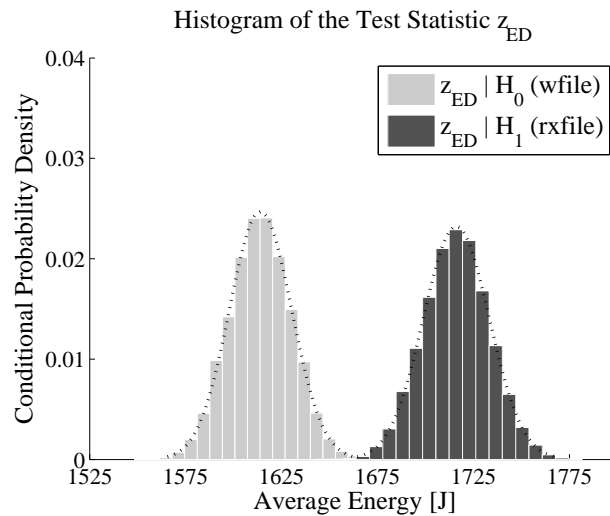
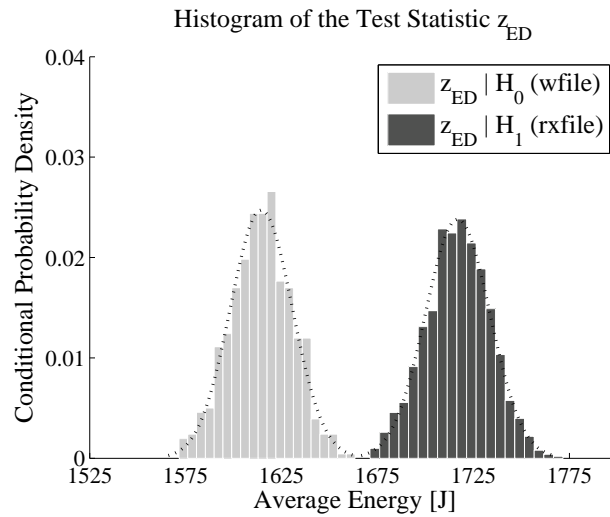
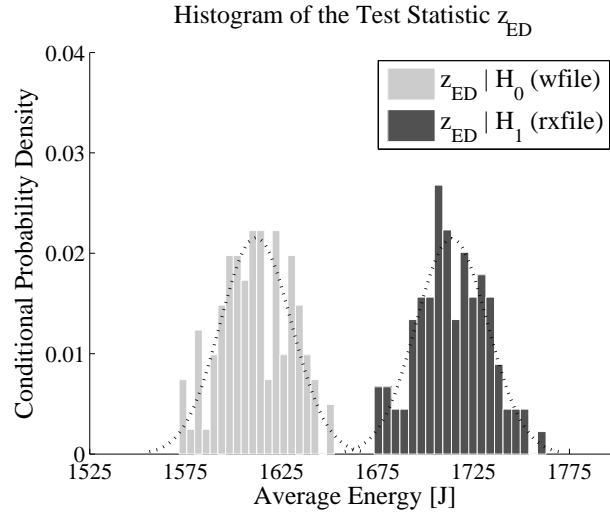
we decided not to use neither IS nor any variance-reduction technique in this dissertation. Instead, recalling that our run-time limitations are mild thanks to the availability of the high-performance computer cluster system mentioned earlier in this section, we use a “brute force” approach that relies on large  $N_r$ . To determine  $N_r$  in a MC experiment, a popular rule of thumb is to use a ratio where the numerator is on the order of 10 to 100 and the denominator is the a priori probability of the event of interest. Assuming that the resolution of the measured probabilities should be in the range from 0.1 to 0.01, this corresponds to  $100 \leq N_r \leq 10000$  for each experiment, *e.g.* for each simulated SNR point. By assigning values from this range to  $N_r$ , we ensure that the error associated to the MC estimates will be on the order of 0.1 to 0.01. We could pick the setting giving the smallest error but, before starting with large scale simulations, it is advisable to analyze how these different settings influence other aspects of the data gathered through simulation.

Among a number of statistical tools available for data visualization [149], *histograms* can be used to estimate the p.d.f. of the data set under analysis from the distribution of the data values. Exemplary histograms are provided in Figure 4.1 for the case of ECMA-392 signals detected via ED under AWGN conditions. In this case, the approximation in (2.11) relies on the central limit theorem and, as such, we expect the conditional p.d.f.’s  $p(z_{\text{ED}}|H_0)$  and  $p(z_{\text{ED}}|H_1)$  to follow asymptotic normal distributions. This is exactly the case here, as the histograms of  $z_{\text{ED}}$  under both hypotheses clearly approach the estimated bell-shaped p.d.f.’s, superimposed on the plots as dashed lines, as  $N_r$  increases. Notwithstanding the intuitive nature of Figure 4.1, detecting normality from a histogram is often a hard task, particularly when the data set is small as in Figure 4.1(a). In such cases, it is useful to obtain additional information about the data set via *normal probability plots*. As illustrated in Figure 4.2 for the statistic collector “rxfile”, this tool allow us to verify on a graphic manner whether our sample data comes from a normal distribution. The bottom line here is to compare the sample data in “rxfile” to a straight line resulting from a linear fit of the sample order statistics of that statistic collector. The closer the points are from the straight, the more difficult it is to distinguish the sample data from normal data. The *outliers*, *i.e.* points that do not lie on the straight, account for deviations from normality and the number of outliers clearly decreases as  $N_r$  increases.

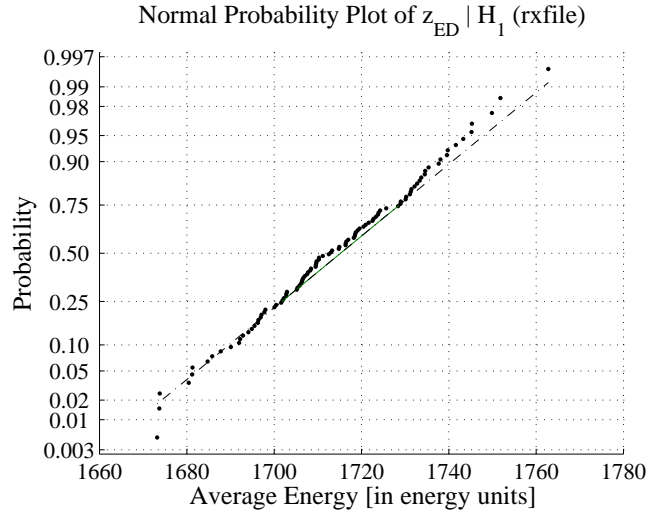
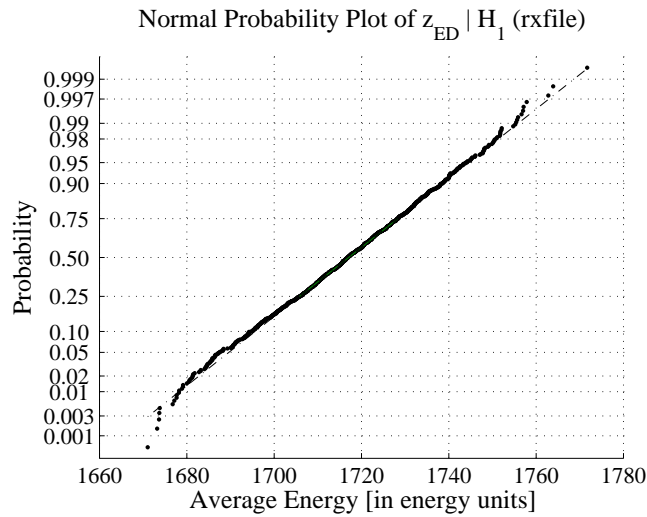
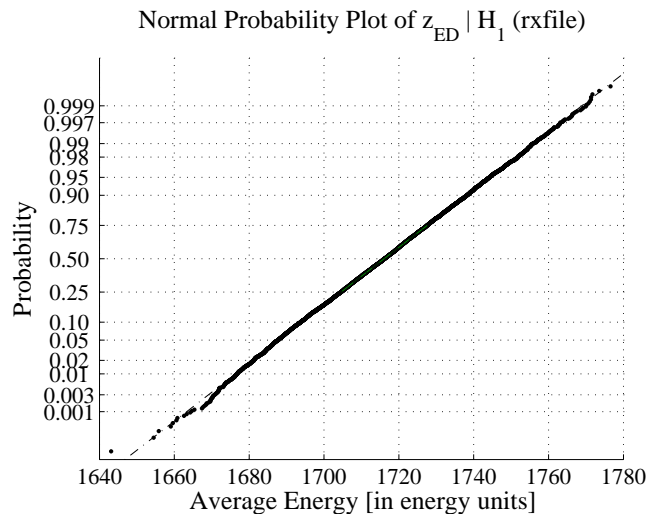
The statistical analysis presented in this section has illustrated only the case of ED, but similar results for the remaining methods implemented in MESS are straightforward to obtain. Setting  $N_r = 10000$  is more than enough for the central limit theorem to hold, so all the method distributions considered in this dissertation can be treated as asymptotically normal. This number of runs keeps the error of our MC estimates on the order of 0.01, which is low enough to allow accurate analysis in the operation region of interest.

## 4.2 AWGN Performance

Having the system and simulation settings put in place, it is now time to start presenting our results. In this section, we present a set of results that reflect simulations carried out when no source of uncertainty is present in the operation environment and the noise is pure AWGN. The performance derived in such idealized scenario will serve as the baseline for comparisons with the more challenging scenarios investigated later on in this section when different sources of uncertainty are taken into account.



**Fig. 4.1:** Impact of number of runs on the distribution of the test statistic  $z_{ED}$ . The exemplary histograms depicted here were obtained by using ED to detect ECMA-392 signals under AWGN ( $CP = 1/8$ ,  $SNR|_{dB} = -15$  dB, 20 bins).

(a)  $N_r = 100$  runs.(b)  $N_r = 1000$  runs.(c)  $N_r = 10000$  runs.

**Fig. 4.2:** Impact of number of runs on the normality of the statistic collector “rxfile”. The exemplary normal probability plots depicted here were obtained by using ED to detect ECMA-392 signals under AWGN ( $CP = 1/8$ ,  $SNR|_{dB} = -15$  dB).



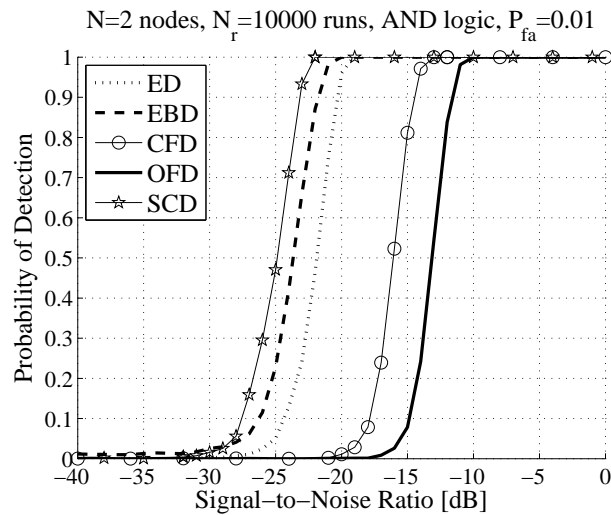
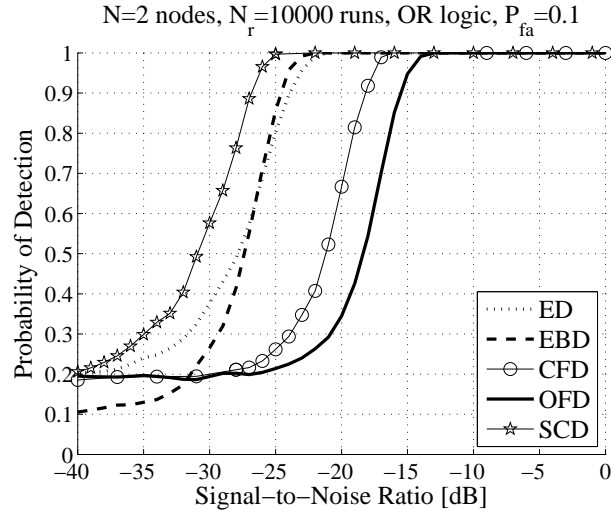


**Fig. 4.3:** Detection performance of DVB-T signals under AWGN (Mode 2k, CP=1/4).

### 4.2.1 OFDM-based Target Signals

When the target signals are based on DVB-T, it is seen in Figure 4.3 that losses ranging from 3 dB to 4 dB are introduced by switching from the best- to the worst-case curves. If we keep the fusion rule unchanged, decreasing the CFAR requirement from 0.1 to 0.01 yields a degradation of 1 dB for all methods. Changing the fusion rule from OR logic to AND logic introduces additional losses of 1 dB to 2 dB depending on the class and CFAR requirement. The EBD class works independently of fusion rule but its performance still depends on the specific method used. Here, RLRT is the best EBD method and AGM, GLRT, and MME perform essentially the same and about 2 dB worse than RLRT. Since ED and SCD are singleton classes, the losses observed are caused only by fusion rule and CFAR requirement. As for CFD and OFD, the specific method used also plays a role in the achievable performance and the best (worst) methods within these classes are BTPD (ACD) and TDSC-MRC (TDSC-NP). All in all, the top performers are SCD and EBD while CFD and OFD account to the least and second least accurate classes. The sensing time is 1.12 ms for all but the OFD class, where it is 4.48 ms.

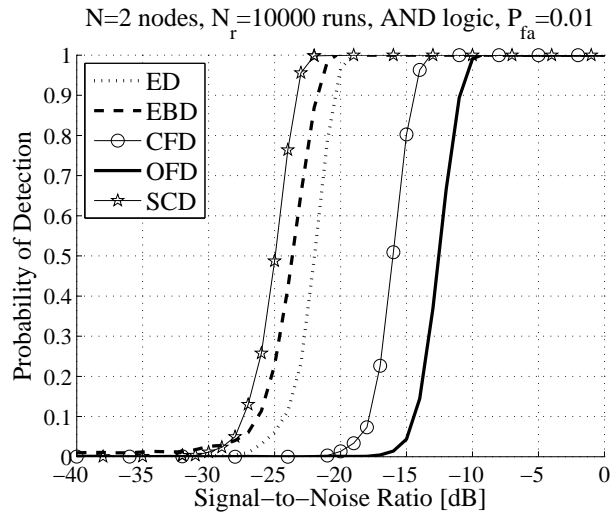
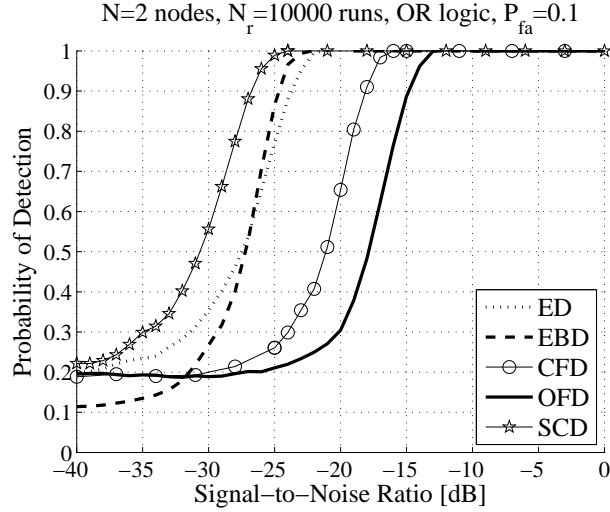
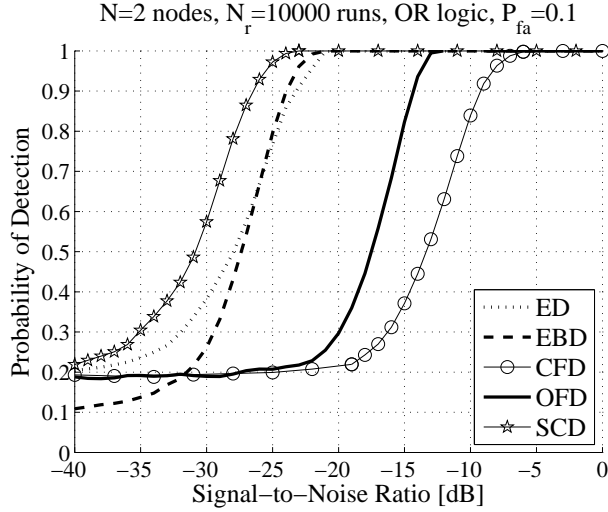
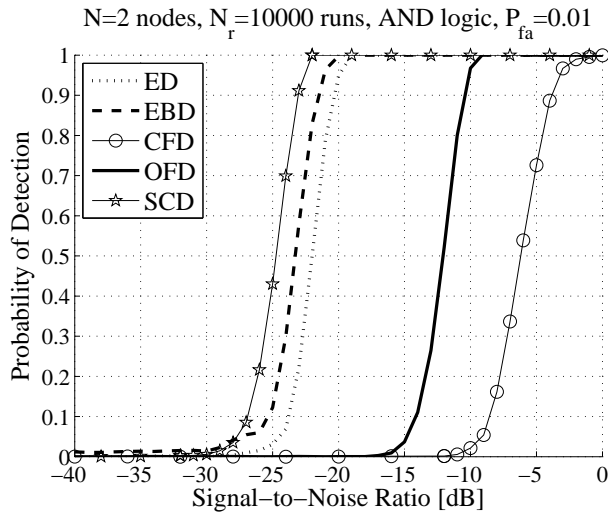


**Fig. 4.4:** Detection performance of ISDB-T signals under AWGN (Mode 2k, CP=1/4).

Recalling from Table 3.1 and Figure 3.3 that the OFDM parameterizations used in DVB-T and ISDB-T are quite similar, we expect no significant changes when comparing these standards. This is confirmed in Figure 4.4, where the sensing time is again set to 4.48 ms for OFD and 1.12 ms for the remaining classes. This comparison suggests that performance does not vary much if WSD operate collocated with licensed transmitters based only on OFDM-based standards. However, the detection of OFDM signals is known to be largely dependent of the CP ratio, symbol length, or both depending on the class used [115][121]. To confirm the results in the related work, we first examine the influence of the CP ratio by comparing the results shown in Figure 4.4 (CP=1/4) to those in Figure 4.5 (CP=1/32). EBD and ED are composed by blind and semi-blind methods and therefore immune to variations in the CP ratio. SCD is robust too because the PSD of an OFDM signal remains essentially the same as we vary the CP ratio. As for OFD, we confirm that TDSC-MRC and TDSC-NP are only slightly susceptible to such changes, and the 1 dB loss observed here matches well to that reported in [121]. In contrast, CFD gives losses of 9 dB (best-case curves) and 12 dB (worst-case curves) as expected from [115].



(a) Best case.



(b) Worst case.

**Fig. 4.5:** Detection performance of ISDB-T signals under AWGN (Mode 2k, CP=1/32).

From Table 3.1 we also see that DVB-T and IEEE 802.22 follow the *same* OFDM parameterization, except for the slightly larger bandwidth occupied by signals based on the former. Therefore, we expect ED and EBD to achieve similar performance for both standards. CFD and SCD should not be affected much neither because of the same symbol length, same CP ratio, and similar spectra (see Figure 3.4) used in DVB-T and IEEE 802.22. We confirm this in Figure 4.6, where the results shown for all but the OFD class are essentially the same as those obtained for DVB-T under both best- and worst-case conditions. In case of OFD, we know from Figure 3.3 that the SP cells are “boosted” by a factor  $4/3$  in DVB-T but transmitted with unitary gain in IEEE 802.22. Since both standards adopt the same symbol length, the performance gap of OFD observed between Figures 4.3 and 4.6 can be explained in terms of the ratio of the power of SP cells to the power of all cells (SP and data) of any subcarrier in a single PRU. The PRU adopted in DVB-T repeats itself every four symbols, so its power ratio  $(s_p/s)^2$  is:

$$\frac{(4/3)^2}{1^2 + 1^2 + 1^2 + (4/3)^2} = \frac{16}{43}. \quad (4.1)$$

In IEEE 802.22, the pilot insertion rate is lower than in DVB-T so that the PRU repeats itself only every seven symbols. In this case, we have  $(s_p/s)^2$  equal to:

$$\frac{1^2}{1^2 + 1^2 + 1^2 + 1^2 + 1^2 + 1^2 + 1^2} = \frac{1}{7}. \quad (4.2)$$

Since the power ratio in (4.1) is larger than in (4.2), it is easier to detect DVB-T using TDSC methods than IEEE 802.22. Indeed, the performance gap due to differences in the amplitude and periodicity of the pilot insertion pattern used in DVB-T and IEEE 802.22 can be as high as 20 dB. This is better seen at the detailed analysis given in Figure 4.6(c), where the  $x$ -axis is rescaled up to 10 dB. We also see in this figure that, in contrast to in DVB-T and ISDB-T, the performances of TDSC-MRC and TDSC-NP are essentially the same for IEEE 802.22. In this case, the reduced computational complexity of TDSC-NP makes it more attractive than TDSC-MRC.

To complete our analysis about the detection of OFDM-based target signals, we still need to examine the impact that the symbol length exerts on this process. DVB-T and ISDB-T use  $T_{\text{SYM}}$  up to 1.49 ms (in 8K mode with CP=1/4), whereas ECMA-392 conveys information using shorter symbols around only 20  $\mu\text{s}$  long. Hence, despite the fact that DVB-T, ISDB-T, and ECMA-392 are all OFDM-based standards, the detection of target signals complying with these standards clearly imposes different requirements on the design of WSD. We analyze this impact by comparing Figure 4.3 ( $T_{\text{SYM}} = 0.37$  ms) to Figure 4.7 ( $T_{\text{SYM}} = 19$   $\mu\text{s}$ ). ECMA-392 signals are detected using 0.75 ms for the OFD class and 57.75  $\mu\text{s}$  for all remaining classes. Slightly larger than in DVB-T, the performance gap between best- and worst-case curves in ECMA-392 lies between 2 dB and 7 dB. The most and the least accurate performers remain the same as in DVB-T. Depending on the class used to detect ECMA-392 signals, the impacts of fusion rule and CFAR requirement account for losses ranging from 1 dB to 6 dB. Since the impact of such design options is more severe in ECMA-392 than in DVB-T, our results suggest that method selection should be carried out on a target-dependent basis. Specifically, for ED, EBD, and CFD, we observe a relatively mild average loss ( $\approx 4$  dB) that can be explained by adding up the impacts above. With losses as high as 11 dB (best-case curves) and 13 dB (worst-case curves), OFD is the class most significantly impacted by a shorter  $T_{\text{SYM}}$ . This matches well our expectations because, as seen in Figure 3.3, ECMA-392 transmits SP cells using unitary power and employs a PRU that repeats itself only every 13 symbols. The ratio  $(s_p/s)^2$  that results from this setting is:

$$\frac{1^2}{1^2 + 1^2 + 1^2 + 1^2 + 1^2 + 1^2 + 1^2 + 1^2 + 1^2 + 1^2 + 1^2 + 1^2 + 1^2} = \frac{1}{13}. \quad (4.3)$$

However, different  $T_{\text{SYM}}$  are used here, so we cannot predict performance deviations by comparing (4.1) to (4.3) directly. In such cases, we should also consider the number of OFDM symbols observed over the sensing time considered. For the specific case of Figures 4.3 and 4.7, the number of fully observed symbols is 14 and 35, respectively. Multiplying these numbers by the corresponding power ratios in (4.1) and (4.3) yields average power ratios of 5.21 and 2.69. Hence, when TDSC methods are employed along the lines in Table 3.7, it is evident that ECMA-392 signals should be more difficult to detect than DVB-T signals. The same reasoning can be applied to Figures 4.6(c) and 4.7(c) to explain why TDSC methods perform better for ECMA-392 than for IEEE 802.22 despite of the fact that the ratio  $(s_p/s)^2$  is larger in (4.2) than in (4.3).

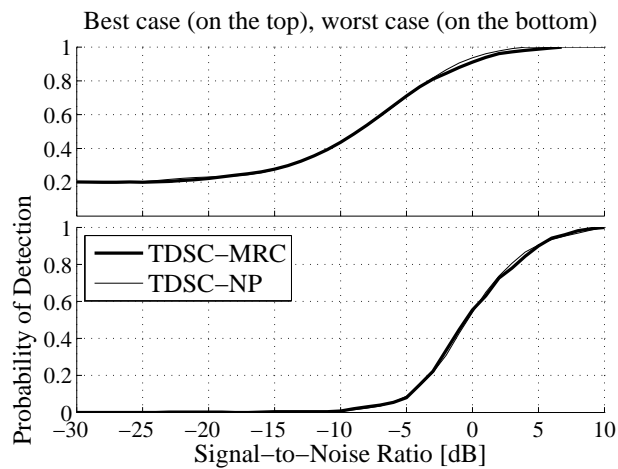
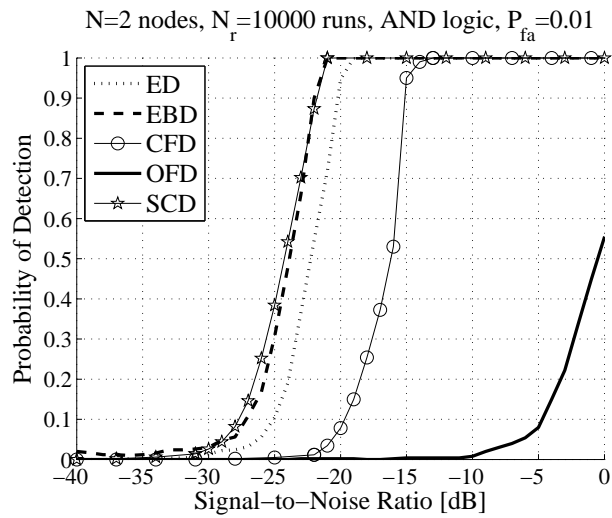
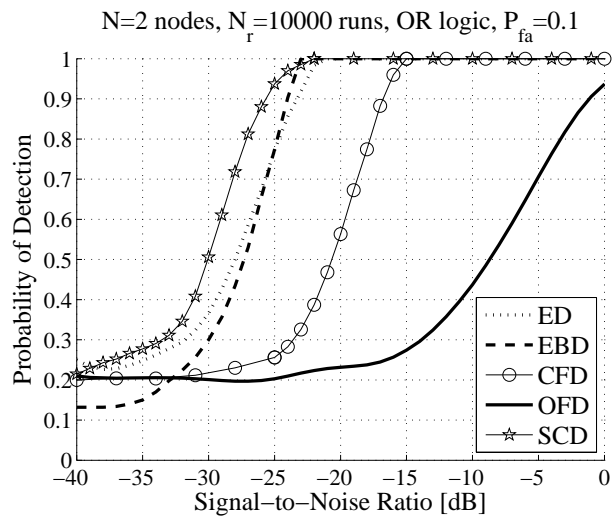
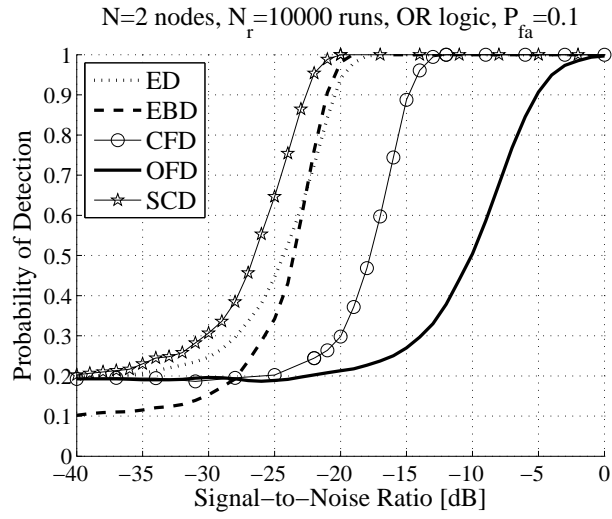
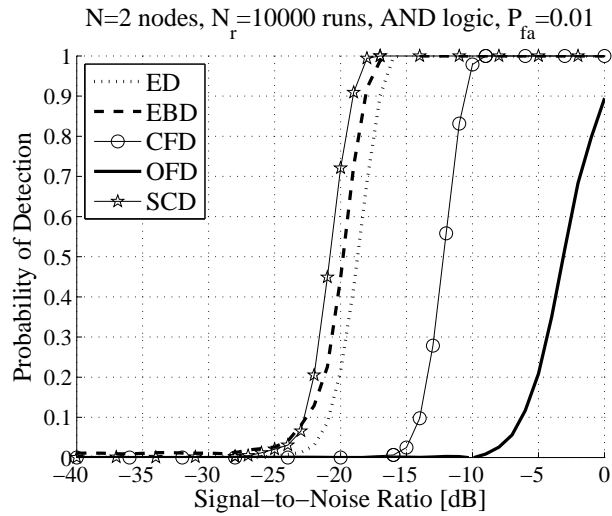


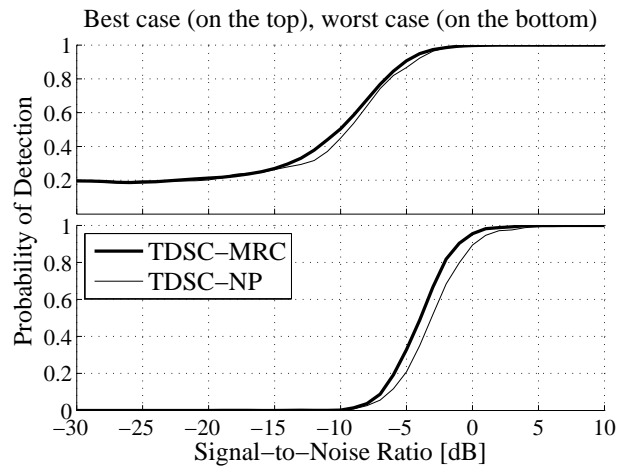
Fig. 4.6: Detection performance of IEEE 802.22 signals under AWGN (CP=1/4).



(a) Best case.



(b) Worst case.



(c) Detailed analysis of OFD: TDSC methods.

**Fig. 4.7:** Detection performance of ECMA-392 signals under AWGN (CP=1/8).

Further insight about the joint impact of CP ratio and symbol length can be obtained by comparing Figure 4.5 (CP= 1/32,  $T_{\text{SYM}} = 0.26$  ms) to Figure 4.7 (CP= 1/8,  $T_{\text{SYM}} = 19$   $\mu\text{s}$ ). It can be seen that the ability of CFD in reliably detecting target signals is limited to  $-7$  dB (best-case curves) or  $-1$  dB (worst-case curves) in ISDB-T but it is still possible at  $-13$  dB (best-case curves) and  $-9$  dB (worst-case curves) in ECMA-392. This means that, depending on the CP ratio used and in contrast to all other classes, the performance of CFD may degrade even when  $T_{\text{SYM}}$  increases.

### 4.2.2 Non-OFDM Target Signals

By comparing Figure 4.3 to Figure 4.8, we observe some similarities in the detection of DVB-T and ATSC signals. First, all but the OFD class incur losses of 2 dB to 5 dB when we move from the best- to the worst-case curves. Second, a performance degradation of 1 dB is verified for all but the OFD class when we decrease the CFAR requirement from 0.1 to 0.01. Third, SCD and OFD are the most and the least accurate classes. Recalling that the sensing time used in the simulations is roughly five times longer for DVB-T than for ATSC (see Table 3.7), it is clear that signals based on the former are harder for SCD to detect than those based on the latter. This is expected because, as seen in Figure 3.4(a), only the edges of the DVB-T spectrum can be exploited by SCD. In contrast, 3.5(a) shows that the ATSC spectrum can be better “seen” by SCD because the ATSC pilot creates a sharp spectral feature whose position does not change much over time. As for the OFD class, here represented by the ASSD method, switching from OR to AND logic with CFAR requirement kept unchanged yields losses up to 5 dB. Conversely, by increasing  $P_{\text{fa}}$  from 0.1 to 0.01 with fusion rule kept unchanged yields losses of 2 dB. Adding up these losses explains the performance gap of 7 dB between best- and worst-case curves.

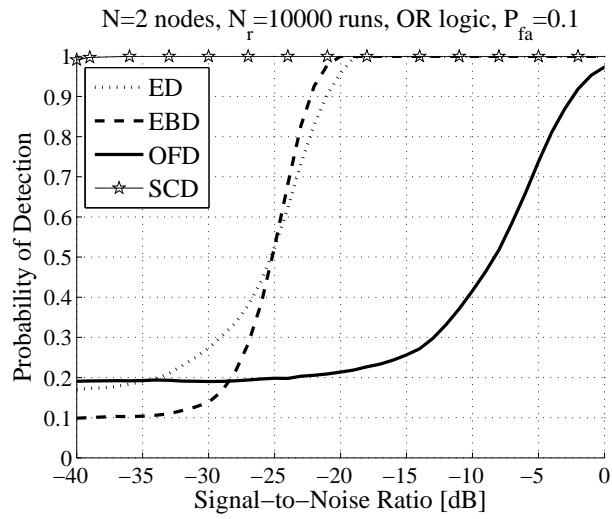
The poor performance of ASSD observed here is, in part, due to an issue that arises in the threshold setting process and the way we tackle this issue in MESS. The symbols conveying data segment SYNC signals are designed to have better SNR than ordinary data symbols. While intended to facilitate synchronization in typical ATSC systems, here this imposes the need for a threshold setting process able to *adaptively* set  $\gamma$  according to the type of symbol (SYNC or data). We have seen in Section 3.3.3 that MESS determines the value of  $\gamma$  solely on the basis of the  $\sigma_w^2$  simulated for each SNR value. To avoid the condition that  $\gamma$  cannot be suitably set because MESS does not know the type of symbol currently being detected, we normalize each segment before transmission. Both conditions are shown at the detailed analysis in Figure 4.8(c), where the  $x$ -axis is rescaled up to 20 dB. The dotted curves reflect the inability of MESS to operate with fixed  $\gamma$  when ATSC signals are generated as in [135]. This condition occurs only at specific SNR values, namely those where a segment conveying data segment SYNC symbols is generated more than  $P_{\text{fa}} \times N_r$ , *e.g.*  $0.01 \times 10000 = 100$  times. The continuous curves reflect the performances obtained using different CFAR requirements to detect ATSC signals with normalized data segment SYNC symbols. It can be seen from this figure that segment normalization solves the threshold issue but introduces some sort of “saturation” as we approach the operation region of interest, *i.e.* 4 dB are needed to improve from  $P_d = 0.9$  to  $P_d = 0.99$  regardless of fusion rule and CFAR requirement. Hence, beside being the method most sensitive to changes in the design options adopted, the lack of an adaptive threshold setting procedure makes ASSD need SNR higher than all remaining methods to reliably detect ATSC signals. Under worst-case assumptions and sensing time of 0.23 ms, this need translates into 9 dB

(all other methods achieve the same performance below  $-18$  dB). Alternatively, longer sensing time can improve performance.

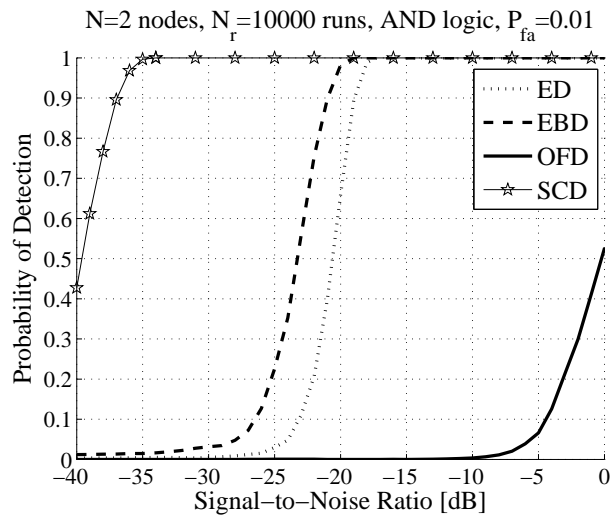
Recalling that the system settings adopted in NTSC and PAL are only slightly different (see Table 3.2), we do not expect substantial differences in performance when detecting signals based on these standards. This is confirmed in Figures 4.9 and 4.10 for sensing times of 0.76 ms and 0.57 ms, respectively. It can be seen that the performance of all but the EBD class degrade up to 4 dB when we switch from best- to worst-case curves. Also, both figures exhibit losses of 2 dB when we change the fusion rule from OR to AND logic with the CFAR requirement kept unchanged, and of 3 dB when we increase  $P_{fa}$  from 0.1 to 0.01 with the fusion rule kept unchanged. The impact of such design options in NTSC and PAL is thus similar as in the other TV broadcast standards analyzed thus far. As in ATSC, the synchronization signals adopted in NTSC and PAL introduced issues in the threshold setting process and the way we found to suitably set  $\gamma$  was to normalize HSYNC signals before transmission. However, since the SYNC lines used in NTSC/PAL are more abundant than the segment SYNC signals used in ATSC, this solves the threshold issue at the expense of some degradation in the performance of energy-based methods, *e.g.* ED, RLRT, and SCD. In case of ED, a comparison among Figures 4.8, 4.9, and 4.10 reveals that the losses due to normalization of NTSC and PAL signals are up to 5 dB and 10 dB as compared to ATSC. Due to the same reason, the performance degradation verified for the EBD class when we switch from the best- to the worst-case curves is of 6 dB in NTSC and 11 dB in PAL. As shown at the detailed analyses in Figures 4.9(c) and 4.10(c), AGM, GLRT, and MME give essentially the same performance whereas RLRT is here the worst EBD method. SCD remains by far the best method but, despite of the longer sensing times used in the simulations of NTSC and PAL (see Table 3.7), its performance is only slightly better than in case of ATSC. The reason is that, beside the reduction in the signal energy caused by normalization, we do not generate audio in NTSC and PAL. Once the audio information is omitted, SCD can only exploit the two spectral features created by the luminance and chrominance subcarriers.

Figure 4.11 suggests that all but the SCD class perform the same regardless of the WM speaker mode used (see Table 3.3). Accounting to losses of 2 dB, changes in the fusion rule and CFAR requirement impact the detection of WM in a manner similar to that observed for analog TV broadcast. In general, the performance gap between the best- and the worst-case curves ranges from 1 dB to 4 dB. OFD, here representing MF, and ED are the second-worst and worst performers though we observe that the number of lags used to compute (2.96) is critical to the achievable performance of MF. For instance, a 3 dB gain can be derived by increasing  $\tau_s$  from 30 to 100 lags, so that MF becomes able to detect WM signals in SNR as low as that observed for EBD. This, however, comes at the expense of longer simulation time. As for SCD, the loud and soft speaker modes are respectively 2 dB and 3 dB harder to detect than the silent speaker mode. This is expected because, as seen in Figure 3.6, typical WM spectra exhibit spectral features that are sharper for the silent speaker mode than for the other speaker modes. This is better seen at the detailed analysis in Figure 4.11(c). Even at  $-30$  dB, the strongest spike (centered at  $f_c$ ) in the PSD of the silent speaker mode still can be distinguished from the noise floor, whereas the spikes exhibited by the spectra of soft and loud speaker modes are large in number, weaker in amplitude, and sit close to one another, thus making it more difficult for SCD to detect WM signals based on these modes. Therefore, and as in [103], all simulations of WM signals presented throughout the remainder of this dissertation will be based only on the soft speaker mode.

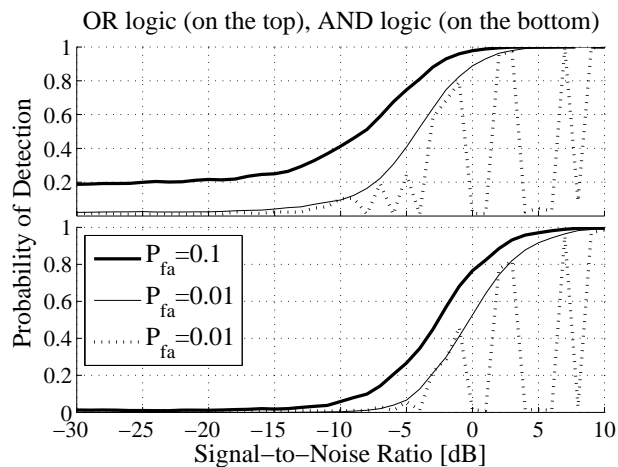




(a) Best case.



(b) Worst case.



(c) Detailed analysis of OFD: ASSD method.

**Fig. 4.8:** Detection performance of ATSC signals under AWGN.

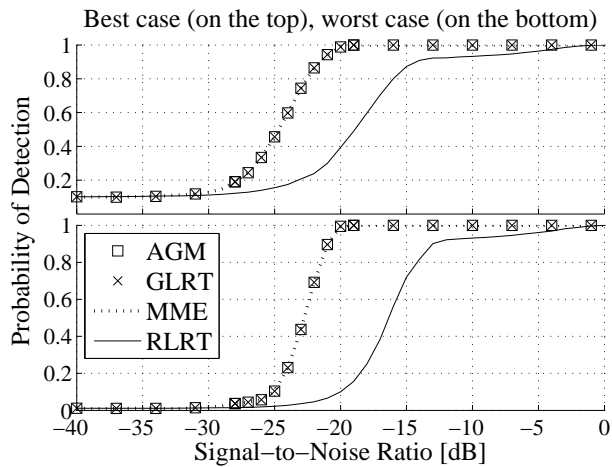
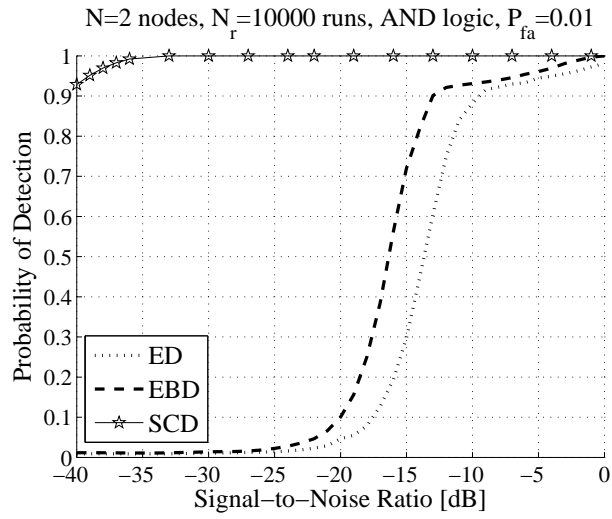
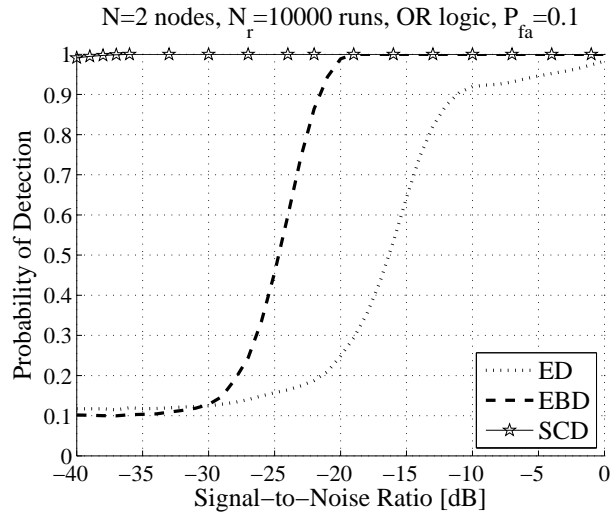


Fig. 4.9: Detection performance of NTSC signals under AWGN.

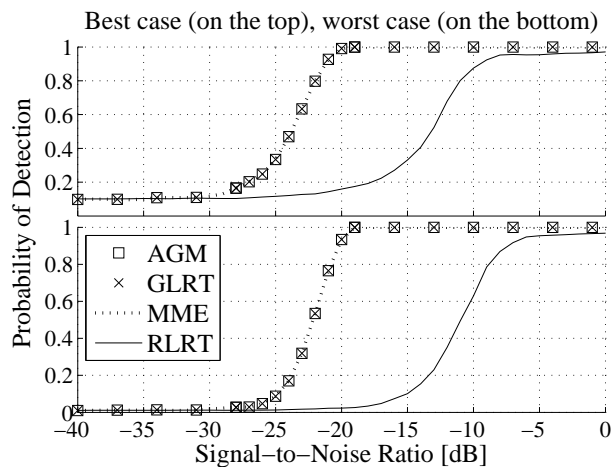
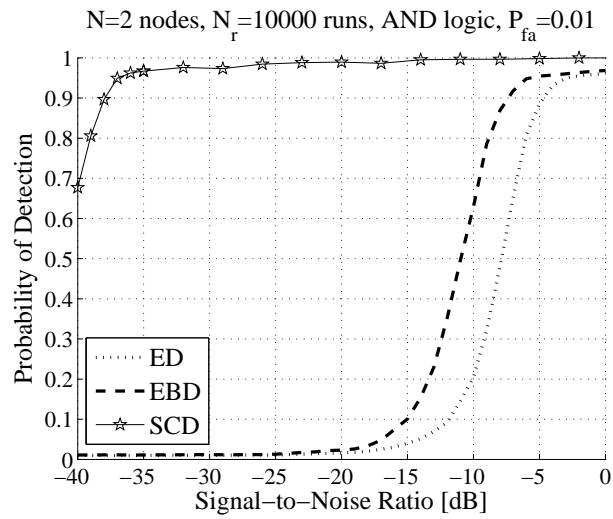
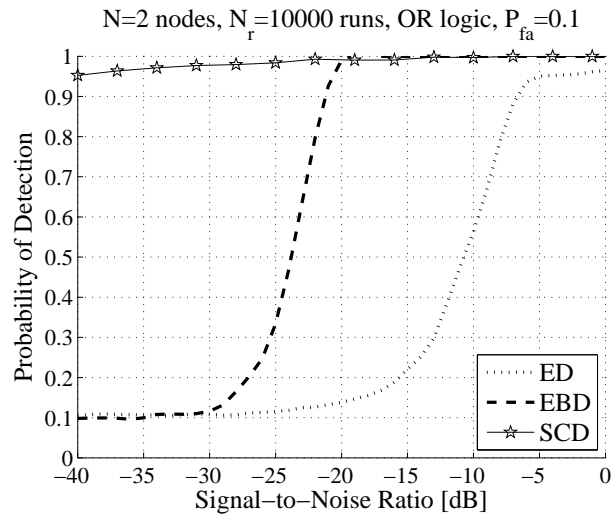
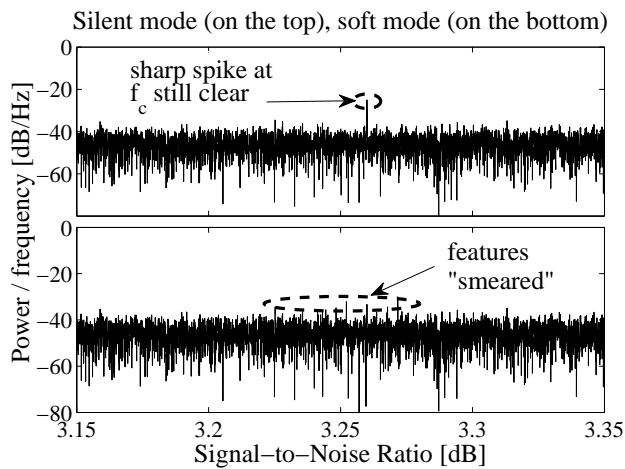
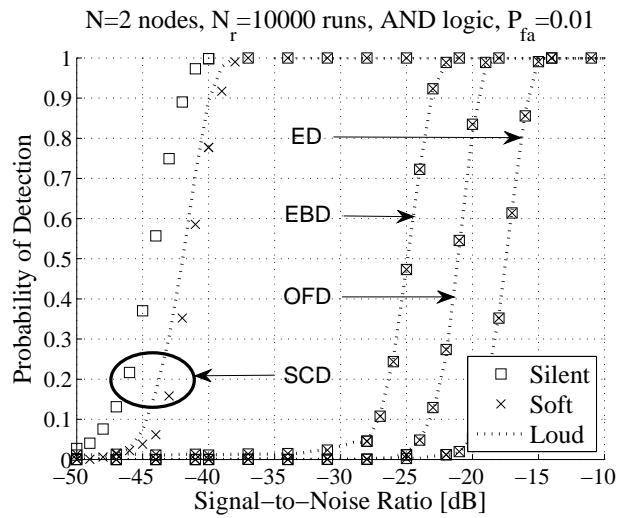
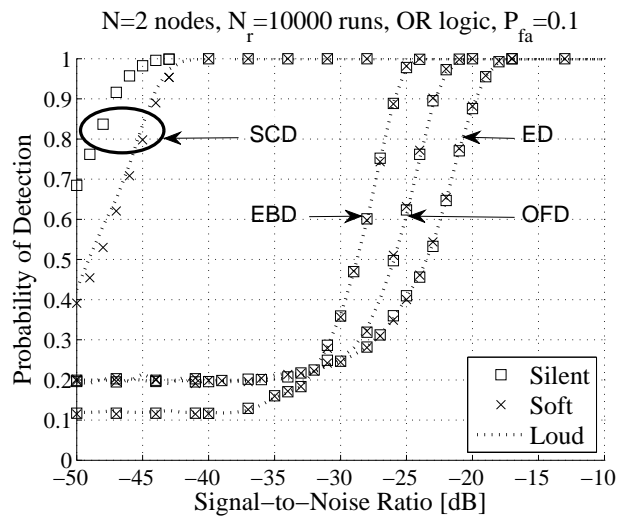


Fig. 4.10: Detection performance of PAL signals under AWGN.



**Fig. 4.11:** Detection performance of PMSE under AWGN (different WM speaker modes).

## 4.3 Multipath Fading

Now that we have analyzed the AWGN channel, our next step is to extend the analysis in Section 4.2 with practical issues that can substantially impair the detection process. To begin with, we consider the case where the target signals are detected under fading conditions. The channel is a six-tap multipath fading channel, created by making  $L = 6$  in Figure 3.7 and fed with the profiles B and D in Table 3.5. In Tables 4.1 and 4.2, we summarize the simulation results obtained for this setting in terms of the deviations (in dB) observed when we switch from the ideal AWGN case to the more practical case of multipath fading. Negative and positive deviations reflect losses and gains, respectively, as compared to the AWGN case. Throughout the remainder of this dissertation, we refer to *average method deviation* (AMD) as the total deviation averaged over all types of target a method can detect. This allows us to rank the multipath robustness of that method as poor ( $\text{AMD} \leq -5$ ), fair ( $-5 < \text{AMD} \leq -3$ ), average ( $-3 < \text{AMD} \leq -2$ ), good ( $-2 < \text{AMD} \leq -1$ ), and excellent ( $\text{AMD} > -1$ ).

### 4.3.1 Impact of Target Signal Type

It may seem from Tables 4.1 and 4.2 that OFDM-based target signals become in general more difficult to detect than non-OFDM target signals when multipath fading is considered. However, care should be taken in this kind of statement because of the different sensing times (see Table 3.7) and sampling frequencies (see Tables 3.1 and 3.2) used in the simulations. Deviations in the performance of most methods do not vary much with fusion rule and CFAR requirement for a *given* type of target signal, but substantial discrepancies are observed when we direct a given method to detect its *whole* set of target signals (see Table 3.6). For instance, the AMD values of ED and SCD indicate that they are robust against multipath when non-OFDM target signals are considered but perform poorly when it comes to OFDM-based target signals. Indeed, this impact of the target signal type on detection performance is expected due to the two following reasons. The first, responsible for the fairly positive AMD observed when ED and MF detect PMSE, relates to the SNR boost in the vicinity of the WM signal created by  $W \ll B$ . Probably, and again because of the small  $W/B$ , the multipath fading channel is behaving linearly. If the channel frequency response is linear, the replicas of  $s(t)$  are only being shifted in time and this does not affect performance negatively. Hence, since “what” the MF is picking up is actually better than the sum of FM signals and noise described by  $r(t)$ , the (filtered) received energy is larger in the multipath case than in the AWGN case. The second reason is that, in contrast to in the other OFDM-based standards, the  $T_{\text{CP}}$  adopted in ECMA-392 are too short to absorb the maximum delay spreads  $\tau_{\text{max},B}$  and  $\tau_{\text{max},D}$  (see Tables 3.1 and 3.5). Since  $T_{\text{CP}} < \tau_{\text{max}}$ , ISI is certain to occur under both profiles. This explains the low AMD of most methods when detecting ECMA-392 signals.

In view of the above, the emphasis of the discussion that follows is placed on ECMA-392 only. Operation under ISI best supports the development of an understanding about how detection performance is impaired by multipath. Of particular interest for us are ACD, BTPD, and SCD, as highlighted using light grey color in Table 4.1. We begin looking at the full set of results of these worst performers under both profiles B and D. Then, we increase the number of nodes to investigate whether and under what circumstances CSS can effectively mitigate the losses introduced by the multipath fading channel.

**Table 4.1:** Performance deviation in dB introduced by multipath fading for OFDM-based target signals (compared to AWGN).

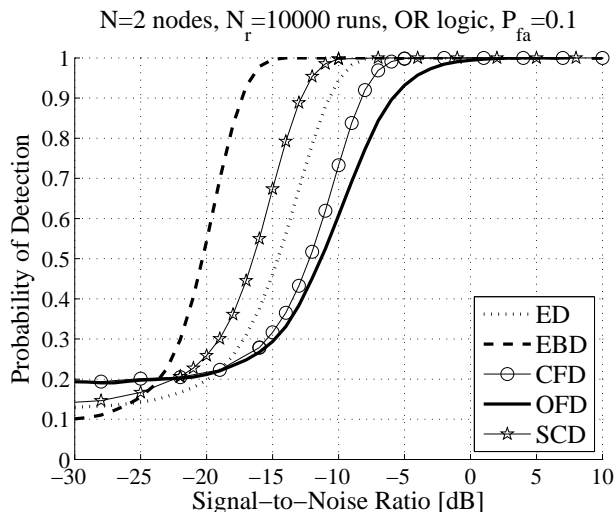
| Method   | DVB-T     |       |           |       | ISDB-T    |       |           |       | IEEE 802.22 |       |           |       | ECMA-392  |       |           |       | AMD  | Robustness |           |
|----------|-----------|-------|-----------|-------|-----------|-------|-----------|-------|-------------|-------|-----------|-------|-----------|-------|-----------|-------|------|------------|-----------|
|          | Profile B |       | Profile D |       | Profile B |       | Profile D |       | Profile B   |       | Profile D |       | Profile B |       | Profile D |       |      |            |           |
|          | Best      | Worst | Best      | Worst | Best      | Worst | Best      | Worst | Best        | Worst | Best      | Worst | Best      | Worst | Best      | Worst |      |            |           |
| ED       | -4        | -3    | -4        | -4    | -4        | -3    | -4        | -4    | -3          | -3    | -3        | -3    | -3        | -9    | -9        | -11   | -12  | -5.19      | Poor      |
| AGM      | -1        | -1    | -1        | -1    | -1        | -1    | -1        | -1    | -1          | -1    | -1        | -1    | -1        | -2    | -2        | -2    | -2   | -1.25      | Good      |
| GLRT     | -1        | -1    | -1        | -1    | -1        | -1    | -1        | -1    | -1          | -1    | -1        | -1    | -1        | -1    | -2        | -1    | -2   | -1.13      | Good      |
| MME      | -1        | -1    | -1        | -1    | -1        | -1    | -1        | -1    | -1          | -1    | -1        | -1    | -1        | -2    | -2        | -2    | -2   | -1.25      | Good      |
| RLRT     | -4        | -4    | -4        | -4    | -4        | -4    | -4        | -4    | -1          | -1    | -1        | -1    | -1        | -7    | -8        | -12   | -12  | -4.81      | Fair      |
| SCD      | -4        | -3    | -3        | -2    | -4        | -3    | -3        | -2    | -1          | -2    | -1        | -2    | -2        | -10   | -7        | -22   | -20  | -5.56      | Poor      |
| ACD      | -2        | -1    | -2        | -2    | -2        | -1    | -2        | -2    | 0           | +1    | 0         | +1    | +1        | -6    | -6        | FAIL  | FAIL | -1.71      | Poor      |
| BTPD     | -1        | -1    | -2        | -2    | -1        | -1    | -2        | -2    | +1          | +2    | +2        | +3    | +3        | -9    | -10       | -20   | -22  | -4.06      | Fair      |
| TDSC-NP  | 0         | 0     | 0         | +1    | -1        | 0     | -1        | -1    | +3          | +6    | +3        | +5    | +5        | 0     | 0         | +3    | +3   | +1.31      | Excellent |
| TDSC-MRC | 0         | 0     | 0         | 0     | -1        | 0     | -1        | 0     | +4          | +2    | +4        | +2    | +2        | -1    | -1        | +1    | +1   | +0.63      | Excellent |

Best: OR logic and  $P_{fa} = 0.1$ , Worst: AND logic and  $P_{fa} = 0.01$ , AMD: Average Method Deviation.

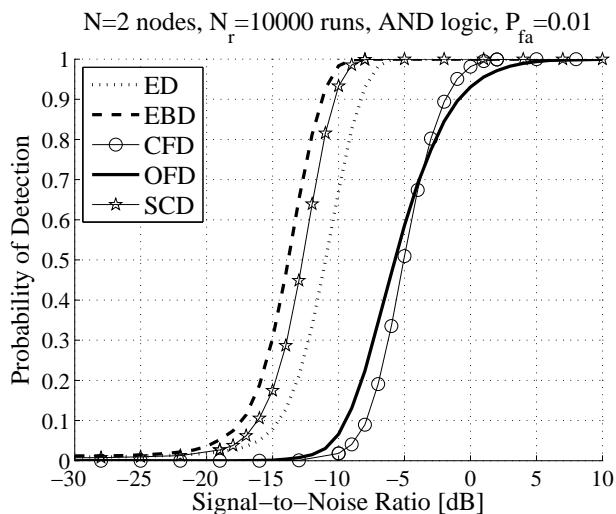
**Table 4.2:** Performance deviation in dB introduced by multipath fading for non-OFDM target signals (compared to AWGN).

| Method | ATSC      |       |           |       | NTSC      |       |           |       | PAL       |       |           |       | PMSE (Soft Mode) |       |           |       | AMD | Robustness |           |
|--------|-----------|-------|-----------|-------|-----------|-------|-----------|-------|-----------|-------|-----------|-------|------------------|-------|-----------|-------|-----|------------|-----------|
|        | Profile B |       | Profile D |       | Profile B |       | Profile D |       | Profile B |       | Profile D |       | Profile B        |       | Profile D |       |     |            |           |
|        | Best      | Worst | Best      | Worst | Best      | Worst | Best      | Worst | Best      | Worst | Best      | Worst | Best             | Worst | Best      | Worst |     |            |           |
| ED     | -1        | -1    | -3        | -3    | +1        | 0     | +1        | +1    | 0         | 0     | +1        | 0     | 0                | +4    | +4        | +4    | +4  | +0.75      | Excellent |
| AGM    | 0         | 0     | 0         | 0     | 0         | 0     | 0         | 0     | 0         | 0     | 0         | 0     | 0                | 0     | 0         | 0     | 0   | 0.00       | Excellent |
| GLRT   | 0         | 0     | 0         | 0     | 0         | 0     | 0         | 0     | 0         | 0     | 0         | 0     | 0                | 0     | 0         | 0     | 0   | 0.00       | Excellent |
| MME    | 0         | 0     | 0         | 0     | 0         | 0     | 0         | 0     | 0         | 0     | 0         | 0     | 0                | 0     | 0         | 0     | 0   | 0.00       | Excellent |
| RLRT   | 0         | 0     | -2        | -2    | -1        | 0     | 0         | 1     | 0         | 0     | 0         | 0     | 0                | -2    | -2        | -2    | -2  | -0.75      | Excellent |
| SCD    | 0         | 0     | -1        | 0     | 0         | +2    | 0         | +1    | +2        | -1    | +2        | -1    | -3               | -3    | -2        | -2    | -2  | -0.38      | Excellent |
| ASSD   | -1        | -1    | 0         | +1    | NA        | NA    | NA        | NA    | NA        | NA    | NA        | NA    | NA               | NA    | NA        | NA    | NA  | -0.25      | Excellent |
| MF     | NA        | NA    | NA        | NA    | NA        | NA    | NA        | NA    | NA        | NA    | NA        | NA    | NA               | +7    | +5        | +7    | +7  | +6.00      | Excellent |

Best: OR logic and  $P_{fa} = 0.1$ , Worst: AND logic and  $P_{fa} = 0.01$ , AMD: Average Method Deviation.



(a) Best case.



(b) Worst case.

**Fig. 4.12:** Detection performance of ECMA-392 signals under multipath (profile B).

By switching from the best- to the worst-case curves in Figure 4.12, the losses in performance for profile B are relatively mild for ED and SCD (2 dB) and only moderate for the remaining classes (6 dB). Figure 4.13 suggests that the impact of profile D is similar to that of profile B for all classes but EBD and CFD. In case of EBD, the methods AGM, MME, GLRT, and RLRT perform the same ( $P_d = 0.99$  is achieved at  $-20$  dB), so the 10 dB gap between profile B and profile D is caused solely by the more stringent CFAR requirement adopted under worst case conditions. However, when AND logic is used as fusion rule and each node is imposed to deliver  $P_{fa} = 0.01$ , the CFD class, representing the ACD method in this setting, performs poorly under profile B but *entirely* fails under profile D. This is expected because our previous work in [90] shows that a single ACD-based node performs poorly when ECMA-392 signals are taken into consideration in conjunction with profile A (see Table 3.5). In that paper, the simulated performance of ACD at 20 dB is limited to  $P_d \approx 0.40$  while BTPD achieves  $P_d = 0.99$  at the same SNR. In the sequel, we provide a more detailed analysis of this issue not presented in [90] due to the space limitations imposed to that conference paper.

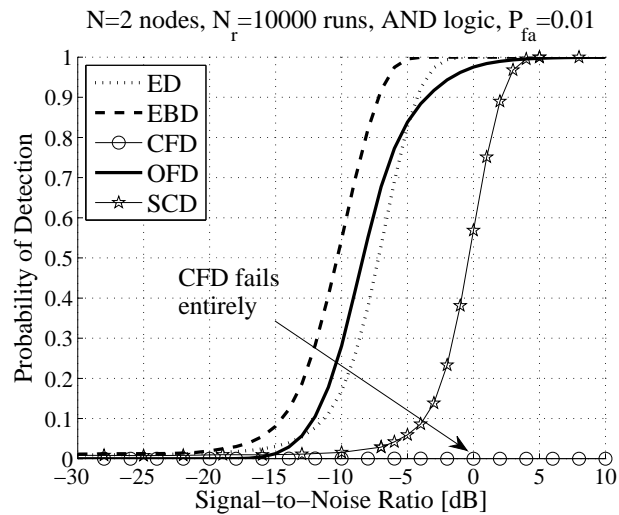
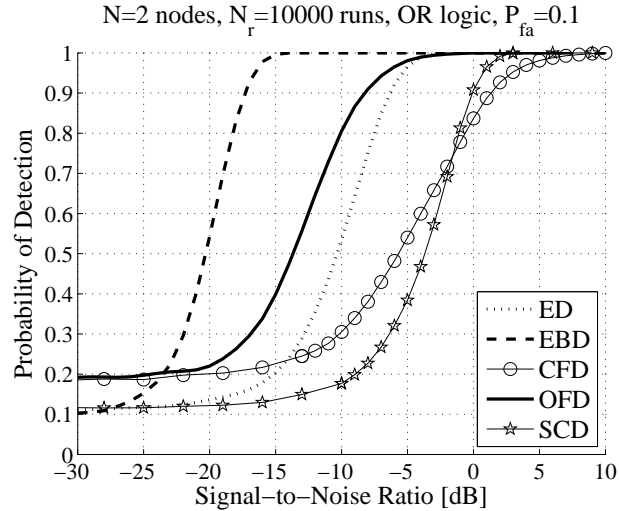


**Fig. 4.13:** Detection performance of ECMA-392 signals under multipath (profile D).

### 4.3.2 Impact of Number of Nodes

As said earlier in this section, we are interested in investigating the extent to which CSS can alleviate the losses introduced by multipath fading. Thus far, we have worked with  $N = 2$ , so the natural next step is to look at the impact caused on performance when the number of nodes engaged in cooperation increases. Some simulation results for  $N = 10$  and  $N = 20$  are presented in Figure 4.14, where the curves for  $N = 2$  are plotted again to serve as baseline for the computation of the cooperation gains derived for larger  $N$ . In case of ACD, it can be seen from Figure 4.14(a) that cooperation buys us *nothing* when under worst case conditions. Also, the improvement in the global probability of detection achievable under best case conditions comes at the expense of deteriorated probabilities of false alarm. Specifically, for  $P_{fa} = 0.1$ , ACD provides  $Q_d^{OR} \approx Q_{fa}^{OR}$  with the latter assuming values in the ranges  $[0.6320, 0.6720]$  for  $N = 10$  and  $[0.8650, 0.8920]$  for  $N = 20$ . This corresponds to global probabilities of false alarm that are respectively degraded in more than 300% and 400% as compared to the  $N = 2$  case.



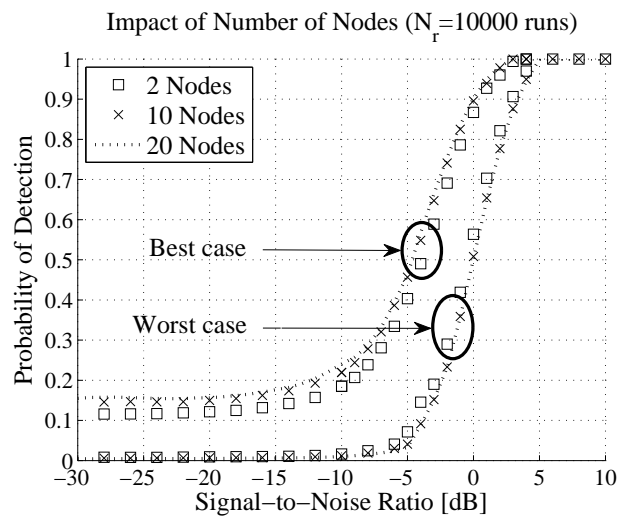
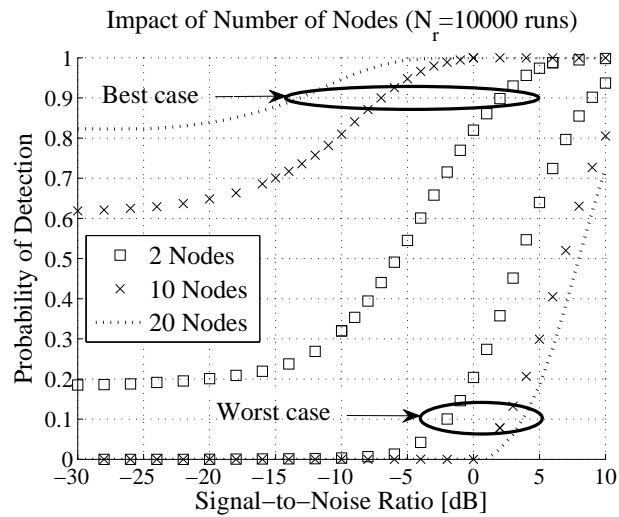
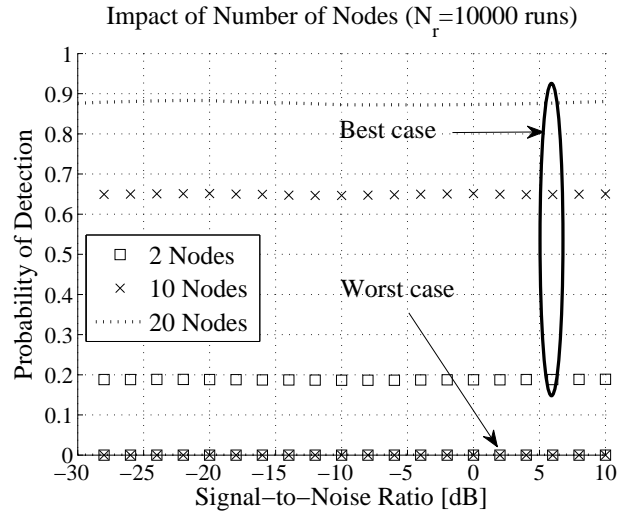


**Fig. 4.14:** Detection performance of ECMA-392 signals under multipath (profile D) for different number of nodes. Best (worst) case curves reflect the use of OR (AND) logic and  $P_{fa} = 0.1$  ( $P_{fa} = 0.01$ ).

As for BTPD, Figure 4.14(b) shows that an increased number of nodes yields losses under worst-case conditions but a substantial 12 dB gain can be achieved by increasing  $N$  from 2 to 20 when under best-case conditions. In this case, it may be tempting to further increase  $N$  until the resulting cooperation gain “neutralizes” the losses due to multipath. We do not pursue on this here because the cooperation gains do not increase linearly with the number of nodes<sup>2</sup>, so it is unlikely that we can manage to obtain the remaining 8 dB required to provide AWGN-like performance under multipath fading conditions this way. Another aspect worth mentioning is that, like in ACD, the cooperation gains derived in BTPD come at the expense of a degradation in  $Q_{\text{fa}}^{\text{OR}}$ . For  $P_{\text{fa}} = 0.1$ ,  $Q_{\text{fa}}^{\text{OR}}$  varies (as a function of the SNR) in the ranges  $[0.1800, 0.1930]$  for  $N = 2$ ,  $[0.5900, 0.6320]$  for  $N = 10$ , and  $[0.7920, 0.8430]$  for  $N = 20$ . However, BTPD differs from ACD in the sense that it is able to detect ECMA-392 signals for all combinations of system options tested, *e.g.* a better balance between  $Q_{\text{d}}^{\text{OR}}$  and  $Q_{\text{fa}}^{\text{OR}}$  can be achieved by combining OR logic with  $P_{\text{fa}} = 0.01$ . For  $N = 20$ , this allows us to improve the range of values of  $Q_{\text{fa}}^{\text{OR}}$  to  $[0.1490, 0.1770]$  while the resulting  $Q_{\text{d}}^{\text{OR}}$  still outperforms that obtained for  $N = 2$  in 10 dB.

When SCD is used at the local level, 4.14(c) shows that less can be achieved in terms of cooperation gains by increasing the number of nodes. The absence of improvement in  $Q_{\text{d}}$  under both best- and worst-case conditions suggests that the additional costs introduced by cooperation (see Section 1.3) may become difficult to justify here. On the other hand, it is important to note that the global probability of false alarm provided by SCD is low, as compared to ACD and BTPD, and does not vary much as  $N$  increases. For instance,  $Q_{\text{fa}}^{\text{AND}}$  lies in  $[0.0020, 0.0070]$  for  $N = 10$  and in  $[0.0010, 0.0070]$  for  $N = 20$ , whereas  $Q_{\text{fa}}^{\text{OR}}$  lies in  $[0.1330, 0.1520]$  for  $N = 10$  and in  $[0.1400, 0.1690]$  for  $N = 20$ . So, we think it is more appropriate to refer to SCD as method suitable for CSS applications requiring low  $Q_{\text{fa}}$ , rather than as a “poor” performer in terms of cooperation gains.

It turns out from the above findings that the use of different methods allows us to derive different cooperation gains. The gains observed here are essentially different in terms of how much  $Q_{\text{d}}$  overcomes  $P_{\text{d}}$ , but may differ in terms of  $Q_{\text{fa}}$  too. Methods able to provide big improvements in  $Q_{\text{d}}$ , even if at the expense of some degradation in  $Q_{\text{fa}}$ , are interesting for those applications where the emphasis is on protecting licensed systems that operate collocated. In contrast, methods that cannot improve  $Q_{\text{d}}$  that much, but have potential to keep  $Q_{\text{fa}}$  as low as  $P_{\text{fa}}$  (or even lower than  $P_{\text{fa}}$  if using AND logic), are interesting for applications that focus on efficient white space utilization. This suggests that, in order to realize the theoretical benefits of cooperation, special care is needed when selecting the method to be used at the local level. With respect to the methods analyzed here, the combined use of BTPD and SCD seems particularly promising to *balance* such contrasting goals thus serving *both* types of applications. For instance, a two-stage WSD could first detect the faded OFDM signals using BTPD (high  $Q_{\text{d}}$ ) and then further refine results by using SCD (high  $Q_{\text{fa}}$ ). However, it can be seen from (2.83) and (2.84) that the double time lags required in BTPD makes it twice as complex as ACD. Hence, it is desirable to determine the reasons why ACD fails to detect ECMA-392 signals under worst-case conditions while BTPD does not. Finding a remedy for this issue, if there is any, would make of ACD a less complex alternative to couple with SCD. The natural starting point for such an investigation is the underlying working principle used by both ACD and BTPD, namely the ACF of the received signal.

---

<sup>2</sup> The cooperation gain saturates as  $N$  increases without limit. For instance, it is shown in [64] that a small number of ED-based nodes ( $N \sim 10$ -20) is enough to realize the full benefits of cooperation.

After being passed through the multipath fading channel, the discrete-time received signal can be written as

$$r(n) = \sum_{k=1}^L \alpha_k s(n-k) + w(n), \quad (4.4)$$

where the coefficients  $\alpha_k$  are the complex channel amplitudes and  $L$  is the channel order. In the discrete-time domain, we can rewrite the ACF of the received signal in (2.44) as

$$R_r(\tau_s) = E[r(n + \tau_s)r^*(n)], \quad (4.5)$$

where  $\tau_s$  are discrete time lags normalized by a sampling period  $T_s$ . Plugging (4.4) into (4.5) and rearranging the terms, we get

$$\begin{aligned} R_r(\tau_s) &= E \left[ \sum_{k=1}^L \alpha_k s(n + \tau_s - k) \sum_{k=1}^L \alpha_k^* s^*(n - k) \right] \\ &= \sum_{k=1}^L \sum_{j=1}^L \alpha_k \alpha_j^* E[s(n + \tau_s - k)s^*(n - j)]. \end{aligned} \quad (4.6)$$

The values assumed by the expectation in (4.6) are known to be

$$E[s(n + \tau_s - k)s^*(n - j)] = \begin{cases} R_s(\tau_s), & \text{if } k = j \\ 0, & \text{otherwise,} \end{cases}$$

so we can simplify it as:

$$R_r(\tau_s) = R_s(\tau_s) \sum_{k=1}^L |\alpha_k|^2, \quad \text{if } k = j. \quad (4.7)$$

However, if we increase the number of discrete time lags in one unit (4.6) becomes

$$\begin{aligned} R_r(\tau_s + 1) &= \sum_{k=2}^L \sum_{j=1}^L \alpha_k \alpha_j^* E[s(n + \tau_s + 1 - k)s^*(n - j)] \\ &= R_s(\tau_s) \sum_{k=2}^L \alpha_k \alpha_{k-1}^*, \end{aligned} \quad (4.8)$$

for  $k - 1 = j$  and zero otherwise. Further increasing  $\tau_s$  yields:

$$R_r(\tau_s + 2) = R_s(\tau_s) \sum_{k=3}^L \alpha_k \alpha_{k-2}^* \quad (4.9)$$

$$R_r(\tau_s + 3) = R_s(\tau_s) \sum_{k=4}^L \alpha_k \alpha_{k-3}^* \quad (4.10)$$

⋮

$$\vdots$$

$$R_r(\tau_s + L - 2) = R_s(\tau_s) \sum_{k=L-1}^L \alpha_k \alpha_{k-L+2}^* \quad (4.11)$$

$$R_r(\tau_s + L - 1) = R_s(\tau_s) \sum_{k=L}^L \alpha_k \alpha_{k-L+1}^*. \quad (4.12)$$

Expanding the sums in (4.7)-(4.12) and writing the result in matrix form gives

$$\underbrace{\begin{bmatrix} R_r(\tau_s) \\ R_r(\tau_s + 1) \\ \vdots \\ R_r(\tau_s + L - 2) \\ R_r(\tau_s + L - 1) \end{bmatrix}}_{\mathbb{R}_L} = R_s(\tau_s) \underbrace{\begin{bmatrix} \alpha_1 & \alpha_2 & \alpha_3 & \dots & \alpha_{L-1} & \alpha_L \\ \alpha_2 & \alpha_3 & \alpha_4 & \dots & \alpha_L & 0 \\ \vdots & \vdots & \vdots & \ddots & 0 & 0 \\ \alpha_{L-1} & \alpha_L & 0 & \dots & 0 & 0 \\ \alpha_L & 0 & 0 & \dots & 0 & 0 \end{bmatrix}}_{\mathbb{T}_L} \underbrace{\begin{bmatrix} \alpha_1^* \\ \alpha_2^* \\ \vdots \\ \alpha_{L-1}^* \\ \alpha_L^* \end{bmatrix}}_{\mathbb{S}_L}, \quad (4.13)$$

which for the six-tap channel used in MESS becomes:

$$\underbrace{\begin{bmatrix} R_r(\tau_s) \\ R_r(\tau_s + 1) \\ R_r(\tau_s + 2) \\ R_r(\tau_s + 3) \\ R_r(\tau_s + 4) \\ R_r(\tau_s + 5) \end{bmatrix}}_{\mathbb{R}_6} = R_s(\tau_s) \underbrace{\begin{bmatrix} \alpha_1 & \alpha_2 & \alpha_3 & \alpha_4 & \alpha_5 & \alpha_6 \\ \alpha_2 & \alpha_3 & \alpha_4 & \alpha_5 & \alpha_6 & 0 \\ \alpha_3 & \alpha_4 & \alpha_5 & \alpha_6 & 0 & 0 \\ \alpha_4 & \alpha_5 & \alpha_6 & 0 & 0 & 0 \\ \alpha_5 & \alpha_6 & 0 & 0 & 0 & 0 \\ \alpha_6 & 0 & 0 & 0 & 0 & 0 \end{bmatrix}}_{\mathbb{T}_6} \underbrace{\begin{bmatrix} \alpha_1^* \\ \alpha_2^* \\ \alpha_3^* \\ \alpha_4^* \\ \alpha_5^* \\ \alpha_6^* \end{bmatrix}}_{\mathbb{S}_6} \quad (4.14)$$

Finally, by taking the inner product  $\langle \mathbb{R}, \mathbb{R} \rangle$  we arrive at

$$\mathbb{R}^\dagger \mathbb{R} = |R_s(\tau_s)|^2 \mathbb{S}^\dagger \mathbb{T}^\dagger \mathbb{T} \mathbb{S}, \quad (4.15)$$

where the term  $|R_s(\tau_s)|^2$  reflects the AWGN contribution and the term  $\mathbb{S}^\dagger \mathbb{T}^\dagger \mathbb{T} \mathbb{S}$  reflects the fading contribution, *i.e.* if detection is carried out only in the presence of AWGN and the number of samples collected is large enough, then  $\mathbb{S}^\dagger \mathbb{T}^\dagger \mathbb{T} \mathbb{S} = 1$  and  $\mathbb{R}^\dagger \mathbb{R} = |R_s(\tau_s)|^2$ .

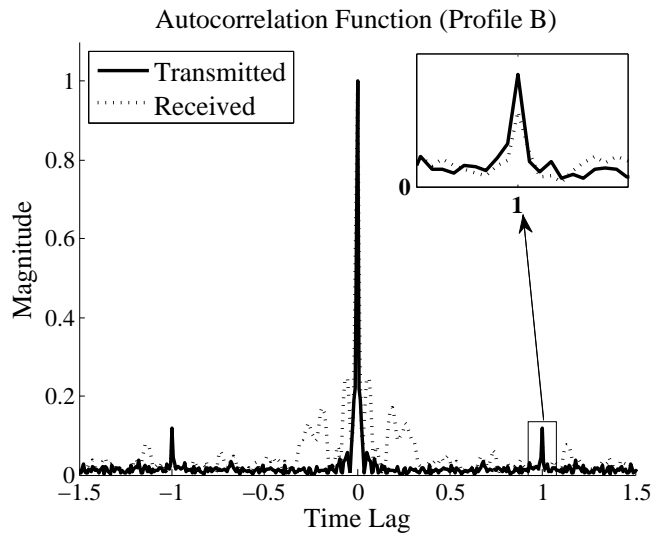
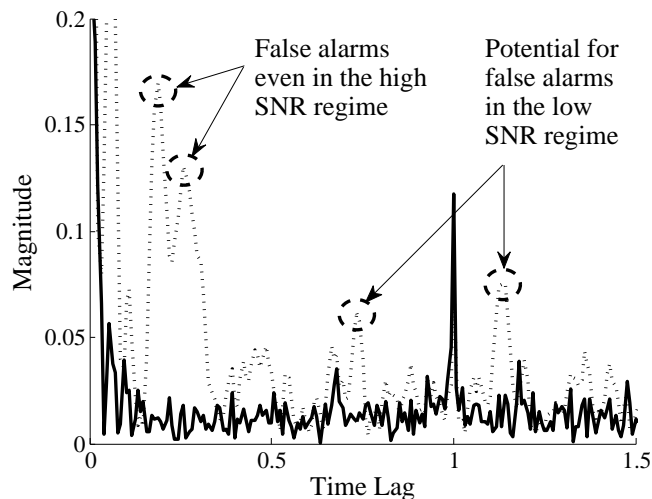
The following conclusions can be drawn from the derivation above. First, the PDP describing the multipath fading channel accounts for a performance limiting aspect of any ACF-based method. Second, as seen from the matrix  $\mathbb{T}_L$  in (4.13), the extent to which the detection performance is impacted by the PDP will be in general more dependent of the contribution of the latest path than those of the earlier paths. For the specific channel at hand, we see from the matrix  $\mathbb{T}_6$  in (4.14) that the contribution of the sixth tap is the one that dominates the overall degradation caused by the fading. The excess delays and amplitudes defining the sixth tap in Table 3.5 are substantially different for profiles B and D, so it is reasonable to expect different levels of performance. However, while (4.15) explains the variations observed in the performance of ACD under multipath fading, it does not provide much insight on why the method works under profile B but not under profile D. In the sequel, we show that the answer to this question also depends on aspects other than the channel amplitudes and channel delays in (4.15).

We have seen in Chapter 2 that detection methods can be implemented in different ways, depending on the amount of prior knowledge of target signals available for detection. In the specific case of ACD, this prior knowledge may involve information about the symbol length [118], CP length, and synchronization [116]. BTPD, in contrast, is regarded to as a blind technique in [119] and [120] because it does not require any information to work. However, BTPD additionally needs to perform a peak search followed by a symmetry check in order to determine the secondary peaks introduced by the CP on both sides of  $R_r(\tau_s)$ . Having that said, it is clear that the assumptions above can be used *interchangeably* in the implementation of both ACD and BTPD.

Consider the case where the useful symbol length  $T_{\text{FFT}}$  is known a priori. Since the desired side peaks of  $R_r(\tau_s)$  will sit at  $\tau_s = \pm 1$ , we can derive substantial run-time savings by evaluating *only* those two time lags of interest. Under this assumption, Figure 4.15(a) shows that multipath fading created by profile B should not be an issue as long as the SNR is high enough. The reason is that the PDP described by the profile B does not impact the position of the side peaks. This can be clearly seen by zooming in the vicinity of  $\tau_s = +1$ , as shown in the upper right side of Figure 4.15(a). Suppose now that information about  $T_{\text{FFT}}$  entirely lacks and it is hard to estimate it on a timely manner<sup>3</sup>. If this is the case, we need to evaluate  $R_r(\tau_s)$  over a range of time lags and search its side peaks inside that range. Such peak search procedure consists of departing from  $\tau_s = 0$  and progressively increasing (or decreasing and increasing in case of BTPD) the time lag index until peaks are eventually found. However, without exact knowledge of  $T_{\text{FFT}}$ , ACD has no “reference” that allows distinction between the desired peaks and other undesired peaks, *e.g.* that may have been introduced by the multipath fading channel. While BTPD relies on the symmetry of  $R_r(\tau_s)$  to resolve for the desired peaks, this works only if the undesired peaks are not symmetric. This condition is illustrated in Figure 4.15(b), where it is seen that some of the unintended peaks are strong enough in magnitude to be misperceived as the desired peak even in the high SNR regime. The presence of such unintended peaks in  $R_r(\tau_s)$  yields high FAR for both ACD and BTPD. Also, since they are exactly symmetric, they may compromise the process of determining  $T_{\text{FFT}}$  blindly using BTPD.

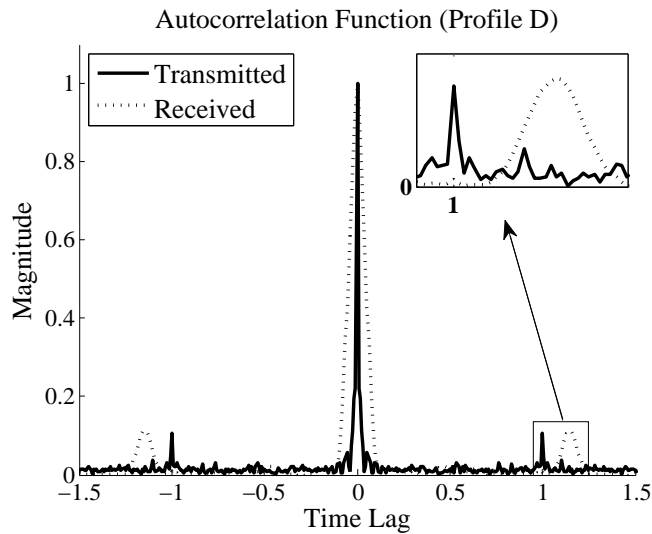
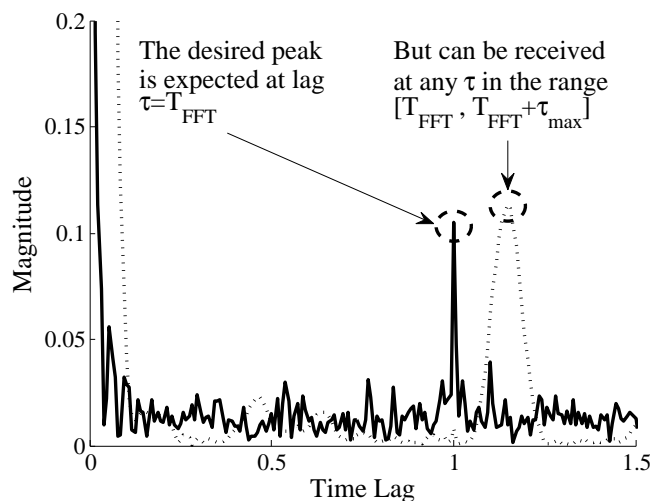
Let us now extend our analysis to the profile D. Under the assumptions that  $T_{\text{FFT}}$  is exactly known and only the time lags  $\tau_s = \pm 1$  are used for detection, Figure 4.16(a) shows that the desired side peak cannot be detected at the time lag where it is expected to be sitting at. Instead, it is “spread” around a different time lag whose value depends on the maximum delay spread  $\tau_{\text{max}}$ . This is better seen by zooming in the vicinity of  $\tau_s = +1$ , as shown in the upper right side of Figure 4.16(a). The maximum values of the received side peak (actually a pulse) will lie somewhere within the range  $\tau \in [T_{\text{FFT}}, T_{\text{FFT}} + \tau_{\text{max}}]$ . Hence, even if knowledge of  $T_{\text{FFT}}$  is available, ACD does not work properly when profile D is considered. BTPD works fine thanks to its peak search. Apart from the spreading caused by the multipath fading channel, Figure 4.16(b) differs from Figure 4.15(b) in the sense that it exhibits no strong unintended peaks that could cause false alarms. Therefore, the FAR of ACD and BPTD are lower here than for profile B. Also, the detection of ECMA-392 under profile D should *not* be an issue using ACD as long as some peak search is carried out. As for BTPD, the spreading of the desired side peaks will cause the blind determination of the useful symbol length to overestimate the actual  $T_{\text{FFT}}$ .

<sup>3</sup> The set of possible  $T_{\text{FFT}}$  values increases as a function of the number of OFDM standards operating collocated and the number of operation modes allowed within each standard. Hence, the estimation of  $T_{\text{FFT}}$  via successive testing may yield unacceptably high detection delays in practical multi-standard operation scenarios.

(a)  $T_{\text{FFT}}$  known a priori.(b)  $T_{\text{FFT}}$  determined based on peak search.

**Fig. 4.15:** Autocorrelation function of ECMA-392 signals received at 20 dB under multipath fading described by profile B. The autocorrelation function of the transmitted (noiseless) ECMA-392 signal is provided for comparison.

It turns out from our analysis that the level of performance achieved by ACD and BTPD depends not only on the PDP describing the fading process (as shown in (4.15)), but also on both knowledge of  $T_{\text{FFT}}$  available for detection and how that knowledge is exploited by the detection process. Unintended peaks introduced by the channel decrease in number and amplitude as  $\tau_{\text{max}}$  increases, but very long delays (as in profile D) cause the secondary peaks in the ACF to be spread around the expected time lag. When  $T_{\text{FFT}}$  is known a priori and  $\tau_{\text{max}}$  is small (as in profile B), satisfactory detection performance can be derived by evaluating  $R_r(\tau_s)$  only at those time lags where the side peaks introduced by the CP are expected to be sitting at. In contrast, when  $\tau_{\text{max}}$  is large (as in profile D), we may need to ensure performance through peak search regardless of the amount of information about  $T_{\text{FFT}}$  available for detection. This maximizes the likelihood of detecting spread side pulses and avoids ACD to fail entirely when ECMA-392 signals are considered.

(a)  $T_{\text{FFT}}$  known a priori.(b)  $T_{\text{FFT}}$  determined based on peak search.

**Fig. 4.16:** Autocorrelation function of ECMA-392 signals received at 20 dB under multipath fading described by profile D. The autocorrelation function of the transmitted (noiseless) ECMA-392 signal is provided for comparison.

## 4.4 Noise Uncertainty

Another issue that arises in the practical operation of WSD is uncertainty about the noise level. In this section, we present simulation results obtained when the target signals are “buried” in noise of uncertain power. Firstly, we consider the impact exerted by the type of target signal on the performance degradation introduced by the SNR wall phenomenon. Specifically, we check if there exist methods that suffer from SNR walls when detecting a certain type of target signal but not all types of target signals. We then investigate whether the fundamental detection limits of those methods susceptible to noise uncertainty can be further shifted by using an increased number of cooperating nodes. As in the multipath case, this allows us to assess whether CSS can mitigate the impact of noise uncertainty. To close our analysis, we look at other operation conditions known to influence performance in the ideal case, e.g, fusion rule, CFAR requirement, and symbol length.

The AMD values shown in Tables 4.3 and 4.4 suggest that all methods but ED, RLRT, and SCD are robust against noise uncertainty when the channel is AWGN. Indeed, it is evident from (2.11) and (2.30) that ED and RLRT are susceptible to noise uncertainty. As for SCD, nothing can be inferred by inspecting (2.54) directly but our simulation results show that, depending on the type of target signal, the absence of exact knowledge of  $\sigma_w^2$  may introduce SNR walls that substantially degrade detection performance. The same behavior is also verified for multipath fading channels, as illustrated for the case of profile B in Tables 4.5 and 4.6. By comparing Table 4.3 to Table 4.5, we see that AMD does not change much for most methods when the target signals are based on OFDM. This reflects well the fact that most methods are virtually immune to multipath, as seen in Section 4.3. However, unlike most methods, ED, RLRT, and SCD show AMD improvements of 3.75, 3.44, and 2.38, respectively, when we switch the channel from AWGN to multipath. The reason is that, while the ideal performances of these methods decrease substantially under multipath, their SNR walls remain the same as when under AWGN. Hence, since the deviations in performance decrease in average, the observed AMD increases. A similar analysis of the joint effects of noise uncertainty and multipath fading can be carried out for the case of non-OFDM signals by comparing Tables 4.4 and 4.6. Extensions for profile D are also straightforward to obtain.

In what follows, our emphasis is placed on the analysis of methods that are susceptible to noise uncertainty: ED, RLRT, and SCD. In order to allow direct comparisons between ideal operation conditions ( $\sigma_w^2$  is perfectly known) and noise uncertainty conditions (knowledge of  $\sigma_w^2$  is imperfect), we use the  $\rho$  values in Table 3.4.

#### 4.4.1 Impact of Target Signal Type

ED and RLRT are methods that perform independent of the target signal type even if the noise is of uncertain power. This is confirmed in Figures 4.17 and 4.18, where some minor performance variations are due to the different sensing times used in the simulations (see Table 3.7). In either case, a small deviation of only  $\pm 0.5$  dB ( $\rho = 1.12$ ) about the true value of  $\sigma_w^2$ , *e.g.* noise level changes or due to some irreducible residual uncertainty after  $\sigma_w^2$  has been estimated, introduces SNR walls that degrade the detection performances in up to 13 dB relative to the ideal case ( $\rho = 1.00$ ). In the particular case of ED, for which nominal SNR walls can be computed in closed form, our results in Figure 4.17 support well those presented in [100] and [102] as they suggest that (2.19) provides a lower bound on the actual detection limit. For the types of target signal in Figure 4.17, we can clearly see that the simulated SNR wall is *always* better than that computed via (2.19).

In contrast to ED and RLRT, SCD largely depends on the type of target signal when  $\sigma_w^2$  is only imperfectly known. If the target signals are non-OFDM, as originally proposed in [50], it is easy to improve performance because no SNR wall is created. In such cases, where the spectrum of the target signal exhibits sharp spectral features (see Figure 3.5), SCD is virtually immune to noise uncertainty. This is confirmed in Figure 4.19 for ATSC, NTSC, and PAL. Similar results can be obtained for WM signals, regardless of the speaker mode used. In contrast, performance losses ranging from 5 dB to 11 dB are observed in Figure 4.20 when we direct SCD to detect OFDM-based signals. Before pursuing on this specific issue of SCD (and along the same lines used in our analysis of multipath), let us first investigate whether CSS can alleviate the losses in performance caused by SNR walls in more general cases.



**Table 4.3:** Performance deviation in dB introduced by noise uncertainty for OFDM signals detected under AWGN as compared to  $\sigma_w^2$  ideally known ( $\rho = 0$ ).

| Method   | DVB-T         |       |               |       | ISDB-T        |       |               |       | IEEE 802.22   |       |               |       | ECMA-392      |       |               |       | AMD    | Robustness |
|----------|---------------|-------|---------------|-------|---------------|-------|---------------|-------|---------------|-------|---------------|-------|---------------|-------|---------------|-------|--------|------------|
|          | $\rho = 1.12$ |       | $\rho = 1.24$ |       | $\rho = 1.12$ |       | $\rho = 1.24$ |       | $\rho = 1.12$ |       | $\rho = 1.24$ |       | $\rho = 1.12$ |       | $\rho = 1.24$ |       |        |            |
|          | Best          | Worst | Best          | Worst | Best          | Worst | Best          | Worst | Best          | Worst | Best          | Worst | Best          | Worst | Best          | Worst |        |            |
| ED       | -13           | -11   | -15           | -12   | -13           | -9    | -15           | -12   | -11           | -11   | -13           | -12   | -10           | -8    | -11           | -9    | -11.56 | Poor       |
| AGM      | -1            | -1    | -1            | -1    | -1            | 0     | -1            | 0     | +1            | +1    | +1            | +1    | 0             | -1    | -1            | -1    | +0.06  | Excellent  |
| GLRT     | -1            | -1    | -1            | -1    | -1            | 0     | -1            | 0     | +1            | +1    | +1            | +1    | -1            | 0     | -1            | -1    | +0.06  | Excellent  |
| MME      | -1            | -1    | -1            | -1    | 1             | 0     | -1            | 0     | +1            | +1    | +1            | +1    | 0             | -1    | -1            | -1    | +0.06  | Excellent  |
| RLRT     | -12           | -11   | -14           | -13   | -11           | -11   | -14           | -13   | -12           | -10   | -14           | -12   | -8            | -7    | -11           | -10   | -11.44 | Poor       |
| SCD      | -11           | -8    | -12           | -9    | -11           | -8    | -12           | -9    | -9            | -9    | -11           | -10   | -9            | -5    | -10           | -7    | -9.38  | Poor       |
| ACD      | 0             | +1    | +1            | +1    | 0             | +1    | +1            | +1    | 0             | +1    | +1            | +1    | +1            | +1    | +1            | +1    | +0.81  | Excellent  |
| BTPD     | 0             | 0     | 0             | 0     | 0             | 0     | 0             | 0     | +1            | 0     | +1            | 0     | 0             | 0     | 0             | 0     | +0.13  | Excellent  |
| TDSC-NP  | 0             | 0     | 0             | 0     | 0             | 0     | 0             | 0     | 0             | 0     | 0             | 0     | +1            | 0     | +1            | 0     | +0.13  | Excellent  |
| TDSC-MRC | 0             | 0     | 0             | 0     | 0             | 0     | 0             | 0     | 0             | 0     | 0             | 0     | +1            | 0     | +1            | 0     | +0.13  | Excellent  |

$\rho = 1.12 \leftrightarrow \sigma_w^2 \pm 0.5$  dB,  $\rho = 1.24 \leftrightarrow \sigma_w^2 \pm 1.0$  dB Best: OR logic and  $P_{fa} = 0.1$ , Worst: AND logic and  $P_{fa} = 0.01$ , AMD: Average Method Deviation.

**Table 4.4:** Performance deviation in dB introduced by noise uncertainty for non-OFDM signals detected under AWGN as compared to  $\sigma_w^2$  ideally known ( $\rho = 0$ ).

| Method | ATSC          |       |               |       | NTSC          |       |               |       | PAL           |       |               |       | PMSE (Soft Mode) |       |               |       | AMD   | Robustness |
|--------|---------------|-------|---------------|-------|---------------|-------|---------------|-------|---------------|-------|---------------|-------|------------------|-------|---------------|-------|-------|------------|
|        | $\rho = 1.12$ |       | $\rho = 1.24$ |       | $\rho = 1.12$ |       | $\rho = 1.24$ |       | $\rho = 1.12$ |       | $\rho = 1.24$ |       | $\rho = 1.12$    |       | $\rho = 1.24$ |       |       |            |
|        | Best          | Worst | Best          | Worst | Best          | Worst | Best          | Worst | Best          | Worst | Best          | Worst | Best             | Worst | Best          | Worst |       |            |
| ED     | -10           | -8    | -11           | -10   | -6            | -6    | -7            | -7    | -3            | -3    | -4            | -4    | -10              | -7    | -11           | -8    | -7.19 | Poor       |
| AGM    | 0             | +1    | +1            | +1    | +1            | 0     | +2            | +1    | 0             | 0     | +1            | +1    | +1               | 0     | +1            | +1    | +0.75 | Excellent  |
| GLRT   | 0             | +1    | +1            | +1    | +1            | 0     | +2            | +1    | 0             | 0     | +1            | +1    | +1               | 0     | +1            | +1    | +0.75 | Excellent  |
| MME    | 0             | +1    | +1            | +1    | +1            | 0     | +2            | +1    | 0             | 0     | +1            | +1    | +1               | 0     | +1            | +1    | +0.75 | Excellent  |
| RLRT   | -8            | -7    | -11           | -10   | -7            | -5    | -10           | -7    | -3            | -3    | -5            | -5    | -12              | -11   | -15           | -14   | -8.31 | Poor       |
| SCD    | -1            | 0     | -1            | 0     | 0             | 0     | 0             | 0     | 0             | -1    | 0             | -1    | -1               | 0     | -2            | 0     | -0.44 | Excellent  |
| ASSD   | -1            | -2    | -1            | -2    | N/A           | N/A   | N/A           | N/A   | N/A           | N/A   | N/A           | N/A   | N/A              | N/A   | N/A           | N/A   | -1.50 | Good       |
| MF     | N/A           | N/A   | N/A           | N/A   | N/A           | N/A   | N/A           | N/A   | N/A           | N/A   | N/A           | N/A   | 0                | 0     | -1            | 0     | -0.25 | Excellent  |

$\rho = 1.12 \leftrightarrow \sigma_w^2 \pm 0.5$  dB,  $\rho = 1.24 \leftrightarrow \sigma_w^2 \pm 1.0$  dB Best: OR logic and  $P_{fa} = 0.1$ , Worst: AND logic and  $P_{fa} = 0.01$ , AMD: Average Method Deviation.

**Table 4.5:** Performance deviation in dB introduced by noise uncertainty for OFDM signals detected under multipath as compared to  $\sigma_w^2$  ideally known ( $\rho = 0$ ).

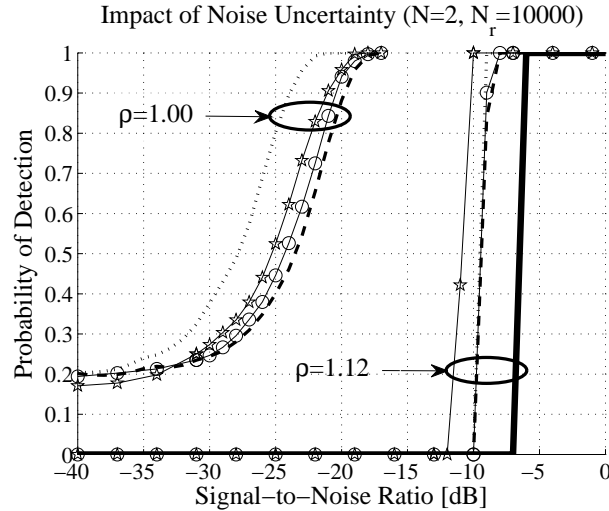
| Method   | DVB-T         |       |               |       | ISDB-T        |       |               |       | IEEE 802.22   |       |               |       | ECMA-392      |       |               |       | AMD   | Robustness |
|----------|---------------|-------|---------------|-------|---------------|-------|---------------|-------|---------------|-------|---------------|-------|---------------|-------|---------------|-------|-------|------------|
|          | $\rho = 1.12$ |       | $\rho = 1.24$ |       | $\rho = 1.12$ |       | $\rho = 1.24$ |       | $\rho = 1.12$ |       | $\rho = 1.24$ |       | $\rho = 1.12$ |       | $\rho = 1.24$ |       |       |            |
|          | Best          | Worst | Best          | Worst | Best          | Worst | Best          | Worst | Best          | Worst | Best          | Worst | Best          | Worst | Best          | Worst |       |            |
| ED       | -10           | -8    | -11           | -9    | -10           | -6    | -11           | -9    | -11           | -9    | -9            | -10   | -3            | -2    | -4            | -3    | -7.81 | Poor       |
| AGM      | 0             | +1    | +1            | +1    | 0             | +1    | +2            | +1    | 0             | +1    | +1            | +1    | 0             | +1    | +1            | +1    | +0.81 | Excellent  |
| GLRT     | 0             | +1    | +1            | +1    | 0             | +2    | +1            | +2    | 0             | +1    | +1            | +1    | 0             | +1    | +1            | +1    | +0.88 | Excellent  |
| MME      | 0             | +1    | +1            | +1    | +2            | +2    | +1            | +2    | 0             | +1    | +1            | +1    | 0             | +1    | +1            | +1    | +1.00 | Excellent  |
| RLRT     | -8            | -7    | -11           | -10   | -7            | -7    | -11           | -10   | -10           | -9    | -11           | -12   | -4            | -2    | -5            | -4    | -8.00 | Poor       |
| SCD      | -8            | -6    | -9            | -7    | -8            | -6    | -9            | -7    | -11           | -7    | -12           | -8    | -3            | -3    | -4            | -4    | -7.00 | Poor       |
| ACD      | +1            | 0     | +1            | +1    | +1            | 0     | +1            | +1    | 0             | +1    | +1            | +1    | +1            | 0     | +1            | 0     | +0.69 | Excellent  |
| BTPD     | 0             | 0     | 0             | 0     | 0             | 0     | 0             | 0     | 0             | 0     | 0             | 0     | 0             | 0     | 0             | 0     | +0.00 | Excellent  |
| TDSC-MRC | 0             | 0     | 0             | 0     | 0             | 0     | 0             | 0     | 0             | 0     | 0             | 0     | 0             | 0     | 0             | 0     | +0.00 | Excellent  |
| TDSC-NP  | 0             | 0     | 0             | 0     | 0             | 0     | 0             | 0     | 0             | 0     | 0             | 0     | 0             | 0     | 0             | 0     | +0.00 | Excellent  |

$\rho = 1.12 \leftrightarrow \sigma_w^2 \pm 0.5$  dB,  $\rho = 1.24 \leftrightarrow \sigma_w^2 \pm 1.0$  dB Best: OR logic and  $P_{fa} = 0.1$ , Worst: AND logic and  $P_{fa} = 0.01$ , AMD: Average Method Deviation.

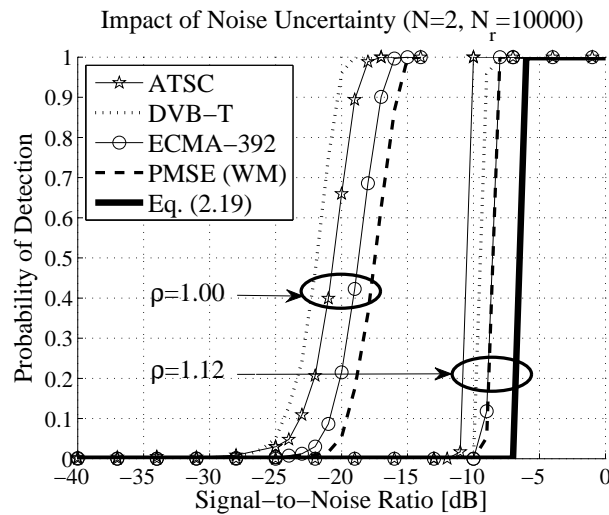
**Table 4.6:** Performance deviation in dB introduced by noise uncertainty for non-OFDM signals detected under multipath as compared to  $\sigma_w^2$  ideally known ( $\rho = 0$ ).

| Method | ATSC          |       |               |       | NTSC          |       |               |       | PAL           |       |               |       | PMSE (Soft Mode) |       |               |       | AMD   | Robustness |
|--------|---------------|-------|---------------|-------|---------------|-------|---------------|-------|---------------|-------|---------------|-------|------------------|-------|---------------|-------|-------|------------|
|        | $\rho = 1.12$ |       | $\rho = 1.24$ |       | $\rho = 1.12$ |       | $\rho = 1.24$ |       | $\rho = 1.12$ |       | $\rho = 1.24$ |       | $\rho = 1.12$    |       | $\rho = 1.24$ |       |       |            |
|        | Best          | Worst | Best          | Worst | Best          | Worst | Best          | Worst | Best          | Worst | Best          | Worst | Best             | Worst | Best          | Worst |       |            |
| ED     | -10           | -7    | -11           | -9    | -7            | -6    | -8            | -7    | -3            | -3    | -5            | -4    | -14              | -11   | -16           | -13   | -8.38 | Poor       |
| AGM    | 0             | +1    | +1            | +1    | +1            | 0     | +1            | +1    | 0             | 0     | +1            | +1    | 0                | 0     | +1            | +1    | +0.63 | Excellent  |
| GLRT   | 0             | +1    | +1            | +1    | +1            | 0     | +1            | +1    | 0             | 0     | +1            | +1    | 0                | 0     | +1            | +1    | +0.63 | Excellent  |
| MME    | 0             | +1    | +1            | +1    | +1            | 0     | +1            | +1    | 0             | 0     | +1            | +1    | 0                | 0     | +1            | +1    | +0.63 | Excellent  |
| RLRT   | -8            | -7    | -11           | -10   | -6            | -8    | -7            | -10   | -3            | -3    | -5            | -5    | -11              | -11   | -14           | -13   | -8.25 | Poor       |
| SCD    | 0             | 0     | 0             | 0     | 0             | 0     | 0             | 0     | 0             | 0     | 0             | 0     | -2               | -1    | -2            | -1    | -0.38 | Excellent  |
| ASSD   | 0             | -1    | -1            | -1    | N/A           | N/A   | N/A           | N/A   | N/A           | N/A   | N/A           | N/A   | N/A              | N/A   | N/A           | N/A   | -0.75 | Excellent  |
| MF     | N/A           | N/A   | N/A           | N/A   | N/A           | N/A   | N/A           | N/A   | N/A           | N/A   | N/A           | N/A   | 0                | -1    | -1            | -1    | -0.75 | Excellent  |

$\rho = 1.12 \leftrightarrow \sigma_w^2 \pm 0.5$  dB,  $\rho = 1.24 \leftrightarrow \sigma_w^2 \pm 1.0$  dB Best: OR logic and  $P_{fa} = 0.1$ , Worst: AND logic and  $P_{fa} = 0.01$ , AMD: Average Method Deviation.



(a) Best case.



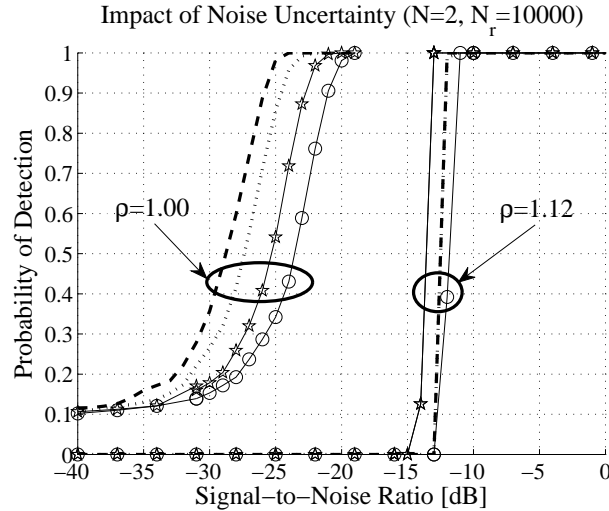
(b) Worst case.

**Fig. 4.17:** AWGN performances of ideal ED ( $\rho = 1.00$ ) and ED under noise uncertainty of  $\Delta\hat{\sigma}_w^2 = \sigma_w^2 \pm 0.5$  dB ( $\rho = 1.12$ ) for different target signals.

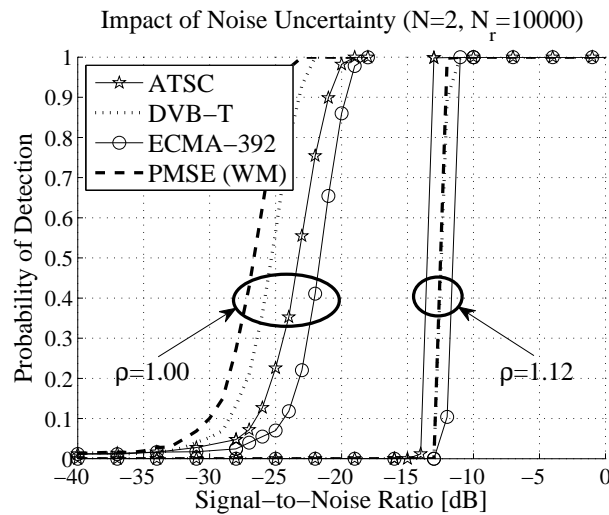
#### 4.4.2 Impact of Number of Nodes

Thus far, our simulation work has shown that ED and RLRT are always susceptible to noise uncertainty but SCD suffers from the SNR wall phenomenon only when it comes to the detection of OFDM-based target signals. Our next step is to analyze the impact of an increased number of nodes on the detection performances that these methods can deliver when  $\sigma_w^2$  is not perfectly known. As in our multipath fading analysis, the cooperation gains derived when  $N$  increases are assessed by comparing simulation results obtained for  $N = \{2, 10, 20\}$  nodes. We restrict the analysis that follows to the case of OFDM-based target signals and, without any loss of generality, consider the ECMA-392 standard. Similar results for DVB-T, ISDB-T, and IEEE 802.22 are straightforward to obtain along the lines used here.

According to the best-case curves shown in Figures 4.21(a) and 4.22(a), the ideal gains ( $\rho = 1.00$ ) derived by increasing  $N$  from 2 to 20 nodes are 4 dB and 5 dB when ED and



(a) Best case.

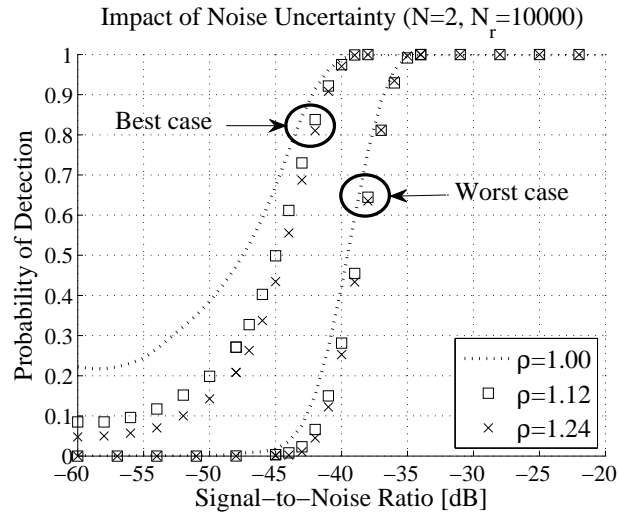


(b) Worst case.

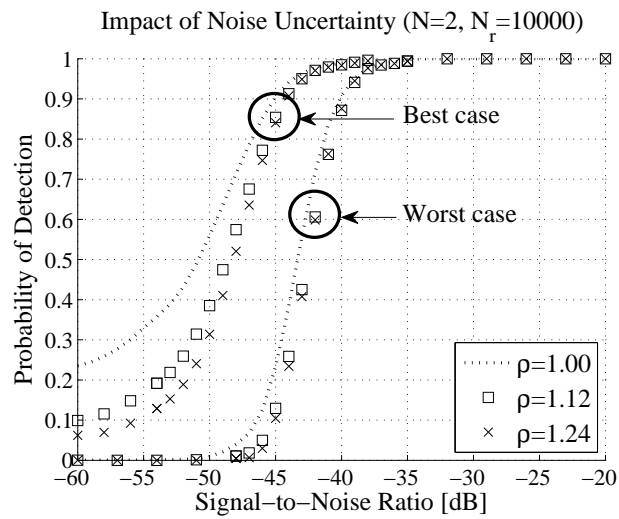
**Fig. 4.18:** AWGN performances of ideal RLRT ( $\rho = 1.00$ ) and RLRT under noise uncertainty of  $\Delta\hat{\sigma}_w^2 = \sigma_w^2 \pm 0.5$  dB ( $\rho = 1.12$ ) for different target signals.

SCD are respectively employed at the local level. On the other hand, if the fluctuation about the true value of  $\sigma_w^2$  is of  $\pm 0.5$  dB ( $\rho = 1.12$ ), the same increase in the number of nodes buys us *nothing* in terms of performance improvement. The SNR walls remain fixed at around  $-9$  dB for ED and  $-13$  dB for SCD, regardless the number of nodes used. In case of ED, this matches well to the related work in [98]–[102] where it is shown that SNR walls cannot be “shifted” via CSS. If we now look at the worst-case curves on Figures 4.21(b) and 4.22(b), it is clear that hard combining local contributions using AND logic results in a global performance that deteriorates as  $N$  increases with  $\sigma_w^2$  perfectly known ( $\rho = 1.00$ ). When the uncertainty about the true noise floor is of  $\pm 0.5$  dB ( $\rho = 1.12$ ), any visible losses are introduced as  $N$  increases. Nevertheless, and like in the best-case curves where OR logic is used, the global detection performances of ED and SCD are limited by SNR walls respectively located at  $-8$  dB and  $-11$  dB.

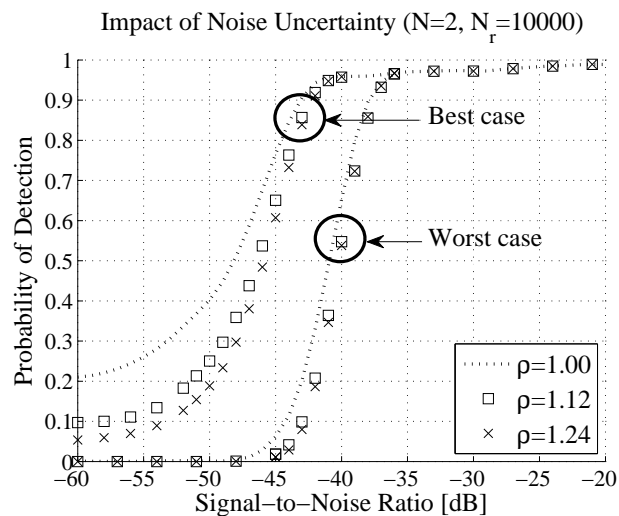
As explained in Section 3.5, the use of SCD to detect OFDM-based target signals has been motivated due to its potential to improve the third stage of the generic signal classification



(a) ATSC.

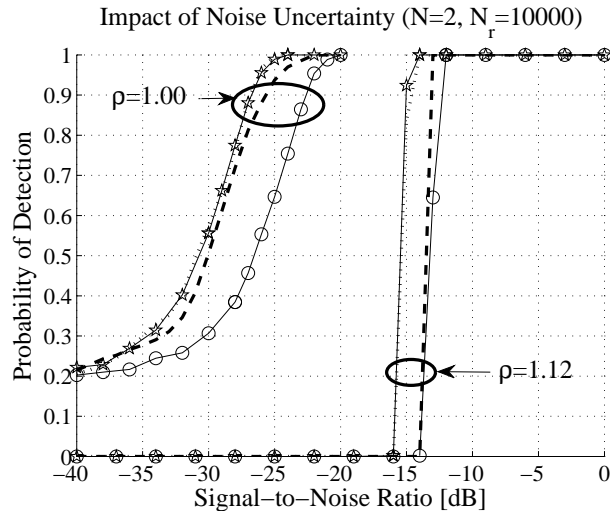


(b) NTSC.

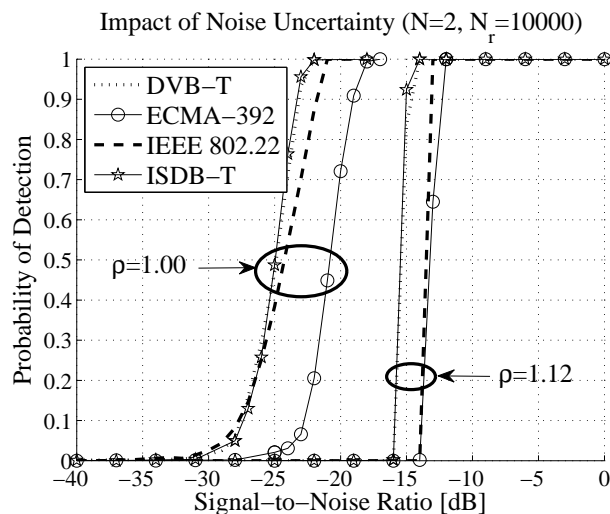


(c) PAL.

**Fig. 4.19:** AWGN performances of SCD under different amounts of noise uncertainty for different non-OFDM target signals. Best (worst) case curves account to the use of OR (AND) logic and  $P_{fa} = 0.1$  ( $P_{fa} = 0.01$ ).



(a) Best case.



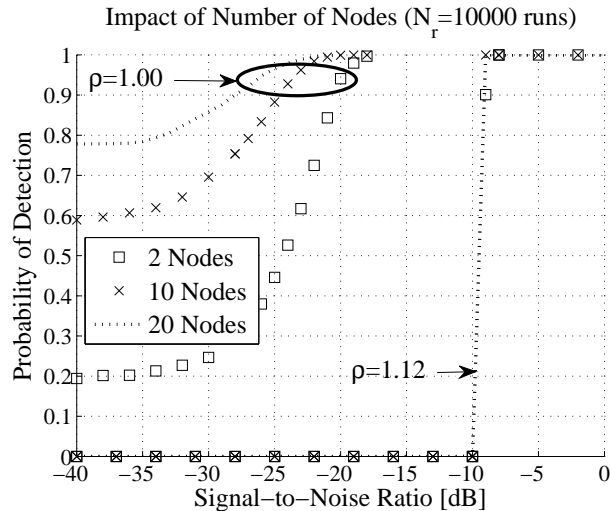
(b) Worst case.

**Fig. 4.20:** AWGN performances of ideal SCD ( $\rho = 1.00$ ) and SCD under noise uncertainty of  $\Delta\hat{\sigma}_w^2 = \sigma_w^2 \pm 0.5$  dB ( $\rho = 1.12$ ) for different OFDM signals.

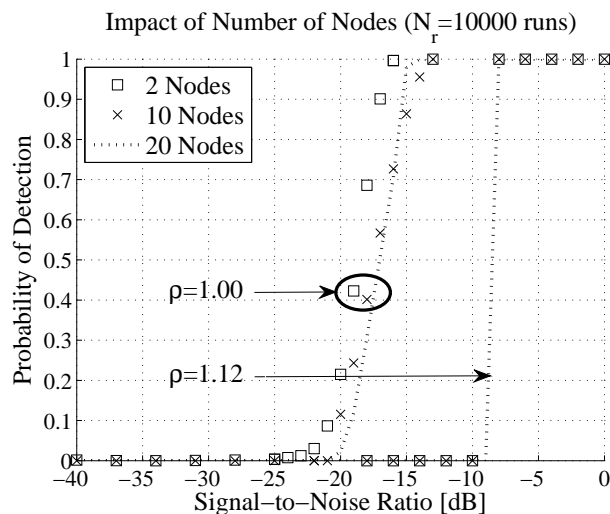
block in Figure 3.11 in terms of agility and complexity. However, the coupling SCD-OFDM has shown some “bad signs” as the achievable performance is limited by SNR walls that, as in ED, cannot be shifted through CSS. Though SCD can still be regarded as the most promising candidate to detect non-OFDM signals, the reason for its “signal-dependent” susceptibility to noise uncertainty is worth investigating.

Our starting point for such investigation are the spectral masks of OFDM signals received at different SNR levels, as Figure 4.23 illustrates for ECMA-392 when the knowledge of  $\sigma_w^2$  is perfect<sup>4</sup>. It is seen in Figure 4.23(a) that the signal edges are sharp in the high SNR regime but, in Figure 4.23(b), they progressively degrade, and subsequently disappear, as the SNR decreases. The region where the signal edges undergo critical deterioration spans from  $-10$  dB to  $-15$  dB and, thus, encompasses the values where walls occur in Figures 4.20 and 4.22. Since the signal edges are the only spectral features that can be exploited

<sup>4</sup> We omit the plots for  $\sigma_w^2 = 1.12$  and  $\sigma_w^2 = 1.24$  because OFDM spectra do not seem to change much in the presence of noise uncertainty.



(a) Best case.



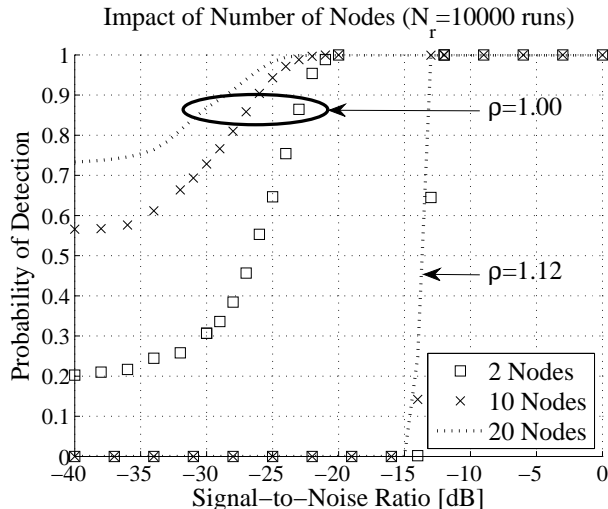
(b) Worst case.

**Fig. 4.21:** AWGN performances of ideal ED ( $\rho = 1.00$ ) and ED under noise uncertainty of  $\Delta\hat{\sigma}_w^2 = \sigma_w^2 \pm 0.5$  dB ( $\rho = 1.12$ ) when ECMA-392 signals are detected using different number of nodes.

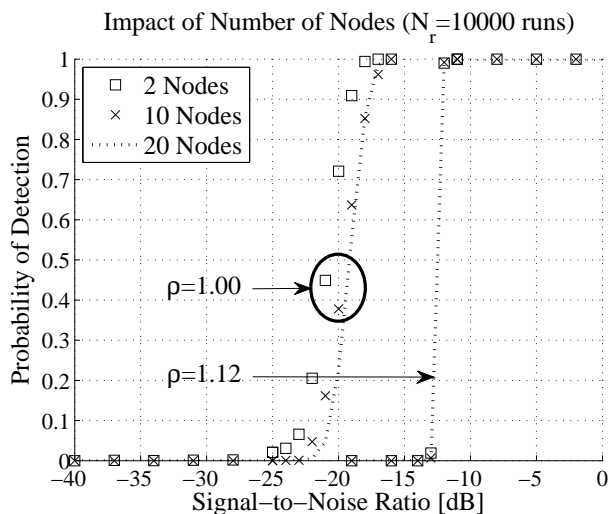
for detection in OFDM, the uncertainty about their positions seems to contribute *jointly* with the noise uncertainty to the SNR walls of SCD.

The next aspect to verify is whether the SNR walls observed here really characterize the detection limits of SCD, *i.e.* whether the sample complexity of the method approaches infinity in their neighborhoods. If this is the case, then the use of an increased number of samples  $M$  should not yield any performance improvement when  $\sigma_w^2$  is not exactly known. However, what we see in Figure 4.24 actually contradicts this expectation. First, Figure 4.24(a) shows that it becomes possible to distinguish the signal edges from the noise floor when  $M$  is one order of magnitude larger than before. Second, since the edges are now visible at lower SNR, it is evident that the global detection performance of SCD should improve. This is confirmed in Figure 4.24(b), where the SNR walls improved in roughly 10 dB (as compared to Figures 4.20 and 4.22) when  $\sigma_w^2 = 1.12$ .

Summing up our analysis on the SNR walls experienced by SCD, we observe that the



(a) Best case.

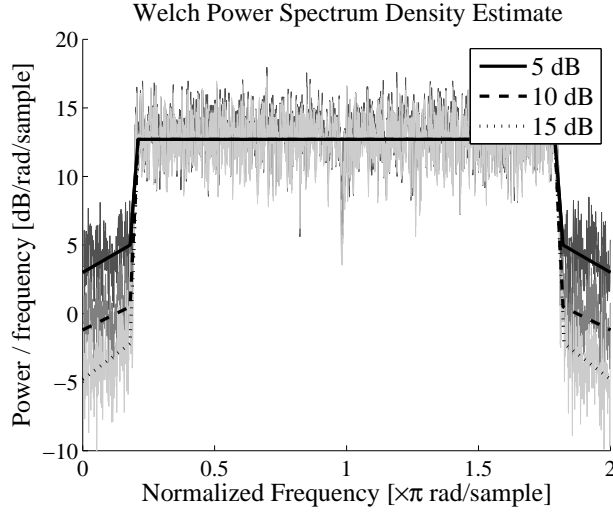


(b) Worst case.

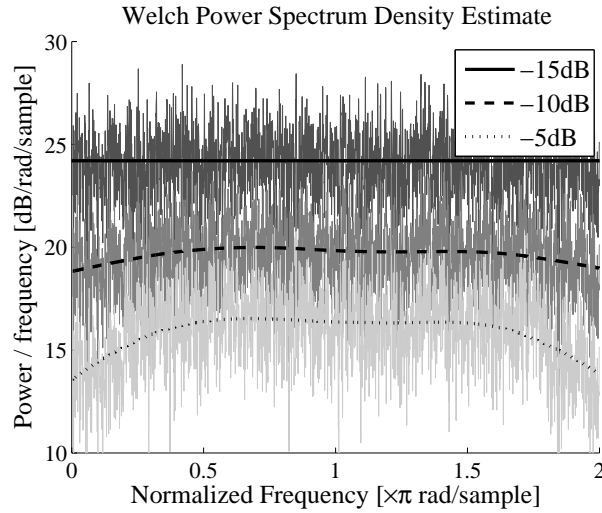
**Fig. 4.22:** AWGN performances of ideal SCD ( $\rho = 1.00$ ) and SCD under noise uncertainty of  $\Delta\hat{\sigma}_w^2 = \sigma_w^2 \pm 0.5$  dB ( $\rho = 1.12$ ) when ECMA-392 signals are detected using different number of nodes.

robustness of the method depends on the joint uncertainty about the actual  $\sigma_w^2$  and the actual position of the spectral feature exploited for detection. If the target signals are non-OFDM, SCD does not suffer from SNR walls because the spikes related to the ATSC pilot and the subcarriers (luminance and chrominance) used in NTSC/PAL occur at fixed positions. In contrast, the detection of OFDM-based target signals is more challenging in the presence of noise uncertainty because the exact position of the signal edges exploited by SCD becomes hard to determine as the SNR decreases. The use of an increased number of samples makes it possible for SCD to “see” the signal edges at lower SNR, thus improving the performance of the method also under noise uncertainty. However, if the SNR keeps decreasing, there will be some value for which the signal edges will disappear again, *e.g.* around  $-22$  dB in Figure 4.24(b). Hence, while we can shift SNR walls at the expense of complexity, this does not prevent the occurrence of the SNR wall phenomenon. It is also worth noting that, though intuitive, these findings are based on observations only and thus not intended to replace a formal proof justifying the behavior of SCD.





(a) High SNR regime.

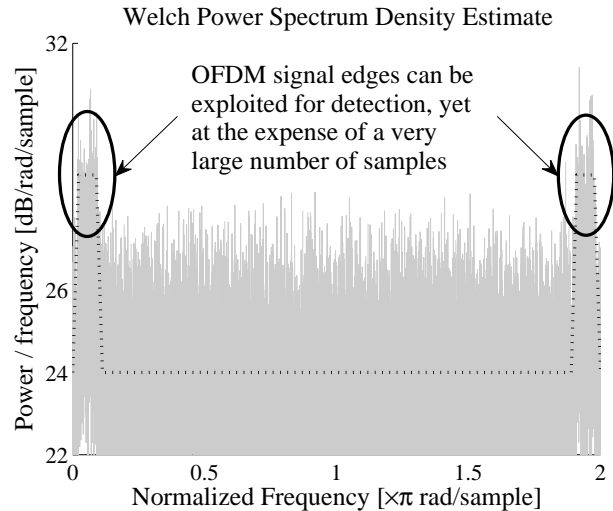
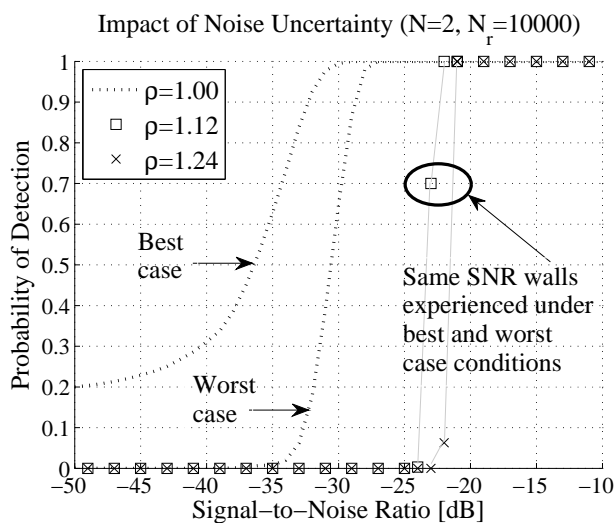


(b) Low SNR regime.

**Fig. 4.23:** Spectral masks of ECMA-392 signals received at different SNR levels ( $\rho = 1.00$ ,  $M \approx 10000$  samples).

Now that we have shed some light on what might be introducing SNR walls in SCD, it is time to turn our attention to the case shown in Figure 4.25 where an increased number of RLRT-based nodes engage in cooperation. When we assume perfect knowledge of  $\sigma_w^2$ , Figure 4.25(a) shows that the cooperation gains achievable by RLRT can be as large as 7 dB when we increase  $N$  from 2 to 20 nodes. The same increase in  $N$  yields gains of 9 dB and 10 dB when the uncertainty about the true  $\sigma_w^2$  is of  $\pm 0.5$  dB ( $\rho = 1.12$ ) and  $\pm 1.0$  dB ( $\rho = 1.24$ , not depicted), respectively. This suggests that, unlike what we have observed for ED and SCD, cooperation can effectively alleviate the detrimental effects caused by noise uncertainty when RLRT is used at the local level. In order to understand why CSS yields rather different results when based on ED and RLRT, we need to find the distributions of the test statistics  $z_{\text{ED}}^{\text{CSS}}$  and  $z_{\text{RLRT}}$ .

Deriving an approximation to the distribution of  $z_{\text{RLRT}}$  corresponds to finding an accurate representation for the p.d.f. of  $\lambda_{\text{max}}$  under  $H_0$  and  $H_1$ . This has been an open problem in multivariate analysis for several decades and no acceptable method for dimension larger

(a) Spectral mask received at  $-15$  dB ( $\rho = 1.00$ ).(b) AWGN performance of SCD for different  $\rho$ .

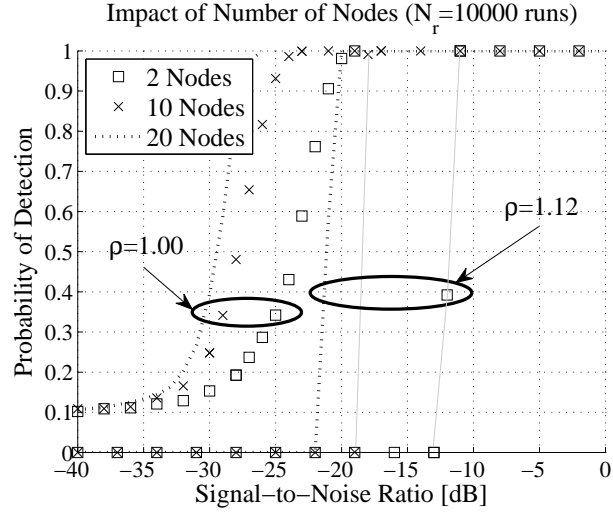
**Fig. 4.24:** Impact of number of samples on the spectral masks and on the performance of SCD for ECMA-392 signals ( $M \approx 100000$  samples).

than two ( $N > 2$ ) is known to date [151]. Moreover, though substantial research effort has been carried out to study  $\lambda_{\max}$  in the high dimensional setting, *i.e.* in the joint limit as both  $N, M \rightarrow \infty$  (see, *e.g.* [105], [151], and the references therein), we should not use asymptotic approaches here because both  $N$  and  $M$  are finite in our case.

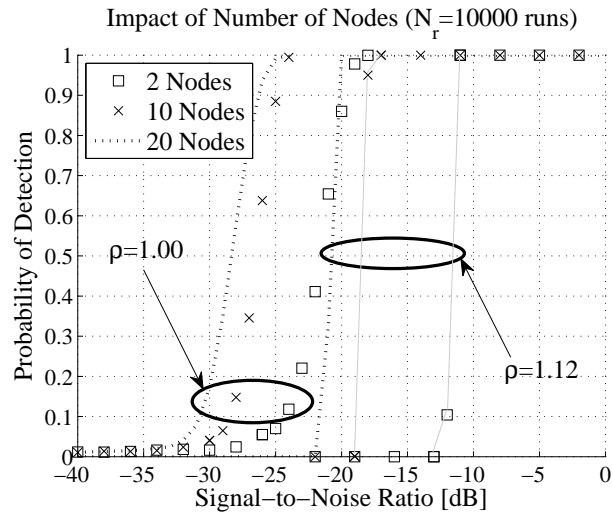
As for  $z_{\text{ED}}^{\text{CSS}}$ , the test statistic of the  $i$ th node under the assumption that all nodes collect the same number of channel samples

$$z_{\text{ED}}^i(n) = \frac{1}{M} \sum_{n=0}^{M-1} |r_i(n)|^2 \quad (4.16)$$

is essentially the same as (2.10). If each node reports its entire set of samples, *i.e.* soft combining is used, the master node can issue a decision using (2.31). In this case, since the sum of Gaussian random variables is itself a Gaussian random variable [147], it is evident that the distribution of  $z_{\text{ED}}^{\text{CSS}}$  can be approximated as asymptotically normal. In MESS,



(a) Best case.



(b) Worst case.

**Fig. 4.25:** AWGN performances of ideal RLRT ( $\rho = 1.00$ ) and RLRT under noise uncertainty of  $\Delta\hat{\sigma}_w^2 = \sigma_w^2 \pm 0.5$  dB ( $\rho = 1.12$ ) when ECMA-392 signals are detected using different number of nodes.

however, we use hard combining. Thereby, instead of reporting its full test statistic, each node reports only a single-bit decision described by:

$$\pi_i(n) = \begin{cases} 0, & z_{\text{ED}}^i < \gamma_i \\ 1, & z_{\text{ED}}^i \geq \gamma_i. \end{cases} \quad (4.17)$$

Recalling that any censoring scheme is implemented in MESS (see Section 3.3.2), *i.e.* all nodes are allowed to report their local findings to the master node, the presence of target signals on the channel currently being scanned can be determined using

$$z_{\text{ED}}^{\text{CSS}}(n) = \begin{cases} H_0 : \sum_{i=1}^N \tilde{\pi}_i < \gamma_{\text{master}} \\ H_1 : \sum_{i=1}^N \tilde{\pi}_i \geq \gamma_{\text{master}} \end{cases} \quad (4.18)$$

with the detection threshold used at the master node set according to the fusion rule used to combine the received decision bits<sup>5</sup>, *i.e.*  $\gamma_{\text{master}} = 1$  for OR logic and  $\gamma_{\text{master}} = N$  for AND logic. Suppose now that individual node decisions are collected into the vector  $\tilde{\boldsymbol{\pi}} = [\tilde{\pi}_1, \tilde{\pi}_2, \dots, \tilde{\pi}_N]^T$ . Our next step consists of finding the probability mass function (p.m.f) of the vector  $\tilde{\boldsymbol{\pi}}$  under  $H_0$  and  $H_1$ . However, we observe that even if these p.m.f's were available and we could use (2.6) to construct the LRT

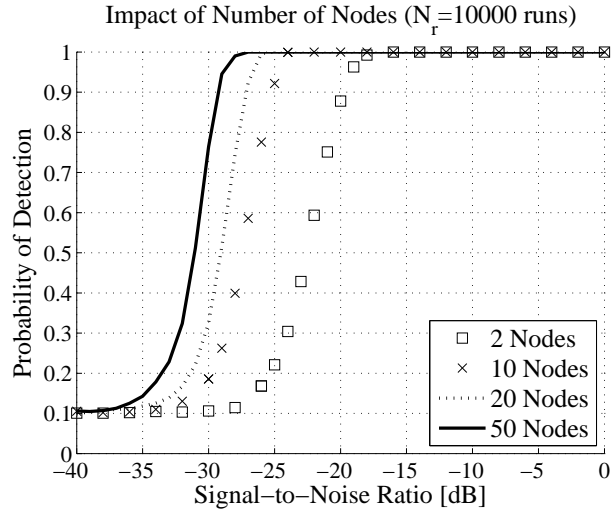
$$\frac{p(\tilde{\boldsymbol{\pi}}|H_0)}{p(\tilde{\boldsymbol{\pi}}|H_1)} \underset{H_1}{\overset{H_0}{\gtrless}} \gamma_{\text{opt}}, \quad (4.19)$$

the computation of an optimal detection threshold  $\gamma_{\text{opt}}$  for each individual node is mathematically intractable under the NP criterion (see [52] and the references therein). Indeed, by assuming uncorrelated node decisions, we could manage to formulate a decision problem that can be verified in polynomial time. We do not pursue on this here because, even if we are able to approximate the distribution of  $z_{\text{ED}}^{\text{CSS}}$ , we will still lack that of  $z_{\text{RLRT}}$ .

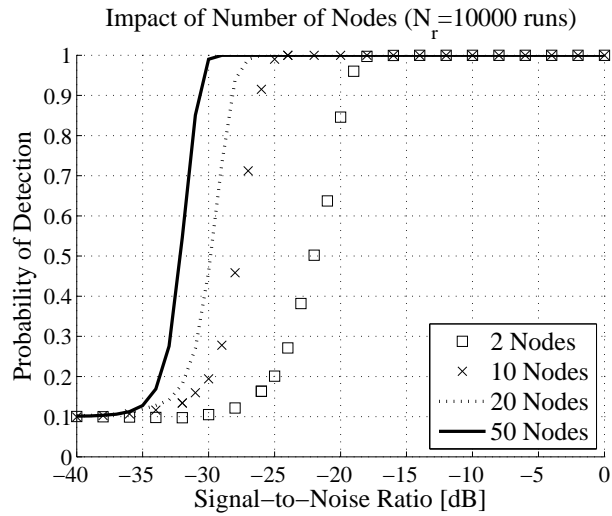
It turns out from the above discussion that the task of finding closed-form approximations for the distributions of  $z_{\text{ED}}^{\text{CSS}}$  and  $z_{\text{RLRT}}$  becomes difficult when hard combining is used and the number of cooperating nodes is larger than two (but finite), respectively. A less formal, yet possible, explanation for the fact that cooperation shifts SNR walls in RLRT but not in ED might go as follows. While the ED-based CSS approach adopted here performs hard combining to issue a decision about the current channel status, RLRT relies solely on  $\lambda_{\text{max}}$ . This means that only the contribution of the node experiencing the best channel realization matters for the detection process. Hence, what RLRT actually does is far from suboptimum hard combining and can be interpreted as some kind of “node selection” (see Chapter 1). It seems therefore interesting to investigate whether, when under noise uncertainty, node selection can make ED-based CSS achieve cooperation gains similar to those observed for RLRT. We do not pursue on this issue here because, even if the SNR walls in Figure 4.21 improve as in Figure 4.25, the best-case performance derived thereby will still lie below what can be achieved using blind EBD methods.

The exact extent to which blind EBD outperforms semi-blind EBD can be analyzed with the help of Figures 4.26 and 4.27. In these figures, we consider ECMA-392 signals detected under best- and worst-case conditions, respectively, when the uncertainty about the true value of  $\sigma_w^2$  is of  $\pm 0.5$  dB ( $\rho = 1.12$ ). By comparing Figure 4.25(a) to Figure 4.26, we see that the performance gap between RLRT and any of the blind EBD methods under best-case conditions lies around 6 dB provided that  $N \geq 10$ . Similar gaps can be observed under worst-case conditions by comparing Figure 4.25(b) to Figure 4.27, though in this case the gains of blind EBD over semi-blind EBD can be realized even when the number of nodes is small, *e.g.*  $N = 2$ . Hence, recalling that all EBD methods pose roughly the same computational complexity (see Table 3.8), it does not seem to exist any advantage in using semi-blind techniques in our setting. Within blind EBD methods, it is clear from Figures 4.26 and 4.27 that, unless  $N = 2$ , AGM is outperformed in up to 2 dB by both GLRT and MME. This is expected since, compared to (2.41), the test statistics (2.39) and (2.43) are clearly suboptimal for  $N$  is large enough. Therefore, despite the slightly better robustness of MME ( $\approx 1$  dB) against noise uncertainty observed in our simulations, GLRT is the method of choice when it comes to EBD.

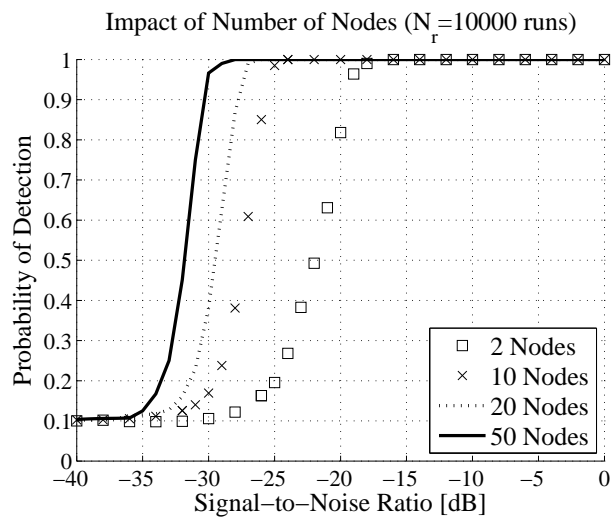
<sup>5</sup> MESS does not care about how the information exchange process takes place, so the control channel between any ordinary node and the master node can be assumed as perfect ( $\tilde{\pi}_i = \pi_i$ ).



(a) AGM.

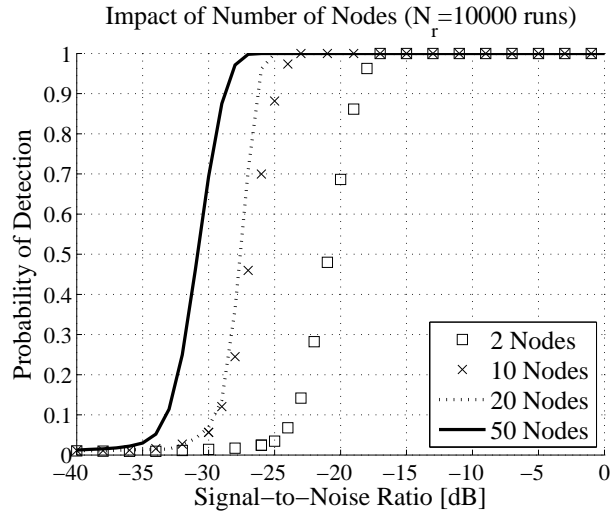


(b) GLRT.

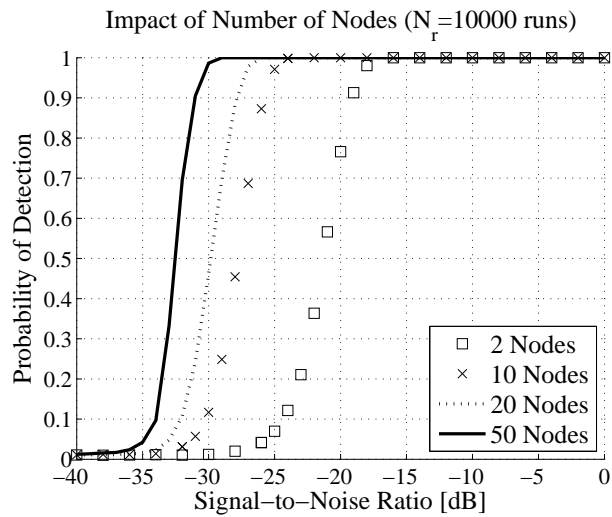


(c) MME.

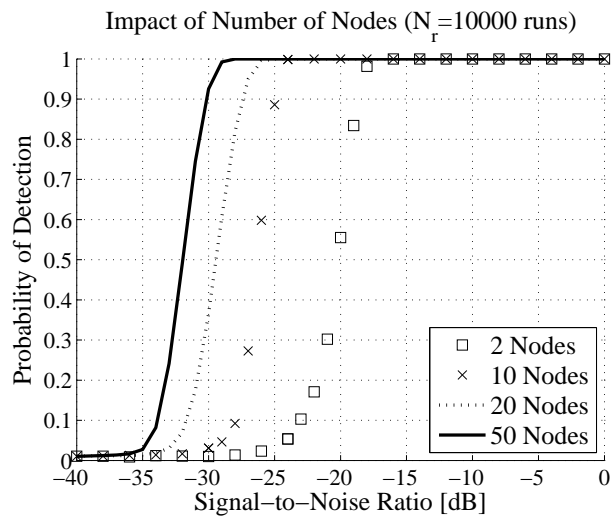
**Fig. 4.26:** Best-case AWGN performance of blind EBD methods under noise uncertainty of  $\Delta\hat{\sigma}_w^2 = \sigma_w^2 \pm 0.5$  dB ( $\rho = 1.12$ ) when ECMA-392 signals are detected using different number of nodes.



(a) AGM.



(b) GLRT.



(c) MME.

**Fig. 4.27:** Worst-case AWGN performance of blind EBD methods under noise uncertainty of  $\Delta\hat{\sigma}_w^2 = \sigma_w^2 \pm 0.5$  dB ( $\rho = 1.12$ ) when ECMA-392 signals are detected using different number of nodes.

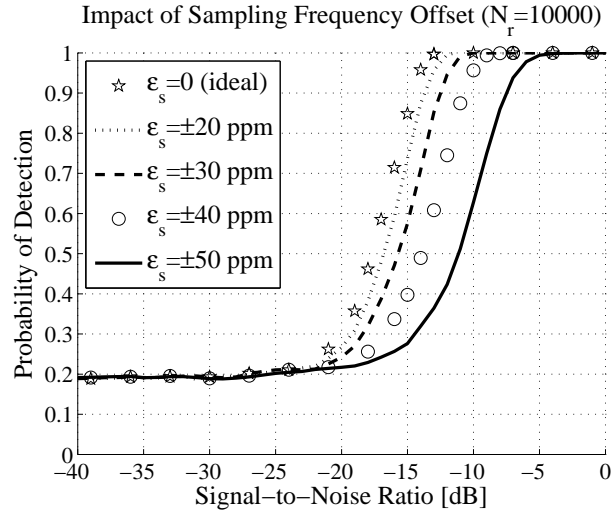
## 4.5 Frequency Offsets

The last practical issue taken into account in this dissertation is raised by the presence of mismatches between the local oscillators used at the licensed transmitter and WSD. As seen in Chapter 2, such oscillator mismatches cause CFO that can reduce the amplitude and shift the phase of the received signals. Earlier in this chapter, we have also seen that single carrier systems are usually less susceptible to CFO but OFDM-based systems may experience demodulation problems in the presence of CFO. Therefore, our analysis of CFO focussed on OFDM-based target signals only. In order to assess the impact of CFO on detection performance, we assigned values to the normalized CFO out of two possible ranges. To define the first range, we departed from the ideal AWGN case ( $\epsilon_c = 0$ ) and increased the normalized CFO until  $\epsilon_c = \Delta f$ . The second range starts with  $\epsilon_c > \Delta f$  and ends up with some exact multiple of  $\Delta f$ , e.g.  $3 \times \Delta f$ . The step size used is  $0.1 \times \Delta f$  for both ranges. Despite of the loss of orthogonality between subcarriers experienced when  $\epsilon_c > \Delta f$ , the losses compared to the case  $\epsilon_c = 0$  were of  $\approx 1$  dB (and not larger than 2 dB) for all methods. Though the losses observed are slightly lower for ECMA-392, due to its smaller number of subcarriers, this suggests that the methods implemented in MESS are robust against CFO regardless the type of target signal. However, we know that clock offsets also impose the need for WSD to operate in the absence of perfect synchronization with the licensed transmitter. In this case, our simulation results suggest that the performances of all but TDSC methods are not affected much by non-synchronized sampling. The AMD values shown in Table 4.7 suggest that the performance of TDSC-NP is good, whereas TDSC-MRC can only be regarded as a fair performer when under SFO. In case of DVB-T, this matches well the results presented in [132]. We know from Table 4.1 that TDSC methods are excellent performers under multipath fading, so the joint effect of fading and SFO yields results that are virtually the same as those in Table 4.7.

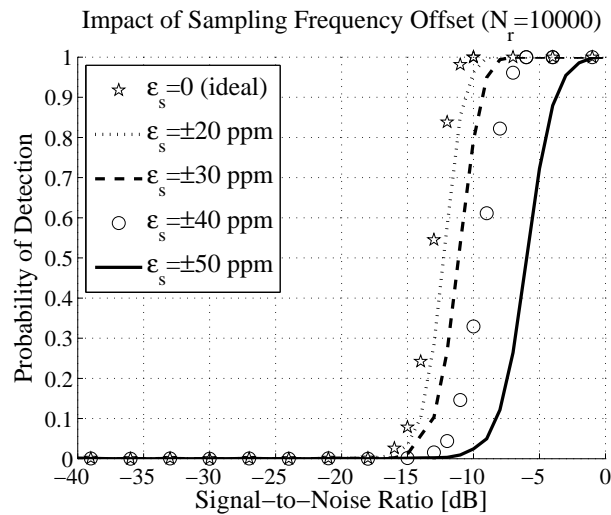
In the sequel, we present some simulation results obtained in the presence of frequency offsets. In view of the preliminary discussion above, our focus will be on the performance that TDSC methods derive under different levels of synchronization. As done in the analyses of multipath fading and noise uncertainty, we begin with an assessment of the impact that the type of target signal exerts on the detection process. Then, we show that the performance degradation caused by SFO *cannot* be alleviated by taking longer sensing times because the deteriorating effects introduced thereby accumulate over the time. To support this finding, we extend the derivation provided for CFO in [121] to the case of SFO. As a by-product, the expression for the TDSC function obtained in this derivation will help us explaining why TDSC-NP outperforms TDSC-MRC in the presence of SFO. Finally, we show that it is possible to mitigate the performance losses due to SFO by increasing the number of nodes engaged in CSS.

**Table 4.7:** Performance deviation in dB introduced by sampling frequency offsets in TDSC methods (as compared to the AWGN case with  $\epsilon_s = 0$ ).

| Method   | DVB-T        |       |              |       | ISDB-T       |       |              |       | ECMA-392     |       |              |       | AMD   | Robustness |
|----------|--------------|-------|--------------|-------|--------------|-------|--------------|-------|--------------|-------|--------------|-------|-------|------------|
|          | $\pm 20$ ppm |       | $\pm 40$ ppm |       | $\pm 20$ ppm |       | $\pm 40$ ppm |       | $\pm 20$ ppm |       | $\pm 40$ ppm |       |       |            |
|          | Best         | Worst | Best         | Worst | Best         | Worst | Best         | Worst | Best         | Worst | Best         | Worst |       |            |
| TDSC-NP  | -1           | -1    | -4           | -4    | 0            | -2    | -3           | -3    | 0            | 0     | -1           | 0     | -1.58 | Good       |
| TDSC-MRC | -2           | -2    | -8           | -8    | -2           | 0     | -7           | -8    | 0            | 0     | 0            | -1    | -3.17 | Fair       |



(a) Best case.



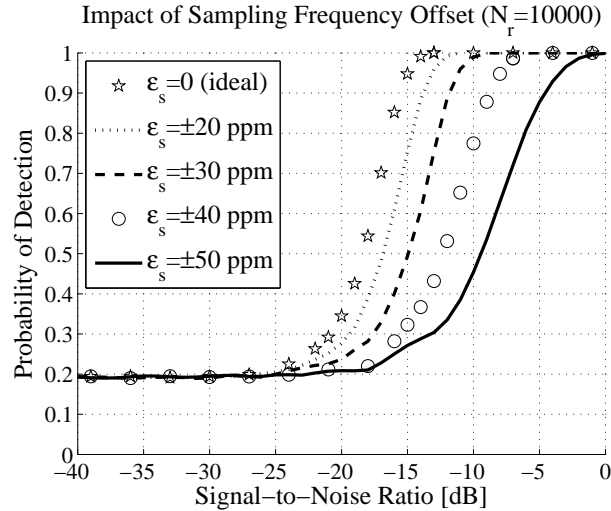
(b) Worst case.

**Fig. 4.28:** AWGN performance of TDSC-NP when DVB-T signals Mode 2k CP= 1/4 are detected under different synchronization levels using a sensing time of 4.48 ms (equivalent to three PRU).

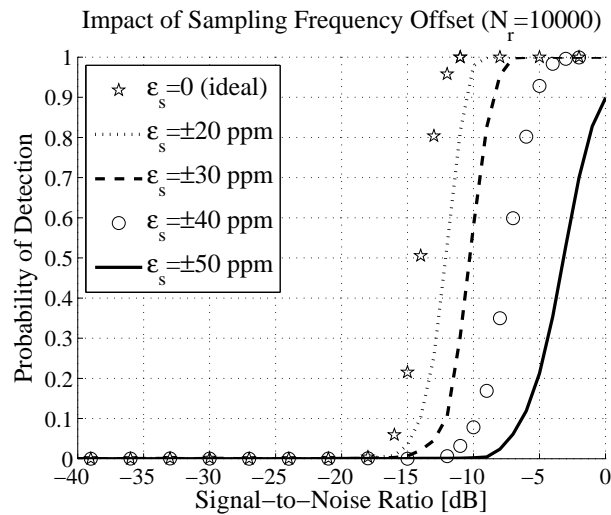
#### 4.5.1 Impact of Target Signal Type

When the target signal is compliant with the DVB-T standard, Figure 4.28 shows the performance derived by TDSC-NP when different levels of synchronization levels are considered. As expected, it is seen from this figure that the loss in performance due to SFO increases as  $\epsilon_s$  increases. By varying  $\epsilon_s$  from 0 ppm to  $\pm 50$  ppm, the maximum loss can be as high as 7 dB under best-case conditions or 9 dB under worst-case conditions. This means that the degradation caused when we switch from best- to worst-case conditions is basically the same as in the ideal AWGN case ( $\epsilon_s = 0$ ). One might argue at this point that  $\epsilon_s = \pm 50$  ppm represents a SFO that is too large to occur in practical systems. However, we observe that this actually depends on the sensing time. In [132], the authors consider  $\epsilon_s \in [2, 6]$  ppm but use a sensing time of 50 ms, while here we use only 4.48 ms (equivalent to three PRU). The role played by the sensing time in the impact of SFO on the detection performance of TDSC methods will be clarified later on in Section 4.5.2.





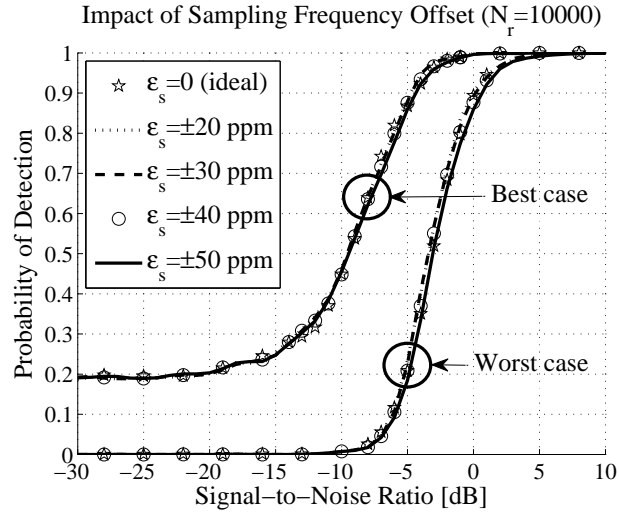
(a) Best case.



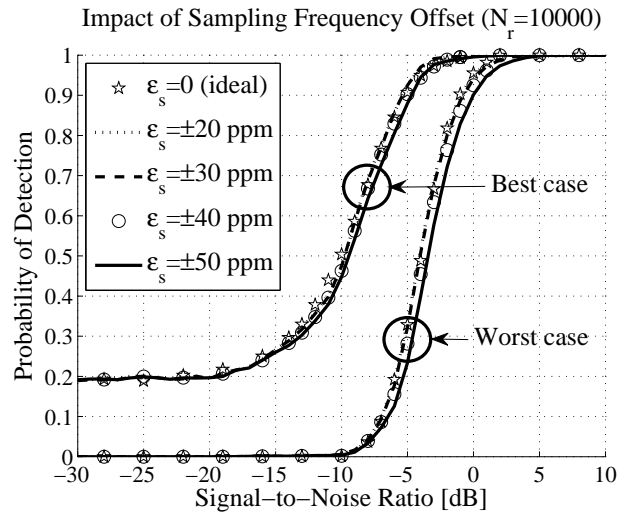
(b) Worst case.

**Fig. 4.29:** AWGN performance of TDSC-MRC when DVB-T signals Mode 2k CP= 1/4 are detected under different synchronization levels using a sensing time of 4.48 ms (equivalent to three PRU).

With all settings kept unchanged, Figure 4.29 shows the performance derived by TDSC-MRC with non-synchronized sampling. Here, the losses introduced by SFO can be as high as 13 dB under best-case conditions or 15 dB under worst-case conditions. By comparing Figures 4.28 and 4.29, it is clear that the susceptibility of TDSC-MRC to SFO is similar to that of TDSC-NP as long as the licensed transmitter and WSD are perfectly synchronized or the normalized SFO is relatively low, *i.e.*  $\epsilon_s \leq \pm 30$  ppm under best-case conditions or  $\epsilon_s \leq \pm 20$  ppm under worst-case conditions. If this is not the case, the performance of TDSC-MRC degrades much faster than that of TDSC-NP. This suggests that the statement in [121] that TDSC-MRC outperforms TDSC-NP at the expense of increased computational complexity holds true, yet only under the assumption of tight or nearly-tight synchronization. For more practical cases, where synchronization between the licensed transmitter and WSD may entirely lack, lower complexity and better robustness against SFO makes of TDSC-NP the best choice among TDSC methods.



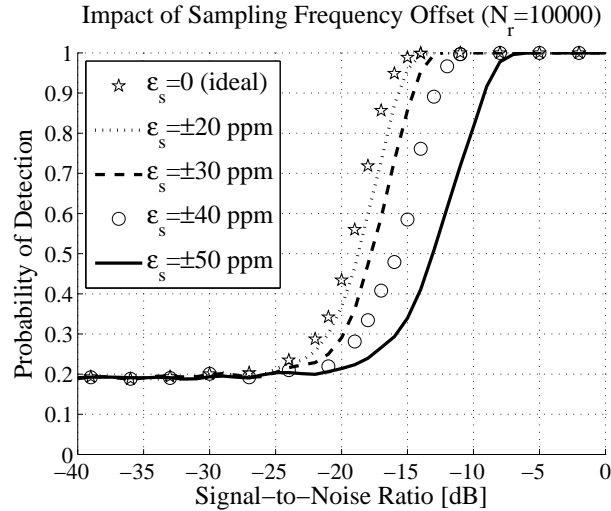
(a) TDSC-NP.



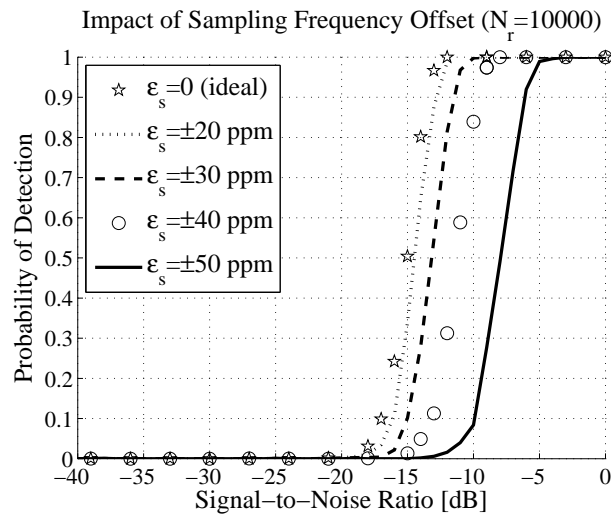
(b) TDSC-MRC.

**Fig. 4.30:** AWGN performance of TDSC methods when ECMA-392 signals  $CP = 1/8$  are detected under different synchronization levels using a sensing time of 0.75 ms (equivalent to three PRU).

The superiority of TDSC-NP is shown in Figure 4.30, this time for ECMA-392. The loss in performance is less than 1 dB for TDSC-NP, regardless of CFAR requirement, fusion rule, and synchronization level. In contrast, the performance degradation experienced by TDSC-MRC exceeds 2 dB when  $\epsilon_s \leq \pm 50$  ppm under worst-case conditions. This means that, whether using TDSC-NP or TDSC-MRC, the impact of SFO is milder when it comes to the detection of ECMA-392 signals. Despite of the shorter sensing time of 0.75 ms used to detect ECMA-392 signals, the robustness of TDSC-NP against SFO observed in Figure 4.30(a) outperforms that in Figure 4.28 in up to 8 dB. As for TDSC-MRC, the robustness improvement is better and up to 13 dB according to Figures 4.30(b) and 4.29. The deviations in performance observed here are, in part, due to the different number of subcarriers used in DVB-T and ECMA-392 (see Table 3.1). However, in the presence of SFO, the sensing time affects the detection performance of TDSC methods in a fashion different than that observed thus far. We take a closer look at this issue in the sequel.



(a) Best case.

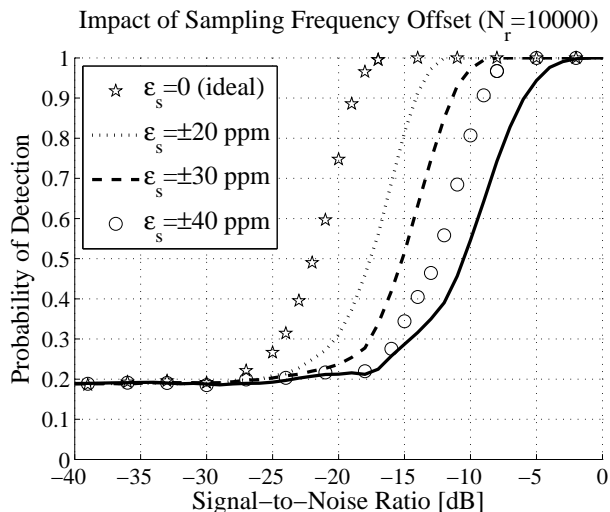


(b) Worst case.

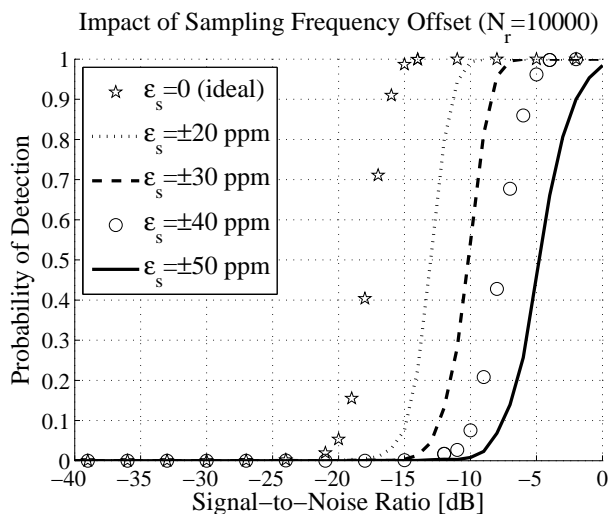
**Fig. 4.31:** AWGN performance of TDSC-NP when DVB-T signals Mode 2k CP= 1/4 are detected under different synchronization levels using a sensing time of 8.96 ms (equivalent to six PRU).

## 4.5.2 Impact of Sensing Time

Figure 4.31 shows the performance derived by TDSC-NP when we double the sensing time used in Figure 4.28 with all other simulation settings kept unchanged. Though the longer sensing time of 8.96 ms can improve the performance achieved using non-synchronized sampling in up to 2 dB under best-case conditions and 3 dB under worst-case conditions, the losses due to SFO observed here remain essentially the same as in Figure 4.28. Similarly, the performance obtained by TDSC-MRC in Figure 4.32 outperforms that in Figure 4.29 in about 3 dB to 4 dB. Nevertheless, with respect to the performance degradation introduced by SFO, TDSC-MRC reacts to longer sensing times in a different fashion than TDSC-NP. The losses observed for sensing time equal to 8.96 ms are typically larger than those for 4.48 ms. Hence, in contrast to TDSC-NP, the degradation in the performance of TDSC-MRC with non-synchronized sampling *increases* with the sensing time. The same behavior is verified also for ECMA-392 signals, as shown in Figure 4.33.



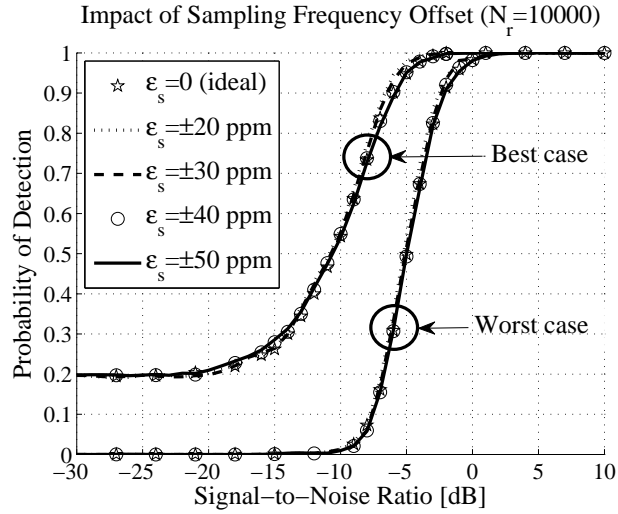
(a) Best case.



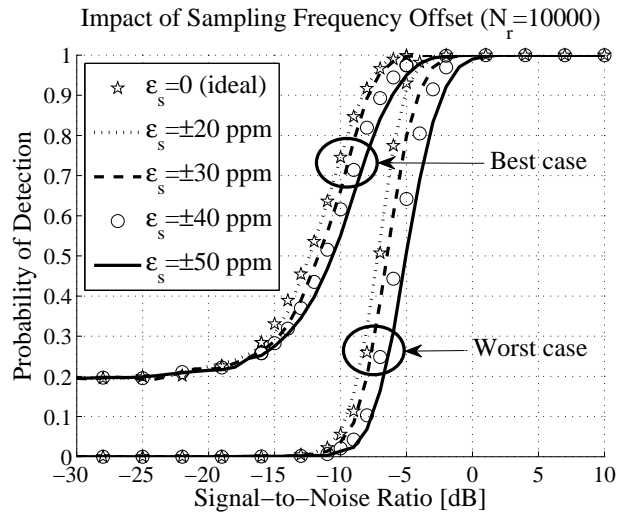
(b) Worst case.

**Fig. 4.32:** AWGN performance of TDSC-MRC when DVB-T signals Mode 2k CP= 1/4 are detected under different synchronization levels using a sensing time of 8.96 ms (equivalent to six PRU).

We have verified via simulations two aspects related to the performance of TDSC methods that deserve an analytical analysis. First, we are interested in finding out why TDSC-NP outperforms TDSC-MRC when the normalized SFO is large. Second, a better understanding about why TDSC-NP and TDSC-MRC behave differently when we increase the sensing time in the presence of SFO is needed. The bottom line of such an analysis involves the derivation of an expression that models the impact caused by non-synchronized sampling in the detection performance of TDSC methods. In our context, this basically consists of feeding the accumulated TDSC function in (2.87) with OFDM symbols that have been received using an incorrect sampling period  $T'_s$  as in (2.91). For the sake of simplicity, we begin with a single pair of symbols whose indexes  $l$  and  $l'$  indicate that both symbols in that pair have the same SP pattern. In this case, since we do not accumulate the correlations due to multiple symbol pairs,  $N_1 = 1$  and (2.87) reduces to the TDSC



(a) TDSC-NP.



(b) TDSC-MRC.

**Fig. 4.33:** AWGN performance of TDSC methods when ECMA-392 signals CP= 1/8 are detected under different synchronization levels using a sensing time of 1.50 ms (equivalent to six PRU).

function of two OFDM symbols [121]:

$$R(l, l') = \frac{1}{N_s} \sum_{n=0}^{N_s-1} r_l(n) r_{l'}^*(n). \quad (4.20)$$

From (2.91) we know that:

$$r_l(n) = \frac{1}{N_s} \sum_{k=0}^{N_s-1} H(k) C_l(k) e^{j \frac{2\pi}{N_s} k \left[ n \left( \frac{T'_s}{T_s} \right) - l T_{\text{SYM}} \left( \frac{\epsilon_s}{1+\epsilon_s} \right) \right]} + w_l(n) \quad (4.21)$$

$$r_{l'}^*(n) = \frac{1}{N_s} \sum_{k'=0}^{N_s-1} H^*(k') C_{l'}^*(k') e^{-j \frac{2\pi}{N_s} k' \left[ n \left( \frac{T'_s}{T_s} \right) + l' T_{\text{SYM}} \left( \frac{\epsilon_s}{1+\epsilon_s} \right) \right]} + w_{l'}^*(n). \quad (4.22)$$

Plugging (4.21) and (4.22) into (4.20) yields:

$$\begin{aligned}
R(l, l') &= \frac{1}{N_s^3} \sum_{n=0}^{N_s-1} \sum_{k=0}^{N_s-1} \sum_{k'=0}^{N_s-1} H(k) H^*(k') C_l(k) C_{l'}^*(k') e^{j \frac{2\pi}{N_s} (k-k')} \left\{ n \left( \frac{T'_s}{T_s} \right) + \left[ \frac{\epsilon_s (l-l')}{1+\epsilon_s} \right] T_{\text{SYM}} \right\} \\
&+ \frac{1}{N_s^2} \sum_{n=0}^{N_s-1} \sum_{k=0}^{N_s-1} H(k) C_l(k) w_{l'}^*(n) e^{j \frac{2\pi}{N_s} k \left[ n \left( \frac{T'_s}{T_s} \right) - l \left( \frac{\epsilon_s}{1+\epsilon_s} \right) T_{\text{SYM}} \right]} \\
&+ \frac{1}{N_s^2} \sum_{n=0}^{N_s-1} \sum_{k'=0}^{N_s-1} H^*(k') C_{l'}^*(k') w_l(n) e^{-j \frac{2\pi}{N_s} k' \left[ n \left( \frac{T'_s}{T_s} \right) + l' \left( \frac{\epsilon_s}{1+\epsilon_s} \right) T_{\text{SYM}} \right]} \\
&+ \frac{1}{N_s} \sum_{n=0}^{N_s-1} w_l(n) w_{l'}^*(n). \tag{4.23}
\end{aligned}$$

Expanding the exponentials and rearranging the sums we get:

$$\begin{aligned}
R(l, l') &= \frac{1}{N_s^2} \sum_{k=0}^{N_s-1} \sum_{k'=0}^{N_s-1} H(k) H^*(k') C_l(k) C_{l'}^*(k') e^{j \frac{2\pi}{N_s} (k-k')} \left[ \frac{\epsilon_s (l-l')}{1+\epsilon_s} \right] T_{\text{SYM}} \\
&\cdot \left[ \frac{1}{N_s} \sum_{n=0}^{N_s-1} e^{j \frac{2\pi}{N_s} \left( \frac{T'_s}{T_s} \right) (k-k') n} \right] \\
&+ \frac{1}{N_s^2} \sum_{k=0}^{N_s-1} H(k) C_l(k) e^{-j \frac{2\pi}{N_s} k \left( \frac{\epsilon_s l}{1+\epsilon_s} \right) T_{\text{SYM}}} \left[ \sum_{n=0}^{N_s-1} w_{l'}^*(n) e^{j \frac{2\pi}{N_s} \left( \frac{T'_s}{T_s} \right) k n} \right] \\
&+ \frac{1}{N_s^2} \sum_{k'=0}^{N_s-1} H^*(k') C_{l'}^*(k') e^{-j \frac{2\pi}{N_s} k' \left( \frac{\epsilon_s l'}{1+\epsilon_s} \right) T_{\text{SYM}}} \left[ \sum_{n=0}^{N_s-1} w_l(n) e^{-j \frac{2\pi}{N_s} \left( \frac{T'_s}{T_s} \right) k' n} \right] \\
&+ \frac{1}{N_s} \sum_{n=0}^{N_s-1} w_l(n) w_{l'}^*(n). \tag{4.24}
\end{aligned}$$

Recalling the shift theorem of the DFT, it turns out that the last sum in the first term of (4.24) corresponds to a circularly shifted Kronecker Delta [152]

$$\frac{1}{N_s} \sum_{n=0}^{N_s-1} e^{j \frac{2\pi}{N_s} \left( \frac{T'_s}{T_s} \right) (k-k') n} = \delta \left[ \left( \frac{T'_s}{T_s} \right) (k-k') \right] = \begin{cases} 0, & k \neq k' \\ 1, & k = k' \end{cases}, \tag{4.25}$$

which thanks to the orthogonality property of the DFT is still a Kronecker Delta, *i.e.* a single peak that exists iff  $k = k'$ . Similarly, the noise contributions due to the last sum in the second and in the third terms of (4.24) account both for the circularly shifted DFT of the noise process. The statistical properties of  $w(n)$  are not affected neither by phase rotation nor by circular shift, so we can define

$$W_l(k') = e^{-j \frac{2\pi}{N_s} k' \left( \frac{\epsilon_s l'}{1+\epsilon_s} \right) T_{\text{SYM}}} \left[ \sum_{n=0}^{N_s-1} w_l(n) e^{-j \frac{2\pi}{N_s} \left( \frac{T'_s}{T_s} \right) k' n} \right] \tag{4.26}$$

with  $W_{l'}^*(k)$  defined in the same fashion.

Using (4.25) and (4.26), we rewrite (4.24) as:

$$\begin{aligned}
R(l, l') &= \frac{1}{N_s^2} \sum_{k=0}^{N_s-1} |H(k)|^2 C_l(k) C_{l'}^*(k') e^{j \frac{2\pi}{N_s} k \left[ \frac{\epsilon_s(l-l')}{1+\epsilon_s} \right]} T_{\text{SYM}} \\
&+ \frac{1}{N_s^2} \sum_{k=0}^{N_s-1} H(k) C_l(k) W_{l'}^*(k) \\
&+ \frac{1}{N_s^2} \sum_{k'=0}^{N_s-1} H^*(k') C_{l'}^*(k') W_l(k') \\
&+ \frac{1}{N_s} \sum_{n=0}^{N_s-1} w_l(n) w_{l'}^*(n). \tag{4.27}
\end{aligned}$$

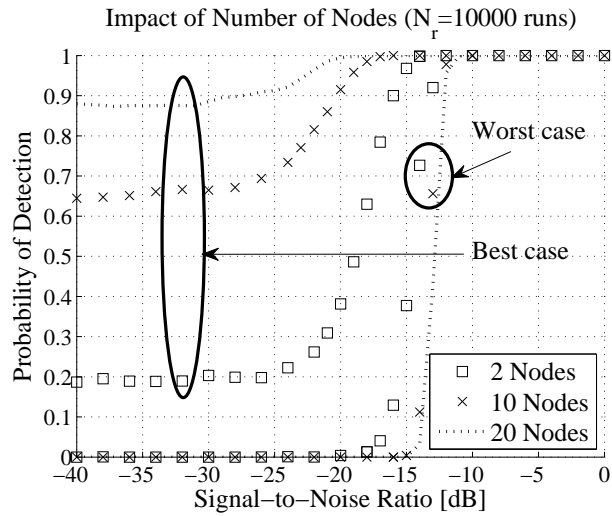
$W_l(k')$  and  $W_{l'}^*(k)$  are zero-mean random variables, so that multiplying them by complex channel gains and complex constellations that are independent yields zero. This allows us to drop the second and the third terms in (4.27) when  $N_s$  large enough (this is reasonable because we can make  $N_s$  in (4.20) as large as the number of collected samples  $M$ ). Breaking the first term of (4.27) in pilot subcarriers and non-pilot subcarriers yields

$$\begin{aligned}
R(l, l') &= \frac{1}{N_s^2} \sum_{k \in \mathbb{P}} |H(k) \sigma_{\text{SP}}|^2 e^{j \frac{2\pi}{N_s} k \left[ \frac{\epsilon_s(l-l')}{1+\epsilon_s} \right]} T_{\text{SYM}} \\
&+ \frac{1}{N_s^2} \sum_{k \notin \mathbb{P}} |H(k)|^2 C_l(k) C_{l'}^*(k) e^{j \frac{2\pi}{N_s} k \left[ \frac{\epsilon_s(l-l')}{1+\epsilon_s} \right]} T_{\text{SYM}} \\
&+ \frac{1}{N_s} \sum_{n=0}^{N_s-1} w_l(n) w_{l'}^*(n) \tag{4.28}
\end{aligned}$$

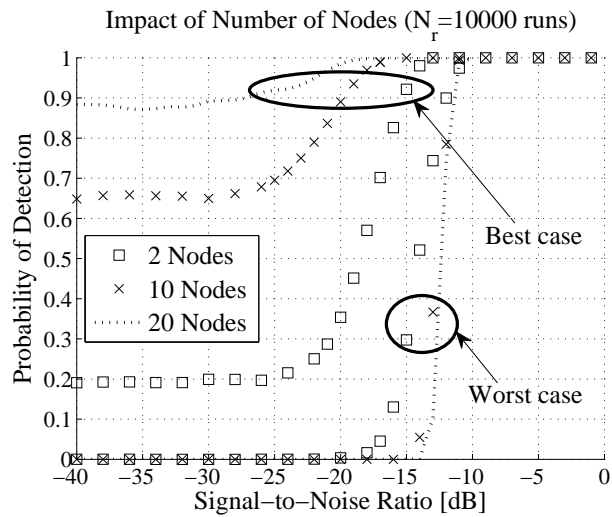
where  $\sigma_{\text{SP}}^2$  denotes the squared amplitudes of the SP signal, which are fixed and known for  $k \in \mathbb{P}$ . It can be shown, *e.g.* along the lines in [121], that the contribution due to the non-pilot subcarriers has zero mean and its variance is small as compared to the variance of the noise in the low SNR regime. Hence, ignoring the second term in (4.28), we can approximate the TDSC function as

$$R(l, l') \approx \frac{\sigma_{\text{SP}}^2}{N_s^2} \sum_{k \in \mathbb{P}} |H(k)|^2 e^{j \frac{2\pi}{N_s} k \left[ \frac{\epsilon_s(l-l')}{1+\epsilon_s} \right]} T_{\text{SYM}} + \frac{1}{N_s} \sum_{n=0}^{N_s-1} w_l(n) w_{l'}^*(n), \tag{4.29}$$

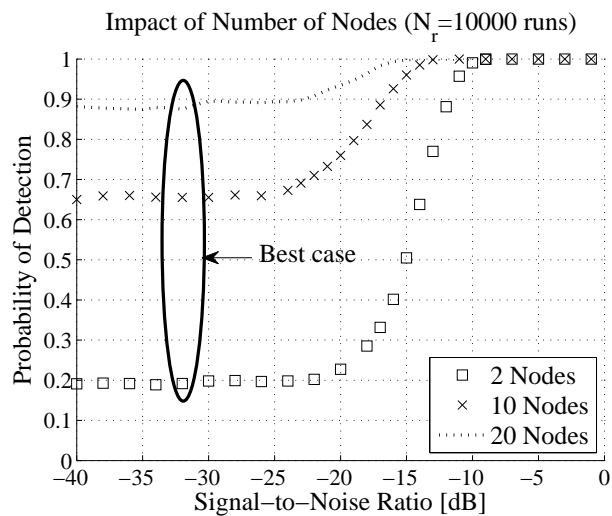
where the first term is deterministic and the second one is a zero-mean noise term. The following conclusions can be drawn from (4.29). First, and in contrast to (3) derived in [121] for the case of CFO, the amplitude reduction and phase rotation caused by SFO affect each subcarrier independently. Second, these deteriorating effects are dependent of the symbol index difference  $\Delta l = l' - l$ . Hence, in the accumulation of TDSC functions in (2.87), we are also accumulating the SFO related to each of the  $N_1$  symbol pairs considered in the correlation. This explains why longer sensing times can provide some performance gain but the losses due to SFO remain essentially the same as those verified for shorter sensing times. Third, it is clear from (2.89) that TDSC-MRC allows to SP symbols having different  $\Delta l$ . This increases the number of symbols used in the correlation, thus making TDSC-MRC to be more susceptible to SFO than TDSC-NP.



(a)  $\epsilon_s = 0$ .



(b)  $\epsilon_s = \pm 20$  ppm.



(c)  $\epsilon_s = \pm 50$  ppm.

**Fig. 4.34:** AWGN performances of TDSC-NP when ISDB-T signals Mode 2k CP= 1/4 are detected under different synchronization levels using different number of nodes. The sensing time is 8.96 ms (equivalent to six PRU).



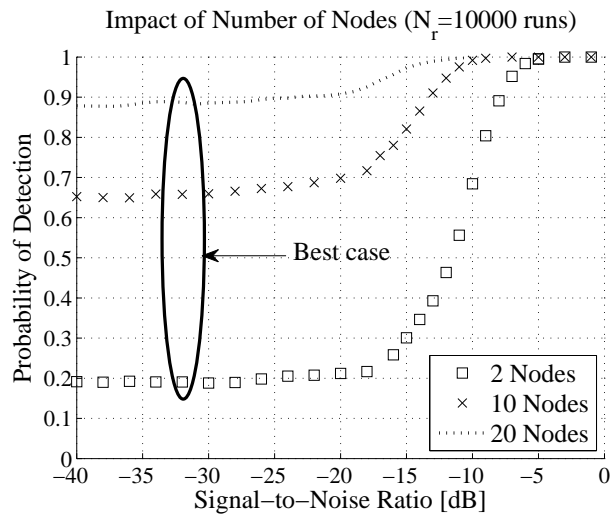
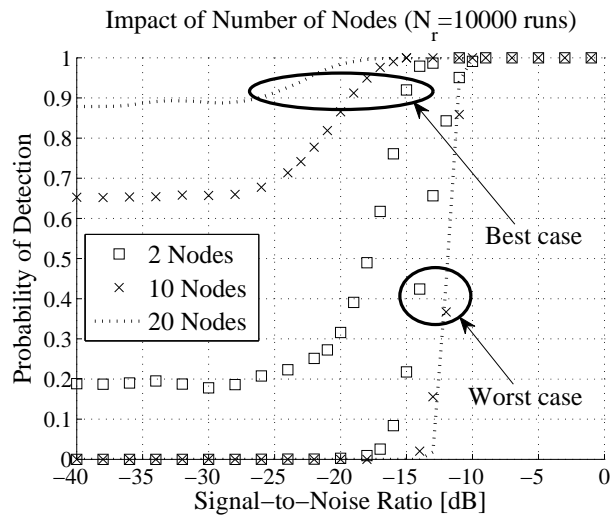
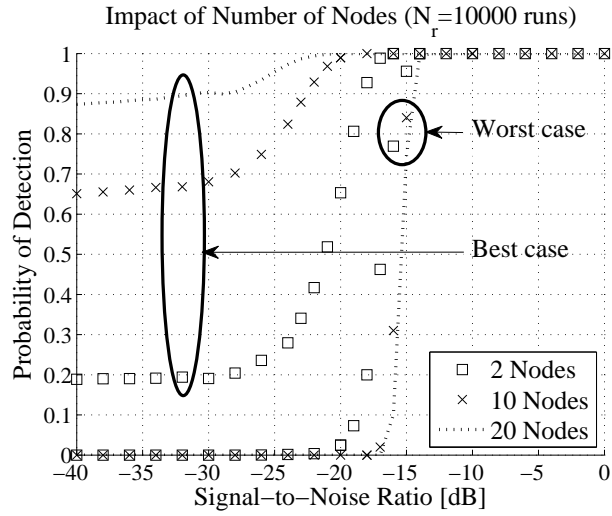


**Fig. 4.35:** AWGN performances of TDSC-MRC when ISDB-T signals Mode 2k CP= 1/4 are detected under different synchronization levels using different number of nodes. The sensing time is 8.96 ms (equivalent to six PRU).

### 4.5.3 Impact of Number of Nodes

We have seen that we can improve the performance of TDSC methods by increasing the sensing time but this does not affect the losses introduced by SFO. We now look at the case where an increased number of nodes relies on cooperation as an attempt to mitigate those losses. In what follows, we consider the detection of IDSB-T signals using sensing time equal to 8.96 ms. As before, our simulation results are generated for  $N = 10$  and  $N = 20$ , with additional curves for  $N = 2$  provided as baseline for the computation of cooperation gains.

Figure 4.34 shows that the gains achieved by TDSC-NP under best-case conditions are of 3 dB and 6 dB when we increase  $N$  from 2 to 10 from and 2 to 20, respectively. As seen before for ACD and BTPD, the cooperation gains derived in TDSC-NP come at the expense of a degradation in  $Q_{fa}^{OR}$ . For  $P_{fa} = 0.1$ ,  $Q_{fa}^{OR}$  varies (as a function of the SNR) in the ranges  $[0.1840, 0.1960]$  for  $N = 2$ ,  $[0.6270, 0.6730]$  for  $N = 10$ , and  $[0.8610, 0.9000]$  for  $N = 20$ . A better balance between  $Q_d^{OR}$  and  $Q_{fa}^{OR}$  can be achieved by combining OR logic with  $P_{fa} = 0.01$ . For  $N = 20$ , this allows us to improve the range of values of  $Q_{fa}^{OR}$  to  $[0.1740, 0.1890]$  while the resulting  $Q_d^{OR}$  still outperforms that obtained for  $N = 2$  in 6 dB. Since these gains are observed *regardless* of the amount of SFO present in the operation environment, they suggest that CSS based on TDSC-NP can provide the *same* improvement in performance whether synchronization is tight ( $\epsilon_s = 0$ ), imperfect ( $\epsilon_s = \pm 20$  ppm), or lacks ( $\epsilon_s = \pm 50$  ppm).

In contrast, as seen in Figure 4.35, the cooperation gains derived by TDSC-MRC slightly depend on the synchronization level available. For instance, if the licensed transmitter and WSD are relatively well synchronized ( $\epsilon_s \leq \pm 20$  ppm), Figure 4.35(b) shows that TDSC-MRC achieves the same cooperation gains as TDSC-NP. However, in the practical case that synchronization lacks or be very imprecise as in Figure 4.35(c) ( $\epsilon_s = \pm 50$  ppm), the gains achieved by increasing  $N$  from 2 to 10 and from 2 to 20 are of 5 dB and 7 dB, respectively. The degradation in the global probability of detection introduced by cooperation is similar to that reported above for TDSC-NP, so the use of a more stringent individual CFAR requirement is recommended also for TDSC-MRC.

## 4.6 Signal Classification Block (Revisited)

The goals of the present section are to summarize the major conclusions drawn from our simulation work and, based on them, determine the best methods to be used in the generic signal classification block in Figure 3.11.

The simulation outcomes are summarized in Table 4.8. Method robustness, imported from Tables 4.1-4.7, is as before expressed in terms of AMD. The cooperation gain accounts to the improvement (in dB) observed in the global probability of detection when we increase  $N$  from 2 to 20. Methods giving average gains show improvements between 4 dB and 10 dB, whereas improvements below and above this range characterize low and high gains, respectively. In the sequel, we use this table to discuss the pros & cons of each of the methods considered in this dissertation. For ease of explanation, we group methods according to the amount of prior knowledge they require to work.

**Table 4.8:** Summary of the major results of the simulation work carried out in this chapter.

| Method   | Robustness Under Different Operation Conditions |           |                   |           |                  |           | Cooperation Gain |
|----------|---|-----------|-------------------|-----------|------------------|-----------|------------------|
|          | Multipath Fading                                |           | Noise Uncertainty |           | Sampling Offsets |           |                  |
|          | OFDM  | Non-OFDM  | OFDM              | Non-OFDM  | OFDM             | Non-OFDM  |                  |
| ED       | Poor  | Excellent | Poor              | Poor      | Excellent        | Excellent | High             |
| AGM      | Good  | Excellent | Excellent         | Excellent | Excellent        | Excellent | Average          |
| GLRT     | Good  | Excellent | Excellent         | Excellent | Excellent        | Excellent | Average          |
| MME      | Good  | Excellent | Excellent         | Excellent | Excellent        | Excellent | Average          |
| RLRT     | Fair  | Excellent | Poor              | Poor      | Excellent        | Excellent | Average          |
| SCD      | Poor  | Excellent | Poor              | Excellent | Excellent        | Excellent | Low              |
| ACD      | Poor  | NA        | Excellent         | NA        | Excellent        | NA        | High             |
| BTPD     | Fair  | NA        | Excellent         | NA        | Excellent        | NA        | High             |
| TDSC-NP  | Excellent                                       | NA        | Excellent         | NA        | Good             | NA        | Average          |
| TDSC-MRC | Excellent                                       | NA        | Excellent         | NA        | Fair             | NA        | Average          |
| ASSD     | NA  | Excellent | NA                | Good      | NA               | Good      | Average          |
| MF       | NA  | Excellent | NA                | Excellent | NA               | Excellent | Average          |

### 4.6.1 Blind Techniques

The candidate blind techniques for the first stage are AGM, GLRT, and MME.

- **Pros:** Our simulation work has shown that blind techniques outperform both semi-blind and signal specific techniques in terms of detection performance, robustness, and agility in most cases studied. This has been verified under different operation conditions (AWGN, multipath fading, noise uncertainty, frequency offsets) and for a number of target signals types having different characteristics (digital vs. analog, OFDM vs. non-OFDM, wideband vs. narrowband). The blind techniques evaluated deliver similar performance and are virtually immune to noise uncertainty, CFO, and SFO. Good performance is delivered also in the presence of multipath fading. In this case, GLRT is slightly better than AGM and MME when target signals are based on the ECMA-392 standard.
- **Cons:** All blind techniques studied in this dissertation perform EBD, which basically consists of estimating the sample covariance matrix and decomposing its eigenvalues. Estimation of  $\mathbf{R}_r(n)$  usually requires a large number of samples, but can be carried out offline. Also, the use of algorithms such as SVD allows to obtain the vector  $\boldsymbol{\lambda}_r$  directly without the need to compute the whole  $\mathbf{R}_r(n)$ . Even though, the complexity posed by EBD methods is linear with  $M$  but on the order of  $\mathcal{O}(N^3\iota^3)$ . Fortunately, the smoothing factor  $\iota$  can be set arbitrarily low and the number of nodes  $N \sim 10$ -20 required to realize the benefits of cooperation is also relatively low.
- **Conclusion:** Unless only two nodes engage in cooperation, AGM is outperformed by both GLRT and MME in most cases studied. For the number of nodes considered  $N \in \{2, 10, 20, 50\}$ , MME performs the same as GLRT and is slightly more robust against noise uncertainty. However, since  $\frac{1}{N} \text{Tr}[\mathbf{R}_r(n)]$  becomes lower than  $\lambda_{\min}$  as  $N$  increases, GLRT has potential to outperform MME for a number of cooperating nodes large enough. **This makes of GLRT the method of choice to implement the first stage of the proposed signal classifier.**

### 4.6.2 Semi-blind Techniques

The candidate semi-blind techniques for the first stage are ED and RLRT.

- **Pros:** Provided that the noise level is exactly known, our simulation work has shown that RLRT performs similar to its blind EBD counterparts. For the particular case of OFDM-based target signals detected in the presence of AWGN, RLRT outperforms AGM, GLRT, and MME in up to 2 dB. RLRT outperforms ED in most cases studied, but the latter is  $N\iota$  times less complex than the former. Also, the cooperation gains achieved by using ED and RLRT at the local level are high and average, respectively. This suggests that ED may be suitable for reducing fast sensing complexity in some applications, *e.g.* where  $N$  is large and the noise level can be estimated on the basis of noise-only samples collected prior to initiating WSD operation.
- **Cons:** Due to the susceptibility of semi-blind techniques to uncertain in the marginal noise distribution, a deviation of only  $\pm 0.5$  dB about the true  $\sigma_w^2$  is usually enough to create SNR walls. In case of ED and RLRT, our study suggests that SNR walls are essentially the same regardless of target signal type, channel type, fusion rule, and CFAR requirement. The distinguishing aspect in favor of RLRT is the improvement in SNR walls observed as  $N$  increases. While this illustrates the potential of CSS in alleviating the SNR wall phenomenon, the resulting performance derived thereby is still below what can be achieved using blind EBD methods.
- **Conclusion: Recalling that all EBD methods pose roughly the same computational complexity (see Table 3.8), there seems to exist no advantage in using RLRT in our setting. Despite of the pros highlighted above, it is hard to find application for ED too because there will always exist some residual uncertainty after the noise power has been estimated.**

### 4.6.3 Signal-specific Techniques for the 2nd Stage

The candidate signal specific techniques to implement the CP-based classifier at the second stage are ACD and BTPD.

- **Pros:** All in all not the best but not the worst methods, ACD and BTPD can be used as fast OFDM classifiers with agility and computational complexity comparable as ED. They are virtually immune to CFO and SFO, and, in contrast to ED, robust against noise uncertainty. Besides, yielding the highest cooperation gains among the methods studied (up to 12 dB), the use of CP-based methods at the local level allows a group of nodes to maximize the benefits of cooperation.
- **Cons:** The CP-based methods investigated are very sensitive to variations in the CP length. If the target signals are transmitted in 2k mode, changing the CP ratio from 1/4 to 1/32 deteriorates performance in 12 dB. Our simulation work also suggests that this loss relates to the number of subcarriers and will be larger for larger modes, *e.g.* 4k and 8k. Another aspect common to ACD and BTPD is their susceptibility to variations in the symbol length, again dictated by the number of subcarriers used. However, it is possible to distinguish between ACD and BTPD when it comes to multipath fading. Both methods undergo major losses (up to 22 dB) but, while the performance of BTPD increases with the SNR in all cases studied, ACD fails entirely when operating under worst-case conditions and in the presence of very long echoes (profile D). This disadvantage is inherent to ACD and cannot be alleviated via cooperation.

- **Conclusion:** For the number of nodes considered  $N \in \{2, 10, 20\}$ , the degradation in the global probability of false alarm due to hard combining based on the OR logic can be alleviated at the expense of better sensors, *i.e.* by setting  $P_{fa} = 0.01$  at each node. This combination of OR logic and more stringent CFAR requirement brings  $Q_{fa}$  up to an acceptable level while keeping the cooperation gain almost unchanged. **Assuming that ACD and BTPD are to be implemented “as is”, the latter is the method of choice to implement the second stage of the proposed signal classifier<sup>6</sup>.**

## 4.6.4 Signal-specific Techniques for the 3rd Stage

### 4.6.4.1 SP-based Classifier

The candidate signal specific techniques considered to implement the SP-based classifier at the third stage are TDSC-NP and TDSC-MRC.

- **Pros:** TDSC methods play a key role in our setting because, among the methods studied, they are the only capable of distinguishing between DVB-T 2k and IEEE 802.22. They are virtually immune to noise uncertainty, CFO, and provide superior robustness against multipath fading even under ISI, *i.e.* when  $T_{CP} < \tau_{max}$ . When under imperfect synchronization conditions, the degradation introduced by SFO in the performance of TDSC methods can be effectively alleviated via cooperation. In contrast to CP-based methods, TDSC-NP is robust against CP length variations. TDSC-MRC is only slightly sensitive ( $\leq 1$  dB) to such variations.
- **Cons:** Our simulation work has shown that TDSC methods are dramatically affected by variations in the pilot power ratio. Such variations are practical, and reflect the different amplitudes and periodicities mandated for SP in different standards. Losses up to 20 dB are observed when we compare IEEE 802.22 (SP have unitary gain and repeat themselves every seven symbols) to DVB-T 2k (SP are boosted by 4/3 factor and repeat themselves every four symbols). The performance of TDSC methods also varies according to symbol length changes. In this case, the loss observed can be as high as 13 dB when  $T_{SYM}$  decreases from 0.37 ms (DVB-T 2k CP= 1/4) to 0.19  $\mu$ s (ECMA-392 CP= 1/8). As another drawback, TDSC-NP and TDSC-MRC are the only among the methods studied that are impacted by non-synchronized sampling. Both methods perform similarly for  $\epsilon_s \leq \pm 30$  ppm, but TDSC-NP is more robust than TDSC-MRC against SFO in at least 6 dB for  $\epsilon_s \geq \pm 50$  ppm.
- **Conclusion:** As seen in Figure 3.11, the SP-based classifier is triggered on-demand, only in the particular case that distinction between DVB-T 2k and IEEE 802.22 is made necessary. This means that the longer sensing time required by TDSC methods to achieve desirable performance levels (*e.g.* 50 ms) is affordable in our setting. In most cases studied, TDSC-NP has been shown less susceptible to SFO than TDSC-MRC. Also, when nodes team up to compensate for performance degradations due to SFO, the cooperation gains derived by TDSC-NP are independent of  $\epsilon_s$  whereas

---

<sup>6</sup> We are currently working on the incorporation of peak search procedures into ACD. We expect that the resulting modified ACD (MAD) allows us to exploit the benefits of both ACD and BTPD, yet posing computational complexity similar to the original ACD (half of BTPD).

the gains derived by TDSC-MRC vary with the level of synchronization. **In view of its lower complexity and better behavior in the lack of perfect synchronization, TDSC-NP is the method of choice to implement the SP-based classifier at the third stage of the proposed signal classifier.**

#### 4.6.4.2 PSD-based Classifier

The candidate signal specific technique considered to implement the PSD-based classifier at the third stage is SCD. In what follows, we also comment on the possibility of dropping the SP-classifier and using only the PSD-classifier at the third stage.

- **Pros:** Our simulation work has shown that SCD is the top performer in most cases studied. In particular, when directed to detect non-OFDM signals in the presence of AWGN, SCD has confirmed its ability of accurate signal detection at very low SNR, *e.g.* as low as  $-44$  dB for WM signals (silent mode) and  $-40$  dB for TV broadcast. The method delivers similar performance also under more practical operation conditions due to its excellent robustness against multipath fading, noise uncertainty, CFO, and SFO. Among the signal specific techniques evaluated, SCD is the method that gives the lowest  $Q_{fa}$  (comparable to that of blind EBD methods) regardless of the target signal type.
- **Cons:** One disadvantage of SCD is that it is the only method among those evaluated whose performance varies (up to 3 dB) with the WM speaker mode. However, since it still outperforms all other methods in at least 14 dB, this is a minor issue. In contrast, two major concerns arise when it comes to detection of OFDM-based target signals. The first relates to the poor performance of SCD in the presence of multipath fading, *e.g.* losses observed in case of ECMA-392 (up to 22 dB) are comparable to those of CP-based methods. The second issue is that SCD experiences SNR walls that, unlike in ED and RLRT, seem to be caused by the joint uncertainty about the actual  $\sigma_w^2$  and the position of the OFDM signal edges exploited for detection.
- **Conclusion:** SCD can be employed to detect OFDM-based signals at the expense of some performance degradation when in the presence of multipath fading. Under noise uncertainty, a very high number of samples is required to shift SNR walls so as to provide performance similar to blind EBD methods. TDSC-NP also needs many samples to achieve the desired performance, but it is clearly more advantageous than SCD due to its superior robustness against multipath fading and noise uncertainty. On the other hand, if the targets are non-OFDM signals, SCD is by far the best method in all disciplines evaluated. **Hence, while its use seems less interesting when it comes to resolve both condition  $C_2$  and condition  $C_3$  (see Figure 3.11), SCD is the method of choice to resolve condition  $C_3$  in isolation, *i.e.* to implement the PSD-based classifier at the third stage of the proposed signal classifier.**

## 4.7 Chapter Summary

This chapter has provided a thorough assessment of the performance derived by 12 different signal processing techniques, some of them currently regarded as the most promising for WSD and applications based thereon. Over 50000 hours of simulations were carried out by running the MESS platform (see chapter 3) on a high-performance parallel computing cluster system. This extensive series of simulations allowed us to rank each of the candidate methods in terms of its robustness against multipath fading, noise uncertainty, and clock offsets.

It turns out from the above study that CP- and PSD-based methods can exhibit substantial performance degradation as compared to the AWGN case when detecting *some* but *not all* types of target signals in the presence of modeling uncertainties. Such signal-type dependencies were first observed when we directed ACD to detect ECMA-392 signals under multipath fading. If the false alarm rate at each node is 0.01 and the fading process is characterized by profile D, ACD fails entirely and this drawback cannot be alleviated via cooperation. The presence of very long delays, which cannot be resolved by the short CP length mandated in ECMA-392, spreads the secondary peaks in the ACF of the received signal around the expected time lag. Hence, and in contrast to BTPD, ACD fails because of its reliance on prior knowledge of  $T_{\text{FFT}}$  and the lack of a peak search procedure. Our findings further suggest that the detection performance of SCD under noise uncertainty is strongly dependent of whether the target signals are based on OFDM. As the SNR becomes fairly negative, SCD cannot keep track of the position of the OFDM signal edges and the method start suffering from the SNR wall phenomenon. As for TDSC methods, performance is shown to be dramatically affected even if the noise is pure AWGN because of variations in the pilot power ratio of the received signal. In this case, the losses observed are due to the different amplitudes mandated for SP in different standards. TDSC methods are also the only among those studied that are impacted by non-synchronized sampling, TDSC-NP being more robust than TDSC-MRC.

The learning outcomes of the above study, which provide insights also on other operation conditions such as fusion rule, CFAR requirement, symbol length, and CP ratio, were used to populate the blocks of the generic signal classifier described in chapter 3. The resulting three-stage cascade classifier was designed having in mind a feature set of practical interest: agility, robustness, context-awareness, and universality. Its agility follows from the fact that channel monitoring is carried out blindly using GLRT, and fast classification of OFDM-based signals (accounting for most standards deployed today) is done by BTPD. Robustness is achieved by combining individual methods that possess complementary features, *i.e.* GLRT is robust against all practical issues studied, the performances of BTPD and TDSC-NP under multipath and sampling frequency offsets, respectively, can both be improved via CSS, and, in our setting, SCD works well at very low SNR in all cases studied. The proposed cascade classifier is context-aware in that it allows WSD to coexist with the TV broadcast standards most deployed worldwide. Alternatively, it can be employed to protect PMSE systems on a proactive fashion, and to provide a contingency for self-coexistence between IEEE 802.22 and ECMA-392 in case other methods fail. Finally, our cascade classifier was conceived to take advantage of cooperation among nodes. The minimization of CAPEX and OPEX makes it attractive for developing countries, so universality follows.





# Chapter 5

## Conclusions

A task of utmost importance in the modern ICT society relates to make efficient use of RF spectrum, specially when it comes to accommodate the growing bandwidth demands introduced along with new wireless devices, services, and applications. However, despite of the significant progress witnessed in engineering, economics, and regulation thus far, spectrum underutilization remains a big issue to date. Recently, novel spectrum management policies, models, and techniques have been advanced to improve current spectrum utilization levels. Among the approaches to spectrum reform, DSA is regarded as one of the most promising due to its potential to leverage innovative reconfigurable systems. In the last decade, DSA-capable systems have received increasing attention thanks to advances in digital signal processing and the sinergies that arouse between emerging technologies like SDR and CR. Such systems support the deployment of WSD, aimed at exploiting white spaces on an opportunistic (possibly unlicensed) basis. This opens up a new world of opportunities, including broadband Internet access for underserved areas, backhaul for WLAN, offload data traffic from other networks, and M2M, just to name a few.

In parallel to the developments above, the ITU has been advocating an approach in which access to broadband Internet access plays the key role in creating job opportunities, increasing productivity, and boosting economies. In line with the goals set by the ITU, several countries worldwide engaged in releasing larger amounts of spectrum and reallocating them for the purpose of supporting broadband growth. Both North America and Europe, which are the world's leading regions in WSD regulation and ICT infrastructure, respectively, are considering the use of white spaces. Collaboration efforts between the FCC and CEPT are being undertaken, so unnecessary regulatory work is reduced to a minimum and some harmonization is ensured. Notwithstanding the value of these efforts towards the ITU's millenium goals and the introduction of WSD into the market, one aspect seems to have been overlooked in this process: Do solutions adopted in developed markets fit developing markets too?

In this dissertation, we have argued that the benefits envisioned by the ITU will only be achieved if WSD can contribute to reduce digital divides. This calls for methods capable of determining white spaces in most operation environments, while posing low CAPEX, low OPEX, and keeping computational burdens to WSD as low as they can possibly be. Approaches that enforce cooperation among nodes, such as CSS and WSN, become particularly attractive in this context because most of their practical implementation issues can be tackled at the network level. Nevertheless, when fabrication costs come into consideration, it is interesting that such network-centric schemes can achieve economies of scale.

With this respect, we have presented an approach that has potential to leverage economies of scale in the information acquisition process, *i.e.* in terms of the signal processing tasks carried out at the local level. The proposed approach takes advantage of a kind of context awareness that a set of cooperating WSD can obtain as long as it is capable of detecting, and subsequently classifying, the RF signals conveyed in its cooperation footprint. The underlying idea is that, by suitably combining different signal processing techniques offering complementary features, we can design cascade signal classifiers that are able to deal with a number of coexistence situations raised by the introduction of WSD into the market. For the specific case of the TV bands, we have designed a three-stage cascade classifier that allows WSD to coexist with the TV broadcast standards most deployed worldwide. Alternatively, the proposed cascade classifier can be employed to protect PMSE systems on a proactive fashion, and to provide a contingency for self-coexistence between future TVBD standards in case other methods fail, *e.g.* IEEE 802.22 CBP, IEEE 802.22.1 disabling beacons, or ECMA-392 alien beacons. While we have illustrated our concept using the TV bands, the construction of cascade classifiers aimed at facilitating coexistence in whatever underutilized bands should be straightforward along the lines discussed here.

The remainder of this chapter is organized as follows. We start in Section 5.1 with a summary of the contributions made in this dissertation. This includes some final remarks on the proposed three-stage cascade classifier, as well as other key insights gained during the steps of studying, implementing, assessing, and selecting the signal processing techniques used at each of its stages. Section 5.2 closes the chapter, and the dissertation, with a list of directions that we believe are promising for future research. We also discuss two different scenarios where the results presented in this dissertation may find application.

## 5.1 Summary of Contributions

This section summarizes our key contributions. The first contribution, perhaps the most important made in this dissertation, is the concept of multi-standard context-aware WSD. By exploiting the distinguishing features of this concept, we have provided a deeper understanding on CSS using signal specific techniques at the local level. On top of this two contributions, we have then designed a cascade classifier that not only allows to coexistence in the TV bands but can potentially mitigate digital divides and achieve economies of scale. The extensive simulation work needed to substantialize our performance assessments could be realized thanks to MESS, so we have granted the sensing platform a place in the contributions list of this dissertation.

### 5.1.1 Multi-standard Context-aware WSD

This dissertation has introduced the concept of multi-standard context-aware WSD. The novelty of this concept relies on the following distinguishing aspects:

- **Broader scope of application:** At the time of this writing, the majority of publications available in the literature evaluated detection performance having only digital TV broadcast in mind. ATSC and DVB-T were the standards typically considered in the studies about WSD coexistence carried out in North America and Europe. In a few very rare exceptions, the literature addressed the detection of TV broadcast

signals in both digital and analog formats. Even in those cases, the study was always restricted to a single market, *e.g.* detection of ATSC and NTSC in North America, DVB-T and PAL in Europe. The present dissertation can be distinguished from the related work, as well as from the literature on spectrum sensing in general, in the sense that it considers multiple markets where a substantially larger number of different incumbent systems may be operating in. Another distinguishing aspect is that our analysis have been carried out from a post-switchover perspective. This allows the analysis of a broader set of coexistence situations arising between TV simulcast, PMSE, and future TVBD standards such as IEEE 802.22 and ECMA-392.

- **Signal type dependencies:** Built on top of the broader scope of application described above, our analysis has revealed some nuances of signal specific techniques that would have likely remained obscure if we had adopted the traditional single-target single-market approach. As nuances we mean those signal type dependencies that, though negligible in case of blind or semi-blind techniques, yield significant performance variations in case of signal specific techniques. This dissertation has shown that this is particularly true in case of OFDM-based standards, where the use of different number of subcarriers, CP length, symbol length, pilot insertion pattern (both SP amplitude and periodicity) impacts performance in tens of dB. Moreover, as summarized later on in this section, our study on signal type dependencies has allowed the identification of critical drawbacks associated to the use of some signal specific techniques (ACD and SCD) in the presence of modeling uncertainties.
- **Standard classification:** The related work has shown that much has been done in terms of signal detection but, in most cases of interest for WSD, the literature has not managed yet to perform standard classification. We have seen in Chapter 2 that extraction of implicit signal features is made difficult due to the complex and expensive signal processing needs posed by the computation of the SCF. Another shortcoming raised by the use of implicit signal features is that the class labeling is frequently limited to modulation. This is clearly not enough to distinguish among currently deployed standards, particularly those based on OFDM. In contrast, the cascade classifier proposed in this dissertation exploits explicit signal features, which can be extracted without going into the “internal details” of the signal. Accurate standard classification is possible by exploiting complementary explicit features, such as CP, SP, and PSD.

### 5.1.2 Cooperation based on Signal Specific Techniques

The related work reviewed in Chapter 2 reflects well most work found in the CSS literature, where either ED or EBD are typically used to model the information acquisition process. To the best of our knowledge, there exist no counterparts of these analyses where signal specific techniques are used at the local level. In this context, this dissertation has contributed to a deeper understanding on the following aspects:

- **Cooperation gains:** One interesting open question in the context of CSS is whether the use of different methods at the local level yields to different levels of performance improvement. This dissertation has shown that, as the number of cooperating nodes increases, CP-based methods derive the highest gains whereas PSD-based methods

derive the lowest gains. The degradation in the global FAR due to hard combining based on OR logic can be mitigated by imposing more stringent CFAR requirements at each node. However, as summarized in the sequel, we also have shown that the extent to which CSS may be beneficial depends on a number of aspects other than the number of cooperating nodes.

- **Cooperation in the presence of multipath fading:** The benefits of CSS are usually illustrated using nodes that experience fading, shadowing, or are in a deep fade. According to the related work, such local detection issues can be mitigated by enforcing cooperation among nodes. We have confirmed this behavior for all methods but ACD, which fails entirely under some particular condition. To determine this condition, we have shown analytically that the contribution of the last channel tap dominates the degradation caused by fading in the performance of ACF-based methods. Whenever ISI occurs, the channel will either introduce unexpected peaks in the ACF of the received signal (profile B) or spread the peak due to the CP within a range as wide as the maximum channel delay spread (profile D). ACD has prior knowledge of the position of the intended peak but lacks information about the the channel's PDP, so it fails entirely under profile D. This cannot be alleviated by means of node cooperation.
- **Cooperation in the presence of noise uncertainty:** Most work on this subject deals with ED, which is known to suffer from SNR walls when there is uncertainty in the noise marginal distribution. Color of the noise and time-selectivity of the fading process constitute sources of uncertainty that may jointly contribute to the creation of SNR walls, but less is known about how exactly they impact the signal specific techniques studied in this dissertation. Our contribution with this respect has been twofold. First, our simulation work has suggested that there may be a chance to improve the SNR walls of ED provided that node selection algorithms are used. This observation has been drawn on the basis of insights gained for RLRT, whose cooperation gains under noise uncertainty are similar to under ideal conditions. Second, we have shown that, regardless of target signal type, operation in noise of uncertain power affects all methods equally. The only exception is due to SCD, which may become susceptible to noise uncertainty depending on the sharpness of the spectral features and changes in the positions where such features occur in the PSD of the received signals.
- **Cooperation in the presence of frequency offsets:** Another practical issue that WSD will likely have to cope with is raised by imperfect synchronization. This calls for methods that are robust against frequency offsets, both CFO and SFO. This dissertation has shown that, among the methods evaluated, only TDSC methods are sensitive to SFO. Our contribution with this respect has been multi-fold. First, we have shown that the performance of TDSC methods is largely affected by the target signal type, *e.g.* due the use of different symbol lengths and pilot insertion patterns. Second, we have confirmed that TDSC-MRC outperforms TDSC-NP at the expense of increased complexity, yet only under tight synchronization requirements. Third, we have modeled analytically the impact exerted by SFO in the TDSC function. This has made it possible to visualize the accumulation of SFO over time, thus justifying the better robustness of TDSC-NP. Fourth, our simulations have suggested that CSS can compensate for degradations due to SFO, but the gain of TDSC-MRC varies with the level of synchronization whereas that of TDSC-NP is fixed.

### 5.1.3 A Cascade Classifier for Coexistence in the TV Bands

The three-stage cascade signal classifier proposed in this dissertation has been designed to be of practical interest. Its design has been carried out having the following features in mind:

- **Agility:** Recalling the current levels of spectrum underutilization and the typically static behavior of TV band incumbents, the proposed cascade classifier will likely spend most of its operation time on channel monitoring tasks. Since we have implemented the first stage using GLRT, channel monitoring can be carried out blindly and very fast thus keeping detection delays low. With respect to signal classification, we have exploited the fact that most standards deployed today are OFDM-based. Hence, the natural way to obtain classification ability without increasing detection delays is to use a fast OFDM classifier. This task has been accomplished in the second stage by BTPD, which has agility comparable as simple ED. Those less numerous cases that cannot be resolved on the basis of the CP are treated at the third stage, where we have proposed the use of SCD and TDSC-NP. SCD is fast too, so it is possible to classify non-OFDM standards on a timely manner. TDSC-NP requires longer sensing time, but it is the only method among those studied here that is able to distinguish OFDM standards having the same subcarrier spacing.
- **Robustness:** The choice of GLRT as the method used in the first stage provides excellent robustness against all practical issues studied. In the second stage, BTPD is virtually immune to noise uncertainty and frequency offsets, and its fair performance under multipath fading can be improved via CSS. Cooperation also works effectively in the third stage to improve the performance of TDSC-NP when perfect synchronization lacks. In our setting, SCD works well at very low SNR in all cases studied. Summing up, the highlight of the proposed cascade classifier is that its stages have been designed to possess complementary features. This also includes robustness against variations in the CP length or SP power ratio.
- **Context-awareness:** Knowledge of the structure of standardized target signals is frequently available a priori. When target signals are based on TV broadcast standards, additional information becomes available in the form of deployment related patterns, *e.g.* different standards that have the same format (digital or analog) are usually not deployed collocated, simulcast services are still offered in most markets, etc. Information about the TV standards deployed in a certain market is in general publicly available, so we can use it to facilitate the signal classification process. Specifically, markets where digital TV signals are simulcast in analog format can be determined by classifying both the standards they adopt. If market determination is less straightforward only on this basis, we can additionally scan the spectrum for variations of the PAL standard or TVBD standards. The context-awareness obtained thereby renders our cascade classifier able to operate in most markets worldwide. Also, the use of our cascade classifier in WSD poses reduced fabrication costs, which would increase otherwise if we had one specific WSD design for each market considered. This has clear potential to leverage economies of scale.
- **Universality:** Our cascade classifier has been conceived to take advantage of cooperation among nodes. As compared to other methods for determining white spaces,

CSS reduces infrastructure costs, eliminates costs associated with location-aware hardware, and poses milder connectivity issues since it does not necessarily require access to the Internet. The minimization of both CAPEX and OPEX resulting from these advantages makes CSS attractive for developing countries, where the telecommunications infrastructure is precarious and the household income is low. Provided that the proposed cascade classifier can be made of low cost (out of the scope of this dissertation), its use at the local level of CSS can realize all the above features while respecting our commitment to promote white space use also in developing countries. Hopefully, this can contribute to the decrease of digital divides in both regional and global levels.

### 5.1.4 The MESS Platform

The performance assessments in this dissertation rely on extensive simulation work that has only been possible thanks to MESS, the Matlab-based spectrum sensing platform to which we have dedicated the Chapter 3. Originally envisioned as a standardized evaluation scenario to comparing approaches proposed by different research groups on a fair basis, MESS has ended up becoming much more than we had ever thought it could be. MESS is based on what we call virtual testbed, a concept that differs from conventional Matlab simulation in the sense that all target signals are implemented in detailed accordance to corresponding standards. This allows to visualize (and gain insight on) issues that cannot be captured by other means.

Beside of having accomplished its major goal of allowing a thorough assessment of several signal processing techniques (not available in the literature at the time of this writing), the work on MESS has been proven extremely rewarding in the following ways:

- **Integrating research framework:** MESS has played a key role as the framework integrating our contributions on the gaps identified in the related work (see Chapter 2). Perhaps, if we had looked at each of those gaps in isolation, we would not had come up with the concept of multi-standard context-aware WSD introduced in this dissertation.
- **Own algorithm development:** MESS has given us the chance to develop novel signal processing skills, both in analog and digital formats. Implementation efforts, such as amendments needed to overcome the lack of accurate documentation, careful evaluation of simulation outcomes, and extensive code debugging, have all left us valuable insights. These insights can be used to improve the methods implemented or even in the development of our own algorithms, *e.g.* MAD.
- **Commercial feasibility:** MESS has been attracting interest in both North America and Europe due to its potential for becoming a commercial product to support the assessment, development, and implementation of signal processing techniques for WSD. To the best of our knowledge, such a product is not currently available neither in the academy nor in the industry. Unfortunately, we had to freeze negotiations with the company<sup>1</sup> that was willing to collaborate due to the time constraints raised by the writing of the present dissertation.

---

<sup>1</sup> Though we did not come to sign a non-disclosure agreement, for the time being we think that letting the interested company anonymous is convenient to both parties involved.

- **Encourage future research:** Now that the main code and core functions have been put in place, a number of extensions can be envisioned for MESS at the expense of minimum implementation effort. We discuss some of them in the next section.

## 5.2 Suggestions for Future Research

This dissertation has touched on many aspects crucial to the design of WSD. Some of these aspects have received an in-depth treatment, while others have been studied more superficially. In either case, and despite the progress that has been made in this dissertation, there exist a variety of open issues related to WSD that deserve further investigation. In this section, we list some key issues in which we believe promising future research can be carried out. This includes two different scenarios where the results presented in this dissertation may find application.

### 5.2.1 Emerging Coexistence Situations

Due to superior propagation and building penetration characteristics the TV bands have been selected by regulatory agencies worldwide to accommodate the first CR-based services and applications. Not surprisingly, most research efforts carried out thus far have assumed that WSD will operate collocated with a single licensed transmitter ( $P = 1$ ). Under this assumption, this dissertation has considered the coexistence between TV band incumbents, such as TV broadcast and PMSE, and WSD based on the standards IEEE 802.22 and ECMA-392. Possible extensions of this setting include:

- **Other targets:** The types of target signals currently implemented in MESS suffice to assess the performance of different detection methods, whether blind or signal specific, CP- or pilot-based. The results presented here can also be used to provide an estimate about how performance would look like in case other target signals come into consideration. However, recalling that MESS is very flexible and scalable, it seems interesting to improve the signal generation block with other signal sources. Among the candidate sources, the most promising are those based on emerging standards that consider the use of white spaces, *e.g.* Long Term Evolution (LTE), Super Wireless Fidelity (Super WiFi) within the scope of the IEEE 802.11af standard, and Worldwide Interoperability for Microwave Access (WiMAX) within the scope of the IEEE 802.16h standard. All of these standards are OFDM-based, so implementation in MESS is just a matter of creating new “flags” that point to the mandatory sets of system parameters and pilot insertion patterns.
- **Other bands:** While the  $P = 1$  assumption models coexistence in typical broadcast scenarios, it may not suit forthcoming coexistence situations created by approaches that jointly consider TV white space and licensed services operating in frequencies other than the TV bands. This is the case, for instance, of cellular networks where TV white spaces are currently being viewed as a promising means to offload data traffic and/or deploy smart grid services. In such cellular scenarios, there will likely be multiple licensed transmitters sharing the same frequencies. Therefore, the development of algorithms that need not rely on the  $P = 1$  assumption have received

great attention recently [103][107][109]. This related work can serve as initial guide for the amendments in the MESS code, as required to simulate  $P \geq 2$ .

## 5.2.2 Practical Implementation

Despite of the “brute force” simulation-based approach adopted in this dissertation, we recognize that accurate knowledge of the distributions of a certain test statistic  $z$  under both hypotheses are valuable quantities. First, efficient approximations for the distribution of  $z$  enable the analytical computation of that test’s performance in terms of  $P_d$  and  $P_{fa}$ . Second, and as a consequence of the former, the minimum number of samples needed to provide a given performance can be determined in closed-form, *e.g.* as in (2.15) and (2.18). Notwithstanding the importance of this knowledge to practical WSD, the search for such approximations implies analytical work that is time consuming and does not necessarily ends up with something efficient. Now that the amount of methods to analyze has been reduced to one third of the initial candidate set via simulation, one possible next step would be to update and deepen the related work in Chapter 2 with emphasis on the distributions of ACD, GLRT, TDSC-NP, and SCD. This could include:

- **ACD:** As explained in Chapter 4, we are currently working on the incorporation of peak search procedures into ACD. We expect that the resulting MAD allows us to exploit the benefits of both ACD and BTPD, *i.e.* the robustness against multipath fading of the latter with computational complexity of the former. In case this idea turns out to be fruitful, the work in [116] can serve as starting point for an asymptotic analysis of MAD. Within this framework, we also can study the impact on the performance, particularly the classification performance, of MAD when information about subcarrier spacings is available a priori.
- **GLRT ( $P = 1$ ):** For the low dimensional setting (both  $N$  and  $M$  are finite), exact distributions for MED, EME, and MME have been recently derived in [104]. Represented in terms of complex zonal polynomials, the proposed distributions allow to formulate closed-form expressions for  $P_{fa}$  that can be used to exactly set the detection threshold  $\lambda$ . In case of MME, the performance derived via this procedure is shown to outperform the asymptotical approaches in [103] and [106]. At the time of this writing, and to the best of our knowledge, the literature had not yet found efficient approximations for GLRT. Therefore, it might be worth investigating whether it is possible to express the distributions of GLRT using complex hypergeometric functions along the lines in [104].
- **GLRT ( $P \geq 2$ ):** The related work discussed in Chapter 2 is by no means intended to be a complete treatment of signal processing techniques for WSD. In case of EBD, for instance, a number of methods can be constructed to exploit the eigenvalues of  $\mathbf{R}_r(n)$ . Derived under the GLRT criterion, the spherical test (ST) detector

$$z_{\text{ST}}(n) = \frac{\prod_{i=1}^N \lambda_i}{\left(\frac{1}{N} \sum_{i=1}^N \lambda_i\right)^N}$$

has been receiving attention due to the closed-form approximations recently proposed in [153]. Therein, easily computable analytical formulae for  $P_{fa}$ ,  $P_d$ , and  $Q_d$



are derived by matching the moments of  $z_{\text{ST}}$  to the Beta distribution. It is shown that the proposed Beta approximation fits almost exactly the simulations and, for large  $P$ , outperforms  $z_{\text{GLRT}}$ . In view of these facts, and recalling that some advantages may be achieved by relaxing the  $P = 1$  assumption, the state of the art points out  $z_{\text{ST}}$  as the currently most promising EBD method. Minimum implementation effort is required to introduce the method into MESS.

- **TDSC:** For the high dimensional setting ( $N_1, M \rightarrow \infty$ ), the distribution of TDSC is close to being circularly symmetric complex Gaussian [121]. By exploiting the fact that  $|z_{\text{TDSC-NP}}|$  and  $|z_{\text{TDSC-MRC}}|$  are both asymptotically Rayleigh distributed under  $H_0$ , it is possible to derive an accurate closed-form expression to compute  $\lambda$  in terms of  $P_{\text{fa}}$ . While this suffices to demonstrate the potential of TDSC, real-world WSD require approaches that can estimate detection power and define  $\lambda$  for arbitrary values of  $N_1$  and  $M$ . At the time of this writing, and to the best of our knowledge, the literature had not yet studied the distributions of TDSC for practical low dimensional settings where the number of samples and the number of observed symbol pairs having the same SP pattern are both limited.
- **SCD:** The asymptotic optimality of SCD, in the sense that the method asymptotically approaches the LRT detector at low SNR when  $M$  is large enough, is proven in [50] using the periodogram to estimate the PSD of the received signal. However, the derivation of  $\chi_{\kappa}^2(o)$  used therein to approximate the distribution of  $z_{\text{SCD}}$ , and in turn set  $\lambda$  via (2.63), relies on the Bartlett method. As explained in Section 3.3, we used both the Bartlett and Welch methods in the beginning but our preliminary results indicated that, despite of substantially longer simulation times, periodogram averaging gives the same detection performance as the simple periodogram. In view of this, two distinct lines of investigation can be adopted. The first is to assess the accuracy of using  $\chi_{\kappa}^2(o)$  to approximate the distributions of the periodogram-based SCD,  $z_{\text{PER}}$ , following the steps done in [50] for the Bartlett-based SCD,  $z_{\text{BAR}}$ . The second one is to study the asymptotic optimality of  $z_{\text{BAR}}$  ( $z_{\text{BAR}}$  is likely suboptimum compared to  $z_{\text{PER}}$ , so the first line of investigation seems more promising).

### 5.2.3 Characterization of Classification Performance

Under the  $P = 1$  assumption used in this dissertation, the probability of correctly classifying signals based on a given standard corresponds to the probability of correctly detecting those signals. This allowed us to assess the classification performance that a certain method delivers in a multi-standard operation environment by performing distinct simulation campaigns, one for each standard. Possible extensions of this setting include:

- **Simultaneously active transmitters of different kind:** The actual setting does not model those practical events where WSD *simultaneously* pick up signals of different formats and types. This is clear to occur in markets where simulcast services are still offered. Alternatively, the assumption of multiple target signals of different kind can be justified by the condition where WSD interfere with licensed transmissions, *e.g.* due to missed detections or shadowed beacon signals from other WSD operating in the same area. Though this assumption does not invalidate the results obtained thus far using MESS (unintended received signals are treated as noise),

it requires an assessment of classification performance in terms of probability of missed classification  $P_{mc}$ . If  $Z = \{z_A, z_B, \dots, z_Z\}$  denote the set of values assumed by a generic test statistic  $z$  in the presence of noisy signals based on the standards A, B,  $\dots$ , Z, respectively,  $P_{mc}$  is the probability that  $z > z_A, \forall z \neq z_A$ , given that A is true. Currently, we are working on the code amendments required to compute  $P_{mc}$  using MESS. They are relatively simple (depending on the size of  $Z$ ), but must avoid storage issues raised by the size of the resulting variables/workspaces.

- **Categorical data analysis:** According to the extension above, the test statistic  $z$  has a measurement scale consisting of a set of categories, *e.g.* it may be measured as “standard A present”, “standard B present”,  $\dots$ , “standard Z present”. Hence, in the context of standard classification, we can treat  $z$  as a categorical response variable. This allows us to use standard statistical models to describe how the distribution of  $z$  changes according to levels of explanatory variables, which in our case can be either categorical (*e.g.* channel type) or continuous (*e.g.* SNR). In multi-standard operation environments, categorical responses with more than two categories account to the prevailing condition. Within this framework, the *simultaneous* determination of the odds of outcome in one category instead of in all others calls for multi-category logit models [154]. We have not assessed yet the effort to increment MESS with such models, but we are aware that other statistical computing software such S-Plus, R, Stata, and SPSS may have advantages over Matlab.

## 5.2.4 Applications

A number of applications can be envisioned to demonstrate the feasibility of the cascade signal classifier proposed in this dissertation. Two of them, specific for the case of the TV bands, are described in the sequel.

### 5.2.4.1 On-demand Return Path for Interactive Television

The context-awareness achieved via signal detection and classification can be exploited to provide a return path for interactive television (iTV) over white spaces. This first application is illustrated by the interaction channel model shown in Figure 5.1. In this figure, TV broadcast and forward interaction path are both conveyed in a single downstream which can be based on ATSC, DVB-T, ISDB-T, or any digital TV standard supporting interactivity. The interface between the TV set and the broadcaster is provided by the cognitive interactive terminal (CIT). The CIT’s building blocks (not depicted) are a network interface unit and a set-top box, the latter equipped with our three-stage signal classifier. In practice, the interaction network adapter can be viewed as a BS deployed collocated with the broadcast transmitter site. Since the broadcast and forward interaction channels conveyed in the downstream have priority (licensed) access to spectrum, the (unlicensed) upstream used to send interactive data from the home user back to the broadcaster needs to be set in overlay with the downstream on a non-interfering basis. Spectrum resources assigned to the return path should be then selected from available white spaces, *e.g.* channels found to be unused within the frequency band licensed to the broadcaster.

Once having selected a channel and started using it, the CIT periodically monitors this channel to ascertain that it remains free of licensed activity. To that end, we can enforce

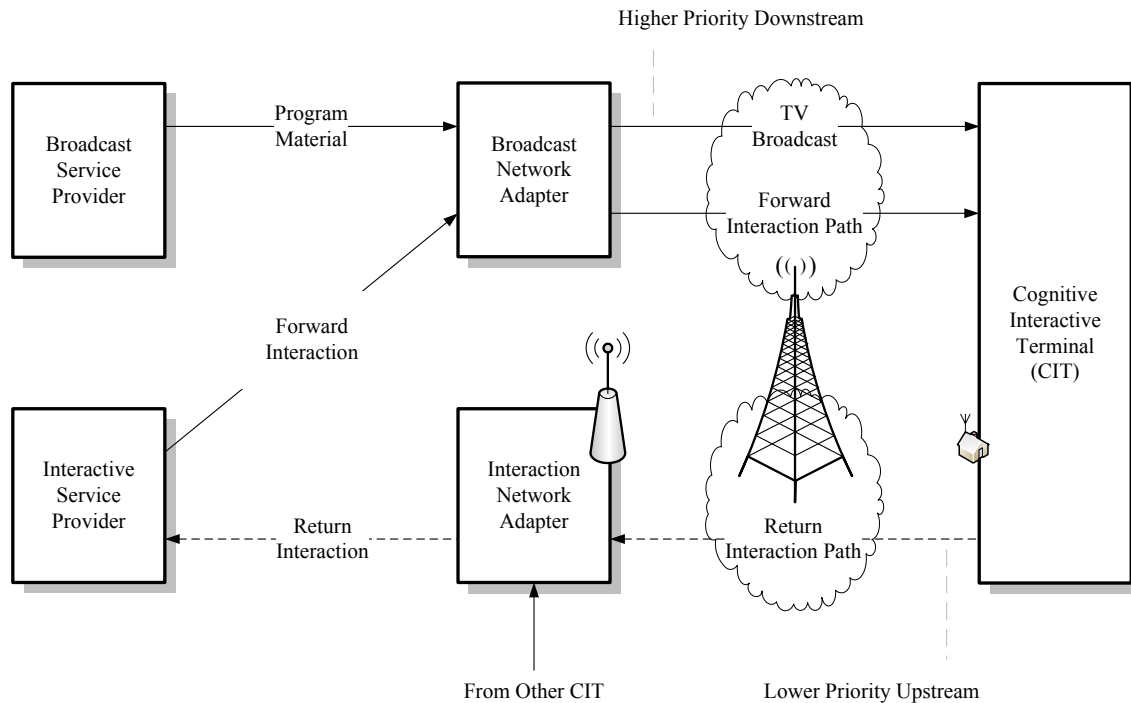


**Fig. 5.1:** An interaction channel model for iTV over TV white spaces (adapted from [159]).

quiet periods during which transmissions on the return path cease and the CIT performs spectrum sensing as shown in Figure 5.2. The channel samples collected over a quiet period allow the CIT to issue a local decision about whether licensed signals are present or absent. In this process, an individual CIT has to cope with fading, shadowing, and penetration losses. These local detection issues can be mitigated by using CSS, in which multiple CIT share sensing information to get a more accurate picture of current spectrum occupancy. This implies that, besides its typical control tasks, the BS has to send enabling signals to instruct the CIT in its coverage area about what channel to sense, when to sense, and for how long to sense. The task of defining how long the quiet periods last is of utmost importance here since it determines *both* the accuracy of the channel monitoring scheme *and* the duration of the transmit periods over which CIT are allowed to transmit interactive over the return path.

The reason why such an application is desirable is multi-fold. First, iTV has been considered a key feature to make digital TV appealing to end users and provide additional revenue to manufacturers and broadcasters [155]. Through services that facilitate digital inclusion, such as t-learning, t-government, and t-commerce, iTV has gained attention as an efficient way to bring the Internet to mass markets [156]. Hence, iTV seems to be the perfect application to supporting our goal of mitigating digital divides. Second, the interaction channel model proposed in Figure 5.1 is dynamic, smart, and spectrally efficient. It is dynamic in the sense that it exploits the fact that home users are not likely to interact all the time to set the return path on an on-demand basis. Smart here means that it provides an alternative way for gaining access to spectrum in case licenses are difficult to obtain. As for spectral efficiency, better use of spectrum is achieved by using the same medium to transmit interactive data in overlay with higher priority broadcast data. Third, ATSC and ISDB-T are flexible standards in the sense that they mandate no specific access technology to provide the interaction channel [157][158]. Though flexibility is

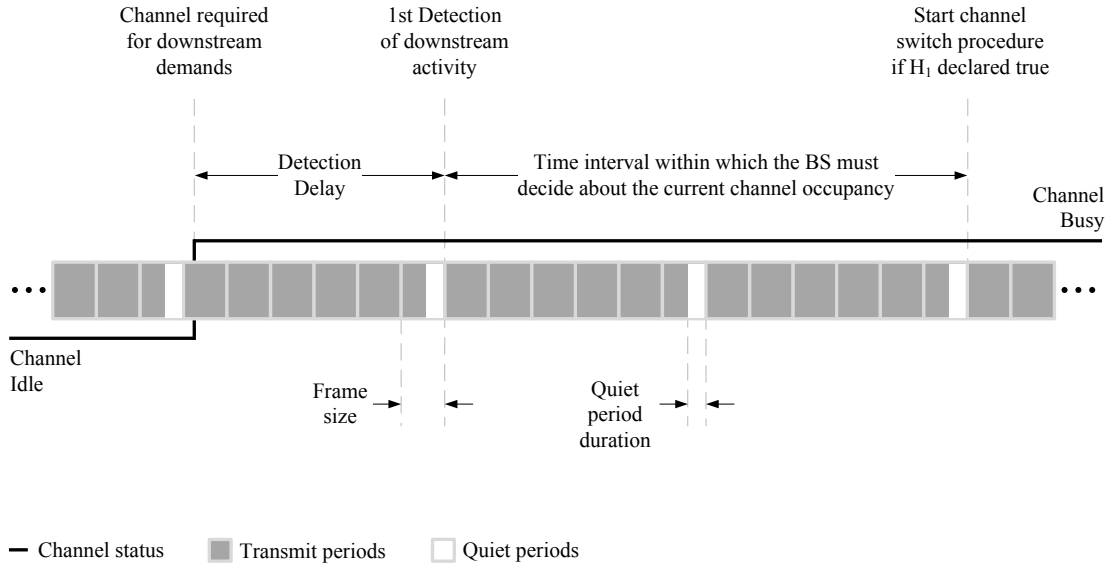


**Fig. 5.2:** In-band channel monitoring process carried out by a single CIT. To ascertain that the return path remains free of PU activity, the BS orders its served CIT to perform periodic sensing tasks.

almost always welcome, the access technologies currently considered for this purpose usually require broadcasters to cooperate (thus sharing revenues) with telecommunications or Internet service providers. In its family of standards, DVB specifies a return channel terrestrial (RCT) to convey data in the forward and return interaction paths [159]. Unfortunately, DVB-RCT is not straightforward to implement because neither sensing method nor channel monitoring mechanisms are specified in the standard. Hence, in contrast to other access technologies, white space technologies do not require broadcasters to cooperate. This cuts down revenue sharing, thus increasing broadcasters' profits.

To the best of our knowledge, our previous work in [89] was the first study on the application of a TVBD standard as access technology for the return path of iTV. We considered the settings for sensing periodicity, sensing duration, and number of cooperating CIT needed to fulfill the requirements on dynamic frequency selection mandated in the IEEE 802.22 standard. Possible extensions of this work might include:

- **Improve local level performance:** Carried out in the “early days of MESS”, when only a few methods were implemented, the numerical analysis, simulation work, and testbed experimentation all rely on ED. Strictly speaking, CIT do not need advanced classification abilities but the extent to which their detection performance can be improved by using blind techniques (GLRT) or signal specific techniques (ACD and TDSC-NP) is worth investigating. To update the numerical analysis accordingly, we depend on the availability of approximations for the distributions of these methods as highlighted earlier in this section. Updating the simulation work is straightforward using the current version of MESS. As for the testbed, substantial implementation work is required, particularly with respect to the estimation of the eigenvalues of the covariance matrix required in GLRT. Among the tools available to that end, the literature has been typically calling upon SVD algorithms [160] or symmetric bidiagonalization methods [161].

- **Improve system and channel models:** The system model used in the numerical analysis assumes that CIT contributions are uncorrelated and the noise process is AWGN. The simulation work is done for both AWGN channel and multipath fading channel generated according to profile A (see Table 3.5). However, these models do not reflect the correlated shadowing experienced in the testbed measurements due to the fact that the cooperating CIT are placed too close to one another. In order to produce numerical, simulative, and experimental results that are comparable, we need to relax the assumption of uncorrelated contributions and improve MESS with correlated fading channel models. A different system aspect that might be improved is the single-channel perspective. By extending analysis to a multi-channel environment, as considered in the experiment, we would be able to quantify the agility gain suggested as tie-break criterion for making the sensing settings.

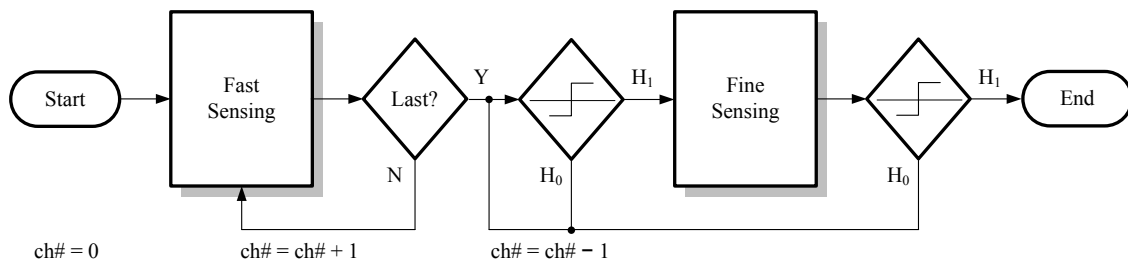
#### 5.2.4.2 Channel Monitoring Mechanisms for Cognitive PMSE

PMSE systems have been thus far allowed to operate in the TV bands with lower priority than broadcast TV. However, the transition from analog to digital TV has been viewed with some worry by the WM industry, particularly in the U.S. where the FCC will allow unlicensed operation of WSD in the spectrum freed up by the digital switchover. Two major concerns are about how to mitigate harmful interference from WSD to PMSE and how to ensure that the WM operated by PMSE will still be able to find idle frequencies where they can operate. Indeed, both are relevant concerns because providing coexistence between WSD and PMSE is a challenging task for both GDA (see Chapter 1) and spectrum sensing (see Chapter 2).

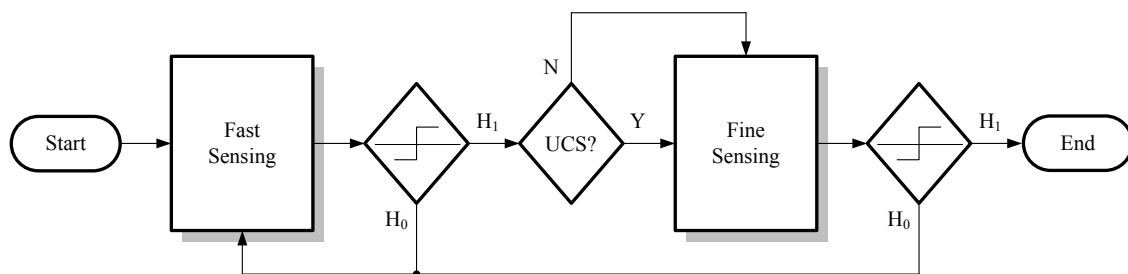
In this context, the trend consists of applying CR principles to enhance the sensing capabilities of the scanning receiver units (SRU) used in current WM systems, mostly based on simple ED, thus improving immunity to interference [162][163]. Such CR-based systems are referred to as cognitive PMSE (C-PMSE). Unlike in the usual overlay-based hierarchical access model, where opportunistic unlicensed users should detect and avoid licensed users, C-PMSE are concerned about sensing carried out *by* WM rather than *for* WM. Within this framework, specific channel monitoring mechanisms are needed to ensure quality of service of PMSE. Assuming that at least one dedicated antenna is available for sensing, the SRU can carry out the channel monitoring mechanisms depicted in Figure 5.3 in an alternated fashion.

The first mechanism, shown in Figure 5.3(a), considers out-of-band channel monitoring, *i.e.* it is intended for channels not currently occupied by WM transmissions. The number of channels to be sensed is always limited in practice, so SRU can use fast sensing to scan all channels in acceptable time. Preliminary fast sensing results serve to populate a list of reserve channels based on radio environment maps (REM) [164]. After all channels have been scanned and the REM entries initialized, the SRU performs fine sensing on the last channel that it has declared idle through fast sensing. Basically, this means that the SRU declares a channel as suitable for WM transmissions only if it has been declared idle also through fine sensing.

Upon having selected a channel and assigned it for WM transmitter use, the SRU initiates in-band channel monitoring using the second mechanism shown in Figure 5.3(b). Here, whenever the channel is declared occupied through fast sensing, the SRU has to rely on other link quality parameters to determine the existence of a urgent coexistence situa-



(a) Out-of-band channel monitoring.



(b) In-band channel monitoring.

**Fig. 5.3:** Generic channel monitoring mechanisms to ensure quality of service in future C-PMSE systems.

tion (UCS). This may include additional mechanisms to monitor bit error rate and/or received signal strength indication, as proposed in [163]. By comparing current channel measurements to the thresholds stated in the service level agreement (depends on the PMSE application), the SRU decides about triggering fine sensing or handling transmissions immediately to a new channel. Out-of-band channel monitoring maintains the REM updated, so a reserve channel can be retrieved on-the-fly in case of UCS or detection of target signals during fine sensing. In either case, and before initiating the channel switch procedure, the SRU double-checks the status of the reserve channel using the fine sensing loop of Figure 5.3(a).

The channel monitoring mechanisms described above are characterized by two distinguishing features. First, since WM transmitters are powered off during out-of-band channel monitoring, the methods used at both fast and fine sensing blocks in Figure 5.3(a) do not need possess any classification ability. Second, unlike the bursty interactive data conveyed in the return path of iTV, WM systems have 100% duty cycle. Consequently, we cannot enforce quiet periods (as in Figure 5.2) in case of in-band channel monitoring and the SRU should perform sensing tasks while WM transmitters are powered on. This calls for methods with classification ability for both fast and fine sensing blocks in Figure 5.3(b), particularly methods capable of distinguishing WM signals from other signals found in the TV bands.

In our previous work [90], we analyze the pros & cons of five potential detection methods with respect to computational complexity, amount of prior information required for detection, classification ability, and performance under AWGN and frequency-selective fading.

Our analysis suggests that methods based on the CP can be used for fast sensing as long as ECMA-392 can be detected. For fine sensing, we suggest methods that exploit SP and have complementary features to fast sensing methods. For most cases of interest, we show through computer simulations that the combined uses of ED and TDSC-NP (out-of-band monitoring), and BTPD and TDSC-NP (in-band monitoring) incur no performance loss in comparison to fast sensing methods in isolation.

Possible extensions of this work might include:

- **Improve operation environment:** The proposed channel mechanisms suit well operation environments where C-PMSE need coexist with OFDM-based systems only. This may not be realistic in those markets where digital TV is still simulcast in analog format or the digital standard adopted is non-OFDM, *e.g.* ATSC. Recalling that in C-PMSE sensing is carried out by WM rather than for WM, it is evident that prior knowledge of the structure of WM signals will be available because the entity managing the system exactly knows  $f_c$ ,  $f_{dev}$ ,  $W$ , side-tone placements, and other operational parameters that can be exploited by the detection process. Under the assumption that this is exactly the case, SCD can distinguish WM signals from most types of non-OFDM signals currently found in the TV bands. This renders the three-stage classifier proposed in this dissertation a better option for both in-band and out-of-band monitoring.
- **Improve system and channel models:** Besides suiting most practical scenarios, the extension above improves both local level performance and robustness against noise uncertainty. The simulation work has been updated throughout this dissertation, where we have also considered frequency offsets and extended the single-node analysis to the case of multiple cooperating nodes. Nevertheless, we have not managed yet to address two aspects that are crucial to C-PMSE. The first consists of improving MESS to consider a multi-channel perspective, as required to realize REM. Further implementation effort is also required in a second aspect, which relates to the integration of MESS and the additional mechanisms required to determine UCS. Both aspects are currently under investigation within the broader scope of the “C-PMSE Project” [165], organized in a consortium of research and industry and funded by the German Federal Ministry of Economics and Technology.





# Bibliography

- [1] L. E. Doyle, “Essentials of Cognitive Radio”, 1st Ed., Cambridge University Press 2009.
- [2] M. J. Marcus, “Unlicensed Cognitive Sharing of TV Spectrum: The Controversy at the Federal Communications Commission”, *In Proc. IEEE Communications Magazine*, pp. 24-25, May 2005.
- [3] FCC. Et docket no. 02-155. Report of the Spectrum Efficiency Working Group, Nov. 2002.
- [4] D. Cabric, S. M. Mishra, and R.W. Brodersen, “Implementation Issues in Spectrum Sensing for Cognitive Radios”, *In Proc. Asilomar Conference on Signals, Systems and Computers*, vol. 1, pp. 772-776, Nov. 2004.
- [5] T. A. Weiss and F. K. Jondral, “Spectrum Pooling: An Innovative Strategy for the Enhancement of Spectrum Efficiency”, *In IEEE Communications Magazine*, vol. 42, no. 3, pp. S8-S14, Mar. 2004.
- [6] J. van de Beek, J. Riihijärvi, A. Achtzehn, and P. Mähönen, “UHF white space in Europe – a quantitative study into the potential of the 470-790 MHz band”, *In Proc. IEEE DySPAN*, pp. 1-9, May 2011.
- [7] Q. Zhao and B. M. Sadler, “A Survey of Dynamic Spectrum Access: Signal Processing, Networking, and Regulatory Policy”, *IEEE Signal Processing Magazine*, pp. 79-89, May 2007.
- [8] V. Chakravarthy et al., “Novel Overlay/Underlay Cognitive Radio Waveforms using SD-SMSE Framework to enhance Spectrum Efficiency - Part I: Theoretical Framework and Analysis in AWGN Channel”, *In IEEE Transactions on Communications*, vol. 57, no. 12, pp. 3794-3804, Dec. 2009.
- [9] P. Sutton, “Rendezvous and Coordination in OFDM-based Dynamic Spectrum Access Networks”, Ph.D. Thesis, University of Dublin, Trinity College, Ireland, Sept. 2008.
- [10] V. Chakravarthy et al., “Novel Overlay/Underlay Cognitive Radio Waveforms using SD-SMSE Framework to enhance Spectrum Efficiency - Part II: Analysis in Fading Channels”, *In IEEE Transactions on Communications*, vol. 58, no. 6, pp. 1868-1876, June 2010.
- [11] D. Gurney, G. J. Buchwald, L. M. Ecklund, S. L. Kuffner, and J. Grosspietsch, “Geolocation Database Techniques for Incumbent Protection in the TV White Space”, *In Proc. IEEE DySPAN*, pp. 1-9, Oct. 2008.

- [12] I. F. Akyildiz, B. F. Lo, and R. Balakrishnan, "Cooperative Spectrum Sensing in Cognitive Radio Networks: A Survey", *In Physical Communication (Elsevier) Journal*, vol. 4, no. 1, pp. 40-62, Mar. 2011.
- [13] IEEE 802.22.1, "IEEE Standard for Information Technology–Telecommunications and information exchange between systems–Local and metropolitan area networks–Specific requirements Part 22.1: Standard to Enhance Harmful Interference Protection for Low-Power Licensed Devices Operating in TV Broadcast Bands", Nov. 2010.
- [14] P. Sutton, K. E. Nolan, and L. E. Doyle, "Cyclostationary Signatures in Practical Cognitive Radio Applications", *In IEEE Journal of Selected Areas in Communications*, vol. 26, no. 1, pp. 13-24, Jan. 2008.
- [15] S. Delaere and P. Ballon, "Multi-Level Standardization and Business Models for Cognitive Radio: The Case of the Cognitive Pilot Channel", *In Proc. IEEE DySPAN*, pp. 1-18, Oct. 2008.
- [16] Cisco Systems, Inc. Cisco Visual Networking Index: Global Mobile Data Forecast Update, 2010-2015, Feb. 2011.
- [17] Cisco Systems, Inc. Cisco Visual Networking Index: Forecast and Methodology, 2010-2015, June 2011.
- [18] FCC. Et docket no. 10-174. Second Memorandum Opinion and Order, Sept. 2010.
- [19] FCC. Et docket no. 11-131. Order, Jan. 2011.
- [20] Spectrum Bridge Inc. Summary Report of the Spectrum Bridge TVWS Database Public Trial Report, Nov. 2011.
- [21] FCC. Et docket no. 08-260. Second Report and Order and Memorandum Opinion and Order, Nov. 2008.
- [22] OET Report. FCC/OET 08-TR-1005. Evaluation of the Performance of Prototype TV-Band White Space Devices Phase II, Oct. 2008.
- [23] Ofcom. Digital Dividend: Cognitive Access. Statement on license-exempting cognitive devices using interleaved spectrum, Jul. 2009.
- [24] Ofcom. Digital Dividend: Geolocation for Cognitive Access. A discussion on using geolocation to enable licence-exempt access to the interleaved spectrum, Nov. 2009.
- [25] Ofcom. Implementing geolocation, Nov. 2010.
- [26] CEPT. ECC Report 159. Technical and operation requirements for the possible operation of cognitive radio systems in the "white spaces" of the frequency band 470-790 MHz, Jan. 2011.
- [27] IETF. Report of the IETF 80, Apr. 2011.
- [28] ETSI. TR 102 683 v.1.1.1, Technical Report on "Reconfigurable Radio Systems (RRS); Cognitive Pilot Channel (CPC)", Oct. 2009.

- [29] International Telecommunication Union. A 2010 Leadership Imperative: The Future built on Broadband, Sept. 2010.
- [30] International Telecommunication Union. Broadband: A Platform for Progress, June 2011.
- [31] FCC. Connecting America: The National Broadband Plan, Mar. 2010.
- [32] European Commission. Europe 2020 - A strategy for smart, sustainable, and inclusive growth, Mar. 2010.
- [33] European Commission. A Digital Agenda for Europe, Oct. 2010.
- [34] Department for Culture, Media, and Sport. Enabling UK growth - Releasing public spectrum, Mar. 2011.
- [35] C.-S. Sum, H. Harada, F. Kojima, Z. Lan, and R. Funada, "Smart Utility Networks in TV White Space", *In IEEE Communications Magazine*, pp. 132-139, July 2011.
- [36] S. J. Shellhammer, V. Tawil, G. Chouinard, M. Muterspaugh, and M. Ghosh, "Spectrum Sensing Simulation Model", IEEE 802.22-06/0028r10, Sept. 2006.
- [37] CEPT. ECC Annex 3 to doc. SE43(10)103. Technical and operation requirements for the possible operation of cognitive radio systems in the "white spaces" of the frequency band 470-970 MHz, June 2010.
- [38] Comments of the Coalition of Wireless Microphone Users in the Matter of the FCC's Wt. docket no. 08-166, Wt. docket no. 08-167, and Et. docket no. 10-24, Mar. 2010.
- [39] R. Murty, R. Chandra, T. Moscibroda, and P. Bahl, "SenseLess: A Database-Driven White Spaces Network", *In Proc. IEEE DySPAN*, pp. 10-21, May 2011.
- [40] Project COGEU (FP7 ICT-2009.1.1) Cognitive radio systems for efficient sharing of TV white spaces in European context. Deliverable Report D4.1, "Spectrum measurements and anti-interference spectrum database specification", Nov. 2010.
- [41] C. Ghosh, S. Roy, and D. Cavalcanti, "Coexistence Challenges for Heterogeneous Cognitive Wireless Networks in TV White Spaces", *In IEEE Wireless Magazine*, vol. 18, no. 4, pp. 22-31, Aug. 2011.
- [42] M. Rabinowitz and J. J. Spilker Jr., "A New Positioning System using Television Synchronization Signals", *In IEEE Transactions on Broadcasting*, vol. 51, no. 1, pp. 51-61, Mar. 2005.
- [43] J. Ma, G. Y. Li, and B. H. Juang, "Signal Processing in Cognitive Radio", *In Proceedings of the IEEE*, vol. 97, no. 5, pp. 805-823, May 2009.
- [44] T. Shu and M. Krunz, "Exploiting Microscopic Spectrum Opportunities in Cognitive Radio Networks via Coordinated Channel Access", *In IEEE Transactions on Mobile Computing*, vol. 9, no. 11, pp. 1522-1534, Nov. 2010.
- [45] B. Wild and K. Ramchandran, "Detecting Primary Receivers for Cognitive Radio Applications", *In Proc. IEEE DySPAN*, pp. 124-130, Nov. 2005.

- [46] S. Park, L. E. Larsson, and L. B. Milstein, "An RF Receiver Detection Technique for Cognitive Radio Coexistence", *In IEEE Transactions on Circuits and Systems II: Express Briefs*, vol. 57, no. 8, pp. 652-656, Aug. 2010.
- [47] T. Yücek and H. Arslan, "A Survey of Spectrum Sensing Algorithms for Cognitive Radio Applications", *In IEEE Communications Surveys & Tutorials*, vol. 1, no. 1, pp. 116-130, First Quarter 2009.
- [48] S.-J. Kim, G. Li, and G. B. Giannakis, "Minimum-Delay Spectrum Sensing for Multi-Band Cognitive Radios", *In Proc. IEEE Globecom*, pp. 1-5, Dec. 2010.
- [49] Y. Zeng, Y.-C. Liang, A. T. Hoang, and R. Zhang, "A Review on Spectrum Sensing for Cognitive Radio: Challenges and Solutions", *EURASIP Journal on Advances in Signal Processing*, vol. 2010, pp. 1-15, 2010.
- [50] Z. Quan, W. Zhang, S. J. Shellhammer, and A. H. Sayed, "Optimal Spectral Feature Detection for Spectrum Sensing at Very Low SNR", *In IEEE Transactions on Communications*, vol. 59, no. 1, pp. 201-212, Jan. 2011.
- [51] H. -S. Chen and W. Gao, "Spectrum Sensing for TV White Space in North America", *In IEEE Journal on Selected Areas in Communications*, vol. 29, no. 2, pp. 316-326, Feb. 2011.
- [52] Z. Quan, S. Cui, H. V. Poor, and A. H. Sayed, "Collaborative Wideband Sensing for Cognitive Radios", *IEEE Signal Processing Magazine*, vol. 25, no. 6, pp. 60-73, Nov. 2008.
- [53] B. Le, T. W. Rondeau, J. H. Reed, and C. W. Bostian, "Analog-to-Digital Converters", *IEEE Signal Processing Magazine*, pp. 69-77, Nov. 2005.
- [54] S. Pollin et al., "Digital and Analog Solution for Low-Power Multi-Band Sensing", *In Proc. IEEE DySPAN*, pp. 1-2, Apr. 2010.
- [55] E. J. Candès, J. Romberg, and T. Tao, "Robust Uncertainty Principles: Exact Signal Reconstruction From Highly Incomplete Frequency Information", *In IEEE Transactions on Information Theory*, vol. 52, no. 2, pp. 489-509, Feb. 2006.
- [56] D. L. Donoho, "Compressed Sensing", *In IEEE Transactions on Information Theory*, vol. 52, no. 4, pp. 1289-1306, Apr. 2006.
- [57] Y. Wang, Z. Tian, and C. Feng, "A Two-Step Compressed Spectrum Sensing Scheme for Wideband Cognitive Radios", *In Proc. IEEE Globecom*, pp. 1-5, Dec. 2010.
- [58] J. Meng, W. Yin, H. Li, E. Hossain, and Z. Han, "Collaborative Spectrum Sensing from Sparse Observations in Cognitive Radio Networks", *In IEEE Journal on Selected Areas in Communications*, vol. 29, no. 2, pp. 327-337, Feb. 2011.
- [59] D. J. Rogers, R. Elkins, S. Chin, and M. A. Wayne, "Compressive RF Sensing using a Physical Source of Entropy", *IEEE Statistical Signal Processing Workshop*, pp. 609-612, June 2011.

- [60] J. Park et al., "A Fully Integrated UHF-Band CMOS Receiver With Multi-Resolution Spectrum Sensing (MRSS) Functionality for IEEE 802.22 Cognitive Radio Applications", *In IEEE Journal of Solid-state Circuits*, vol. 44, no. 1, pp. 258-268, Jan. 2009.
- [61] Z. Quan, S. Cui, A. H. Sayed, and H. V. Poor, "Optimal Multiband Joint Detection for Spectrum Sensing in Cognitive Radio Networks", *In IEEE Transactions on Signal Processing*, vol. 57, no. 3, pp. 1128-1140, Mar. 2009.
- [62] Y. Zeng, Y. -C. Liang, and M. W. Chia, "Edge based Wideband Sensing for Cognitive Radio: Algorithm and Performance Evaluation", *In Proc. IEEE DySPAN*, pp. 538-544, May 2011.
- [63] D. Tse and P. Viswanath, "Fundamentals of Wireless Communication", Cambridge University Press 2005.
- [64] S. M. Mishra, A. Sahai, and R. W. Brodersen, "Cooperative Sensing among Cognitive Radios", *In Proc. IEEE International Conference on Communications*, pp. 1658-1663, Dec. 2006.
- [65] W. Zhang and K. B. Letaief, "Cooperative Spectrum Sensing with Transmit and Relay Diversity in Cognitive Radio Networks", *In IEEE Transactions on Wireless Communications*, vol. 7, no. 12, pp. 4761-4766, Dec. 2008.
- [66] A. Nosratinia, T. E. Hunter, and A. Hedayat, "Cooperative Communication in Wireless Networks", *In IEEE Communications Magazine*, pp. 74-80, Oct. 2004.
- [67] G. Ganesan and Y. G. Li, "Cooperative Spectrum Sensing in Cognitive Radio - Part I: Two User Networks", *In IEEE Transactions on Wireless Communications*, vol. 6, no. 6, pp. 2204-2213, Aug. 2007.
- [68] X. Wang, J. Liu, W. Chen, and Z. Cao, "CORE-4: Cognition Oriented Relaying Exploiting 4-D Spectrum Holes", *In Proc. IEEE Wireless Communications and Mobile Computing Conference*, pp. 1982-1987, Aug. 2011.
- [69] C. Sun, W. Zhang, and K. B. Letaief, "Cluster-Based Cooperative Spectrum Sensing in Cognitive Radio Systems", *In Proc. IEEE International Conference on Communications*, pp. 2511-2515, June 2007.
- [70] C. Sun, W. Zhang, and K. B. Letaief, "Cooperative Spectrum Sensing for Cognitive Radios under Bandwidth Constraints", *In Proc. IEEE Wireless Communications and Networking Conference*, pp. 1-5, Mar. 2007.
- [71] A. Ghasemi and E. S. Sousa, "Collaborative Spectrum Sensing for Opportunistic Access in Fading Environments", *In Proc. IEEE DySPAN*, pp. 131-136, Nov. 2005.
- [72] C. Lee and W. Wolf, "Energy Efficient Techniques for Cooperative Spectrum Sensing in Cognitive Radios", *In Proc. IEEE Consumer Communications & Networking Conference*, pp. 968-972, Jan. 2008.
- [73] M. Mustonen, M. Matinmikko and A. Mämmelä, "Cooperative Spectrum Sensing Using Quantized Soft Decision Combining", *In Proc. Crowncom*, pp. 1-5, July 2009.

- [74] K. Arshad, M. A. Imran, and K. Moessner, "Collaborative Spectrum Sensing Optimisation Algorithms for Cognitive Radio Networks", *International Journal of Digital Multimedia Broadcasting*, vol. 2010, pp. 269-299, Mar. 2010.
- [75] P. Pawełczak, C. Guo, R. V. Prasad, and R. Hekmat, "Cluster-Based Spectrum Sensing Architecture for Opportunistic Spectrum Access Networks", Technical Report IRCTR-S-004-07, Feb. 2007.
- [76] V. Fodor and I. Glaropoulos, "On the Gains of Deterministic Placement and Coordinated Activation in Sensor Networks", *In Proc. IEEE Globecom*, pp. 1-6, Nov. 2008.
- [77] V. Fodor, I. Glaropoulos, and L. Pescosolido, "Detecting Low-Power Primary Signals via Distributed Sensing to Support Opportunistic Spectrum Access", *In Proc. IEEE International Conference on Communications*, pp. 1-6, Jun. 2009.
- [78] S. J. Shellhammer, "A Comparison of Geo-Location and Spectrum Sensing in Cognitive Radio", *In Proc. IEEE ICCCN*, pp. 1-6, Aug. 2009.
- [79] ITU-R. Recommendation P.1546-4. Method for point-to-area predictions for terrestrial services in the frequency range 30 MHz to 300 MHz, Oct. 2009.
- [80] V. Gonçalves and S. Pollin, "The Value of Sensing for TV White Spaces", *In Proc. IEEE DySPAN*, pp. 231-241, May 2011.
- [81] M. Cave, C. Doyle, and W. Webb, "Essentials of Modern Spectrum Management", 1st Ed., Cambridge University Press 2007.
- [82] International Telecommunication Union. Measuring the Information Society, v. 1.01, 2010.
- [83] International Telecommunication Union. Measuring the Information Society, 2011.
- [84] Organisation for Economic Cooperation and Development (OECD). Understanding the Digital Divide, 2001.
- [85] M. B. H. Weiss, M. Altamaimi, and L. Cui, "Dynamic Geospatial Spectrum Modelling: Taxonomy, Options and Consequences", *In Proc. Telecommunications Policy Research Conference*, Oct. 2010.
- [86] M. B. H. Weiss and M. Altamaimi, "The Cost of Knowing: An Economic Evaluation of Context Acquisition in DSA Systems", *In Proc. Telecommunications Policy Research Conference*, Sept. 2011.
- [87] O. Grøndalen, M. Lähteenoja, and P. Grønsund, "Business case proposal for a Cognitive Radio Network based on Wireless Sensor Network", *In Proc. Crowncom*, pp. 1-5, Sept. 2010.
- [88] J. Li and V. Samarasekera, "Designing a TV White Space Spectrum Sensor to Exceed FCC Requirements", WiLAN Technical White Paper, 2011.
- [89] J. P. Miranda, H. Tchouankem, J. Kibilda, and L. A. DaSilva, "Return Path for iTV using Whitespaces: A Novel Application for 802.22 WRAN", *In Proc. of IEEE Wireless Advanced*, pp. 95-100, June 2011.

- [90] J. P. Miranda, J. Kibilda, and L. A. DaSilva, "Semi-blind Channel Monitoring Mechanisms for Post-switchover Wireless Microphones", *In Proc. of IEEE Globecom*, pp. 1-6, Dec. 2011.
- [91] B. Sklar, "Digital Communications: Fundamentals and Applications", 2nd Ed., Prentice Hall 2001.
- [92] P. K. Varshney and C. S. Burrus, "Distributed Detection and Data Fusion", Springer 1996.
- [93] H. V. Poor, "An Introduction to Signal Detection and Estimation", 2nd Ed., Springer 1994.
- [94] T. Pany, "Navigation Signal Processing for GNSS Software Receivers", Artech House 2010.
- [95] F. F. Digham, M. S. Alouini, and M. K. Simon, "On the Energy Detection of Unknown Signals over Fading Channels", *In Proc. International Conference on Communications*, vol. 5, pp. 3575-3579, May 2003.
- [96] A. Mariani, A. Giorgetti, and M. Chiani, "SNR Wall for Energy Detection with Noise Power Estimation", *In Proc. International Conference on Communications*, pp. 1-6, June 2011.
- [97] A. Sonnenschein and P. M. Fishman, "Radiometric Detection of Spread-spectrum Signals in Noise of Uncertain Power", *In IEEE Transactions on Aerospace and Electronic Systems*, vol. 28, no. 3, pp. 654-660, July 1992.
- [98] R. Tandra and A. Sahai, "Fundamental Limits on Detection in Low SNR under Noise Uncertainty", *In Proc. International Conference on Wireless Networks, Communications and Mobile Computing*, pp. 464-469, June 2005.
- [99] R. Tandra and A. Sahai, "SNR Walls for Signal Detection", *In IEEE Journal of Selected Topics in Signal Processing*, vol. 2, no. 1, pp. 4-17, Feb. 2008.
- [100] H. Wang, Y. Xu, X. Su, and J. Wang, "Cooperative Spectrum Sensing in Cognitive Radio under Noise Uncertainty", *In Proc. IEEE Vehicular Technology Conference*, pp. 1-5, May 2010.
- [101] Q. Liu, J. Gao, Y. Guo, and S. Liu, "Robustness Improvement against Noise Uncertainty by Cooperative Spectrum Sensing", *In Proc. International Conference on Wireless Communications and Signal Processing*, pp. 1-6, Oct. 2010.
- [102] H. Wang et al., "SNR Wall and Cooperative Spectrum Sensing in Cognitive Radio under Noise Uncertainty", *In Journal of Electronics (China)*, vol. 27, no. 5, pp. 611-617, Sept. 2010.
- [103] Y. Zeng and Y.-C. Liang, "Eigenvalue-Based Spectrum Sensing Algorithms for Cognitive Radio", *In IEEE Transactions on Communications*, vol. 57, no. 6, pp. 1784-1793, June 2009.
- [104] T. Ratnarajah, C. Zhong, A. Kortun, M. Sellathurai, and C. B. Papadias, "Complex Random Matrices and Multiple-antenna Spectrum Sensing", *In Proc. International Conference on Acoustics, Speech and Signal Processing*, pp. 3848-3851, May 2011.

- [105] B. Nadler, F. Penna, and R. Garello, "Performance of Eigenvalue-based Signal Detectors with Known and Unknown Noise Level", *In Proc. IEEE International Conference on Communications*, pp. 1-5, June 2011.
- [106] P. Bianchi, M. Debbah, M. Maida, and J. Najim, "Performance of Statistical Tests for Single-Source Detection Using Random Matrix Theory", *In IEEE Transactions on Information Theory*, vol. 57, no. 4, pp. 2400-2419, Apr. 2011.
- [107] F. Penna, R. Garello, and M. A. Spirito, "Cooperative Spectrum Sensing Based on the Limiting Eigenvalue Ratio Distribution in Wishart Matrices", *In IEEE Communications Letters*, vol. 13, no. 7, pp. 507-509, Jul. 2009.
- [108] Y. Zeng, Y.-C. Liang, and R. Zhang, "Blindly Combined Energy Detection for Spectrum Sensing in Cognitive Radio", *In IEEE Signal Processing Letters*, vol. 15, pp. 649-652, 2008.
- [109] R. Zhang, T. J. Lim, Y.-C. Liang, and Z. Zeng, "Multi-Antenna Based Spectrum Sensing for Cognitive Radios: A GLRT Approach", *In IEEE Transactions on Communications*, vol. 58, no. 1, pp. 84-88, Jan. 2010.
- [110] M. H. Hayes, "Statistical Digital Signal Processing and Modeling", Wiley 1996.
- [111] J. F. Adlard, "Frequency Shift Filtering for Cyclostationary Signals", Ph.D. Thesis, University of York, Sept. 2000.
- [112] W. A. Gardner, "Introduction to Random Processes with Applications to Signals and Systems", Ed. MacMillan, 1985.
- [113] W. A. Gardner, "Signal Interception: A Unifying Theoretical Framework for Feature Detection", *In IEEE Transactions on Communications*, vol. 36, no. 8, pp. 897-906, Aug. 1988.
- [114] J. Antoni, "Cyclic spectral analysis in practice", *Journal of Mechanical Systems and Signal Processing*, vol. 21, No. 2, pp. 597-630, Feb. 2007.
- [115] N. Han, S. H. Sohn, and J. M. Kim, "A Blind OFDM Detection and Identification Method based on Cyclostationarity for Cognitive Radio Application", *IECE Transactions on Communications*, vol. E92-B, no. 6, pp. 2235-2238, June 2009.
- [116] S. Chaudhari, V. Koivunen, and H. V. Poor, "Autocorrelation-Based Decentralized Sequential Detection of OFDM Signals in Cognitive Radios", *In IEEE Transactions on Signal Processing*, vol. 57, no. 7, pp. 2690-2700, July 2009.
- [117] ETSI EN 300 744 v.1.6.1. Digital Video Broadcasting (DVB); Framing structure, channel coding and modulation for digital terrestrial television, Jan. 2009.
- [118] D. Danev, E. Axell, and E. G. Larsson, "Spectrum Sensing Methods for Detection of DVB-T Signals in AWGN and Fading Channels", *In Proc. IEEE International Symposium on Personal, Indoor and Mobile Radio Communications*, pp. 2721-2726, Dec. 2010.
- [119] L. P. Goh, Z. Lei, and F. Chin, "DVB Detector for Cognitive Radio", *In Proc. IEEE International Conference on Communications*, pp. 6460-6465, June 2007.



- [120] L. P. Goh, Z. Lei, and F. Chin, "Feature Detector for DVB-T Signal in Multipath Fading Channel", *In Proc. Crowncom*, pp. 234-240, Aug. 2007.
- [121] H.-S. Chen, W. Gao, and D. G. Daut, "Spectrum Sensing for OFDM Systems employing Pilot Tones", *In IEEE Transactions on Wireless Communications*, vol. 8, no. 12, pp. 5862-5870, Dec. 2009.
- [122] K. Jack, "Video Demystified - A Handbook for the Digital Engineer", 5th Ed., Newnes 2007.
- [123] A. M. Mossa and V. Jeoti, "Cyclostationarity-based Spectrum Sensing for Analog TV and Wireless Microphone Signals", *In Proc. International Conference on Computational Intelligence, Communications Systems and Networks*, pp. 380-385, July 2009.
- [124] B. A. Adoum and V. Jeoti, "Cyclostationary Feature based Multiresolution Spectrum Sensing Approach for DVB-T and Wireless Microphone Signals", *In Proc. IEEE International Conference on Computer and Communications Engineering*, pp. 1-6, May 2010.
- [125] A. M. Mossa and V. Jeoti, "The Performance of Cyclostationarity-based WRAN Classification Approach in Multipath Fading Channel", *In Proc. IEEE International Conference on Computer Applications and Industrial Electronics*, pp. 636-640, Dec. 2010.
- [126] IEEE 802.22. Standard for Wireless Regional Area Networks Part 22: Cognitive Wireless RAN Medium Access Control (MAC) and Physical Layer (PHY) specifications: Policies and procedures for operation in the TV Bands. Draft D3.0, Mar. 2011.
- [127] Ecma International. Ecma TC48-2009-061. MAC and PHY for Operation in TV White Space. 1st Ed., Dec. 2009.
- [128] G. J. Buchwald et al., "The Design and Operation of the IEEE 802.22.1 Disabling Beacon for the Protection of TV Whitespace Incumbents", *In Proc. IEEE DySPAN*, pp. 1-6, Oct. 2008.
- [129] ARIB Standard STD-B31. Transmission System for Digital Terrestrial Television Broadcasting. Version 1.6, Nov. 2005.
- [130] H.-S. Chen, W. Gao, and D. G. Daut, "Spectrum Sensing for DMB-T Systems Using PN Frame Headers", *In Proc. IEEE International Conference on Communications*, pp. 4889-4893, May 2008.
- [131] M. K. Simon and M.-S. Alouini, "Digital Communication over Fading Channels - A Unified Approach to Performance Analysis", Wiley 2000.
- [132] H. Cao, S. Daoud, A. Wilzeck, and T. Kaiser, "Practical Issues in Spectrum Sensing for Multi-carrier System employing Pilot Tones", *In Proc. International Symposium on Applied Sciences in Biomedical and Communication Technologies*, pp. 1-5, Nov. 2010.

- [133] J. Lee and H. Lee, "Baseband-to-Mobile Clock Synchronization in the Presence of Carrier Frequency Offset", *In Proc. IEEE Vehicular Technology Conference*, pp. 1940-1944, Sept. 2005.
- [134] M. Sliskovic, "Carrier and Sampling Frequency Offset Estimation and Correction in Multicarrier Systems", *In Proc. IEEE Globecom*, vol. 1, pp. 285-289, Nov. 2001.
- [135] ATSC Standard. A/53. ATSC Digital Television Standard Part 2 - RF/Transmission System Characteristics, 2007.
- [136] C. Cordeiro, M. Ghosh, D. Cavalcanti, and K. Challapali, "Spectrum Sensing for Dynamic Spectrum Access of TV Bands", *In Proc. CrownCom*, July 2007.
- [137] Homepage of CSR, "aptX Live" audio codec, <http://www.csr.com/products/59/aptx-live>, Jan. 2011.
- [138] S. J. Shellhammer, A. K. Sadek, and W. Zhang, "Technical Challenges for Cognitive Radio in the TV White Space Spectrum", *In Proc. Information Theory and Applications Workshop*, pp. 323-333, Feb. 2009.
- [139] S. J. Orfanidis, "Optimum Signal Processing - An Introduction", 2nd Ed., McGraw-Hill Publishing Company 1988.
- [140] D. Zhang, L. Dong, and N. B. Mandayam, "Sensing Wireless Microphone with ESPRIT from Noise and Adjacent Channel Interference", *In Proc. IEEE Globecom*, pp. 1-5, Dec. 2010.
- [141] K. Ahmad, U. Meier, and H. Kwasnicka, "Fuzzy Logic Based Signal Classification with Cognitive Radios for Standard Wireless Technologies", *In Proc. CrownCom*, pp. 1-5, June 2010.
- [142] W. Bratton, "Managing The Analogue Switch-Off Process: Timelines, Difficulties and Questions", *In Proc. Broadcast Asia International Conference*, May 2005.
- [143] C. Clanton, M. Kenkel, and Y. Tang, "Wireless Microphone Signal Simulation Method", IEEE 802.22-07/0124r0, Mar. 2007.
- [144] E. Sofer and G. Chouinard, "WRAN Channel Modeling", IEEE 802.22-05/0055r7, Sept. 2005.
- [145] A. van der Veen, E. F. Deprettere, and L. Swindlehurst, "Subspace-based Signal Analysis using Singular Value Decomposition", *In Proc. of the IEEE*, vol. 81, no. 9, pp. 1277-1308, Sept. 1993.
- [146] Homepage of the Regional Computing Center of Lower Saxony (RRZN), "The RRZN Cluster System", <http://www.rrzn.uni-hannover.de/clustersystem.html>, Jan. 2011.
- [147] A. Papoulis and S. U. Pillai, "Probability, Random Variables, and Stochastic Processes", 4th Ed., McGraw-Hill 2002.
- [148] M. C. Jeruchim, P. Balaban, and K. S. Shanmugan, "Simulation of Communication Systems: Modeling, Methodology, and Techniques", 2nd Ed., Springer 2000.

- [149] D. P. Kroese, T. Taimre, and Z. I. Botev, “Handbook of Monte Carlo Methods”, Wiley 2011.
- [150] J. F. Hayes and T. V. Babu, “Modeling and Analysis of Telecommunications Networks”, Wiley 2004.
- [151] B. Nadler and I. M. Johnstone, “On the Distribution of Roy’s Largest Root Test in MANOVA and in Signal Detection in Noise”, Technical Report No. 2011-04, May 2011.
- [152] D. Sundararajan, “A Practical Approach to Signals and Systems”, Wiley 2009.
- [153] L. Wei and O. Tirkkonen, “Spectrum Sensing in the Presence of Multiple Primary Users”, *In IEEE Transactions on Communications*, vol. 60, no. 5, pp. 1268-1277, May 2012.
- [154] A. Agresti, “An Introduction to Categorical Data Analysis”, 2nd Ed., Wiley 2007.
- [155] S. Morris and A. Smith-Chaigneau, “Interactive TV Standards: A Guide to MHP, OCAP, and JavaTV”, Elsevier Inc. 2005.
- [156] E. Tsekleves, J. Cosmas, A. Aggoun, and J. Loo, “Converged Digital TV Services: The Role of Middleware and Future Directions of Interactive Television”, *International Journal of Digital Multimedia Broadcasting*, 19 pages, vol. 2009.
- [157] ATSC Standard. A/96. ATSC Interaction Channel Protocols, Feb. 2004.
- [158] ISDB Standard. STD-B21. Receiver for Digital Broadcasting, June 2006.
- [159] ETSI. EN 301 958 v.1.1.1, European Standard “Digital Video Broadcasting (DVB); Interaction channel for Digital Terrestrial Television (RCT) incorporating Multiple Access OFDM”, 2002.
- [160] N. Björzell, L. De Vito, and S. Rapuano, “A GNU Radio-based Signal Detector for Cognitive Radio Systems”, *In Proc. IEEE Instrumentation and Measurement Technology Conference*, pp. 1-5, May 2011.
- [161] P. Alvarez, N. Pratas, A. Rodrigues, N. R. Prasad, and R. Prasad, “Energy Detection and Eigenvalue Based Detection: An Experimental Study Using GNU Radio”, *In Proc. International Symposium on Wireless Personal Multimedia Communications*, pp. 1-5, Oct. 2011.
- [162] Working Document RSCOM10-61, Report and Follow-up from the EU Workshop on “A Long Term Approach to Radio Spectrum for PMSE in Europe”, Dec. 2010.
- [163] ETSI. TR 102799 v.1.1.1, Technical Report on “Electromagnetic compatibility and Radio spectrum Matters (ERM); Operation methods and principles for spectrum access systems for PMSE technologies and the guarantee of a high sound production quality on selected frequencies utilising cognitive interference mitigation techniques”, Dec. 2010.
- [164] J. Zhang, Q. Zhao, and J. Zou, “The IEEE802.22 WRAN System Based on Radio Environment Map (REM)”, *In Proc. International Workshop on Education Technology and Computer Science*, vol. 1, pp. 98-101, Mar. 2009.

- [165] Homepage of the Project CPMSE, “A Research Project to Improve the Frequency Utilization and Coexistence for PMSE Systems by Cognitive Methods”, <http://www.c-pmse.research-project.de/index.php/en/>, June 2012.

# Wissenschaftlicher Werdegang

## Persönliche Daten

João Paulo Cruz Lopes Miranda  
geboren am 05.04.1974 in Recife, Brasilien  
verheiratet mit Daniela Julio de Almeida Miranda  
Adresse: Apt. 517, The Arcs  
Beacon South Quarter  
Sandyford, Dublin 18  
Ireland  
Email: joao.paulo.cl.miranda@googlemail.com

---

## Studienverlauf

- 12.1991                      Abitur, Contato Colégio e Curso, Recife, Brasilien
- 02.1992–12.1996            Studium der Ingenieurwissenschaften  
an der Escola Politécnica de Pernambuco, Recife, Brasilien
- 03.1999–08.2001            Masterstudium in Ingenieurwissenschaften  
an der Universidade Federal de Pernambuco, Recife, Brasilien,  
bei Prof. Docteur Hélio Magalhaes de Oliveira. Titel der  
Masterarbeit: “*Digital Multiplexing and Multiple Access  
based on Finite Field Transforms*”
- 04.2008–06.2012            Promotion zum Dr.-Ing.  
an der Leibniz Universität Hannover  
bei Prof. Dr.-Ing. Markus Fidler. Titel der Dissertation:  
“*Multi-standard Context-aware Cognitive Radio: Sensing and  
Classification Mechanisms*”
- 08.2012–Jetzt                Post-doctoral Research Fellow  
an der Trinity College Dublin, Ireland

**Stipendien & Preise**

|                  |   |
|------------------|---|
| 10.2007–03.2008  | DAAD-Stipendium<br>für einen Deutschkurs am Goethe-Institut Göttingen   |
| 04.2008–06.2012  | CAPES/Brasilien-Stipendium<br>für eine Promotion an der Leibniz Universität Hannover                          |
| 02.2011, 04.2011 | Grant der COST Action IC0902 für Short-term Scientific Missions (STSM) an der Trinity College Dublin, Ireland |

---

**Forschungsaufenthalte**

|         |  |
|---------|--|
| 02.2011 | Trinity College Dublin, Ireland (Prof. Dr. Luiz DaSilva).<br>Title der STSM: “Coexistence Issues in Cognitive Radio” |
|---------|--|

---

**Liste der Publikationen**

H. Cao, Q. Cai, J. P. Miranda, and T. Kaiser, “Cyclostationary Multitone Beacon Signal for Opportunistic Spectrum Access”, In Proc. of the Crowncom, pp. 1-6, Hannover, Germany, June 2009.

J. P. Miranda, C. König, and M. D. Pérez Guirao, “Implementation of a Simple Air-interface for Overlay-based Cognitive Radio”, Skriptum zum Laboratorium für Netze und Protokolle (NUP), chapter 4, pp. 59-86, Apr. 2010.

J. P. Miranda, M. D. Pérez Guirao, A. Lambertucci, and L. A. DaSilva, “Worst Case Analysis of Single-stage Sensing in WRANs”, 1st Workshop of the COST Action IC0902, Bologna, Italy, Nov. 2010.

H. Cao, Q. Cai, J. P. Miranda, and T. Kaiser, “Cyclostationary Beacon for Assisting Spectrum Sensing in Opportunistic Spectrum Access”, Majlesi Journal of Electrical Engineering, vol. 5, No. 1, pp. 65-72, Mar. 2011.

J. P. Miranda and H. Tchouankem, “Simple Air-interface for Energy-based Cooperative Spectrum Sensing”, Skriptum zum Laboratorium für Netze und Protokolle (NUP), chapter 5, pp. 55-75, Apr. 2011.

J. P. Miranda, H. Tchouankem, J. Kibiłda, and L. A. DaSilva, “Return Path for iTV using Whitespaces: A Novel Application for 802.22 WRAN”, In Proc. of IEEE Wireless Advanced, pp. 95-100, London, U.K., June 2011.

J. P. Miranda, J. Kibiłda, and L. A. DaSilva, “Spectrum Sensing by Program Making and Special Events in the Post-switchover Era: Achievements of a STSM”, 2nd Workshop of the COST Action IC0902, Barcelona, Spain, Oct. 2011.

J. P. Miranda, J. Kibiłda, and L. A. DaSilva, “Semi-blind Channel Monitoring Mechanisms for Post-switchover Wireless Microphones”, In Proc. of IEEE Globecom, pp. 1-6, Houston, USA, Dec. 2011.

J. P. Miranda and H. Tchouankem, “Simple Air-Interface for Energy-based Cooperative Spectrum Sensing”, Skriptum zum Laboratorium für Netze und Protokolle (NUP), chapter 5, pp. 53-73, June 2012.

H. Cao, J. P. Miranda, and J. Peissig, “Enhanced Spectrum Awareness with Extended Information Carried on Embedded Cyclostationary Signatures for Cognitive Radio”, In Proc. of IEEE Globecom, pp. 1506-1512, Anaheim, USA, Dec. 2012.

---

### Reviewertätigkeit

IEEE Journal on Selected Areas in Communications • IEEE Transactions on Wireless Communications • IEEE Communication Letters • IEEE Transactions on Vehicular Technology • IEEE Signal Processing Magazine • Transactions on Emerging Telecommunications Technologies • IET Journal of Communications • IEEE DySPAN • IEEE Globecom • IEEE ICC • Crowncom • IEEE VTC • IEEE ICUWB • IEEE CCNC

---

### Kollaborationen

Prof. Dr. Luiz DaSilva, Virginia Tech, USA  
Prof. Dr. Giuseppe Abreu, Jacobs University, Bremen

---

### Zusätzliche Informationen

Für ein vollständigen Lebenslauf siehe mein LinkedIn Profil unter [http://www.linkedin.com/profile/view?id=118166085&trk=tab\\_pro](http://www.linkedin.com/profile/view?id=118166085&trk=tab_pro)

